Corrected Copy

GUGGENHEIM AERONAUTICAL LABORATORY

CALIFORNIA INSTITUTE OF TECHNOLOGY

HYPERSONIC RESEARCH PROJECT

Memorandum No. 61

June 15, 1961

ENERGY TRANSFER PROCESSES IN A PARTIALLY IONIZED GAS

by

Gordon L. Cann

ARMY ORDNANCE CONTRACTS

NO. DA-04-495-Ord-1960 and 3231

GUGGENHEIM AERONAUTICAL LABORATORY
CALIFORNIA INSTITUTE OF TECHNOLOGY
Pasadena, California

HYPERSONIC RESEARCH PROJECT

Memorandum No. 61

June 15, 1961

ENERGY TRANSFER PROCESSES IN A PARTIALLY IONIZED GAS

by

Gordon L. Cann

Clark B. Millikan, Director
Guggenheim Aeronautical Laboratory

ARMY ORDNANCE CONTRACTS NO. DA-04-495-Ord-1960 and 3231

ACKNOWLEDGMENTS

The author wishes to express his sincere thanks and appreciation to Professor A. Roshko, under whose guidance this work was carried out. The author would also like to acknowledge the many helpful suggestions contributed by other members of the California Institute of Technology Guggenheim Aeronautical Laboratory staff that have led to the completion of this work, especially from Professor H. W. Liepmann and Professor L. Lees.

The author would also like to acknowledge his indebtedness to Mr. A. C. Ducati of the Giannini Scientific Corporation for introducing him to the art of arc jet practice and design.

Thanks are also extended to Mr. Gordon Johnston of the Electro-Optical Company and to Mrs. G. Van Gieson of the California Institute of Technology for their kind help in preparing the figures and typing of this report.

This work was carried out under the sponsorship and with the financial assistance of the Office, Chief of Ordnance, and the Office of Ordnance Research, U. S. Army.

ABSTRACT

The following paper is divided into three more or less separate sections. The first section (Chapters II - VI) deals with an analysis of the transport properties of a partially ionized gas subject to the constraint that the average random energy of all constituent particles is exactly equal (equipartition of energy). This constraint is necessary so that the formal Chapman-Enskog solution of Boltzman's equation can be used to evaluate the various transport coefficients. Subject to this constraint, a set of tractable equations describing the mass and energy diffusion in a partially ionized gas is obtained that includes all terms correct to the order of the square root of the ratio of the electron to atom mass compared to one. The transport coefficients are evaluated for helium and argon over the complete range of partial ionization assuming that the species particle densities are quite close to their equilibrium values.

The analysis indicates that the electron and ion diffusion velocities are more closely coupled than the equations of Chapman and Cowling show. The added coupling implicitly applies the constraint of zero mass velocity to the gas locally. Because of this constraint a current in the direction of (E x B) x B occurs in addition to the direct and Hall currents.

It is shown that the only part of the thermal conductivity that can be influenced by a magnetic field is that part of the energy carried by the diffusion of the charged particles. For this reason, magnetic fields, in general, cannot be nearly as effective in reducing heat transfer rates as was previously thought, e. g., a magnetic field will have no

influence on the thermal conductivity in a fully ionized gas, except through its influence on the current density and the thermal diffusion.

Chapters VII - IX comprise the second section of this paper and deal with the development of a similarity solution for axially symmetric electric discharges. A number of parameters are obtained and discussed. The solution is evaluated for a discharge in argon gas at one atmosphere pressure in which the temperature on the axis of the discharge varies from 6,000°K to 19,000°K. The current-voltage characteristic obtained from this solution is compared with an experimentally determined curve of H. Maecker.

The third section of this paper (Chapters X - XIII) is concerned with the mechanisms of energy transfer in arc jet devices. Use is made of the previous sections of the paper to determine the relative magnitude of the amount of energy that is transferred to the gas in the various parts of the electric discharge. The various possible electrode configurations are discussed in detail and compared. The design and performance of an annular electrode arc heater with a rotating arc is next described and discussed. Because of a number of undesirable performance characteristics of this type of electrode configuration, a modified heater was constructed with the cathode emission occurring along the axis of the applied magnetic field. Details of the unexpectedly good performance of this configuration are given. It is shown that the arc potential drop depends primarily on the strength of the applied magnetic field and the gas enthalpy downstream of the arc. The dependence of the arc potential drop on the arc current and the ambient

pressure is shown to be weak over the ranges tested, e.g., 50 to 300 amperes for the current and 1 to 4 atmospheres for the pressure. Some heat transfer measurements taken with this equipment are presented.

Appendix I is concerned with the evaluation of the transport coefficients in a partially ionized gas. Formulae are developed for determining the viscosity, thermal conductivity, and electric conductivity of the plasma. These coefficients are computed for argon and helium at one atmosphere pressure and over the temperature range of partial ionization.

TABLE OF CONTENTS

LIST OF TABLES

LIST OF FIGURES

LIST OF SYMBOLS

There is some duplication in the symbols used. In general, an attempt has been made to use conventional notation so that the duplication occurs only when some well-known relation is introduced only once or twice and is not used throughout the report.

a	ratio of atom to ion number density
a_i	constants in similarity solution
A^*	collisional interaction parameter
b	distance of closest approach of two particles in a binary collision
b	ratio of ion-atom to electron-ion diffusion cross-section
b_i	constants in similarity solution
b_1	$\left(\frac{2me}{ma} \right)^{\frac{1}{2}} b$
B	magnetic field strength
B^*	collisional interaction parameter
c	ratio of electron-atom to electron-ion diffusion cross-section
c_{p_i}	specific heat at constant pressure for species i
c_ε	Euler's constant
C^*	collisional interaction parameter
d	cut-off distance in coulomb interactions
D_{ij}	multiple particle diffusion coefficient
$\mathcal{D}_{ij}$	binary diffusion coefficient between particles of type i and type j
e_i	internal energy per gas particle of species i
e_i	electric charge of species i
$\|e\|$	absolute value of electronic charge
E	electric field strength

$f_{ij}^{(2)}$	correction term in diffusion coefficient
$f(T_o)$	similarity parameter
F_i	body force on particles of species i
F_1, F_1', F_2	generalized forces
g	relative velocity of particles in a binary collision
$g(T_o)$	similarity parameter
h	Plank's constant
h_i	enthalpy of gas particles of species i
H_{ij}	matrix component in determination of viscosity coefficient
j	electric current density
J	charged particle mass flux density
J_i	mass flux ratio of species i per unit area
k	Boltzmann's constant
k_T	thermal diffusion coefficient as defined by Chapman and Cowling
K_i	thermal diffusion coefficients
ℓ	length of heat transfer nozzles
L_{ij}	coefficients of vector relations in phenomenological equations
$\mathcal{L}_{ij}$	coefficients of 1st set of phenomenological equations
m	ratio of electron to atom mass
m_i	mass of particle of species i
m_{ij}	reduced mass of two particles in a binary collision
n	number density of particles
p	gas pressure
p	collision parameter in coulomb interactions
p_i	partial pressure of species i

P	stress tensor
P_{ea}^{I}	probability of an inelastic collision occurring between an electron and an atom
q_{ea}^{I}	cross-section for inelastic collisions between electrons and atoms
q_{ij}	reference cross-section for collisions between particles of type i and j
$Q_{12}^{(\ )}(g)$	general definition of cross-section
r	radial coordinate in cylindrical coordinate system
s_e'	electron ionizing efficiency
s_i	entropy per particle for species i
t_1	relaxation time for charged particle production
t_2	relaxation time for charged particle recombination
T	absolute temperature
u	gas velocity
u_i	diffusion velocity of species i
U	unit vector
V_I	ionization energy of particles of type i
w	non-dimensional electric potential
W	heat flux rates per unit area
X_i	generalized force applied to species i
y_o'	cut-off parameter in a coulomb collision
z	axial coordinate in cylindrical coordinate system
α	coefficient in the diffusion equations
$\alpha_d = 1+4y_o'^2$	= cut-off parameter in coulomb interactions
α_{iT}	thermal diffusion coefficient
β	coefficient in the diffusion equations
β_1	coefficient in the diffusion equations

γ	coefficient in the diffusion equations
Γ_i	volume production rate of species i
δ	coefficient in the diffusion equations
ϵ	ratio of electron to ion number density
ε_o	dielectric constant of free space
η	coefficient in the diffusion equations
η	non-dimensional radial coordinate
η	non-dimensional energy in binary collision
$[\eta]$	viscosity coefficient
θ	angular coordinate in cylindrical coordinate system
θ	non-dimensional temperature
κ'	coefficient of bulk viscosity
$\kappa_{J=0}$	thermal conduction coefficient when all diffusion currents are zero
μ_i	chemical potential of gas particles of species i
μ_o	permeability of free space
ξ	non-dimensional coordinate in sheath solution
π	non-dimensional pressure
ρ	gas density
σ	electrical conductivity
σ_{ij}	molecular diameter in collision between particles of the type i and j
σ_{sp}	electrical conductivity as derived by Spitzer
τ_i	collision time for a particle of type i

ϕ	coefficient in the diffusion equations
ϕ	similarity parameter
$\phi(v)$	potential energy of interaction for two particles in a binary collision
Φ	similarity parameter
χ	angular parameter in binary collision
χ_i	work function of surface material i
ω_i	gyration frequency of charged particle of type i
ϖ_i	ground state degeneracy of particles of type i
$\Omega_{12}^{(\ell,s)}(T)$	general interaction parameter in binary collision

Subscripts

a	atom
e	electron
g	gas
I	ion

I. INTRODUCTION

I. 1. Historical Sketch

Although electric arcs have been used and studied now for over one hundred and fifty years, their use as a device to heat a gas flow to several thousand degrees Kelvin is comparatively recent. It is only with the advent of the ballistic missile and the projected exploration of the inner planetary system that the need has arisen to develop equipment capable of producing steady-state gas flows in which the stagnation temperature is between 2,000°K and 12,000°K. Considerable work was done on devices of this nature by a number of German workers between 1940 and 1950[1]*, and this research has formed the basis for most of the subsequent work in the United States. During the past six years numerous devices have been built and operated throughout this country[2-4]. They can be divided approximately into three groups, each having its own characteristics. These types, together with their advantages and disadvantages will be discussed in a subsequent section. In general, the design is based upon precedent and trial and error. No one configuration has yet proved itself to be superior to the others for all applications.

Practical applications of arc heaters are being found in more and more widely diversified fields. Hyperthermal wind tunnels using a plasma jet to heat the gas to about 10,000 B. T. U./lb. are in use in many laboratories for studying heat transfer rates and ablation rates of nose cone material. These installations range from a few kilowatts

---

* Superscripts denote references at the end of the text.

to 15 megawatts supplied to the arc[5, 6]. A number of organizations are actively engaged in developing arc heaters as low thrust propulsion devices for space vehicles[7-9]. These engines use a low molecular weight gas for propellant, heat it with the arc and expand it through a sonic orifice and nozzle to an exit velocity greater than 10,000 m/sec. $I_{sp} > 1,000$. Numerous applications are being found for arc heaters outside of the aeronautical industry, e.g., chemical processing, spray coating with ceramic materials and as magnetohydrodynamic research tools.

I.2. Analytical Techniques Available to Describe Arc Phenomena and Thermal Plasmas

Until recently, the literature pertaining to the theory of arcs has consisted mainly of a number of mechanisms that were postulated to explain the various phenomena that have been observed. These mechanisms have been worked out in mathematical detail. In general, the mechanisms can be grouped into two classes, linear and non-linear. The former assumes that changes in gas particle energy over one mean free path are small compared to the gas internal energy, and that changes in velocity over a mean free path are small compared to the velocity of sound. When these assumptions are made it is possible to study a plasma or electric discharge by considering it as a mixture of perfect reacting gases that is perturbed only slightly from equilibrium because of gradients of electrical potential, chemical potential, and temperature. The familiar expressions for

laminar heat transfer	$q = -\kappa \nabla T$
electrical conductivity	$j = -\sigma \nabla \phi$
shear stress	$\bar{\bar{\sigma}} = \mu \nabla : w$

are all simple examples of linear mechanisms. Non-linear mechanisms

are defined as those that involve the treatment of problems where changes in either energy and velocity over a mean free path are of the same order as or larger than the gas internal energy and speed of sound, respectively. The development of turbulence and the phenomenon of run-away electrons in an electric discharge through hydrogen are examples of non-linear mechanisms. The best documented non-linear phenomenon in electric discharges is the dependence of the electron and ion drift velocities on the square root of the electric field in low pressure discharges where the per cent ionization is low. In this case the temperature of the charged particles is assumed to depend upon the electric field only and is evaluated by balancing the energy that these particles gain from the electric field with the energy that they lose due to collisions with uncharged particles. Agreement between experiment and theory is quite good over certain ranges of E/p, the electric field divided by the pressure. This is documented in many curves of the measured diffusion velocity of charged particles plotted as a function of E/p which are shown in References 19 and 23.

Inherent in the usual treatments of linear systems are the assumptions of local equipartition of energy among the particles and local Maxwellian velocity distribution. Neither of these assumptions is in general acceptable in a gas mixture that contains electrons and through which an electric current is passing. Because of the weak coupling in energy transfer from the electrons to gas atoms or ions and because the electrons absorb initially a high percentage of the energy transferred from the electric field to the gas, the mean electron energy is always higher than the mean atom and ion energy, sometimes by a factor of over 10. When the dependence of the cross-sections for energy exchange between electrons and ions or atoms falls rapidly enough with the relative velocity, the local distribution of electron velocity can be distorted far from the

Maxwell distribution. In some cases, e.g., an electron and proton mixture, the interaction cross-section falls so rapidly that the electron energy becomes undirectional in the direction of the applied electric field and the well-known phenomenon of run-away electrons occurs. Unfortunately, the whole theory of the gaseous state, as developed in thermodynamics, statistical mechanics, irreversible thermodynamics, chemical kinetics, and the theory of non-uniform gases do not allow for local departures from equipartition of energy among the species present in a gas mixture, even in the presence of externally applied fields. Recently, some efforts have been made to obtain a solution of Boltzmann's equation for a two-particle system (electron-ion) in which the constraint of equipartition of energy was relaxed[10]. A similar treatment of a three particle system is still not available in the literature, possibly because of the complicated nature of the many new interactions that become available.

Although the general solutions for a three particle system constrained by equipartition has been in existence for many years now, the algebra involved in handling the complete solution is so unwieldy that the physical implications behind the mathematical solution have not yet been fully elucidated. It is felt that before any attempt can be made to develop a complete mathematical theory for a system in which energy equipartition does not occur, the solution for equipartition should be studied in detail, and its implications clearly understood. Finkelnburg and Maecker have attempted to do this in their article, "Thermal Plasmas and Electric Arcs"[1]; however, some algebraic errors have crept into their work and their expressions are still so complicated that it is difficult to interpret them.

I. 3. Extent of Present Analysis

The analytic portion of the present work is mostly concerned with an attempt to simplify the general Chapman-Enskog solution to Boltzman's equation for a system of atoms, ions, and electrons. At the same time the implications of the finite reaction rate in the production and recombination of the electrons and ions is studied. In order to introduce the reaction rates into the general mathematical solution, it is convenient to use irreversible thermodynamics so that all possible interactions can be obtained. In general, irreversible thermodynamics is only a convenient bookkeeping technique for properly cataloguing all of the possible interactions between the various transport processes in the fluid under study. In the general treatment of the species diffusion and energy transport equations using irreversible thermodynamics, no restriction is initially placed upon the species concentrations so that the diffusion and heat transfer relations derived are generally valid and are not coupled to any assumption made concerning the reaction rate. The first section of the analysis reported here is the derivation of the three general sets of relations for the transport properties of a partially ionized gas from the laws of irreversible thermodynamics. The vector equations for species mass diffusion and energy diffusion are each discussed in detail. The scalar reaction rate equation is next derived from chemical kinetic considerations and it is shown under what conditions the linear approximation of irreversible thermodynamics is valid. If desirable, it is possible to introduce any reasonable expression for the reaction-rate equation, valid when the reaction is far from equilibrium, into the general equations for particle and energy diffusion in the gas mixture. The second order tensor equations, involving the stress-strain relations for the fluid are derived

but not discussed in detail.

The general results of the above analysis are used to discuss two problems. The first is a model of a cylindrically symmetric electric discharge, when the reaction rate is fast enough to keep the particle concentrations close to their equilibrium values. The second problem that is discussed is the formation and structure of sheaths between a solid surface and a plasma under conditions close to equilibrium. The interpretation of some arc phenomena in terms of these solutions is then discussed in some detail. In particular, the range of validity of the linear approximation as applied to electrical discharges is clearly outlined.

II. THE FORMULATION OF TRANSPORT PROPERTY ANALYSIS

II. 1. Formulation of the Problem of the Transport Properties in a Gas by the Use of Irreversible Thermodynamics

In formulating the problem of the motion of the various species relative to the center of mass of the gas and of the energy transport it is desirable to list the various phenomena that can be considered to have some bearing on these processes and then see to what extent a comprehensive analysis can be made to include all of them. The following list describes most of the processes of interest that occur in partially ionized plasmas.

(1) An electric current is carried by the diffusion of the electrons relative to that of the ions.

(2) A current of charged particles relative to the neutral particles occurs; this current is known as ambipolar diffusion.

(3) Both of the above phenomena occur when there are gradients of any of the following:

(a) species density

(b) pressure

(c) temperature

(d) electric potential.

(4) Energy is transferred by thermal conduction and by species diffusion.

(5) Energy can be added to the gas from an externally applied electric field.

(6) Recombination of electrons and ions as well as ionization of

atoms is occurring throughout the gas.

(7) Several of these processes do not attain equilibrium instantaneously but must be characterized by relaxations times or reaction rates, e.g., a reaction rate equation is necessary to describe the deviation of the ionization level from equilibrium.

(8) Any, or all of the above processes can be modified by the presence of either an externally applied magnetic field or a self-generated magnetic field.

(9) Shear and compressive stresses in the gas can conceivably affect the above processes.

The ideal method of studying the behavior and interaction of the above quantities is through the use of kinetic theory, usually involving some treatment of the relevant Boltzmann equation. Unfortunately, because of the great complexity of the problem, not even an approximate solution is available as yet. Burgers[10] has considered the equivalent problem for a fully ionized gas, and Chapman and Cowling[11], among many others[12-14], have investigated numerous aspects of the behavior of a partially ionized gas under severely restrictive assumptions, where most of the possible interactions among the phenomena are deliberately omitted so that a solution may be obtained. An alternative, but less self-contained, method of handling this problem is available through the use of the thermodynamics of the steady state, or, as it is commonly called, irreversible thermodynamics[15, 16]. The application of this technique requires that the following steps be carried out:

(1) An expression for the entropy production rate per unit mass of the gas must be derived and the terms representing reversible entropy changes and irreversible entropy production separated.

(2) Each term that involves irreversible entropy production is a product; one part of the product is called a "flux"; the other part is called a "force".

(3) All fluxes and forces that are of the same rank tensor are linearily inter-dependent. In addition other terms may result by the contraction of any other tensors representing forces and fluxes of rank 2 higher than that under consideration if they are symmetric.

(4) The coefficients in the various systems of linear equations have certain symmetry properties that result from the application of the Onsager reciprocity relations.

(5) The coefficients that are left after applying (4) must be evaluated by recourse to either kinetic theory or experiment.

The great advantage of this procedure is that a complete solution to the problem of the transport properties of a gas mixture can be built up by using the results of a number of simplified kinetic theory analyses.

Using this technique, Finkelnburg and Maecker[1] have derived a set of relations for a three component plasma that incorporate most of the required phenomena and their interactions. These equations are extremely complicated and little effort has been made to apply them to specific problems; moreover, they do not consider cases where charge accumulation can occur nor do they allow for finite reaction rates. A recent report by Pipkin[13] discusses the electrical conductivity of a partially ionized gas using very general considerations, but he also does not allow for charge accumulation or finite reaction rates and his expressions are not simple or easy to interpret.

Rather than attempt to modify the treatments discussed above,

we will treat the problem in full.

Before proceeding to the purely mechanical aspects of the derivation it is necessary to examine two rather fundamental problems that arise when efforts are made to apply the thermodynamics of the steady-state to the derivation of equations that can adequately explain transport phenomena occurring in ionized gases when externally applied electric and magnetic fields are present. The first problem arises from the postulate of equipartition of energy among the various gaseous species. In order to apply thermodynamics and irreversible thermodynamics to the system this postulate must be rigorously true to the extent that when perturbations to the equilibrium system are introducted due to gradients of electric and chemical potential and the temperature, no perturbation in the species temperatures develops. This constraint on the system implicitly implies that the gas particles are extremely strongly coupled energetically, so that energy transfer through collisions of the particles of the various species one with another occurs at a rate much faster than that at which any one species can gain energy from or lose it to an external field. Unfortunately, because of their small mass, electrons are coupled energetically much more strongly to the electric field energy than to the internal energy of the ions and atoms of the plasma. Hence the electron energy will, in general, be somewhere between the limits shown below:

$$\left(\frac{|e|\,E\,\tau}{m_e}\right)^2 \frac{m_a}{2} + \left(\frac{3}{2} k T_g\right) \geq \left(\frac{3}{2} k T_e\right) \geq \left(\frac{3}{2} k T_g\right).$$

At present there does not appear to be any simple technique available to introduce into the general analysis a perturbation in electron tem-

perature from the gas temperature. Probably the most serious limit on the range of validity of the procedure adopted here occurs because of this difference between T_e and T_g when the results are applied to electric discharges.

The second problem that arises when irreversible thermodynamics is used to study phenomena in ionized gases, is that of determining how to compute the influence of a magnetic field upon the transport properties of the plasma. Since this problem can best be investigated once some of the formalism of the theory has been outlined, a discussion of this important point will be deferred until after the vector flux and force system has been constructed in the following section.

With these introductory remarks, it is now possible to proceed to the mechanics of computing the transport properties of a partially ionized gas.

II. 2. Entropy Production Rate

The equation for the entropy production rate for an open system of a mixture of gases can be obtained by combining the first and second laws of thermodynamics as follows[17]:

$$T \frac{d}{dt}\left(\frac{s_i n_i}{\rho}\right) = \frac{d}{dt}\left(\frac{e_i n_i}{\rho}\right) + p \frac{d}{dt}\left(\frac{1}{\rho}\right) - \sum_i \mu_i \frac{d}{dt}\left(\frac{n_i}{\rho}\right) . \qquad \text{(II-1)}$$

s_i and e_i are the entropy and internal energy per particle. The various time derivatives on the right-hand side of this equation can now be replaced from the conservation equations. The mass conservation equation for each type of particle is

$$\rho \frac{d}{dt}\left(\frac{n_i}{\rho}\right) = - \nabla \cdot \frac{J_i}{m_i} + \Gamma_i \qquad . \qquad \text{(II-2)}$$

By adding together the Eqs. (II-2), the equation of mass conservation is obtained.

$$\rho \frac{d}{dt}\left(\frac{1}{\rho}\right) = -\nabla \cdot u \quad . \qquad \text{(II-3)}$$

The final equation that is needed is an energy conservation relation, a convenient form of which is the following:

$$\rho \frac{d}{dt}\left(\sum_i \frac{n_i e_i}{\rho}\right) = -\nabla \cdot W - P : \frac{\partial u}{\partial r} + \sum_i \frac{J_i \cdot F_i}{m_i} \quad . \qquad \text{(II-4)}$$

Substituting Eqs. (II-2), (II-3), and (II-4) into Eqs. (II-1) and rearranging some terms, the following entropy conservation equation is obtained.

$$T\rho \frac{d}{dt}\left(\sum_i \frac{n_i s_i}{\rho}\right) + T \nabla \cdot \left(\frac{W}{T} - \sum_i \frac{J_i \mu_i}{T m_i}\right) = W \cdot \frac{\nabla T}{T}$$
$$- (P - pU) : \frac{\partial u}{\partial r} + \sum_i J_i \cdot \left(\frac{F_i}{m_i} - \frac{kT}{m_i} \nabla \frac{\mu_i}{kT}\right) - \sum_i \mu_i \Gamma_i \qquad \text{(II-5)}$$

The second term on the left-hand side of the equation represents the reversible entropy changes while each term on the right-hand side of the equation represents irreversible entropy production. It can be shown[15] that each of the terms on the right-hand side of the equation is intrinsically positive.

II. 3. Flux and Force Systems

Three groups of forces and fluxes, ordered according to the tensor rank, are represented in the terms on the right-hand side of Eq. (II-5). The last term and the trace of the second term fall into the first group, which consists of scalar quantities. The flux quantities are the species production rate Γ_i and the divergence of the mass velocity vector $\nabla \cdot u$. Using the continuity Eq. (II-3), the second flux

$\nabla \cdot u$ can be equated to the Eulerian derivative of the logarithm of the density - $(d/dt)(\ell n \rho)$ and this representation of the flux term is considered preferable. The force terms corresponding to the above fluxes are the chemical potentials μ_i and the pressure increment δp, which is the trace of the stress tensor P, and indicates how much the compressive stresses cause the pressure in the gas to deviate from the thermodynamic pressure. Since only one chemical reaction will be considered, that of ionization and recombination, it is possible to combine the three chemical potentials into one term[15] $\Sigma_i \nu_i \mu_i$, where ν_i is the digit appearing in the reaction equation indicating the number of mols of the constituent taking part in the reaction. The first set of phenomenological equations can hence be written as follows:

$$\begin{aligned} \frac{d}{dt}(\ln \rho) &= \mathcal{L}_{11} \frac{\delta p}{p} + \mathcal{L}_{12} \sum_i \frac{\nu_i \mu_i}{kT} \\ \frac{\Gamma_1}{n_1} &= \mathcal{L}_{21} \frac{\delta p}{p} + \mathcal{L}_{22} \sum_i \frac{\nu_i \mu_i}{kT} \end{aligned} \qquad \text{(II-6)}$$

$$\Gamma_1 = \Gamma_2 = -\Gamma_3 ; \qquad \mathcal{L}_{12} = \mathcal{L}_{21}$$

In this paper, the electrons will be identified with particle 1, the ions with particle 2, and the atoms with particle 3. The various forces and fluxes have been divided by suitable local properties of the gas in such a manner that the coefficients $\mathcal{L}_{ij}$ have the dimensions $(\text{time})^{-1}$; they are inverse relaxation times. The coefficient $\mathcal{L}_{11}$ is generally termed the second coefficient of viscosity and can be interpreted in terms of a relaxation time for internal degrees of freedom. For a gas mixture composed of electrons, ions, and atoms, the processes of excitation and depopulation of excited electronic states can sometimes have a very

long lifetime and contribute substantially to the overall relaxation time as represented by $\mathcal{L}_{11}$. $\mathcal{L}_{22}$ represents a reaction rate, an approximate expression for which will be derived from chemical kinetics in a later section. $\mathcal{L}_{12}$ or $\mathcal{L}_{21}$ is a coupling coefficient about which little is known.

The second group of relations are vector quantities and comprise the first and third terms of the right-hand side of Eq. (II-5). These are the well-known relations that couple diffusion phenomena and energy flux. The flux quantities are the mass flux rate of each species per unit area J_i, and the energy flux rate per unit area W. The corresponding forces are the gradients of chemical and electric potentials and the gradient of the logarithm of the temperature. The phenomenological relations can now be written using a set of forces X_i and coefficients L_{ij}, L_{iT}, which can be tensors, and subsequently will be defined in detail.

$$\begin{aligned} J_1 &= L_{11} X_1 + L_{12} X_2 + L_{13} X_3 + L_{1T} X_T \\ J_2 &= L_{21} X_1 + L_{22} X_2 + L_{23} X_3 + L_{2T} X_T \\ J_3 &= L_{31} X_1 + L_{32} X_2 + L_{33} X_3 + L_{3T} X_T \\ W &= L_{T1} X_1 + L_{T2} X_2 + L_{T3} X_3 + L_{TT} X_T \end{aligned} \qquad \text{(II-7)}$$

Since the J_i are diffusion mass flux vectors, by definition $\sum_i J_i = 0$. It then follows that the relations shown below are valid:

$$\sum_i L_{ij} = 0 \quad ; \quad \sum_i L_{iT} = 0 \quad .$$

Before the symmetry relations among the coefficients can be written out, it is now necessary to discuss the manner in which magnetic field

effects are to be treated. The electric and magnetic fields enter explicitly into the force system through the term F_i/m_i of Eq. (II-5). One consistent definition of F_i/m_i is $(e_i/m_i)\{E + (u \times B)\}$, where E is an applied electric field and u is the mass velocity vector. This is the definition that is generally adopted in most discussions of the irreversible thermodynamics of electrically conducting systems. Consistent with this definition the coefficient L_{ij} of the force term are, in general, tensors due to the magnetic field. Symmetry relations between the various coefficients can still be postulated from general considerations of microscopic reversibility. These arguments do not indicate, however, which of the coefficients do depend upon the magnetic field not do they give any hint as to the nature of the dependence. This information has been obtained in the past through an appeal to some approximate treatment of the relevant Boltzmann equation, usually employing mean free path considerations.

In studying the effects of a magnetic field upon the transport properties of a plasma, a slightly different point of view will be adopted in this report. A set of phenomenological equations will be written for the fluxes in terms of a set of forces that need not be independent of the fluxes. The coefficients in these equations are then assumed to be scalars that can be computed by the Chapman-Enskog method as applied to a gas mixture. The "force" associated with the electric and magnetic fields is now defined as $(e_i/m_i)\left\{E + [(u + u_i) \times B]\right\}$, where u is the mass velocity of the gas mixture and u_i is the diffusion velocity of the i^{th} species. In the nature of a postulate, we shall assume that the entire influence of the magnetic field upon the transport properties of a plasma can be

introduced into the equations through the "force" terms shown above. Without any further attempt at a more precise definition, the magnetic field effects introduced by the above postulate will be called first order magnetic interaction terms. A number of arguments can be developed in favor of adopting this procedure.

(1) The terms involving the "force" components $L_{ij}\ (e_i/m_i)(u_i \times B)$ can all be moved to the left-hand side of the phenomenological equations. A set of linear equations can now be written for the flux components of the various species that are parallel and perpendicular to the magnetic field. By solving for the individual flux components, a set of equations are obtained between the fluxes and the forces. Each coefficient of the force terms now depends upon the magnetic field and has the proper symmetry relations to the other coefficients required by microscopic reversibility considerations.

(2) The expressions for the ion and electron diffusion velocities in the presence of a magnetic field derived by the above procedure can be reduced, under some conditions, to the expressions derived by Chapman and Cowling (Reference 11, page 328), who used mean free path considerations to compute this effect. It will be shown later that the magnetic field influence on the heat transfer rate that is indicated from the present analysis is fundamentally different from that computed by Chapman and Cowling and others. This fact could be used as an argument to show that the hypothesis set forth above is completely untenable. However, in order to obtain their solutions, the above-mentioned authors have had to simplify the problem to such an extent that the answers which they obtain do not necessarily reflect the true

state of the physical situations. In particular, when Chapman and Cowling compute the influence of the magnetic field upon the heat transfer rate (Reference 11, pp. 336, 329, and 342) they find it necessary to assume that the charged particle diffusion rates, the electric field and the gradients in all properties except temperature are zero in the direction of the heat flow. Because of the Thompson thermo-electric effect, these assumptions are incompatible, since either an electric current will flow or an electric field must develop along the temperature gradient. When they discuss the heat transfer rate in a one-particle fluid that is electrically charged (Reference 11, p. 336) these assumptions then are compatible. However, large electric fields must be present, as can be seen from the induction equations $\nabla \cdot D = en$; hence the successive approximation scheme which they use to obtain the zeroth approximation to the velocity distribution (Reference 11, pp. 329-330) is suspect. Since the point of view adopted in this report introduces significant simplifications into the treatment of problems dealing with the influence of magnetic fields upon the transport properties of plasmas and since it does not appear easy to prove a priori that it is fallacious there is some merit in investigating the implications that result from the postulate. Whenever the results differ from those obtained from another approach, as in the influence of a magnetic field upon the heat transfer rate, then precise experimental measurements should be able to establish which procedure leads to the more accurate results over the range of magnetic fields that can be produced in the laboratory.

In general, it is possible to define the "forces" involved in a number of different ways, depending upon what use is to be made of

the equations. As discussed above, the "force" due to the electromagnetic field will be defined as follows:

$$\text{electric force} = (F_i/m_i) = (e_i/m_i)\left[E + \{(u + u_i) \times B\}\right] = X_{E_i} \quad \text{(II-8a)}$$

The definition of the thermal force follows directly from Eq. (II-5).

$$\text{thermal force} = -\nabla T/T = X_T \quad \text{(II-8b)}$$

The remaining force terms, which are the gradients of the chemical potentials, implicitly include the gradients of the partial pressures and hence represent a generalization of Fick's law for diffusion caused by species density gradients. The use of chemical potentials is particularly useful when particle or energy flow occurs across interfaces (e.g., solid to gas) as the potential energy jumps that can occur across the boundary are described by using the continuity of chemical potential across the interface, as in the Peltier effect. However, in treating a gaseous mixture only, it is sometimes more convenient to use the gradient of the logarithm of the partial pressures of the various components as the driving forces, as follows:

$$\text{diffusion force} = -(kT/m_i)\nabla \ln p_i = X_{F_i} \quad . \quad \text{(II-9a)}$$

Since both representations will be used in later sections, a general relation between the gradient of the chemical potential and the gradient of the logarithm of the partial pressure for a perfect gas will be derived now. The chemical potential for a component of a gas mixture is given by Summerfeld[17] on page 90:

$$\mu_i = h_i - T s_i - kT \ln(p/p_i).$$

The expressions for the enthalpy and entropy of a perfect gas are

$$h_i = (c_p)_i T + (h_o)_i$$

$$s_i = (c_p)_i \ln T - k \ln p + (s_o)_i$$

Substituting these relations into the expression for the chemical potential and dividing by the factor kT the following equation is obtained:

$$\frac{\mu_i}{kT} = \frac{(c_p)_i}{k} + \frac{(h_o)_i}{kT} - \frac{(c_p)_i}{k} \ln T - \frac{(s_o)_i}{k} + \ln p_i .$$

When the gradient of this expression is taken the required relation is obtained:

$$\nabla \frac{\mu_i}{kT} = \nabla \ln p_i - \frac{h_i}{kT} \nabla \ln T \quad . \quad \text{(II-9b)}$$

This expression can be written in terms of the "force" of diffusion and the thermal "force" as follows:

$$\frac{kT}{m_i} \nabla \frac{\mu_i}{kT} = \frac{kT}{m_i} \nabla \ln p_i + \frac{h_i}{m_i} X_T \quad . \quad \text{(II-9c)}$$

When the gradient of the partial pressure is used rather than the gradient of the chemical potential in the phenomenological equations it is necessary to redefine the coefficients of the thermal "force" terms. Let the coefficients of the thermal "force" terms be defined as L_{iT} when the gradient of the logarithm of the partial pressure is used, and let them be called α_{iT} when the gradient of the chemical potential is used. The following expression relates these two coefficients

$$\alpha_{iT} = L_{iT} + \sum_j L_{ij} \frac{h_j}{m_j} \quad . \quad \text{(II-9d)}$$

For the 3 particle system under consideration this relation can be simplified by using the condition that $\sum_j L_{ij} = 0$. Equation (II-9d) can now be written as follows:

$$a_{iT} = L_{iT} + \frac{5}{2}\frac{kT}{m_e} L_{i1} + \frac{|e| V_I}{m_a} L_{i2} \quad . \qquad \text{(II-9e)}$$

This coefficient is to be used when the diffusion "force" is given by the following expression:

$$\text{diffusion force} = -(kT/m_i)\nabla(\mu_i/kT) = X_{F_i}' \quad . \qquad \text{(II-9f)}$$

Chapman and Cowling[11] and Hirschfelder, Curtiss, and Bird[15] (page 713) show that the coefficients L_{iT} can be identified with the thermal diffusion coefficients.

For convenience, the definitions for the forces will now be all grouped together and the vector phenomenological equations restated with the Onsager symmetry relations applied to the coefficients. The force system is defined as follows:

$$X_i = (X_E)_i + (X_F)_i = (e_i/m_i)\left\{ E + \left[(u + u_i) \times B\right] - (kT/e_i)\ell n\, p_i \right\} \qquad \text{(II-10)}$$

$$X_T = -\nabla T/T \quad .$$

Using these forces, all the coefficients L_{ij} and L_{iT}, relating the fluxes and forces, are postulated to be scalars. The vector phenomenological relations remain formally identical to Eqs. (II-7):

$$\begin{aligned} J_1 &= L_{11} X_1 + L_{12} X_2 + L_{13} X_3 + L_{1T} X_T \\ J_2 &= L_{21} X_1 + L_{22} X_2 + L_{23} X_3 + L_{2T} X_T \end{aligned} \qquad \text{(II-11)}$$

$$\begin{aligned} J_3 &= L_{31} X_1 + L_{32} X_3 + L_{33} X_3 + L_{3T} X_T \\ W &= L_{T1} X_1 + L_{T2} X_2 + L_{T3} X_3 + L_{TT} X_T \end{aligned} \qquad \text{(II-12)}$$

The Onsager reciprocity relations state that the matrix of the coefficients should be symmetric. In addition, since $\Sigma_i J_i = 0$,

$$\sum_i L_{ij} = 0 \quad ; \quad \sum_i L_{iT} = 0 \quad . \tag{II-13}$$

The coefficients L_{ij} are essentially multiple diffusion coefficients and have been written out by Hirschfelder, Curtiss and Bird[15] for a general three component system. They are evaluated for an electron, ion, atom mixture in our Appendix 1. The thermal diffusion coefficients L_{iT} are also discussed in Appendix 1. The quantity L_{TT} is a heat transfer coefficient. It will be shown later that it is more convenient to work with a heat transfer coefficient that involves L_{iT} as well as L_{TT} and does not include the energy transported by the diffusion of the various species. This heat transfer coefficient, called $\lambda_{J=o}$ is evaluated in Appendix 1.

The third group of forces and fluxes involves the relations between the stress tensor P and the rate of strain tensor $(\partial u/\partial r)$. Consistent with our previous assumptions, the postulate is made that these tensors and the coefficients relating their various terms are independent of the magnetic field. The phenomenological equations for these forces and fluxes are then given by the hydrodynamic viscous stress-strain relations, a convenient form of which is

$$P - p\,U = -\eta\left\{(\partial u/\partial r) + (\partial u/\partial r)^{+}\right\} + \left(\tfrac{2}{3}\eta - \eta'\right) \nabla \cdot u\,U \quad . \tag{II-14}$$

The term $(\partial u/\partial r)^{+}$ represents the transpose of the tensor $(\partial u/\partial r)$.

The three groups of relations (II-6), (II-10), and (II-14) are in general coupled together. The manner in which the Eqs. (II-6) interact with the vector Eqs. (II-11) is discussed in detail in the following sections. It will be immediately recognized that the coefficient L_{11} in the Eqs. (II-6) is effectively the same as the quantity $\left(\tfrac{2}{3}\eta - \eta'\right)$,

defined in Eqs. (II-14) from a purely hydrodynamic viewpoint. Coupling between the vector Eqs. (II-11) and the tensor relations (II-14) takes place through the occurrence of u x B in the vector force terms X_i. It remains to be shown whether, as a result of this coupling, stress-strain relations involving magnetic field interaction terms can be derived which have any relation to the equations presented on page 338 of Chapman and Cowling[11]. Since the problems considered later in this report deal with configurations where $\nabla \cdot u = 0$, the viscous stress terms will not be discussed further.

III. REDUCTION OF THE DIFFUSION EQUATIONS

The three diffusion equations, Eqs. (II-11), represent very general statements of ohm's law and the law of ambipolar diffusion. Before these equations can be of much use, however, they must be simplified and the coefficients L_{ij} and L_{iT} replaced by expressions derived from kinetic theory. For convenience, the equations will be presented in a number of different forms so that they can be readily adopted to a variety of uses and also that they may be compared with expressions derived by other authors. The Eqs. (II-11) can be written out in detail as follows:

$$\begin{aligned} J_i = {} & L_{i1} \frac{e_1}{m_1} \left\{ E + u \times B + \frac{J_1 \times B}{m_1 n_1} - \frac{kT}{e_1} \nabla \ln p_1 \right\} \\ & + L_{i2} \frac{e_2}{m_2} \left\{ E + u \times B + \frac{J_2 \times B}{m_2 n_2} - \frac{kT}{e_2} \nabla \ln p_2 \right\} \\ & + L_{i3} \left\{ - \frac{kT}{m_3} \nabla \ln p_3 \right\} + L_{iT} X_T \end{aligned} \qquad \text{(III-1)}$$

In these equations particle 1 has been identified with the electrons, particle 2 with the ions, and particle 3 with the atoms. These equations can be simplified considerably in a number of ways. It is possible to drop all terms that are of the order of the ratio of the electron to atom mass compared to one. Also, the force terms involving the partial pressures of the three types of particles can be grouped together in some manner to further simplify the force system. One possible way is suggested by the grouping of the chemical potentials in Eq. (II-6). In practice the grouping $\ell n\ p_1 p_2 / p_3$ does aid in simplifying the equations and is, as well, a useful form for studying the interactions of Eqs. (II-6) and (II-11). Since $J_1 + J_2 + J_3 = 0$, it is necessary to

solve only for J_1 and J_2. Putting $e_1 = -|e|$, $e_2 = |e|$, $m_1 = m_e$, $m_2 = m_3 = m_a$ and using relations (II-12), the Eqs. (II-13) can be simplified to the following set of equations.

$$J_i + L_{i1}\frac{|e|}{m_e}\frac{J_1 \times B}{m_e \nu_e} - L_{i2}\frac{|e|}{m_a}\frac{J_2 \times B}{m_a \nu_2}$$

$$= \left(L_{i1}\frac{|e|}{m_e} - L_{i2}\frac{|e|}{m_a}\right)\left\{E + u \times B + \frac{kT}{|e|}\nabla \ln p_e\right\} \qquad \text{(III-2)}$$

$$- L_{i2}\frac{kT}{m_a}\nabla \ln \frac{p_1 p_2}{p_3} + L_{i1}\frac{kT}{m_a}\nabla \ln p_3 + L_{iT} X_T$$

For many applications the diffusion velocity, rather than the mass flux rate of the various particles is more useful, hence the particle velocities will be used in the further reduction of Eqs. (III-1). In order to reduce the number of independent driving forces to a minimum in Eq. (III-1), the following definitions are made:

$$L_{i1}\frac{kT}{m_a}\nabla \ln p_3 = \left(L_{i1}\frac{|e|}{m_e} - L_{i2}\frac{|e|}{m_a}\right) m \frac{kT}{|e|}\nabla \ln p_3 \qquad \text{(III-3)}$$

$$+ L_{i2}\frac{kT}{m_a}\nabla \ln p_3^{\,m}$$

$$L_{iT} X_T = -\frac{kT}{|e|}\left(L_{i1}\frac{|e|}{m_e} - L_{i2}\frac{|e|}{m_a}\right) K_e \nabla \ln T \qquad \text{(III-4)}$$

$$- L_{i2}(K_e - K_I)\frac{kT}{m_a}\nabla \ln T$$

Equation (III-4) is an identity. The quantities K_e and K_I defined in Eq. (III-4) are very closely related to the thermal diffusion ratios as defined by Chapman and Cowling[11]. When these expressions are introduced into Eqs. (III-1), a somewhat simplified expression is obtained:

$$J_i + L_{i1}\frac{|e|}{m_e}\frac{J_1 \times B}{m_e n_e} - L_{i2}\frac{|e|}{m_a}\frac{J_2 \times B}{m_a n_I}$$

$$= -\left(L_{i1}\frac{|e|}{m_e} - L_{i2}\frac{|e|}{m_a}\right)\left\{E + u \times B + \frac{kT}{|e|}\left(\nabla \ln \frac{p_e}{p_a^m} + K_e \nabla \ln T\right)\right\} \quad \text{(III-5)}$$

$$- L_{i2}\frac{kT}{m_a}\left\{\nabla \ln \frac{p_e p_I}{p_a} + (K_e - K_I)\nabla \ln T\right\}$$

Two generalized forces are now defined as follows:

$$F_1' = E + u \times B + \frac{kT}{|e|}\left(\nabla \ln \frac{p_e}{p_a^m} + K_e \nabla \ln T\right) \quad \text{(III-6)}$$

$$F_2 = \frac{kT}{|e|}\left\{\nabla \ln \frac{p_e p_I}{p_a} + (K_e - K_I)\nabla \ln T\right\} \quad \text{(III-7)}$$

When these expressions are used, and the values of the coefficients L_{ij} introduced, the equations for the electron and ion velocities are found to reduce to the following expressions:

$$u_e + \gamma(\beta + \epsilon) u_e \times B - \gamma\phi(1-\delta) u_I \times B$$

$$= -\gamma\{\beta + \epsilon - \phi(1-\delta)\} F_1' - \gamma\phi(1-\delta) F_2 \quad \text{(III-8)}$$

$$u_I + \gamma\epsilon\phi(1-\delta) u_e \times B - \gamma\eta\phi(1+\delta\epsilon m) u_I \times B$$

$$= \gamma\phi\{\beta_1 + 1 - \epsilon(1-\delta)\} F_1' - \gamma\phi(1+\delta\epsilon m)\eta F_2$$

Equations (III-8) are correct to the order of the electron to ion mass ratio compared to one in describing the electron and ion diffusion velocities in a three component gas mixture. They cover the complete range of ion density from zero to complete ionization. When the gas is almost completely ionized ($10^{-4} < (n_a/n_I) < 10^{-2}$) these complete equations must be used to describe the transition from the partially ionized

gas to the completely ionized gas. When $(n_a/n_I) < 10^{-4}$, the gas can be considered completely ionized and great simplifications to Eqs. (III-8) result. When $(n_a/n_I) > 10^{-2}$ important simplifications to Eqs. (III-8) can still be made. Since the expressions (III-8) are still too cumbersome to be of much use, they will not be discussed in detail.

First, we will show how they can be reduced to the ion-electron system by using the values of the coefficients as evaluated in Appendix 1. The group of coefficients $\gamma(\beta + \epsilon) \rightarrow (\sigma_{sp})/(|e| n_I)$ as the atom density approaches zero, and the group $\gamma \phi(1 - \delta) \rightarrow m(\sigma_{sp})/(|e| n_I)$. When these expressions are introduced into the Eqs. (III-8), the terms in the force functions F_1 and F_2 that contain the gradient of the atom partial pressure cancel each other and the simplified equations become:

$$\frac{|e| n_I u_e}{\sigma_{sp}} + u_e \times B - m u_I \times B$$

$$= E + u \times B + \frac{kT}{|e|}\{\nabla \ln p_e + K_e \nabla \ln T\} - m \frac{kT}{|e|}\{\nabla \ln p_e p_I + (K_e - K_I)\nabla \ln T\} \quad \text{(III-9)}$$

$$\frac{|e| n_I u_I}{\sigma_{sp}} + m u_e \times B - \epsilon m^2 u_I \times B$$

$$= \epsilon m\left[E + u \times B + \frac{kT}{|e|}\{\nabla \ln p_e + K_e \nabla \ln T\}\right] - \epsilon m^2 \frac{kT}{|e|}\{\nabla \ln p_e p_I + (K_e - K_I)\nabla \ln T\}$$

As long as the ratio of the electron to ion density ϵ is approximately one, the ion diffusion velocity is smaller than the electron diffusion velocity by the mass ratio (m_e/m_a) and can in general be neglected when computing the current density, which becomes

$$j + \frac{\sigma_{sp}}{|e| n_I} j \times B = \sigma_{sp}\left[E + u \times B + \frac{kT}{|e|}\{\nabla \ln p_e + K_e \nabla \ln T\}\right] \quad \text{(III-10)}$$

This equation is quite similar to the expression derived by Spitzer[12] on page 21. However, Green[21] has pointed out that the manner by which Spitzer derives his equations cannot adequately account for the thermal

diffusion terms and that the expression shown above is probably a more accurate expression for a generalized ohm's law in a fully ionized plasma.

We can next derive a set of equations that will be valid for partial ionization over the range $\infty > (n_a/n_I) > 10^{-2}$. This leaves only the transition region where $10^{-2} > (n_a/n_I) > 10^{-4}$ which requires the full Eq. (III-8) to adequately describe the ion and electron diffusion. This small region of ionization level will not be considered further. In the region of ionization, $\infty > (n_a/n_I) > 10^{-2}$, we can now put $\nabla \ln p_a^m \approx 0$ in F_1' and call the new generalized force F_1. The coefficients are also somewhat simpler when this restriction is made, since $\phi \approx 1$, $\delta \approx 0$ as shown in Appendix I. Equations (III-8) now reduce to the following set:

$$\begin{aligned} u_e + \gamma(\beta + \epsilon)\, u_e \times B - \gamma u_I \times B &= -\gamma(\beta + \epsilon - 1)\, F_1 - \gamma F_2 \\ u_I + \gamma\epsilon\, u_e \times B - \gamma\eta u_I \times B &= \gamma(\beta_1 + 1 - \epsilon)\, F_1 - \gamma\eta F_2 \,. \end{aligned} \tag{III-11}$$

where

$$F_1 = E + u \times B + (kT/|e|)\left(\nabla \ln p_e + K_e \nabla \ln T\right)$$

$$F_2 = (kT/|e|)\left\{\nabla \ln \frac{p_e p_I}{p_a} + (K_e - K_I)\nabla \ln T\right\} .$$

The product $\gamma\beta$ can be written as $(|e|/kT)\, \mathcal{D}_{ea} \dfrac{\nu c}{\nu_I + \nu_a c}$ and interpreted as a modified electron mobility. Similarily, the term $\gamma\beta_1$ is a modified ion mobility and can be written as

$$\gamma\beta_1 = \frac{|e|}{kT} \mathcal{D}_{Ia} \frac{\nu_a \nu}{(\nu_a + \nu_I)^2} \frac{\nu_a c}{\nu_I + \nu_a c} \tag{III-12}$$

The first important difference that we note between a fully ionized and

a partially ionized gas is that in the latter the ions diffuse with a velocity of approximately $(m_e/m_a)^{\frac{1}{2}}$ that of the electrons in an electric field. This entails a reasonable amount of mass flow and is balanced by a flow of atoms in the opposite direction induced by the electron-atom collisions. The parameter γ determines the degree of coupling that occurs between the ion and electron diffusion motions under the influence of magnetic fields. Strong coupling can only occur when either $\beta \lesssim 1$, $\beta_1 \lesssim 1$, or when both occur simultaneously. In terms of the non-dimensional quantities introduced in the appendix

$$\beta = \frac{(1+a)^2}{a+c}\, b(2/m)^{\frac{1}{2}} \text{ and } \beta_1 = ac \quad .$$

Approximately, $\beta \lesssim 1$ when $10 > a > .1$ and $\beta_1 \lesssim 1$ when $a < 10^{-3}$. Since $a = (n_a/n_I)$, this indicates that the electron diffusion is not strongly influenced by the ion diffusion when the gas is ionized either less than 10 per cent or more than 90 per cent. On the other hand, the ion motion is strongly coupled to the electron motion by a magnetic field when the gas is ionized more than 0.1 per cent. In these ranges of ionization $10^3 > (n_a/n_I) > 10$, and $(n_a/n_I) < 10^{-1}$, the electrons move freely under the action of F_1 and hence the plasma electrical conductivity is very similar to that of a fully ionized gas, except that the collision cross-section for the electrons must be modified to include the electron atom collisions.

When the magnetic field is small enough so that the terms $u_e \times B$ and $u_I \times B$ can be neglected, these equations (III-11), become particularly simple to manipulate. However, when the magnetic field is large enough so that the terms containing it cannot be ignored, the rather complicated coupling terms between the electron and ion velocities

makes this form of the equations difficult to handle or to compare with expressions derived by other authors. With a little algebra, the following symmetric and more tractable form of these equations can be derived:

$$\eta u_e - u_I = -\alpha (F_1 + u_e \times B)$$
$$(\beta+\epsilon) u_I - \epsilon u_e = \alpha (F_1 - F_2 + u_I \times B) \tag{III-13}$$

where the definition $a = \gamma\{(\beta+\epsilon)\eta - \epsilon\}$ has been made for convenience. By substituting Eqs. (III-13) into Eqs. (III-11) it is possible to obtain decoupled expressions for the electron and ion velocities. These are

$$u_e + \gamma(\beta+\epsilon-\eta) u_e \times B - \gamma\alpha (u_e \times B) \times B$$
$$= -\gamma(\beta+\epsilon-1) F_1 - \gamma F_2 + \gamma\alpha F_1 \times B \tag{III-14}$$
$$u_I + \gamma(\beta+\epsilon-\eta) u_I \times B - \gamma\alpha (u_I \times B) \times B$$
$$= \gamma(\beta_1 + 1 - \epsilon) F_1 - \gamma\eta F_2 + \gamma\alpha (F_1 - F_2) \times B.$$

For some applications, the electric current and the mass flux rate of the charged particles are more appropriate variables than the electron and ion velocities. These quantities are defined as follows:

$$\text{electric current density } j = |e| (n_I u_I - n_e u_e)$$
$$\text{charged particle mass flux density } J = m_a n_I u_I + m_e n_e u_e . \tag{III-15}$$

These flux rates can be evaluated by using Eqs. (III-14) and are

$$j + \gamma(\beta+\epsilon-\eta) j \times B - \gamma\alpha (j \times B) \times B$$
$$= \gamma n_I |e| \left[\{\epsilon\beta + \beta_1 + (1-\epsilon)^2\} F_1 + (\epsilon-\eta) F_2\right]$$
$$+ \gamma\alpha n_I |e| \{(1-\epsilon) F_1 \times B - F_2 \times B\}. \tag{III-16}$$

$$J + \gamma(\beta+\epsilon-\eta) J \times B - \gamma\alpha (J \times B) \times B$$
$$= \gamma n_I m_a \left[\{\beta_1 - \epsilon m \beta + (1-\epsilon)\} F_1 - \eta F_2\right]$$
$$+ \gamma\alpha n_I m_a \{(F_1 - F_2) \times B\}$$

For completeness we add the equation $J_a = - J$, where J_a is the mass flux rate of the atoms.

Comparing the above results with expressions obtained by other authors[11-14], a number of comments can be made:

(1) The effects of gradients of ion and atom density as well as deviations from charge neutrality are introduced explicitly for the first time to the author's knowledge. These relations are essential for the understanding of phenomena that occur at all interfaces between plasmas and solid boundaries and in particular at the electrodes of gas discharges.

(2) The effect of magnetic fields on the flow of current and mass flux of charged particles is shown to be considerably more complicated than previously thought. In particular, there is a current in the direction of (E x B) x B in addition to the direct and Hall currents.

(3) Equations (III-13) can be directly compared with the equations derived by Chapman and Cowling[11] (page 328). For low per cent ionizations the Eqs. (III-13) become identical to those of Reference 11 except for the linear coupling terms in the velocity. These extra terms implicitly apply the constraint of zero mass motion of the gas locally to the equations describing the electron and ion motion as derived by Chapman and Cowling, and hence remove a discrepancy pointed out by them concerning their equations, which were derived from mean free path considerations.

IV. REDUCTION OF THE HEAT FLUX EQUATION

To study the heat transfer relations, an alternative form of the phenomenological relations given by Eqs. (II-10) and (II-11) will be used. The "forces" X_i will be changed to $X_i' = (X_E)_i + (X'_F)_i$, where the "force" term $(X'_F)_i$ is given by Eq. (II-9b). The coefficients of the thermal "force" terms now change to α_{iT}, as shown in Eq. (II-9e). Making these changes and using some of the identities (II-12), the following equations are obtained:

$$J_1 = L_{11}(X_i' - X_3') + L_{12}(X_2' - X_3') + \alpha_{1T} X_T$$
$$J_2 = L_{21}(X_1' - X_3') + L_{22}(X_2' - X_3') + \alpha_{2T} X_T \qquad \text{(IV-1)}$$

$$W = \alpha_{T1}(X_1' - X_3') + \alpha_{T2}(X_2' - X_3') + L_{TT} X_T \qquad \text{(IV-2)}$$

$$L_{12} = L_{21} \; ; \; \alpha_{1T} = \alpha_{T1} \; ; \; \alpha_{2T} = \alpha_{T2} \; . \qquad \text{(IV-3)}$$

Using the relations (IV-1), the forces X'_i can be eliminated from the energy flux equation, (IV-2). The resulting expression can be written as follows:

$$W = L_1' J_1 + L_2' J_2 - \mathcal{K}_{J=0} \nabla T \qquad \text{(IV-4)}$$

where the following definitions are made:

$$L_1' = \frac{\alpha_{T1} L_{22} - \alpha_{T2} L_{21}}{L_{11} L_{22} - L_{12}^2} \qquad \text{(IV-5)}$$

$$L_2' = \frac{\alpha_{T2} L_{11} - \alpha_{T1} L_{12}}{L_{11} L_{22} - L_{12}^2} \qquad \text{(IV-6)}$$

$$-T\mathcal{K}_{J=0} = \frac{L_{TT} - 2\alpha_{T1}\alpha_{T2} L_{12} - \alpha_{T1}^2 L_{22} - \alpha_{T2}^2 L_{11}}{L_{11} L_{22} - L_{12}^2} \qquad \text{(IV-7)}$$

The coefficients L_1' and L_2' can be evaluated by using the relations (II-9e), (III-4), and Appendix 1. The resulting expressions are found to be:

$$L_1' = \left(\frac{5}{2} + Ke\right)\left(kT/m_e\right) \qquad \text{(IV-8)}$$

$$L_2' = \frac{|e|V_I}{m_a} - \frac{kT}{m_a} K_I \qquad \text{(IV-9)}$$

The definition (III-5) has again proved very useful by simplifying the thermal diffusion terms.

The coefficient $\mathcal{K}_{J=0}$ is the heat transfer coefficient when all diffusion currents are zero. Chapman and Cowling[11], as well as Hirschfelder, Curtiss and Bird[15], give formulas for evaluating $\mathcal{K}_{J=0}$. This is done in Appendix 1.

The heat flux equation can now be written as follows:

$$W = \left(\frac{5}{2} + Ke\right)\frac{kT}{me} J_1 + \frac{|e|V_I - K_I kT}{m_a} J_2 + \left(-\mathcal{K}_{J=0}\right)\nabla T. \qquad \text{(IV-10)}$$

It should be emphasized that this equation is exact. The form of this expression is surprisingly simple, each term being self-explanatory.

For some applications, it is desirable to have the heat flux expressed in terms of the current density and flux rate of charged particles, rather than the electron and ion mass flux rates. The following equation indicates the required relationship in this case:

$$W = \left(\frac{5}{2} + Ke\right)\frac{kT}{|e|} j + \left\{\left(\frac{5}{2} + Ke - K_I\right)\frac{kT}{ma} + |e|V_I\right\} J - \mathcal{K}_{J=0}\nabla T. \qquad \text{(IV-11)}$$

Equations (IV-10) and (IV-11) are somewhat different in form and in the physical interpretation of the processes that are occurring than the expressions of other authors for the thermal conductivity of a partially or fully ionized gas in the presence of a magnetic field. The expressions

given by Chapman and Cowling[11] (pp. 329, 337, 342), Spitzer[12] (p. 88), and Covert[4] (p. 76) all indicate that the magnetic field influences the thermal conductivity in a manner similar to its influence on the charged particle diffusion, namely, that the total thermal conductivity in the direction perpendicular to the magnetic field B, but parallel to the temperature gradient ∇T is reduced by the factor $\frac{1}{1+\omega_e^2 \tau_e^2}$ to $\frac{\mathcal{K}}{1+\omega_e^2 \tau_e^2}$ and that a thermal flow of magnitude $\frac{\omega_e \tau_e \mathcal{K}}{1+\omega_e^2 \tau_e^2} \nabla T$ is induced in a direction perpendicular to both the magnetic field and the temperature gradient ∇T. In direct contradiction to this, Eq. (IV-10) indicates that the magnetic field has no influence on the thermal conductivity due to collisional energy transfer ($\mathcal{K}_{J=0} \nabla T$) and affects the energy transfer rate only through its influence on the diffusion rates of the charged particles and consequently controls the energy carried by these diffusing particles. In a fully ionized gas $J \approx 0$, hence an applied magnetic field will have a direct influence only upon that part of the heat transfer rate that is due to thermal diffusion. In a partially ionized gas, when the reaction rate is fast enough to maintain the gas at near equilibrium electron and ion density even where temperature gradients are present, then, as will be shown later, the dominant part of the heat transfer rate is due to the recombination energy released by the electrons and ions as they diffuse ambipolarily from the hot to the cooler gas. Under these conditions, a magnetic field can have a very pronounced influence on the energy transfer rate in the plasma.

Before any further progress can be made with the diffusion and heat flux equations it is necessary to study the other set of Eqs. (II-6), which describe the reaction rates in the gas mixture. This is done in the next section.

V. REACTION RATE EQUATIONS

The Eqs. (II-6) indicate that there is a coupling between the energy relaxation processes and the species production rate in the gas mixture. In this report the only phenomenon that will be treated is the species production rate, since most of the problems under study occur in regions of the gas where $\nabla \cdot \mu = 0$. The relation that requires investigation is now reduced to the expression shown below:

$$\Gamma_e = n_e \mathcal{L}_{22} \frac{\mu_e + \mu_i - \mu_a}{kT} \qquad \text{(V-1)}$$

In order to compute $\mathcal{L}_{22}$ and to obtain some indication of the range of validity of Eq. (III-1), the kinetics of the reaction will be studied in some detail. In the following discussion a distinction will be made between the electron temperature and that of the heavier particles.

Once a few electrons are present in the gas, the production rate of electrons depends mainly upon the collision rate of atoms with electrons whose energy exceeds the ionization potential, or some excitation potential of the gas. Kinetic theory can be used to obtain an expression for the number density of electron-atom collisions per second that could lead to either ionization or excitation of the atom, (See Reference 18, pp. 685-691.).

$$[\Gamma_e]_+ = n_e n_a \int_{V_{ex}}^{\infty} \left[\frac{2\pi}{(\pi k T_e)^{3/2}} e^{-\frac{\eta}{kT_e}} \left(\frac{2}{m_e}\right)^{1/2} \eta \int_0^{\eta - V_{ex}} \xi^2 S_1(\xi, \eta)\, d\xi \right] d\eta \qquad \text{(V-2)}$$

In this expression η is the electron energy and the integral $\int_0^{\eta - V_{ex}} \xi^2 S_1(\xi, \eta)\, d\xi$ is the cross-section for ionization by electrons of energy η. At pressures of over a few millimeters of mercury, the recombination

mechanism that predominates is that involving the collision of two electrons and an ion. The recombination rate can be expressed by an equation similar to Eq. (V-2) above: (See Reference 18, page 691.).

$$[\Gamma_e]_- = n_e^2 n_I \frac{8}{\pi m_e (kT)^3} \int_0^\infty \left[e^{-\xi/kT_e} \xi \int_0^\infty e^{-\xi/kT_e} \xi\, {}^1S_2(\xi, \xi) d\xi \right] d\xi \quad \text{(V-3)}$$

When V_{ex} is put equal to the ionization energy $|e| V_I$ in Eq. (V-2), a relation exists between ${}^1S_2$ and ${}^2S_1$ due to the assumption of microscopic reversibility incorporated in the equation for the equilibrium concentration of electrons, ions, and atoms which is given below:

$$\frac{n_e n_I}{n_a} = 2 \frac{\varpi_I}{\varpi_a} \left(\frac{2\pi m_e kT_e}{h^2} \right)^{3/2} e^{-\frac{|e| V_I}{kT_e}} \quad \text{(V-4)}$$

Using Eqs. (V-2, 3, and 4), the following relation is obtained:

$$(|e|V_I + \xi + \alpha)^2 {}^2S_1(\xi, |e|V_I + \xi + \alpha) = \frac{16\pi m_e \varpi_I}{\varpi_a h^3} \alpha\, \xi\, {}^1S_2(\xi, \alpha) \quad \text{(V-5)}$$

This equation can be interpreted as follows: ${}^2S_1$ is the cross-section for ionization of an atom by an electron of energy $|e| V_I + \xi + a$, resulting in an ion and electrons of energy ξ and a. ${}^1S_2$ is the cross-section for recombination of an electron and ion under simultaneous bombardment by electrons of energy ξ and a. Approximate expressions for ${}^1S_2$ and ${}^2S_1$ have been obtained by Thomson and Bohr (Reference 18, page 691),

$$\begin{aligned} {}^2S_1(\xi, \eta) &= \frac{\pi}{\eta} \left\{ \frac{|e|^2}{4\pi \varepsilon_0 (\xi + |e| V_I)} \right\}^2 \\ {}^1S_2(\xi, \alpha) &= \frac{\varpi_a h^3}{16\pi m_e \varpi_I} \frac{\pi}{\alpha \xi} \left\{ \frac{|e|^2}{4\pi \varepsilon_0 (\xi + |e| V_I)} \right\}^2 \end{aligned} \quad \text{(V-6)}$$

These expressions can be substituted into Eqs. (V-2, and 3) which can then be integrated to obtain the ionization and recombination rates. In

carrying out the integrals it is necessary to assume that the major contribution to the integral occurs when the electron energy is just a little greater than the ionization energy. The mathematical assumption is as follows:

$$q \int_{q}^{\infty} e^{-p} \frac{dp}{p^2} = \frac{e^{-q}}{q} \qquad \text{when } q >> 1 \qquad \text{(V-7)}$$

The equations that are obtained from these integrations are shown below:

$$[\Gamma_e]_+ = n_e n_a \left(\frac{8kT_e}{\pi m_e}\right)^{1/2} \pi \left(\frac{|e|}{4\pi\varepsilon_0 V_I}\right)^2 e^{-\frac{|e|V_I}{kT_e}} \qquad \text{(V-8)}$$

$$[\Gamma_e]_- = n_e^2 n_I \frac{\omega_a h^3}{2\omega_I \pi^2 m_e^2 kT_e} \pi \left(\frac{|e|}{4\pi\varepsilon_0 V_I}\right)^2 \qquad \text{(V-9)}$$

In these equations it is necessary to modify the production and recombination rates by a term that indicates the probability of an inelastic collision occurring rather than an elastic collision. This factor is given by the following expression:

$$P_{ea}^{I} = \frac{1}{1 + q_{ea}/q_{ea}^{I}}$$

$$q_{ea}^{I} = \pi \left(\frac{|e|}{4\pi\varepsilon_0 V_I}\right)^2 \qquad \text{(V-9a)}$$

The net electron production rate can now be written as follows:

$$\Gamma_e = \left(\frac{8kT_e}{\pi m_e}\right)^{1/2} P_{ea}^{I} \pi \left(\frac{|e|}{4\pi\varepsilon_0 V_I}\right)^2 n_e n_a e^{-\frac{|e|V_I}{kT_e}} \left(1 - \frac{n_e n_I \bar{n}_a}{\bar{n}_e \bar{n}_I n_a}\right) \qquad \text{(V-10)}$$

The barred values of $\bar{n}_e$, $\bar{n}_a$, and $\bar{n}_I$ are the equilibrium values. This may be used to define a characteristic time t_1 for ionization as follows:

$$t_1 = \left(\frac{\pi m_e}{8kT_e}\right)^{1/2} \left(\frac{4\pi\varepsilon_0 V_I}{|e|}\right)^2 \frac{e^{\frac{|e|V_I}{kT_e}}}{\pi n_a P_{ea}^I} \qquad \text{(V-11)}$$

Similarly, a characteristic time for recombinations t_2 is given by the expression:

$$t_2 = \frac{2\varpi_I \pi m_e^2 k T_e}{P_{ea}^I \varpi_a h^3 n_e n_I} \left(\frac{4\pi\varepsilon_0 V_I}{|e|}\right)^2 \qquad \text{(V-12)}$$

Substituting Eq. (V-11) into Eq. (V-10) and taking the natural logarithm of both sides the following relation is obtained:

$$-\ln\left(1 - \frac{t_1}{n_e}\Gamma_e\right) = \frac{\mu_e + \mu_I - \mu_a}{kT} \qquad \text{(V-13)}$$

Comparing this equation with Eqs. (V-1), a criterion can now be given for the range of validity of the relation derived from irreversible thermodynamics and shown in Eqs. (II-6). The condition that the system be close to equilibrium can be written as follows:

$$\left|\frac{t_1}{n_e}\Gamma_e\right| < 1 \qquad \text{so that} \quad \ln\left(1 - \frac{t_1}{n_e}\Gamma_e\right) \approx + \frac{t_1}{n_e}\Gamma_e \qquad \text{(V-14)}$$

When this is the case the coefficient $\mathcal{L}_{22}$ can be determined:

$$\mathcal{L}_{22} = + (1/t_1) \ .$$

The reaction rate equation is then given by the following equation:

$$\Gamma_e = + \frac{n_e}{t_1} \frac{\mu_e + \mu_I - \mu_a}{kT} \qquad \text{(V-15)}$$

In a later section criteria will be worked out to indicate when diffusion

is a more important phenomenon for charged particle removal from a discharge or plasma than is recombination. When this occurs, the system can operate far from equilibrium and in many cases the recombination term can be omitted.

V. 1. Comparison of Electron Production Rate Equation with Experiment

The experimental results for electron production rate are usually expressed in terms of a coefficient between the ionizing efficiency S_e and the electron energy excess over the ionization potential as follows:

$$S_e' = a' p (V - V_I) \quad . \tag{V-16}$$

Using this relation, von Engel[19] has derived an expression for the electron production rate which is shown below:

$$[\Gamma_e]_+ = n_c n_a \frac{kT}{|e|} a' \left(\frac{8kT_e}{\pi m_e}\right)^{1/2} |e| V_I \; e^{-\frac{|e| V_I}{kT}} \tag{V-17}$$

Comparing this equation with Eq. (V-8) corrected for the elastic collisions, a relation between P_{ea}^{I} and a' is obtained.

$$P_{ea}^{I} = \frac{kT \; V_I}{\pi \left(\frac{|e|}{4\pi \varepsilon_0 V_I}\right)^2} \; a' \tag{V-18}$$

If Eqs. (V-8) and (V-9a) are assumed to be reasonably correct, Eq. (V-18) can be used to compute the elastic collision cross-section for the electrons and atoms and this value can be compared with experimentally determined electron-atom cross sections.

Experimental data for electron-atom elastic collisions is available only for mono-energetic electrons, hence direct comparison

of the cross-section as measured directly and as measured by the electron production rate and then computed from Eq. (V-18) cannot readily be made. Rough estimates indicate that they agree to within a factor of 5 or better. Due to the relatively reasonable agreement as indicated above between Eq. (V-8) and experiments, it is felt that for the present Eq. (V-8) adequately represents the ionization rate in high pressure gases.

V. 2. Comparison of Eq. (V-9) and Experimentally Determined Recombination Rates

The recombination coefficient a'' is defined by $\left[\Gamma_e\right]_- = a'' n_e n_I$. Eq. (V-9) can be evaluated and expressed as follows:

$$a'' = \text{recombination coefficient} = 4.25 \times 10^{-18} \frac{\alpha}{1+\alpha} \frac{\omega_a}{\omega_i} \frac{p}{p_{at}} \left(\frac{10}{T}^4\right)^2 \left(\frac{10}{V_i}\right)^2 \frac{m^3}{\text{ion-sec.}}$$

Little experimental information is available for electron-ion recombination rates. Comparing the few measured recombination coefficients with those computed from the above equation, the values agree to within a factor of 5 or less, which is considered adequate.

VI. RELATION BETWEEN REACTION RATE EQUATIONS AND THE DIFFUSION EQUATIONS

Since the rate of reaction in the gas has an important bearing on determining the species density at any point, any of the coefficients or forces in the diffusion equations that contain a particle density term will be affected by the reaction rate equation. In particular, whenever $\nabla \cdot u = 0$, the force F_2 can be replaced by other variables that are already present and hence the system of Eqs. (III-16) can be somewhat simplified. The non-linear form of the reaction rate Eq. (V-13) will be used in what follows, rather than Eq. (V-1).

$$-\ln\left(1-\frac{\alpha_i}{n_e}\Gamma_e\right) = \frac{\mu_e+\mu_I-\mu_a}{kT} \tag{VI-1}$$

From Eq. (III-11) the form of F_2 is given by the following expression:

$$F_2 = \frac{kT}{|e|}\left\{\nabla \ln \frac{p_e p_I}{p_a} + (K_e - K_I)\nabla \ln T\right\} \tag{VI-2}$$

Eq. (II-9c) permits the partial pressures to be replaced by the chemical potentials:

$$\nabla \ln \frac{p_e p_I}{p_a} = \nabla \frac{\mu_e+\mu_I-\mu_a}{kT} + \frac{h_I}{kT}\nabla \ln T \tag{VI-3}$$

The chemical potential can now be eliminated between Eqs. (VI-1) and (VI-3).

$$\nabla \ln \frac{p_e p_I}{p_a} = \frac{+1}{1-\frac{\alpha_i}{n_e}\Gamma_e}\nabla \frac{\alpha_i \Gamma_e}{n_e} + \frac{h_I}{kT}\nabla \ln T \tag{VI-4}$$

When $\nabla \cdot u = 0$, the species continuity equations can be written as follows:

$$m_i \Gamma_i = \nabla \cdot J_i \tag{VI-5}$$

Since $\Gamma_e = \Gamma_I = -\Gamma_a$ it is possible to write Eq. (VI-5) in the form shown below:

$$\Gamma_e = \nabla \cdot J/m_a \quad . \tag{VI-6}$$

This equation can be substituted into Eq. (VI-4) to obtain the final relation for F_2:

$$F_2 = \frac{kT}{|e|}\left[\left(\frac{h_I}{kT} + K_e - K_I\right)\nabla \ln T + \frac{\nabla \frac{t_1}{m_a n_e}\nabla \cdot J}{1 - \frac{t_1}{m_a n_e}\nabla \cdot J}\right] \tag{VI-7}$$

When the reaction rate is fast enough so that $\frac{t_1}{m_a n_e}\nabla \cdot J << 1$, then the non-linear term of Eq. (VI-7) can be omitted.

When the reaction-rate is extremely fast, so that the gas is at equilibrium at all points, in some cases it is possible to neglect the second term of Eqs. (VI-7) compared to the first term. Great care must be exercised, however, whenever this is done, as it involves the mathematical complication of dropping from a differential equation the highest order derivative, a process known as a singular perturbation.

The above procedure is applicable only when $\nabla \cdot \mu = 0$ in the gas, or more generally, when $\rho\,(d/dt)\left(\frac{m_I n_I + m_e n_e}{\rho}\right) = 0$, where (d/dt) is the Euler derivative. The usual method of dealing with problems involving species production is to solve for J and j in terms of F_1 and F_2. These expressions for J and j are then substituted into the species conservation equations

$$\rho\,(d/dt)\left\{\frac{|e|\,(n_I - n_e)}{\rho}\right\} = -\nabla \cdot j$$

$$\rho\,(d/dt)\left\{\frac{m_a n_I + m_e n_e}{\rho}\right\} = -\nabla \cdot J + m_a \Gamma_e$$

and these equations are then solved for the species number densities,

n_I and n_e, by applying appropriate boundary conditions.

The equations representing particle and energy diffusion have now been reduced to a point where it is possible to solve them for some simple models. The only model that will be discussed in detail is the two dimensional motion of charged particles through a gas that has zero mass motion. Gradients can exist only in one dimension. A one dimensional magnetic field can exist in the direction perpendicular to the surface in which the particles move. This model can be applied to either a cylindrically symmetric volume of plasma or to a rectangular box of conducting gas.

VII. RADIAL PARTICLE DIFFUSION

In this section the problem of the radial flow of ions and electrons from an axisymmetric volume of plasma will be discussed. The results, however, are applicable to one dimensional configurations as well. Eqs. (III-13) will be used rather than Eqs. (III-11) for the following study, and are reproduced below:

$$\eta u_e + \alpha u_e \times B = -\alpha F_1 + u_I \qquad \text{VII-1)}$$

$$(\beta+\epsilon) u_I - \alpha u_I \times B = \alpha (F_1 - F_2) + \epsilon u_e \qquad \text{(VII-2)}$$

For convenience the following definition has been made:

$$\alpha = \gamma \{ (\beta+\epsilon)\eta - \epsilon \} \qquad \text{(VII-1a)}$$

Since the general problem of charged particle diffusion is very complicated, as is indicated by Eq. (III-14), the restrictions listed below are imposed:

(1) The gas can have a uniform velocity component parallel to the magnetic field only.

(2) No radial electric current can flow.

(3) The applied magnetic field has only an axial component.

The tangential velocity components of the ions and electrons are calculated first:

$$(u_e)_\theta = \{ (\beta+\epsilon)(u_e)_r - (u_I)_r \} \gamma B_z \qquad \text{(VII-3)}$$

$$(u_I)_\theta = \{ \epsilon (u_e)_r - \eta (u_I)_r \} \gamma B_z \qquad \text{(VII-4)}$$

The conditions for zero radial current can be written as follows:

$$\epsilon(u_e)_r = (u_I)_r \tag{VII-5}$$

Substituting this relation into Eqs. (VII-3) and (VII-4) the tangential particle diffusion equations reduce to those shown below:

$$\begin{aligned}(u_e)_\theta &= \gamma\beta B_z (u_e)_r \\ (u_I)_\theta &= -\gamma\beta_1 B_z (u_I)_r\end{aligned} \tag{VII-6}$$

The radial components of the ion and electrons diffusion velocities is next computed. After some algebra and the use of Eq. (VII-5) they reduce to the following:

$$\begin{aligned}(\eta - \epsilon + \alpha\gamma\beta B_z^2)(u_e)_r - \alpha(u_e)_z B_\theta &= -\alpha(F_1)_r \\ (\beta + \epsilon - 1 + \alpha\gamma\beta_1 B_z^2)(u_I)_r + \alpha(u_I)_z B_\theta &= \alpha(F_{1r} - F_{2r})\end{aligned} \tag{VII-7}$$

This is an acceptable form of the radial flow equations for some applications. In general it is better, however, to replace the axial velocity components by the axial force system. These relations, which are obtained by calculating the axial velocity components of Eqs. (VII-1) and (VII-2), are shown below

$$\begin{aligned}(u_e)_z &= -\gamma(\beta + \epsilon - 1)(F_1)_z - \gamma(F_2)_z - \{\gamma\beta(u_e)_r B_\theta\} \\ (u_I)_z &= \gamma(\beta_1 + 1 - \epsilon)(F_1)_z - \eta\gamma(F_2)_z + \beta_1\gamma(u_I)_r B_\theta\end{aligned} \tag{VII-8}$$

Substituting these equations into the radial flow Eqs. (VII-7), the following relations are obtained:

$$\{\beta_1+1-\epsilon+\gamma\alpha\beta(B_\theta^2+B_z^2)\}(u_e)_r+\{(\beta+\epsilon-1)F_{1z}+F_{2z}\}\alpha\gamma B_\theta = -\alpha(F_1)_r \qquad \text{(VII-9)}$$

$$\{\beta+\epsilon-1+\gamma\alpha\beta_1(B_\theta^2+B_z^2)\}(u_I)_r+\{(\beta_1+1-\epsilon)F_{1z}-\eta F_{2z}\}\alpha\gamma B_\theta = \alpha\{(F_1)_r-(F_2)_r\}$$

Since $(u_I)=\epsilon(u_e)_r$ Eq. (VII-9) implies a relation between $(F_1)_r$ and $(F_2)_r$. If we eliminate $(F_1)_r$ from Eqs. (VII-9), the following expressions for the ion, atom, and electron radial velocities are obtained:

$$(u_e)_r=-\alpha\frac{(F_2)_r+\{(\beta+\beta_1)(F_1)_z-\beta_1(F_2)_z\}\gamma B_\theta}{\beta\epsilon+\beta_1+(1-\epsilon)^2+(\beta_1\epsilon+\beta)\alpha\gamma(B_\theta^2+B_z^2)} \qquad \text{(VII-10)}$$

$$(u_I)_r=\epsilon(u_e)_r$$

$$n_a(u_a)_r=-n_I(u_I)_r$$

The coefficients in the various terms of the first equation of Eq. (VII-10) can be put into a more familiar form using Eqs. (A-61, 62, 63). Omitting second order terms, Eq. (VII-10) can be written as follows:

$$-J_r=\frac{3}{16}\left(\frac{4\pi kT}{m_a}\right)^{1/2}\frac{m_a n_I n_a}{\mathcal{D}_{Ia}(n_a+n_I)^2}\times \qquad \text{(VII-11)}$$

$$\frac{\frac{d}{dr}\ln\frac{n_e n_I}{n_a}+(1+K_e-K_I)\frac{d}{dr}\ln T+\frac{\sigma_{SP}E_z B_\theta}{kT n_I(1+aC)}}{1+\frac{\mathcal{D}_{Ia}\epsilon+\mathcal{D}_{ea}}{\mathcal{D}_{ea}\epsilon+\mathcal{D}_{Ia}}\mathcal{D}_{Ia}\mathcal{D}_{ea}\left(\frac{|e|}{kT}\right)^2\frac{n^2 n_a C(B_\theta^2+B_z^2)}{(n_a+n_I)^2(n_I+n_aC)}}$$

There are a number of interesting features to the above equations that can be pointed out.

(1) The flux rate J_r is dependent upon three forces, the gradient of the product $(n_e n_I/n_a)$, the gradient of the temperature, and the pinch force.

(2) The radial electric field that is induced can affect the flux rate J_γ indirectly through its influence on the radial distribution of ions and electrons, which is determined from Eq. (VII -9).

(3) The manner in which an applied axial magnetic field affects the flux rate J_γ in Eq. (VII -11b) can be written in a more conventional form when $n_I << n_a$ as follows:

$$1 + \frac{\mathcal{D}_{Ia}\epsilon + \mathcal{D}_{ea}}{\mathcal{D}_{ea}\epsilon + \mathcal{D}_{Ia}} \mathcal{D}_{Ia}\mathcal{D}_{ea}\left(\frac{|e|}{kT}\right)^2 (B_\theta^2 + B_z^2) \qquad \text{(VII -12)}$$

The influence of charge concentration ϵ near a wall can have a very pronounced effect upon Eq. (VII -12), changing the magnitude of the coefficient of $B_\theta^2 + B^2$ by as much as the mass ratio m_e/m_a. In order to obtain the highest reduction in the radial ion and electron flux to a surface by the application of a transverse magnetic field, the ratio n_e/n_I should be made as small as possible on the surface.

Although the above equations were not intended to be applicable in cases where $T_e >> T_I$ it is found that they can be easily modified so that they are. Comparing them with equations derived by B. Lehnert[20], for the radial diffusion of charged particles across a magnetic field out of a glow discharge, it is found that with suitable approximations the equations in that report and those derived above are identical except for the term $\frac{\mathcal{D}_{Ia}\epsilon + \mathcal{D}_{ea}}{\mathcal{D}_{ea}\epsilon + \mathcal{D}_{Ia}}$ in Eq. (VII -12).

The equations derived in the above sections will now be applied to the analysis of an axially symmetric electric discharge. A suitable form of the energy equation is first derived and then a similarity solution for some types of high intensity electric discharge is obtained.

VIII. THE ENERGY EQUATION

In regions of the gas where the mass velocity is zero, the steady-state energy equation is

$$\nabla \cdot W = \sum_i \frac{J_i F_i}{m_i} \tag{VIII-1}$$

The external forces F_i are defined by Eq. (II-7) and are reproduced below:

$$F_i = e_i \{ E + (u + u_i) \times B \} \tag{VIII-2}$$

These equations can be combined as follows:

$$\nabla \cdot W = |e| E \cdot \left(\frac{J_I}{m_a} - \frac{J_e}{m_e} \right) \tag{VIII-3}$$

An alternative form of Eq. (VIII-3) is the following:

$$\begin{aligned} \nabla \cdot W &= j \cdot E \\ \nabla \cdot (W + E \times H) &= 0 \end{aligned} \tag{VIII-4}$$

When Eq. (IV-10) is introduced into this expression the final form of the energy equation is obtained:

$$\left\{ \left(\frac{5}{2} + K_e - K_I \right) \frac{k}{m_a} J - \left(\frac{5}{2} + K_e \right) \frac{k}{|e|} j \right\} \cdot \nabla T - \nabla \cdot \mathcal{K}_{J=0} \nabla T$$
$$+ \left\{ \frac{\left(\frac{5}{2} + K_e - K_I \right) k T + |e| V_I}{m_a} \right\} \nabla \cdot J = j \cdot E \tag{VIII-5}$$

One important feature of this equation is that the magnetic field does not appear explicitly in any terms, in particular the coefficient ($\mathcal{K}_{J=0}$) is independent of the magnetic field by definition. This

result leads to the following statements:

(1) When a gas is fully ionized the only influence an applied magnetic field can have on the heat transfer rate is through the changes induced in the electric current in the gas.

(2) When a gas is partially ionized, the magnetic field can influence the heat transfer rate by modifying the currents of charged particles only. If no currents of electrons or ions are present in the gas, the applied magnetic field cannot affect the energy transfer rate. When a plasma is in contact with an electrically insulated wall the energy transfer rate to the wall can be reduced by the application of a magnetic field parallel to the wall only by slowing down the ambipolar diffusion of the ions and electrons from the hot gas to the wall. Examining Eqs. (VI-5), a secondary effect is seen to exist, in that the temperature gradient can be influenced by the charged particle flow rate. In general, these two effects have a tendency to cancel each other, as a reduction of the ion and electron flow rate allows more recombination to occur in the layers adjacent to the wall and thus increases the temperature gradient. If the mean recombination time is very long compared to the transit time of the charged particles across the boundary layer at the surface, then a transverse magnetic field should significantly reduce the heat transfer rate from a partially ionized gas to a wall.

IX. EQUATIONS GOVERNING THE BEHAVIOR OF CYLINDRICAL ELECTRIC DISCHARGES WHEN NO RADIATION OCCURS

In this section the arc column will be studied in detail. Using the results of the previous sections the equations of momentum and energy conservation are set up in radial coordinates, since changes of the variables in the z and θ direction are assumed to be negligible. These equations are second order, non-linear differential equations for the temperature and pressure as functions of radius. A similarity solution is first developed for the case where the thermal and electrical conductivities can be expressed as a power function of the temperature. A generally valid solution is then constructed for cases when the thermal and electrical conductivities are arbitrary functions of the temperature.

When no mass velocity of the gas occurs and there are only radial gradients present in any of the discharge variables, the following set of four equations describes the phenomena that occur in the discharge and outside it where the electrical conductivity is negligible. The energy equation is given by Eq. (VIII-5), which is reproduced below:

$$\left\{\frac{5}{2}kT + (K_e - K_z)kT + |e|V_I\right\}\frac{J_r}{m_a} = \mathcal{K}_{J=0}\frac{dT}{dr} + \frac{B_\theta E_z}{\mu_0} \qquad \text{(IX-1)}$$

The expression for the diffusion of charged particles is obtained by combining Eqs. (VII-11a) and (VI-7).

$$\frac{1 + \dfrac{\mathcal{D}_{Ia}\epsilon + \mathcal{D}_{ea}}{\mathcal{D}_{ea}\epsilon + \mathcal{D}_{Ia}}\mathcal{D}_{Ia}\mathcal{D}_{ea}\left(\dfrac{|e|}{kT}\right)^2 \dfrac{n^2 m_a c(B_\theta^2 + B_z^2)}{(m_a + m_I)^2(m_I + m_a c)}}{\mathcal{D}_{Ia}\dfrac{n m m_a m_I}{(m_a + m_I)^2}} J_r$$

$$= -\left\{\frac{\frac{5}{2}kT + (K_e - K_I)kT + |e|V_I}{kT^2}\right\}\frac{dT}{dr} - \frac{\sigma_{sp} E_z B_\theta}{n_I kT(1+ac)}$$

$$-\frac{d}{dr}\left\{\frac{t_1}{n_e m_a r}\frac{d}{dr}(r J_r)\right\} \qquad \text{(IX-2)}$$

The induction equation shown below can be used to eliminate the magnetic field from the above equations

$$\mu_o j_z = \frac{1}{r}\frac{d}{dr}(r B_\theta) \qquad \text{(IX-3a)}$$

The relation between the axial forces and the current density can be obtained from Eqs. (VII-8). When the charge concentration is less than 1 % and the only axial gradient is that of electric potential, these equations can be written as follows:

$$j_z = \frac{\sigma_{sp}}{1+ac}\left(E_z + \mu_{Ir} B_\theta\right)$$

This equation indicates that the outward ambipolar diffusion of charged particles tends to increase the current density in the outer sections of the discharge. In general the term $u_{Ir} B_\theta << E$ at high pressure and hence it can be neglected or introduced into the equation as a modification to the electric conductivity by substituting $B_\theta = \frac{\mu_o r j}{2}$:

$$j_z = \frac{\sigma}{1 - \frac{\mu_o \mu_{Ir} r \sigma}{2}} E_z$$

In low pressure, high current electric discharges it is possible for the term $\mu_{Ir} B_\theta$ to be of the same order of magnitude as E_z , in which case some interesting non-linear effects could be expected to occur, e.g., a high percentage of the current could be concentrated in the

outer radial regions of the discharge. In the present analysis it will be assumed that $\mu_{I r} B_\theta << E_z$, so that the induction equations can be written as follows:

$$\frac{\mu_o \sigma_{sp} E_z}{1 + ac} = \frac{1}{r} \frac{d}{dr}(r B_\theta) \qquad \text{(IX-3b)}$$

The momentum equation completes the set necessary to describe the system fully.

$$\frac{dp}{dr} = - \frac{\sigma_{sp}}{1+ac} E_z B_\theta \qquad \text{(IX-4)}$$

No attempt will be made to solve these equations as they stand. There are, however, three regimes in which solutions can be obtained with ease by making simplifying assumptions.

(1) Low pressure, low current discharges. These discharges are usually termed glow discharges and are characterized by a high electron temperature relative to the gas temperature and by a low ionization level, ($ac >> 1$). The radial pressure is essentially constant and the radial electron temperature distribution is quite constant. Although the above equations were derived for a gas in which only slight differences between electron and atom temperature occurs, they can be applied to a glow discharge with only a minor modification to Eq. (IX-1).

(2) High pressure discharges where the electron density is at its equilibrium value over the temperature range considered.

When the reaction rate is fast enough so that equilibrium is established very rapidly, the last term of Eq. (IX-2) can be neglected and the flux Jr can be expressed in terms of the temperature gradient

and electromagnetic body force. This situation probably occurs in most arcs that are cold enough to have atoms present in the discharge column. However, in the outer layers of the discharge, where the electron density is low, this approximation is not likely to be valid.

(3) When the gas becomes fully ionized, the terms involving J become zero. The resulting equations are of particular interest because of the manner in which the electromagnetic pinch forces become significant.

The Eqs. (IX- 1-4) will now be applied to discharges of classes 2 and 3.

IX. 1. High Pressure Discharges

When the gas is always near equilibrium it is possible to use the Saha equation to replace $(n_e n_I)/n_a$ as follows:

$$\frac{n_e n_I}{n_a} = \frac{2\varpi_I}{\varpi_a}\left(\frac{2\pi m_e kT}{h^2}\right)^{3/2} e^{-\frac{|e|V_I}{kT}}$$

$$\nabla \ln \frac{n_e n_I}{n_a} = \left(\frac{3}{2} + \frac{|e|V_I}{kT}\right)\frac{\nabla T}{T}$$

By using this relation in Eq. (VII-11a) the mass flux of charged particles can be expressed in terms of a temperature gradient and the radial electromagnetic force

$$J_r = -D_{Ia}\frac{n\, m_a\, n_a\, n_I}{(n_a + n_I)^2} \times \qquad \text{(IX-5)}$$

$$\frac{\left\{\left(\frac{5}{2} + K_e - K_I + \frac{|e|V_I}{kT}\right)\frac{d\ln T}{dr} + \frac{\sigma_{sp} E_z B_\theta}{n_z kT(1+ac)}\right\}}{1 + \frac{D_{Ia}\epsilon + D_{ea}}{D_{ea}\epsilon + D_{Ia}} D_{ea} D_{Ia}\left(\frac{|e|}{kT}\right)^2 \frac{n^2 n_a c\,(B_\theta^2 + B_z^2)}{(n_I + n_a c)(n_a + n_I)^2}}$$

For convenience the following definition will be made:

$$1+\frac{\mathcal{D}_{Ia}\epsilon+\mathcal{D}_{ea}}{\mathcal{D}_{ea}\epsilon+\mathcal{D}_{Ia}}\mathcal{D}_{Ia}\mathcal{D}_{ea}\left(\frac{|e|}{kT}\right)^2\frac{n^2 n_a c(B_\theta^2+B_z^2)}{(n_I+n_a c)(n_a+n_I)^2}=1+\omega_e\tau_e\omega_I\tau_I$$

The three equations that determine the radial temperature distribution can now be written as follows:

$$-\frac{(1+\omega_e\tau_e\omega_I\tau_I)}{\mathcal{D}_{Ia}n n_a\frac{n_a n_I}{(n_a+n_I)^2}}J_r=\left(\frac{5}{2}+K_e-K_I+\frac{|e|V_I}{kT}\right)\frac{1}{T}\frac{dT}{dr}+\frac{\sigma_{sp}E_z B_\theta}{n_I kT(1+ac)} \qquad \text{(IX-6)}$$

$$\left(\frac{5}{2}+K_e-K_I+\frac{|e|V_I}{kT}\right)\frac{kT}{m_a}J_r=\mathcal{K}_{J=0}\frac{dT}{dr}+\frac{B_\theta E_z}{\mu_o} \qquad \text{(IX-7)}$$

$$\frac{\mu_o\sigma_{sp}E_z}{1+ac}=\frac{1}{r}\frac{d}{dr}(rB_\theta) \qquad \text{(IX-8)}$$

J_r can be eliminated from the first two of the above equations:

$$\left\{\mathcal{K}_{J=0}+\frac{n_a n_I\mathcal{D}_{Ia}n k\left(\frac{5}{2}+K_e-K_I+\frac{|e|V_I}{kT}\right)^2}{(n_a+n_I)^2\quad 1+\omega_e\tau_e\omega_I\tau_I}\right\}\frac{dT}{dr}$$

$$=-\left\{1+\frac{\left(\frac{5}{2}+K_e-K_I+\frac{|e|V_I}{kT}\right)\mu_o\sigma_{sp}\mathcal{D}_{Ia}n_a n}{(1+\omega_e\tau_e\omega_I\tau_I)(1+ac)(n_a+n_I)^2}\right\}\frac{E_z B_\theta}{\mu_o} \qquad \text{(IX-9)}$$

The term $\mu_o\sigma_{sp}\mathcal{D}_{Ia}$ can be called the magnetic Reynolds number for this problem. When the pressure is over one atmosphere this term is always less than 10^{-3}; hence it can be neglected. However, when the gas pressure is less than one millimeter of mercury this term must be included. For convenience the coefficient of (dT/dr) is put equal to $\mathcal{K}$.

The term involving the magnetic field can now be eliminated to

give the final form of the energy equation:

$$\frac{1}{r}\frac{d}{dr}\left(r\,\mathcal{K}\,\frac{dT}{dr}\right)+\frac{\sigma_{sp}}{1+ac}\,E_z^2=0 \qquad \text{(IX10a)}$$

Equations (IX-3) and (IX-4) can be combined to eliminate the magnetic field from the pressure equation

$$\frac{1}{r}\frac{d}{dr}\left(r\frac{dp}{dr}\right)-\frac{d}{dr}\left(\ln\frac{\sigma_{sp}}{1+ac}\right)\frac{dp}{dr}+\frac{\sigma_{sp}^2 E_z^2 \mu_0}{(1+ac)^2}=0 \qquad \text{(IX-11a)}$$

In the vicinity of r = 0, let $\mathcal{K} = \mathcal{K}_0\,(T/T_0)^s$; $\sigma_{sp} = (\sigma_{sp})_0\left(\frac{T}{T_0}\right)^{3/2}$.

Equations (IX-10) and (IX-11) can now be non-dimensionalized to give the following relations:

$$\frac{1}{\eta}\frac{d}{d\eta}\left\{\eta(1+s)\frac{\mathcal{K}}{\mathcal{K}_0}\frac{d\theta}{d\eta}\right\}+\frac{\theta^{3/2}}{1+ac}=0 \qquad \text{(IX-10b)}$$

$$\frac{1}{\eta}\frac{d}{d\eta}\left\{\eta\frac{d\pi}{d\eta}\right\}-\frac{d}{d\eta}\left(\ln\frac{\theta^{3/2}}{1+ac}\right)\frac{d\pi}{d\eta}+\phi\frac{\theta^3}{(1+ac)^2}=0 \qquad \text{(IX-11b)}$$

$$\frac{T}{T_0}=\theta;\quad \frac{p}{p_0}=\pi;\quad \frac{E_z\,r}{\left\{\frac{T_0\,\mathcal{K}_0}{(1+s)(\sigma_{sp})_0}\right\}^{1/2}}=\eta;\quad \frac{\mu_0(\sigma_{sp})_0\,\mathcal{K}_0\,T_0}{(1+s)\,p_0}=\phi \qquad \text{(IX-12)}$$

The subscript zero refers to the value of the variable on the axis. The factor (1 + ac) becomes significant only when the ionization level drops to below 0.1 per cent, i.e., in the outer transition region between the discharge core and the gas of zero electrical conductivity.

In general, $\mathcal{K}/\mathcal{K}_0$ is a function of the pressure as well as temperature, hence Eqs. (IX-10b) and (IX-11b) must be integrated simultaneously. The only parameter appearing in the equations is ϕ, which depends upon the temperature and pressure at the center of the discharge. If ϕ is small it can be seen that the pressure throughout

the discharge is relatively constant.

IX. 1. 1. Solution of Equations when $\mathcal{K}/\mathcal{K}_o = \theta^s$

The significance of ϕ can be seen more clearly if $\mathcal{K}/\mathcal{K}_o = \theta^s$ and $\frac{\sigma_{sp}}{(\sigma_{sp})_o} = \theta^l$ throughout the discharge. These relations are approximately true when the gas is fully ionized ($s = 5/2$) or when a strong axial magnetic field is applied to inhibit the radial diffusion of charged particles in the gas when it is partially ionized, in which case $s = 1/2$. Under these conditions, the energy and momentum equations can be combined to give an integral relation between the pressure and the temperature as follows:

$$T_o \mathcal{K}_o \theta^s \frac{d\theta}{dr} = - \frac{E_z B_\theta}{\mu_o}$$

$$p_o \frac{d\pi}{dr} = - \sigma_{sp} E_z B_\theta$$

Combining these equations, the following differential equation is obtained:

$$\frac{\mu_o (\sigma_{sp})_o \mathcal{K}_o T_o}{(1+l+s) p_o} \frac{d}{dr}(\theta^{1+l+s}) - \frac{d\pi}{dr} = 0 \qquad \text{(IX-13a)}$$

This equation has the general solution shown below:

$$\frac{s+1}{s+l+1} \phi (1 - \theta^{1+l+s}) = 1 - \pi \qquad \text{(IX-13b)}$$

The temperature distribution can be obtained quite accurately by means of a series solution in which only the first three terms are retained.

$$\theta^{1+s} = 1-\left(\frac{\eta}{2}\right)^2 + \frac{\ell}{4(1+s)}\left(\frac{\eta}{2}\right)^4 \qquad \text{(IX-13c)}$$

Eqs. (IX-13b and c) are the general solution to the radial pressure and temperature profiles in cylindrically symmetric electric discharge in which radiation is not significant as an energy transport or energy loss mechanism and in which the thermal conductivity can be represented by a function of temperature of the form

$$\mathcal{K} = \mathcal{K}_0\left(\frac{T}{T_0}\right)^s$$

These relations indicate that when $\phi > \frac{1+\ell+s}{1+s}$ the pressure at the outer edge of the discharge will drop to zero for some finite value of θ. This is the condition that has been popularily called the pinch discharge. Since the present problem has been formulated as a steady-state discharge in which the electrical energy dissipated in the discharge is transferred radially outward to a wall or some heat sink by conduction, solutions with $\phi > \frac{1+\ell+s}{1+s}$ cannot be considered as valid, since no heat conduction can occur outside of the region where $p = 0$. The gas must then necessarily heat up and the problem becomes a non-stationary one. The only singular solution that occurs is when $\phi \longrightarrow \infty$ and the temperature distribution becomes constant. This case is not considered to be a physically acceptable solution, since the discharge must pass through all of the range of ϕ from $\frac{1+\ell+s}{1+s}$ to ∞. Under the conditions imposed upon the discharge the values of ϕ are hence restricted to a range of from 0 to $\frac{1+\ell+s}{1+s}$.

The temperature distribution can be obtained by solving Eq. (IX-10b) with the boundary conditions of

$$\theta = 1 \quad ; \quad \frac{d\theta}{d\eta} = 0 \qquad \text{at} \qquad \eta = 0 \ .$$

The solution when $s = \frac{1}{2}$ (partially ionized gas) is as follows:

$$\theta^{3/2} = J_o(\eta) \tag{IX-14}$$

where $J_o(\eta)$ is the zero order Bessel function. When $s = 5/2$ (fully ionized gas) the equation must be integrated numerically or solved approximately. A numerical integration gives the curve shown in Figure 1 which is compared with a series solution shown below:

$$\theta^{7/2} = 1 - \left(\frac{\eta}{2}\right)^2 + \frac{3}{28}\left(\frac{\eta}{2}\right)^4 \tag{IX-15}$$

The temperature distributions for a discharge when $s = \frac{1}{2}$ and $s = 5$ are also plotted.

The total current is obtained from integrating the current density over the radius and is shown below:

$$\begin{aligned} I &= 2\pi r_1^2 \sigma_o E_z \int_o^{\eta_1} \theta^{3/2} \eta \, d\eta \\ &= 2\pi r_1^2 \sigma_o E_z \ f(\eta_1) \end{aligned} \tag{IX-16}$$

This expression is plotted in Figure 2. The electric field is given by the equation shown below:

$$E_z = \frac{2\pi T_o \mathcal{K}_o}{(1+s) I} \ f(\eta_1) \tag{IX-17}$$

The radius of the discharge is a function of the temperature on the axis and the current as follows:

$$r_1 = \left\{ \frac{1+s}{T_o \mathcal{K}_o (\sigma_{sp})_o} \right\}^{\frac{1}{2}} \frac{I \eta_1}{2\pi f(\eta_1)} \tag{IX-18}$$

The magnetic field is found to be given by the same expression that results when the current density is constant:

$$(B_\theta)_1 = \frac{\mu_o I}{2\pi r_1} \qquad \text{(IX-19)}$$

IX. 2. Solution in the Region where the Gas Electrical Conductivity is Zero

Outside the discharge region, the solution of Eq. (IX-10a) and (IX-10b) are as follows:

$$\theta^{3/2} = \theta_1^{3/2} + \eta_1 \left\{ \frac{d\theta}{d\eta}^{1+s} \right\}_{\eta_1} \ln \frac{\eta}{\eta_1} \qquad \text{(IX-20)}$$

$$\left\{ \frac{d\theta}{d\eta}^{3/2} \right\}_{\eta_1^+} = \left(\frac{d\theta}{d\eta}^{1+s} \right)_{\eta_1^-} \qquad \text{(IX-21)}$$

$$\pi = \pi_1 \qquad \text{(IX-22)}$$

If the heat sink is maintained at a finite temperature θ_w, then the distance between the outer edge of the discharge and the wall is given by the following equation

$$\ln \frac{\eta_w}{\eta_1} = - \frac{\theta_1^{3/2} - \theta_w^{3/2}}{\eta_1 \left\{ \frac{d\theta}{d\eta}^{1+s} \right\}_{\eta_1^-}} \qquad \text{(IX-23)}$$

This equation indicates that under some conditions the discharge can be very close to a cold wall.

IX. 3. General Similarity Solution

In a partially ionized gas the thermal conductivity is not a monatonic function of the temperature, but has a peak at the temperature where the gas is 50 per cent ionized. For this reason the above solutions to the radial temperature distribution equation do not suffice and a more general similarity solution is required. The procedure indicated below will give a similarity solution for arbitrary temperature dependences of the electrical and thermal conductivity. Put

$$\sigma(T) = \sigma_0(T_0)\,\sigma(\theta)$$

$$\int_0^T \mathcal{K}(T)\,dT = T_0\,\mathcal{K}(T_0)\,\frac{g(\theta)}{g(T_0)} \quad ; \quad g(1) = 1 \tag{IX. 24}$$

$$\int_0^T \mathcal{K}(T)\,\sigma(T)\,dT = T_0\,\mathcal{K}(T_0)\,\sigma(T_0)\,\frac{k(\theta)}{k(T_0)} \quad ; \quad \begin{matrix} k(1) = 1 \\ k(\theta_1) = 0 \end{matrix}$$

$g(T_0)$ & $k(T_0)$ are normalizing constants and have values of approximately 1-4 and 3-5, respectively. The expression for the radial pressure gradient is obtained at once from Eq. (IX-13):

$$\frac{d}{dr}\left(\frac{\mu_0\,\sigma(T_0)\,\mathcal{K}(T_0)\,T_0}{k(T_0)\,p_0}\,k(\theta) - \pi\right) = 0 \tag{IX-25}$$

This expression integrates to the following relation:

$$\Phi_0 = 1 - \pi_1 = \frac{\mu_0\,\sigma(T_0)\,\mathcal{K}(T_0)\,T_0}{k(T_0)\,p_0} \tag{IX-26}$$

Since the only pressure that can be controlled is p_1, the pressure at the outer edge of the discharge, it is better to define the parameter Φ in terms of p_1. When this is done the following relations hold:

$$\frac{p_0}{p_1} = 1 + \Phi_1(T_0) = 1 + \frac{\mu_0 \sigma(T_0) \mathcal{K}(T_0) T_0}{k(T_0) p_1}$$

$$\Phi_0 = \frac{\Phi_1}{1 + \Phi_1} \qquad \text{(IX-27)}$$

These relations remain valid as long as $p_1 > 0$. When the relations (IX-24) are substituted into Eq. (IX-10), the following equation results

$$\frac{a_1 T_0 \mathcal{K}(T_0)}{\sigma(T_0) E_z^2 g(T_0)} \frac{1}{r} \frac{d}{dr}\left\{ r \frac{d}{dr} g(\theta) \right\} + a_1 \sigma(\theta) = 0 \qquad \text{(IX-28)}$$

Put

$$\frac{E_z r}{\left\{ \frac{a_1(T_0) T_0 \mathcal{K}(T_0)}{\sigma(T_0) g(T_0)} \right\}^{1/2}} = \eta$$

The radial temperature distribution is now determined by the following equation:

$$\frac{1}{\eta} \frac{d}{d\eta}\left\{ \eta \frac{d}{d\eta} g(\theta) \right\} + a_1 \sigma(\theta) = 0 \qquad \text{(IX-29)}$$

Since there is no simple relation between $g(\theta)$ and $\sigma(\theta)$ in general, it is now assumed that the radial distribution of each of these quantities can be represented by a power series solution.

$$g(\theta) = 1 - a_1\left(\frac{\eta}{2}\right)^2 + a_2\left(\frac{\eta}{2}\right)^4 - a_3\left(\frac{\eta}{2}\right)^6 + a_4\left(\frac{\eta}{2}\right)^8$$

$$\sigma(\theta) = 1 - b_1\left(\frac{\eta}{2}\right)^2 + b_2\left(\frac{\eta}{2}\right)^4 - b_3\left(\frac{\eta}{2}\right)^6 \qquad \text{(IX-30)}$$

A relation between the a_i and b_i can next be obtained by substituting Eq. (IX-30) into Eq. (IX-29) and identifying the coefficients of terms to the same power as n as follows:

$$b_1 = 4\frac{a_2}{a_1} \; ; \; b_2 = 9\frac{a_3}{a_1} \; ; \; b_n = (n+1)^2 \frac{a_{n+1}}{a_1} \; .$$

$$g\{\theta(\eta)\} = 1 - a_1\left(\frac{\eta}{2}\right)^2 + a_2\left(\frac{\eta}{2}\right)^4 - a_3\left(\frac{\eta}{2}\right)^6 + a_4\left(\frac{\eta}{2}\right)^8 \qquad \text{(IX-31)}$$

$$\sigma\{\theta(\eta)\} = 1 - \frac{4a_2}{a_1}\left(\frac{\eta}{2}\right)^2 + \frac{9a_3}{a_1}\left(\frac{\eta}{2}\right)^4 - \frac{16a_4}{a_1}\left(\frac{\eta}{2}\right)^6$$

The constants a_i can now be determined from the known temperature dependence of $g(\theta)$ and $\sigma(\theta)$. The constant a_1 has been introduced as a stretching factor for the radial coordinate. The simplest value it could be given is 1, but when this is done the electrical discharge region of the solution is not similar and the electrical conductivity becomes negligible at some arbitrary value of η. The similarity solution that will be chosen is the case where the electrical conductivity is assumed negligible at $\eta = 2$. This statement implies that the following relations among the constants are valid:

$$(1 - \sigma_1)\, a_1 = 4a_2 - 9a_3 + 16a_4$$

$$g_1 = 1 - a_1 + a_2 - a_3 + a_4 \qquad \text{(IX-32)}$$

$$= g(T_0)/T_0 K(T_0) \int_0^{T_1} K(T)\, dT$$

The number of constants a_i that are used in the solution depends only upon the amount of information concerning $g(\theta)$ and $\sigma(\theta)$ that it is desirable to include. A first rough approximation to the solution can be obtained by using only the values of $\sigma(\theta)$ and $g(\theta)$ at $\eta = 0$ and $\frac{\eta}{2} = 1$. In this case the only constants that need be evaluated are a_1 and a_2. These can be determined from Eqs. (IX-28). This solution is rather inaccurate when compared to some numerical integrations.

However, when the constants a_1, a_2, a_3, and a_4 are retained the above polynomial solution agrees to within better than 1 per cent with the numerical integration. The additional equations necessary to determine these constants are obtained by specifying the ratio of the slopes with respect to temperature of the electrical conductivity, σ, and the thermal conductivity integral g, at $\eta = 0$ and $\frac{\eta}{2} = 1.0$. The following equations result:

$$\left\{\frac{d\sigma(\theta)}{d\theta} \Big/ \frac{dg(\theta)}{d\theta}\right\}_{\eta=0} = \left(\frac{\sigma'}{g'}\right)_0 = \frac{4a_2}{a_1^2}$$

$$\left\{\frac{d\sigma(\theta)}{d\theta} \Big/ \frac{dg(\theta)}{d\theta}\right\}_{\eta=2} = \left(\frac{\sigma'}{g'}\right)_1 = \frac{T_0 \kappa(T_0)}{\sigma(T_0) g(T_0) \kappa(T_1)} \left\{\frac{d\sigma(T)}{dT}\right\}_{T_1} \qquad \text{(IX-33)}$$

Using Eqs. (IX-28) and (IX-29) it is now possible to solve uniquely for the parameter a_1 in terms of $\sigma\{\theta(1)\}$, $g\{\theta(1)\}$, $(\sigma'/g')_0$, $(\sigma'/g')_1$, all of which depend only upon T_0, the temperature on the axis of the discharge and T_1, the temperature at the outer edge of the discharge. The value of a_1 is the smallest positive root of the equation shown below:

$$24(1-g_1) - \left\{19 + 5\sigma_1 + 2(1-g_1)\left(\frac{\sigma'}{g'}\right)_1\right\} a_1 + \left\{\frac{13}{6}\left(\frac{\sigma'}{g'}\right)_0 + \left(\frac{\sigma'}{g'}\right)_1\left(1-\frac{\sigma_1}{6}\right)\right\} a_1^2 - \frac{1}{12}\left(\frac{\sigma'}{g'}\right)_1\left(\frac{\sigma'}{g'}\right)_0 a_1^3 = 0 \qquad \text{(IX-34)}$$

The complete similarity solution for the discharge is now given by the following four equations:

$$\frac{p_0}{p_1} = 1 + \Phi_1(T_0) = 1 + \frac{\mu_0 \sigma(T_0) \kappa(T_0) T_0}{k(T_0) p_1} \qquad \text{(IX-35)}$$

$$\frac{I E_z g(T_o)}{4\pi \mathcal{K}(T_o) T_o} = \frac{12}{7}(1-g_1) - \left(\frac{6}{7} - \sigma_1\right) a_1 + \frac{1}{14}\left(\frac{\sigma'}{g'}\right)_o a_1^2 = f(T_o) \quad \text{(IX-36)}$$

$$r_1 = \left\{ \frac{a_1 g(T_o)}{\mathcal{K}(T_o)\, \sigma(T_o)\, T_o} \right\}^{1/2} \frac{I}{4\pi f(T_o)} \quad \text{(IX-37)}$$

$$(B_\theta)_1 = \frac{\mu_o I}{2\pi r_1} = 2\mu_o f(T_o) \left\{ \frac{\mathcal{K}(T_o)\, \sigma(T_o)\, T_o}{a_1\, g(T_o)} \right\}^{1/2} \quad \text{(IX-38)}$$

The similarity between these equations and Eqs. (IX-13a), (IX-17), (IX-18), and (IX-19) is to be noted.

Some criterion must be established to determine the outer edge of the electrical discharge. A glance at Eqs. (IX-34) and (IX-36) indicate that as long as σ_1, the electrical conductivity at the outer edge of the discharge divided by that at the center, is less than .05 it has less than a 1 per cent influence on any of the parameters. It is possible, therefore, to define the outer edge of the discharge by either the point at which $\sigma_1 = .05$ or by some definite temperature T_1, such that $\sigma_1 < .05$ for all values of T_o under consideration. In this paper the outer edge of the discharge will be placed at a definite temperature T_1, where the electrical conductivity is 50 (mhos/m). In choosing this value, discharges of less than approximately 10 amperes current are excluded from consideration.

The expressions for $(\sigma'/g')_o$ and $(\sigma'/g')_1$ can be expressed in terms of T_1 and T_o if we assume that $\sigma \approx T^{3/2}$ in the vicinity of T_o and that $\sigma \approx e^{-\frac{|e|V_I}{2kT}}$ in the vicinity of T_1. When this is done the following relations are obtained:

$$\left(\frac{\sigma'}{g_1'}\right)_0 = \frac{3}{2\,g(T_0)} \tag{IX-39}$$

$$\left(\frac{\sigma'}{g_1'}\right)_1 = \frac{|e|\,V_I\;T_0\;\;\sigma(T_1)\;\;\mathcal{K}(T_0)}{2k\,T_1\;\;T_1\;\;\sigma(T_0)\;\;\mathcal{K}(T_1)\,g(T_0)} \tag{IX-40}$$

In the region outside of the discharge, the energy equation integrates to the following expression:

$$\ln \eta = \frac{g(\Theta_1) - g(\Theta)}{\frac{2\,f(T_0)\,\mathcal{K}(T_0)}{g(T_0)\,\mathcal{K}(T_1)}}$$

This equation can be simplified to the expression shown below:

$$\ln \frac{r_w}{r_1} = \ln \eta = \frac{g(T_0)^2\,\mathcal{K}(T_1)}{2\,\mathcal{K}(T_0)^2\,T_0\,f(T_0)} \int_{T_w}^{T_1} \mathcal{K}(T)\,dT \tag{IX-41}$$

There is still one aspect of the general physics of the arc column that has not yet been introduced into the similarity solution. When the parameter Φ_1 becomes significant, two phenomena occur. The first effect is that a radial pressure distribution develops and the thermal conductivity $\mathcal{K}$ and the electrical conductivity σ become weak functions of the radial pressure as well as of the radial temperature distribution. The second, and more interesting effect that occurs, is that the tangential magnetic field begins to reduce the radial ambipolar diffusion of the charged particles and hence causes a pronounced reduction in the thermal conductivity in the outer regions of the electric discharge. It is not possible to introduce these non-linear effects exactly into the similarity solution shown above. However, it is possible to do so in an approximate manner under certain restrictions.

When the ambient pressure is quite high, of the order of one atmosphere or greater, the temperature on the axis must be over 40,000°K before Φ_1 becomes significant. This implies that the gas will be partially singly ionized only in the very outer regions of the discharge. We shall now assume that the electrical and thermal conductivity are independent of the pressure to a first approximation in the regions of the discharge where the gas is completely singly ionized and that in the region where the gas is partially singly ionized the pressure is equal to the ambient pressure p_1 and that the tangential magnetic field is constant at its maximum value $(B_\theta)_1$, given by Eq. (IX-38). With these assumptions, the electrical conductivity $\sigma(T)$, the thermal conductivity integral $\dfrac{\mathcal{K}(T_o)\,T_o}{g(T_o)}$, and the radial pressure integral $\dfrac{\sigma(T_o)\,\mathcal{K}(T_o)\,T_o}{k(T_o)}$, are once again functions of T_o only. The expression for the thermal conductivity must now be modified, however, to include the influence of the self-generated magnetic field. The expression shown below gives a rough first approximation to the manner in which the self-generated magnetic field of the arc affects the thermal conductivity integral:

$$\int_0^T \mathcal{K}\,dT = \int_0^T \mathcal{K}_{J=0}\,dT + \frac{\int_0^T (\mathcal{K} - \mathcal{K}_{J=0})\,dT}{1 + \mathcal{D}_{ea}\mathcal{D}_{ia}\left(\frac{|e|}{kT}\right)^2 q c \mu_o p_1 \frac{f(T_o)^2 k(T_o)\,\Phi_1(T_o)}{a_1(T_o)\,g(T_o)}} \qquad \text{(IX-42)}$$

$$= \frac{\mathcal{K}(T_o)\,T_o}{g(T_o)}$$

In order to remove the denominator from the integral, it has been evaluated at the Temperature $T_{.5}$ where the gas is 50 per cent ionized. Since $\int_0^T (\mathcal{K} - \mathcal{K}_{J=0})\,dT$ can be an appreciable fraction of $\dfrac{\mathcal{K}(T_o)\,T_o}{g(T_o)}$, even up to values of T_o of 100,000°K, the magnetic field can cause the

integral of the thermal conductivity to decrease as the temperature T_o rises over some range of T_o. Eq. (IX-36) indicates that when this occurs, the power dissipation capability of the arc decreases as T_o rises. Eqs. (IX-36) and (IX-37) indicate also that over this range of T_o the arc will have a negative characteristic, i.e., the potential drop per unit length of arc column will fall as the current is increased.

In the next section the characteristics of an argon gas column will be evaluated for a discharge operating at an ambient pressure of one atmosphere.

IX. 4. Similarity Solution for an Arc Column in Argon at One Atmosphere Ambient Pressure

The various parameters that were derived from the similarity solution in the previous section will now be evaluated for an electric discharge in argon. The solution requires first the evaluation of the electrical and thermal conductivity coefficients of the gas over the range of temperature under investigation. In Appendix I, the transport coefficients for argon are evaluated over the temperature range of $6,000^{\circ}K$ to $20,000^{\circ}K$. Because of the formation of multiple charged ions at temperatures of over $20,000^{\circ}K$ in argon it is necessary to examine the transport properties of a three particle system consisting of electrons, ions, and doubly charged ions before the similarity solution can be carried to higher temperatures. In particular, the contribution of the diffusion currents to the thermal conductivity, if any, is not a priori evident. Since a study of these effects would entail a considerable amount of analysis, the similarity solution will be

evaluated for argon only up to a temperature of 20,000°K on the axis of the discharge. At one atmosphere ambient pressure the self-generated magnetic field of the discharge has a negligible effect at temperatures of less than 20,000°K, hence any influence of the magnetic interaction parameter Φ_1 will be ignored in what follows.

The outer edge of the discharge will be defined as the position on the discharge radius at which the gas temperature had dropped to 6,000°K.

The first step in constructing the solution is to integrate the thermal conductivity coefficient over the temperature to obtain the value of $g(T_o)$. Values of g_1 and σ_1 are next computed by dividing the values of the thermal conductivity integral and the electrical conductivity evaluated at 6,000°K by their respective values at T_o. The values of $(\sigma'/g')_o$ and $(\sigma'/g')_1$ are then computed using Eqs. (IX-39) and (IX-40) or some equivalent expressions. With these values it is now possible to compute a_1 from Eq. (IX-34). Eq. (IX-36) can then be used to calculate $f(T_o)$ and hence the power dissipating capability per unit length of the discharge. The evaluation of the current divided by the discharge radius and the product of the axial electric field times the discharge radius is then straightforward using Eqs. (IX-37) and (IX-36). If we specify that the discharge is to operate in a cylinder of radius γ_w and at a wall temperature of T_w the logarithm of the ratio γ_w/γ_1 can then be computed from Eq. (IX-41). This equation has been evaluated for a wall temperature of 1,000°K. The results of these calculations are shown in Figures 3 and 4.

Figure 3 indicates that the power dissipating capability of the

arc column is only of the order of several kilowatts per cm. of length at temperatures of the order of 20,000°K on the axis of the discharge. Since most arc jet heat transfer devices are capable of transferring as much as 50 - 100 kw of electric power to argon gas through a discharge that is only several centimeters long and operating at atmospheric pressure, there appears to be some experimental evidence to indicate that the analysis is incorrect. Several alternatives present themselves as possible explanations for the discrepancy:

(1) The arc operates with a temperature along the axis of the column that is much higher than has been thought, perhaps as high as 100,000°K.

(2) The values of the electrical and thermal conductivity of the gas that have been computed are in error by as much as an order of magnitude.

(3) The majority of the energy is transferred to the gas through some mechanism other than heat transfer out of the column.

(4) The assumption of equipartition of energy among the species is incorrect.

There is considerable evidence to indicate that the third alternative is the most likely explanation, the most convincing of which is the experimentally determined fact that the heat transfer capability of an arc is practically independent of the arc length[8]. There is also some evidence to indicate that the electron temperature is considerably above the gas temperature in some heat transfer devices[8].

Figure 4 indicates that confined arcs have falling characteristics only over a very limited current range, after which the arc potential

drop rises gradually with increasing current.

An experimental curve for the E - I characteristic of a confined arc in argon is also plotted in Figure 4. This curve is taken from Reference 30 and represents measurements taken by Maecker and his co-worker in Germany. In general, the analysis predicts values of the electric field that are about a factor of 2 low over most of the current range (5 - 200 amps). It was originally thought that this discrepancy between theory and experiment might be due to the value of the thermal conductivity that was used. In the evaluation of the thermal conduction coefficient the term that appeared most likely to be in error was the energy transferred by ambipolar diffusion because of the difficulty in determining the momentum transfer cross-section for atom-ion collisions. For this reason, the similarity solution was reevaluated with the ion-atom cross-section put equal to the atom-atom cross-section instead of being 3.20 times as large as in the original evaluation. The E - I curve resulting from this evaluation is also plotted on Figure 4. Although there is some reduction in the difference between the theoretical and the experimental curve, there is still a wide enough divergence to indicate that probably some other factor, rather than the thermal conductivity, is responsible for the discrepancy. A systematic investigation into the various factors that could be responsible indicated that the most likely candidate was the electrical conductivity coefficient. The value that has been computed appears to be somewhat too high probably by about a factor of two. A much more thorough investigation into this problem is required before this discrepancy can be resolved. Since such an investigation is not in line with the basic aims of the present study, we shall not discuss this problem further here.

X. SHEATHS

Whenever a plasma comes into contact with a solid wall a layer develops in the gas through which some separation of charge occurs so that a steady state may be set up. The details of the structure of the layer are quite complicated and have been extensively studied only for isothermal layers. The basic effect of sheaths of interest in this report is the manner in which they affect the electrode action. Before the electrode mechanisms can be studied, however, it is necessary to investigate some of the properties of sheaths that occur between a hot plasma and a cold container when no electric current is flowing from the gas to the container. Since the sheath thickness is very small when the electron and ion densities are appreciable, the sheath will be considered as a one-dimensional structure, even for cylindrical surfaces.

The only condition under which sheath structure can be studied exactly is when there are no fluxes of particles or energy occurring, so that thermodynamic relations may be used. In order to extend the analysis into regions where fluxes are occurring the relations obtained from irreversible thermodynamics can be used with confidence as long as the energy change of a charged particle over a mean free path due to the electric field is small compared to the gas internal energy ($\frac{|e|\,\delta V}{kT} < 1$) . When the electric field is strong enough so that this condition is not fulfilled, then an alternative approach must be sought.

X. 1. The Equilibrium Wall Sheath

The simplest sheath will be that one which occurs when the electron diffusion and ion velocity perpendicular to the surface are zero. This condition can be obtained in principle by applying an arbitrarily large magnetic field parallel to the wall and by not allowing any electric current to flow through the wall from the gas.

From Eqs. (III-11), the sheath equations are given by the following expressions:

$$E_x + \frac{kT}{|e|}\left(\frac{d}{dx}\ln p_e + K_e \frac{d}{dx}\ln T\right) = 0$$
$$-E_x + \frac{kT}{|e|}\left(\frac{d}{dx}\ln \frac{p_I}{p_a} - K_I \frac{d}{dx}\ln T\right) = 0 \qquad \text{(X-1)}$$

The boundary conditions that are to be applied are given by the equilibrium concentration of electrons and ions in the plasma where $n_e = n_I$, and at the wall. At the wall:

$$(n_e)_w = 2\left(\frac{2\pi m_e k T_w}{h^2}\right)^{3/2} e^{-\frac{|e|\chi}{kT_w}}$$
$$\left(\frac{n_I}{n_a}\right)_w = \frac{\varpi_I}{\varpi_a}\, e^{-\frac{|e|}{kT_w}(V_I - \chi)} \qquad \text{(X-2)}$$

In the plasma where the electric field is essentially zero the other boundary condition can be placed on the sheath:

$$n_e = n_I = \left(1 - \frac{2n_e kT}{p}\right)^{1/2}\left(\frac{2\varpi_I p}{\varpi_a kT}\right)^{1/2}\left(\frac{2\pi m_e kT}{h^2}\right)^{3/4} e^{-\frac{|e|V_I}{2kT}} \qquad \text{(X-3)}$$

Throughout the sheath the Saha equation is valid:

$$\frac{n_I}{n_a} = \frac{2\varpi_I}{n_e \varpi_a}\left(\frac{2\pi m_e kT}{h^2}\right)^{3/2} e^{-\frac{|e|V_I}{kT}} \qquad \text{(X-4)}$$

When Eqs. (X-1) are combined with Eq. (X-4) it is found that the only solution is as follows:

$$T = T_w = T_o$$

$$p_e = (p_e)_o \, e^{\frac{|e|(V-V_o)}{kT_o}} \qquad \text{(X-5)}$$

$$\frac{p_I}{p_a} = \left(\frac{p_I}{p_a}\right)_o e^{-\frac{|e|(V-V_o)}{kT_o}}$$

The subscript zero refers to conditions in the plasma where the electric field is zero. The structure of the sheath can be determined from Poisson's equation and the momentum equation as follows:

$$\frac{d^2V}{dx^2} = -\frac{|e|}{\varepsilon_o}(n_I - n_e) \qquad \text{(X-6)}$$

$$p_o = p - \frac{\varepsilon_o E^2}{2}$$

The general solution to this problem has been given by Fowler[18] for the two cases of $n_{eo} << n_a$ and $n_a = 0$ when the electric field is zero where $V = V_o$ in the plasma. In non-dimensional variables the solution is given as follows:

$$|\tanh \; w/4| = e^{-\xi}$$

ξ is the non-dimensional distance from the wall.

$$(dw/d\xi) = \pm 2 \sinh \; w/2 \qquad \text{(X-7)}$$

$$w = \frac{|e|(V-V_o)}{kT_o} \; ; \; \frac{\alpha}{\xi} = \left(\frac{\varepsilon_o kT_o}{2|e|^2(n_e)_o}\right)^{1/2} = \text{Debye shielding distance}$$

$$\frac{\varepsilon_o E^2}{2} = (p_e)_o \left(\frac{dw}{d\xi}\right)^2 = \text{"electric" pressure}$$

In Figure 5 the quantities w and (dw/d) are plotted as a function of ξ. The plot shows the well-known result that potentials greater than $kT_o/|e|$ can be supported only over distances of the order of the Debye shielding distance. From Eqs. (X-2) and (X-3) it can be seen that the gas will be fully ionized everywhere only when the two conditions shown below are maintained:

$$V_I < \chi$$

$$\frac{2\varpi_I}{\varpi_a}\frac{p}{kT}\left(\frac{2\pi m_e kT}{h^2}\right)^{3/2} e^{-\frac{|e|V_I}{kT}} >> 1$$

Since these conditions are rarely met with in high pressure electrical discharges the discussion that follows will be applied only to isothermal sheaths in which the ionization level is low. The two quantities of interest are the potential drop across the sheath with its sign and the electric field at the wall. The potential drop across the sheath is given by the following relation:

$$V_w - V_o = \frac{V_I}{2} - \chi_w + \frac{kT_w}{2|e|}\ln\left\{\frac{2\varpi_I}{\varpi_a}\frac{kT_w}{p}\left(\frac{2\pi m_e kT_w}{h^2}\right)^{3/2}\right\} \quad \text{(X-8)}$$

$$= \frac{V_I}{2} - \chi_w + \frac{T_w}{1000}\left[.1315 + .0431 \ln \frac{\varpi_I}{\varpi_a}\frac{p}{p_{at}}\left(\frac{T_w}{1000}\right)^{5/2}\right]$$

The electric field at the wall can be found from Eqs. (X-7) and (X-4) together with the curves of Figure 5.

Eq. (X-8) indicates that for most gases in contact with metal walls the potential drop across the wall sheath is practically independent of the temperature and that the wall is several volts positive with respect to the gas across the isothermal sheath.

X. 2. The "Gas" Sheath

Since the gas is usually much hotter than the container walls in problems of interest in this report it is necessary to determine the potential drop and other parameters that occur across the regions where the gas temperature drops from the free stream value to the value at the wall. This drop occurs across a boundary layer in most cases that has a thickness dependent upon the Reynolds number of the gas flow. Typical boundary layer thicknesses are 10^{-1} - 10^{-2} cm. for the flow of several gms/sec. of gas through pipes of a cm. cross-section and several centimeters length. This length is several orders of magnitude larger than the Debye sheath thicknesses that occur, hence it is possible to postulate the existence of a double sheath, one in the gas that is due to the temperature drop alone and an isothermal wall sheath that matches the properties of the gas to those of the wall.

If the reaction rate of the ions, electrons, and atoms is fast enough it can be assumed that the electron density is always at its equilibrium value. When no electric current is flowing through the sheath the potential drop across this gas sheath can be determined by using the first of Eqs. (X-1) and Eq. (X-3), provided $\frac{n_e k T}{p} << 1$. This expression is given below:

$$V_g - V_o = \frac{k}{|e|}\left\{\left(\frac{9}{4} + K_e\right)(T_g - T_w)\right\} + \frac{V_I}{2} \ln \frac{T_g}{T_w} \qquad \text{(X-9)}$$

This equation indicates that the hot gas develops a potential that is positive with respect to the cold gas layer.

From Eqs. (VII-8) and (VII-9) the potential in the vicinity of a

wall in contact with a hot gas has, in general, the form shown in Figure 6. In practice, the temperature gradient will extend up to the wall and the wall and gas sheaths will then interpenetrate. Qualitatively and in many cases quantitatively, this will not materially affect the argument as given above.

These potential wells that develop near the walls prevent the passage of a current if two walls are insulated and have a small potential difference imposed across them. The sketch in Figure 7 indicates how the potential distribution changes as the applied potential drop across the electrodes is increased. From these curves it can be seen that walls are effectively the plates of a condenser. The image forces from the positive charge accumulation on the cathode eventually can neutralize the negative charge of the gas near the cathode surface in the wall sheath so that the potential well disappears and the potential rises monotonically. On the other hand, it is very difficult for the image forces from the positive charge accumulation on the anode to penetrate into the gas far enough to neutralize the positive charges of the gas sheath, hence the potential well near the anode remains. This indicates, that if the gas is close to equilibrium at all points, that an electrical discharge cannot exist under the conditions postulated. As the potential drop acorss the electrodes is increased the electric field immediately outside of the anode becomes very strong and eventually more and more electrons pick up sufficient energy over one mean free path so that they can ionize an atom upon collision. Once the electron production rate reaches a critical value the equilibrium analysis is no longer valid and the development of the discharge from this point on can only

be postulated. Until current starts to flow, the average electron energy or temperature does not rise above that of the gas. However, the energy distribution function does not remain Maxwellian but becomes anisotropic in the direction of the electric field, as indicated in Figure 8. In general, electron and ion production near the anode surface proceeds by an avalanche once the critical production rate per unit volume has been reached. This leads to the concentration of the current density at the anode into a narrow column in order to puncture the sheath. In order to build up a steady state charge distribution in the column through which the current is flowing, that is opposite to that over the rest of the anode surface through the region where the gas temperature falls from the column temperature to the wall temperature, the discharge now develops a new degree of freedom and the electron temperature rises above that of the gas. The electron temperature must stabilize itself at a value where the electrons can produce ions in the anode fall region at the same rate as they are carried into column by the electric field. If some or most of the ions that are produced in the anode fall region can be blown out of the anode fall and allowed to recombine so that they do not enter the arc column, this provides a very useful mechanism for transferring energy from the electric field to the gas.

XI. ENERGY TRANSFER PROCESSES IN ELECTRIC DISCHARGES

Using the results of the analyses carried out above, it is now possible to discuss in some detail the energy transfer mechanisms that occur in plasmas. In particular, in this section we shall be concerned with one problem of immediate practical interest, namely, the manner in which electrical energy can be efficiently transferred from an electric arc discharge to a gas stream. This topic is the central problem of arc heater designs and up until now has been attacked from a purely empirical point of view. The discussion which follows should be considered as only a rather preliminary and incomplete enquiry into this fascinating subject, where a great deal more analytic work is necessary before we can hope to have a sound understanding of all the relevant physical processes that are occurring.

The particular application of the arc heater determines to some extent the desirable performance characteristics of the interaction between the arc and the gas flow. The following list indicates most of these characteristics that are needed at one time or another:

(1) The electric energy should be transferred to the gas with as high an efficiency as is possible.

(2) The gas should be heated to as high a temperature as is possible.

(3) The gas flow should be uniformly heated.

(4) The gas flow should be as free as possible from unevenness, vorticity, and turbulence.

(5) The electrodes should not be allowed to become hot enough locally to either vaporize or erode.

In general, there is an intricate interaction between the gas flow and the electric discharge, hence it is necessary to study the configuration of the arc and gas flow system in order to determine the relative significance of the various mechanisms at work. We distinguish between three energy transfer mechanisms as follows:

(1) The dissipation of electric energy in the column and its transfer by thermal conduction and charged particle diffusion radially outward.

(2) The transport of charged particles out of the arc column and electrode attachment regions by gas flow; their recombination energy then heats up the gas outside the arc.

(3) The transfer of charged particles out of the arc column and electrode attachment regions by means of electromagnetic pumping and their injection into the gas flow so that they recombine and heat the gas.*

In the remainder of this chapter, the following three configurations, involving the above mechanisms, will be investigated:

(1) The gas flow is axial along the axis of the electric discharge.

(2) The gas flow is similar to that in (1) but has a tangential velocity component. This configuration is commonly called the vortex-stabilized arc heater.

(3) The arc is radial in an annulus through which gas is flowing. The arc rotates around the annulus due to its interaction with an applied axial magnetic field. In this configuration, the flow is mainly across the arc, rather than along it.

A complete analysis of any one of the above three configurations is still far beyond the capabilities of techniques developed in this paper and elsewhere. The various regimes of operation can, however, be outlined and their relative merits in the overall scheme of arc heaters qualitatively assessed.

XI. 1. Axial Gas Flow Along the Axis of a Discharge

Figure 15 shows schematically an electrode configuration that has come to be known as the wall stabilized arc. The anode can be contoured in an arbitrary fashion, and is usually brought close to the cathode around the tip in order to have a near sonic gas velocity in this region. Independent of the electrode shape, there are five critical areas of interaction between the flow and the discharge as indicated in Figure 15.

XI. 1. 1. The Cathode Attachment Region

This region is usually characterized by the high excess positive ion concentrations that occur and by the electron temperature rising substantially above the temperature of the heavy particles. Because of the high ion concentration and subsequent strong electric field near the cathode surface, current is carried to the cathode by field emission as well as thermionic emission. The establishment of a strong field requires that the area of attachment of the discharge on the cathode be small, so that there results a large divergence of the current density downstream of the point of attachment due to the excess gas pressure at this point caused by the electromagnetic forces. Because

of this effect large quantities of charged particles are pumped from the cathode attachment region into the column so that a high rate of charged particle production must be maintained there. In addition, efforts are usually made to force the gas to flow at close to sonic velocity over the cathode tip by constricting the anode channel at this point. The axial flow velocity of the gas near the cathode can be high enough so that the ions are swept along with the neutral particles and flow against the electric field. This results in once again necessitating an increase in the ion production rate in the cathode attachment region in order to maintain the discharge. Most of the charged particles formed due to the action of the above two processes enter the gas flow and thus add to the enthalpy of the gas as long as most of the electron-ion recombinations are due to three body collisions rather than radiative collisions. Experience has shown that it is possible to produce as many as 10^{22} ions/sec. in the cathode attachment region. This process consumes electric power at a level of from 20 to 50 kw at the production rate quoted above. A reasonable percentage of the overall arc potential drop can hence occur over the cathode attachment region. No effort has been made to analyse the attachment region because of the dominant role played by the excess temperature of the electrons, which has not yet been incorporated into a comprehensive treatment of the transport properties of a plasma.

XI. 1. 2. The Inlet Heating Region

A wide and varied group of phenomena can occur and many have been observed to do so in this region. Provided that the channel

diameter is not too large, the arc conduction channel increases from the diameter at the point of attachment at the cathode to a diameter fairly close to that of the anode. The similarity solution indicates that as the arc channel increases in diameter the temperature on the axis of the discharge decreases, consequently reducing the power dissipated per unit length of channel and the electric field strength along the channel. The asymptotic radius of the conduction channel depends primarily on the electric current I and the channel radius r_w. For small values of I/r_w the discharge will not come near to filling the channel, and the temperature on the axis of the discharge is barely enough to make the gas electrically conducting. There will be some critical value of $(I/r_w)_{cr}$, such that the thermal conduction to the walls will be unable to stabilize the column for values of I/r_w below the critical value. In this regime, bouyant forces and small irregularities in the gas flow will exert a strong influence on the discharge. Under some flow conditions the discharge has been seen to thresh about in the channel randomly.* Although fluctuations in the arc potential are high when operating in this mode, this is a fairly desirable type of

---

* Private communication with M. Thorpe of Thermal Dynamics. Thorpe's measurements indicate that this mode of arc operation resulted in efficient energy transfer from the discharge to the gas and also that the anode point of attachment moved randomly over the surface of the cylinder, so that no local hot spot developed. The rapid random motion of the discharge throughout the channel mixed the heated and unheated gas quite well so that the emergent gas did not have a pronounced radial enthalpy profile, as occurs when the gas flows through the stabilized discharge.

arc heater design and has proved in practice to be quite reliable while operating within certain limits of gas flow rate and arc current. Increasing the current inevitably results in the arc suddenly striking to a point on the anode surface near the cathode and anode burnout occurs shortly thereafter. The reason for this behavior is obscure, but is probably connected with the inertia of the ions in the discharge column. This topic will be discussed in some detail later when the behavior of an arc column in a strong cross-flow will be discussed.

Although there is little hope that much can be done to analyse the heat transfer from the unstable arc column to the gas, there is much that can be done with the stable expanding column of conducting gas. In addition, criteria for stability can be established for both column bending (kink instability) and column pinching (sausage instability) based on the tendency of the heat transfer rate to stabilize perturbations in the column. For example, if the column attempts to pinch at some point along the axis, the power transferred out radially increases at this point (see similarity solution) and hence the gas just outside of the column is heated sufficiently to become electrically conducting. The column diameter is thus increased at this point and the instability suppressed. In general, the analysis of problems of this type will be complicated by the jet of ionized gas particles that enters the column from the cathode attachment region.

XI. 1. 3. Fully Developed Discharge Region

In this region the electric discharge has expanded radially outward so that it has reached a steady state and the temperature and

density profiles remain identical further on down the channel. The velocity profile in this region is still not that of fully developed pipe flow, however, and many diameters of channel length may be required before the pipe flow regime is reached. In general, arc heaters based on this electrode configuration have anodes that terminate in this region of the arc-gas flow interaction since little heating of the gas occurs with a longer anode, most of the power from the discharge being conducted to the anode cylinder. Little can be done, at present, in analyzing the velocity field in this region, although some useful information might be obtained by the use of similarity parameters coupled with a well instrumented set of experiments.

For configurations similar to that shown in Figure 15, the electric discharge is established in the wake of the cathode. This complicates any attempt to study the velocity profiles in the inlet heating region and from this compute the radial rate of growth of the discharge. Whether or not the gas flow in the wake is turbulent can also have a pronounced influence upon the characteristics of the electrical discharge. This point will be discussed in the section dealing with fully developed pipe flow.

XI. 1. 4. Fully Developed Pipe Flow Region

Provided the parameters of the anode and the electric discharge are within the proper range, a region of interaction between the discharge and the flow will develop in which velocity profiles stay similar along the tube length and the power dissipated per unit length in the discharge is all transferred to the wall by conduction. Only two

regimes of operation are possible here, either the flow is laminar or turbulent. In the former case, it is possible to completely analyse the problem since the interaction of the flow with the discharge is only second order. By this we mean that the viscous dissipation of energy is negligible compared to the electric energy dissipation so that the radial density distribution is determined only by the electric discharge. Also, the gas velocity does not influence the mechanisms of radial energy transport so the discharge is not modified by the gas flow in this region. The rather remarkable properties of the interaction in this region has been recognized by Emmons and Lick of Harvard, who are at present conducting experiments to study some of the characteristics of this asymptotic flow regime. The similarity solution of Section IX. can be used to determine the density and temperature profiles. The velocity profiles can then be computed, including convective effects if they are significant, and from these profiles the mass flow rate, axial pressure gradient and the energy flux rate or power flux along the tube can be determined. Because of the fairly extensive labor involved in computing profiles and numerically integrating the various parameters required, we have not explicitly carried out this important step in this paper, but intend to do it on a computer in the near future.

As mentioned previously, no net energy is transferred to the gas in this region. However, the power flux and hence the average gas enthalpy level that can be attained by the emergent gas is determined by the profiles of velocity and temperature that occur here. In particular, a transition from laminar flow to turbulent flow will alter the velocity

profile quite radically and hence the power flux and the radial enthalpy distribution. A change in power flux would necessitate a change in discharge in the inlet heating region and thus profoundly modify the whole arc. If the anode of an arc heater similar to that shown in Figure 15 were long enough so that a region of fully developed pipe flow occurred, then we would expect an abrupt change in the arc behavior when the flow became turbulent. In general, the transition would occur as the Reynolds number of the flow increased. For a constant mass flow rate, it is possible to increase the flow Reynolds number by increasing the arc current beyond a certain critical value I_{cr} . At values of current below I_{cr} , an increase of current decreases the flow Reynolds number. This reversal occurs because of the relation between the plasma viscosity and the temperature as shown in Figures 9 and 10. Experiments conducted by Mr. A. C. Ducati, at Giannini Plasmadyne, (private communication) indicate that, in fact, a transition similar to that discussed above has been observed, and occurs in practically all arc heaters that have cylindrical anodes when an effort is made to obtain high gas enthalpies. Since the transition usually involves an increase in the current by about a factor of two, power losses increase rapidly after the transition and attempts to increase the gas enthalpy much beyond this point usually result in destruction of the equipment.

Since it is necessary to operate the discharge so that it completely fills the anode cylinder in order to get high gas enthalpies, the transition to turbulence can be the factor that determines the maximum average enthalpy to which the gas can be heated in this configuration.

XI. 1. 5. Point of Discharge Attachment to the Anode

In the desirable type of arc behavior at the anode, the current would enter the anode surface uniformly over a wide area so that no local heating would occur as the electrons give up energy proportional to the surface work function upon entering the metal. Unfortunately, there appears to be little likelihood of this occurring in most arc heaters that operate at pressures high enough so that the charged particle density is close to its equilibrium value. Because of the nature of the sheath structure that develops on the anode surface (See Section X.) whenever the gas is hotter than the surface and the ionization energy of the gas is greater than twice the work function of the metal, it is necessary for the discharge to contract and contact the anode surface at a point. Once again, as at the cathode, the electron temperature rises considerably above the heavy particle temperature in this region, resulting in a plentiful production of ions which are accelerated out into the column by electromagnetic pumping as well as by the electric field.

The actual point of attachment of the anode spot can occur in any one of regions II, III, IV, or V of Figure 15. When the anode ends in region II of Figure 15, then the anode spot will almost always attach on the front surface of the cylinder, rather than on the inside surface. Whenever attachment to the front surface occurs, the discharge path turns through 180° and a considerable number of charged particles are electromagnetically pumped out of the discharge column in this region. The total potential drop across the discharge is usually comparatively high for this reason. However, since the discharge does not fill the cylinder, much of the gas does not pass through the arc

and hence the average gas enthalpy is usually quite low at the outlet of the heater when the current is such that this mode of operation occurs.

Either by lengthening the anode cylinder or by increasing the arc current it is possible to increase the diameter of the discharge until it effectively fills the channel area (see similarity solution). The anode point of attachment will usually now move from the front surface onto the inside surface of the cylinder. This transition is usually accompanied by a marked drop in the total potential of the arc since there is now considerably less electromagnetic pumping of charged particles out of the discharge in the region of anode spot attachment.

Irregularities in the flow usually cause the point of attachment to move about considerably, both axially and radially. Unless this occurs, experience has shown that local heating of the anode spot will cause anode burnout in a relatively short time. When efforts are made to obtain high gas enthalpies, it has been found that some more positive technique of moving the anode spot is required to prevent erosion or burnout at the anode point of attachment. One method that has been adopted to accomplish this is to rotate the gas by introducing it tangentially into the arc chamber. A second technique now in use is to use electromagnetic forces to move the anode spot. Both of these approaches to solving the problem of anode burnout will be discussed in the following sections.

XI. 2. Arc Heaters with a Gas Vortex

Introducing the gas into the arc chamber with a high tangential velocity component appears to have three major effects upon the

operating characteristics of the arc heater.

(1) The gas vortex tends to center the electric discharge along the axis of the anode cylinder. The radial pressure gradient of the vortex leaves a low pressure region along the axis of the anode. In general, the electric discharge will strike through this low pressure region, since this path is one that requires a minimum potential drop. The vortex also smooths out any irregularities in the arc channel that tend to develop and thus has a stabilizing influence upon the discharge against kink instabilities that could develop without the vortex when the column is too far from the cylinder wall to be stabilized by thermal conduction.

When the temperature on the axis of the discharge is high enough so that the self-generated magnetic field of the discharge is sufficiently strong to influence the radial pressure distribution, then there will be a fairly strong interaction between the vortex flow and the structure of the discharge. Besides having a strong influence on the stability of the discharge, the vortex also will be an important factor in determining the radius of the discharge and hence the temperature along the arc axis. Experimentally, it has been observed that the potential drop across a given electrode configuration increases when a gas vortex is introduced into the flow, all other factors being held constant. This could be interpreted to mean that the arc operates at a considerably higher temperature due to the vortex motion of the gas.

(2) The rotational motion of the gas forces the anode spot to rotate around the anode cylinder. This occurs when the anode spot attaches either on the front or on the inside surface of the anode cylinder.

This rotational motion of the anode spot reduces local heating on the metal and thus helps to prevent the anode from melting at the point of attachment of the arc. Even if the local heating of the surface is high enough to vaporize some surface material, the motion of the spot prevents burnout from occurring rapidly at any one point.

(3) Most electrode configurations that are designed to incorporate a gas vortex in the overall heat transfer scheme, have some regions of operation over which the primary flow becomes unstable and secondary gas flows develop. Since these secondary flows usually occur in regions of the device where the electric discharge is operating, undesirable effects almost always occur. In some cases the actual current-voltage operating characteristics of the discharge is interfered with to such an extent that modal operation, relaxation oscillations, or even extinction of the arc can occur. Often, the secondary flows merely carry some of the heated gas from the discharge along the electrode surfaces, greatly reducing the efficiency of energy transfer and, depending upon the particular design, at times burning out the insulators between the electrodes.

There is little hope that a complete understanding or an analysis of the vortex arc jet heater will be obtained in the near future. Many features of the secondary gas flows, independent of the electric discharge, are as yet inaccessible to analytic techniques. This fact alone helps to explain why arc jet design has been an empirical art in the past for the most part. Ingenuity has done much to improve the reliability and general performance characteristics of all types of arc jets, but has been especially fruitful when applied to the designs which

incorporate gas vortices.

Since the vortex introduces new and usually undesirable phenomena (secondary flows, poor enthalpy distributions, flow rotation) while accomplishing its primary purposes of moving the anode spot and centering the electric discharge, it is natural to search for other means of obtaining the desirable effects without introducing the accompanying undesirable secondary effects. This leads us naturally into a discussion of a third type of arc jet configuration in which the anode spot and usually the arc column is made to move rapidly under the influence of an applied magnetic field.

XI. 3. Arc Heaters with Crossflow

Because of the numerous secondary phenomena and modal transitions that are possible in the interaction between an arc discharge and an axial or tangential gas flow in the arc channel, it is desirable to investigate other interaction configurations that could possible lead to an efficient and reliable arc jet design. A configuration that has been subjected to considerable experimental study is one comprising concentric electrodes with a radial arc in the annulus rotated by an applied axial magnetic field. Gas is passed axially through the annulus and is, in theory, heated as it passes through the arc region.

The interaction between the discharge and the gas flow in this configuration raises a number of fairly fundamental problems. Some experimenters indicate that over certain pressure ranges the discharge takes place through an annular sheet rather than through a localized column (Patrick, Reference 24). On the other hand, the experiments

of Early and Dow at Michigan[25] indicated that over a very wide pressure range the discharge in their equipment occurred through a column. At pressures of over one atmosphere, which were used in the experiments reported here, there is little doubt that a column will form. When this column now rotates around the annulus the interaction problem reduces to that of determining the rate of rotation of the column, its cross-sectional shape and area. Since the force per unit length on the column is constant there should be little tendency for column bending so that it is legitimate to consider the arc as a fairly rigid cylinder. The column inertia is provided almost entirely by the ions since the electrons have such a small mass. The structure of the outer radial support of the discharge is probably strongly influenced by the cross-flow so that the heat transfer out of the column as well as the diameter of the electrical conducting path is profoundly modified. No effort is made to calculate the rotation rate of the discharge in this report, since the influence of the phenomena that occur at the cathode and anode attachment points is felt to be decisive in determining the behavior of the whole discharge when the column is only several millimeters long.

Preliminary considerations of this design indicate that it has a number of very attractive features.

(1) The arc length is fixed by the annulus spacing. This enables one to control accurately the arc length and hence determine its significance in the overall heat transfer scheme. In particular, it should be possible to accurately determine the electric field strength in the column by changing the annular spacing.

(2) The arc column diameter remains the same over the discharge

length and is changed only by the sheath structures that occur at the electrodes. This represents, in theory, a decided advantage for this configuration as compared to the axial flow -- axial arc configuration, in which the arc channel diameter must necessarily increase as the gas is being heated.

(3) It should be possible to continually reduce the diameter of the arc channel by increasing the relative velocity of the arc conducting path to that of the ambient gas. A glance at the similarity solution of Section IX. indicates that this should increase the power dissipation per unit length of the column and hence improve the heat transfer characteristics of the arc by increasing the overall potential drop and thus reducing the current for any required power level of operation.

Because of the seeming advantages of this configuration, as outlined above, it was decided to construct an arc heater of this type and subject it to some fairly extensive measurements. The problems encountered and the observations made when operating this arc will be discussed in the next section.

XII. ARC HEATER DEVELOPMENT

XII. 1. The Annular Electrode Arc

The first device that was constructed had the configuration shown in Figure 16. Little difficulty was encountered in striking the arc, and as anticipated, it rotated rapidly in the annulus. However, many undesirable secondary effects occurred and these will be discussed in detail in the sections which follow.

XII. 1. 1. Arc Potential Drop

The dimension of the annulus, that is, the length of the arc, was 1/4 inch. The potential drop across the arc is plotted as a function of the axial magnetic field strength in Figure 17 for various arc current levels. The general trend is for the voltage to increase as the magnetic field increases. During one run, however, the voltage remained relatively constant over the range of 1000 - 4500 gauss in the magnetic field. This anomalous effect is possibly due to the occurrence of intermittent phenomena at the electrodes and will be discussed later. Since the fundamental requirement of a good arc heater is to transfer the most energy to the gas with a minimum of loss, it is immediately apparent that the higher the potential drop across the arc the better. Figure 17 indicates that the potential drop across the arc does not increase indefinitely but approaches some asymptotic value of the order of 50 volts for argon gas. This is true over a current range of 10 - 120 amperes.

XII. 1. 2. Arc Rotation Rate

A number of different techniques were employed in an effort to measure the rotation rate of the arc. Due to the uneven and intermittent nature of the rotation rate, however, the only method of measurement that proved useful was that of mounting a coil in the cathode and measuring the signal generated in it as the current density at that point in the cathode varied due to the motion of the contact point of the arc with the cathode.

In many of the records obtained from the coil (See Figure 23), no consistent signal was obtained; both wave form and frequency varied with time. The rotation rates of the arc obtained from those records that could be used are plotted as a function of the magnetic field strength in Figure 18. A considerable spread in the data occurs. No strong dependence on the arc current is indicated, although there is a general tendency for the totation rate to increase with the arc current. To a first approximation, the following equation gives the rotation rate in cycles/sec. in terms of the magnetic field strength B in webers/m^2.

$$f = 3800\ B \text{ cycles/sec.}$$

Several high speed movies were taken of the arc by a camera borrowed from Mr. Ray E. Reichenbach of the Mechanical Engineering Department. These films indicated that there was an intermittent tendency for more than one discharge path to occur between the anode and cathode and that when this occurred the rotation rates of the arcs became quite random. Many of the records obtained from the coil in the anode could be interpreted from this standpoint. Several strips of these films are reproduced in

Figure 19.

XII. 1. 3. Induced Gas Rotation Rate

The rotating arc induces a certain amount of rotation in the gas as it flows through the arc region. An indication of the magnitude of this induced rotational flow can be obtained by measuring the radial pressure difference that occurs in the flow channel. The static pressure at the outer edge of the flow annulus was measured at two points $\frac{1}{2}$" apart, as shown in Figure 20. It is assumed that the pressure on the inner annulus is atmospheric. The results of several probe pressure measurements are plotted in Figure 21. The radial pressure differential appears to be approximately linear with the magnetic field strength and to decay quite rapidly as the gas flows along the channel. The axial magnetic field is probably quite instrumental in reducing the angular velocity of the gas by the induction of eddy currents in the ionized gas that is not part of the arc. If this pressure differential is used to compute the angular velocity of the gas assuming solid body rotation,

$$p = \tfrac{1}{2} \rho (\omega Y)^2$$

then the maximum gas rotation rate would be 440 cycles/sec. when the arc is rotating at 2100 cycles/sec. When 1 gm/sec. of argon gas is flowing through the annulus and when it is heated to 3800°K by the arc, the axial flow velocity and the angular velocity at the outer edge of the annulus are approximately equal at 80 m/sec. for the condition quoted above with an axial magnetic field of 0.44 (webers/m^2) .

XII. 1. 4. Efficiency of Electric Energy Transfer to the Gas

The fraction of the total electric energy that is retained by the gas as it leaves the orifice ranges between . 10 and . 5 and is, in general, intolerably low. There is a slight tendency for the fraction of energy retained by the gas to increase as the magnetic field increases. The reason for this low value of P_G/P will be discussed in subsequent sections. Besides having a poor efficiency for transferring energy from the electric field to the gas the following other disadvantages of the configuration became apparent over the period that this arc device was in use and they are listed below.

(1) As already mentioned, it was found that the arc dragged the gas around with it to some extent and set up a vortex in the gas with a radial pressure gradient. This introduced an instability into the axial flow of the gas which resulted in a secondary back flow carrying the heated gas over the electrode and quartz surfaces indicated in Figure 22.

(2) The position along the axis at which the arc struck changed with the gas flow rate and with the axial magnetic field strength. Under some conditions the arc took up the position as shown by B - C in Figure 22. The arc was extremely unsteady in this position as was indicated by wide voltage and current fluctuations as well as by a high noise level in the audible range.

(3) The rotation rate of the arc was found to be unstable and to depend upon the phenomena that occurred at the electrodes as well as upon the current and magnetic field strength. A number of the

photographs of the electric signal generated in the coil shown in Figure 20 are reproduced in Figure 23. These indicate the uneven and apparently random changes in the rotation rate of the arc.

(4) The voltage across the arc exhibited a wide spectrum of high amplitude osciallations. At times the oscillation peak to peak voltage was over 50 per cent of the average D. C. potential drop across the arc. It was found that in general these appeared to be two more or less stable modes of operation of the arc, each characterized by a quite different potential drop across the arc, both in its D. C. and its A. C. components. This is well demonstrated in Figure 24 which shows the voltage across the arc when the operating conditions were identical. When the voltage was low and had a high frequency component (top picture) the audible noise level from the arc was quite low and a bright ring could be seen on the anode. While operating in the other mode (lower picture) the audible noise level from the arc was considerably higher. There was no bright ring on the anode in this mode but intermittent flashes were seen on the cathode.

XII. 1. 5. Attempts to Eliminate the Backflow

The anode geometry was changed to that shown in Figure 25 in an effort to reduce the backflow of hot gas. The gas was forced to flow through a small annular orifice (A in Figure 25) formed by extending the cathode to within 0. 020" of the anode. As expected, the high gas velocity through the orifice prevented the arc from striking at the orifices and forced it to strike across the channel width d. Although this cathode configuration prevented the hot gas from flowing

back over the quartz cylinder, a secondary flow still existed as indicated in Figure 25. However, this modification significantly improved the efficiency with which electrical energy was transferred to the gas as it issued from the heater.

XII. 1. 6. Axial Positioning of the Arc

(1) Since the potential drop across the arc increases as the axial magnetic field is increased, it was felt that the arc might station itself at a position where the magnetic field had a minimum value so as to operate according to the well known Steenbeck principle of minimum voltage drop resulting in a minimum entropy production rate. In order to test this hypothesis, a ring of magnet iron was placed around the region of the annulus where the arc was to be positioned. The axial radial magnetic field profiles in the annulus were measured and are shown in Figure 26. However, when the arc was struck there appeared to be no tendency for it to stabilize itself at the position of the minimum axial magnetic field, so attempts along this line were abandoned.

(2) The electric current generates a magnetic field that could possibly be used to electromagnetically exert an axial force on the arc and hence help to position it. In the normal configuration the axial electromagnetic force on the arc tended to be cancelled out as indicated in Figure 27. In an effort to exert a force on the arc in the direction opposite to the drag force exerted by the gas, the cathode was lengthened and the current made to flow out the front of the cathode. This formed a

current loop that should exert a reasonable axial force on the arc in a downstream direction. However, as the axial magnetic field was increased the arc again blew out of the annulus and attached itself to the front of the anode.

(3) The only reliable way to hold the arc in the annulus immediately in front of the orifice appeared to require insulation of the rest of the annulus electrically. The configuration shown in Figure 28 was designed for this purpose. The insert sketched in Figure 28 was made of copper and was insulated from the anode by the two O-rings. In order to protect the O-ring nearest to the arc and to prevent a secondary arc from striking to the insert a small amount of gas was fed into the small annulus between the anode and the insert as shown in the diagram. This configuration successfully confined the arc to the position A as shown in Figure 28.

Although this design of arc heater appeared to have some merit in that the energy was transferred to the gas with reasonable efficiency (50 per cent) and the enthalpy appeared to be distributed quite uniformly throughout the gas due to the electromagnetic mixing effect of the rotating arc, the arc operation still appeared to be quite unsteady, exhibiting sudden transition from one mode of operation to another which was characterized by abrupt changes in voltage across the arc and by high amplitude oscillations in the arc voltage. As mentioned previously, these transitions appeared to be caused by phenomena occurring at the electrode surfaces. One well-documented phenomenon that could cause this type of behavior of the arc is the tendency for the cathode spot to move in the retrograde direction in a transverse magnetic field.

If the arc column near the cathode had a force on it in the retrograde direction and the rest of the column had a force on it trying to rotate it in the normal direction then unstable operation, exhibited by voltage oscillations and unsteady rotation rate, is to be expected. In order to eliminate this possible source of the voltage fluctuations the design of the electrodes was changed so that the current density at the cathode was in the direction of the magnetic field.

XII. 2. The Point to Ring Electrode Arc

The electrode configuration adopted is shown in Figure 29. Besides having the current density at the cathode parallel to the axial magnetic field, this design of heater incorporated the additional features discussed below.

(1) The arc was forced to turn through a 90^{o} angle rather abruptly. This causes some electromagnetic pumping of the charged particles out of the arc conduction channel resulting in a high energy transfer rate from the arc and a consequent higher voltage drop across the arc.

(2) The arc must contact the anode on a narrow ring.

(3) The gas flow over the anode surface prevents a back flow from developing.

(4) The buffer electrode forces the gas to flow over the cathode at a high velocity near the tip so that good cooling in this region occurs, large quantities of charged particles are blown out of the cathode attachment regions, and the cathode operates as a field emitter over a wide range of current. Some difficulty was encountered in preventing

the arc current from passing through the buffer electrode. Careful contouring of the exit orifice on the buffer electrode eventually led to a configuration that performed reliably and reproducibly over a very wide range of gas enthalpy and power level. No modal transitions were detected at any time in this arc. The heater performed equally well on argon, helium, and nitrogen, although some difficulty was encountered in starting the discharge with the latter two types of gas. The measured performance characteristics are discussed in the following sections.

XII. 2. 1. Arc Potential Drop

The arc potential drop was found to depend upon the following variables:

(1) The arc current

(2) The gas mass flow rate

(3) The applied axial magnetic field strength.

A plot of a number of measurements made when the arc power was held fairly constant is shown in Figure 30. This graph indicates that the dependence of the arc potential drop on the magnetic field strength is quadratic, as may reasonably be expected.

Numerous attempts to obtain some reasonable correlation of the relation between the arc current and potential and gas mass flow rate finally led to the plot shown in Figures 31 and 32. In plotting the arc potential drop as a function of the average enthalpy of the gas, any attempt at separating out the dependence on arc current and gas mass flow rate individually is abandoned. This represents a rather fundamental departure from the methods used to analyze static arcs, where the plot

of arc voltage vs. arc current is considered to be the most important relation of the discharge performance characteristics. As seen in Figures 31 and 32, there is a considerable scatter of the points about the mean curves that are drawn, however, the correlation appears to be adequate to represent a valid relation.

The pressure in the arc chamber was raised only over the comparatively small range of from 1 to 3 atmospheres. Over this range, there was no detectable change in the arc potential that would indicate a dependence on the pressure, when the potential drop was plotted as a function of the average gas enthalpy. Figure 33 shows that it is possible to reduce the potential drop plot for any one gas to a single curve by assuming that the magnetic field influence is quadratic.

An explanation of the mechanism by which an increase in the axial magnetic field strength increases the arc potential drop is not immediately obvious. Since the current enters the anode at a point and is not spread symmetrically around the anode ring there is probably no tangential Hall current. Instead, there is probably an electric field set up across the diameter of the arc which will act to just compensate for the direct decrease in the electrical conductivity of the discharge path by the magnetic field so that no change in the resistance of the current path is to be expected.

If all of the discharge path were perpendicular to the axial magnetic field as in the annular channel configuration, then it would be reasonable to postulate that the increase in potential drop was due to an increase in the rotation rate of the column resulting in a reduction of column diameter due to the stronger cross-flow, thus increasing the

dissipation per unit length and the radial electric field. In the present configuration, however, it will be shown later that probably as much as 65 per cent of the overall potential drop occurs in the vicinity of the cathode, that is, along the axis of the applied magnetic field; hence it does not appear possible to explain all of the increase of the arc potential with increases in the magnetic field strength by using the argument outlined above.

Investigating other possible mechanisms to explain the increase in arc potential with the increasing magnetic field would involve a more thorough study of the manner by which most of the energy is transferred from the discharge to the gas and the actual positions in the arc where this occurs. In this respect, the following general observations are relevant.

(1) The similarity solution of Section IX. indicates that the power dissipation in the column falls very rapidly with increases in the column diameter for a given arc current. This indicates that one would expect the power dissipation to be highest in the contracted regions of the anode and cathode fall spaces.

(2) Coupled with the above energy transfer by thermal conduction to the gas away from the contracted portions of the arc, is the energy transfer out of these regions that occurs by electromagnetic pumping of the charged particles into the other parts of the discharge. This is a phenomenon that always occurs whenever a conducting column of plasma expands, resulting in a decrease of current density.

(3) The electron temperature in the contracted regions is always higher and in some cases higher by orders of magnitude, than

the heavy particle temperature, especially near the electrode surfaces. This results in a high production rate of charged particles. When these charged particles are removed from the contracted regions of the discharge by either gas dynamic forces or electromagnetic pumping or both, large amounts of energy are transferred from the electric field to the gas and a high percentage of the overall arc potential drop would be expected to occur in these regions.

In view of the above discussion, the following postulate is made: In the configuration shown in Figure 29 and in many other configurations of arc jet heaters, a high percentage of the electric-energy is transferred to the gas in the vicinity of the points where the discharge contacts the electrodes. The most important mechanism for transferring energy from the electric field to the gas is through the production of charged particles in these contracted regions and their subsequent injection into and recombination in the gas volume proper. In support of this conclusion the following experimental evidence is cited:

(1) Experiments reported in Reference 7 indicate that the total potential drop across the arc did not increase appreciably when the arc length was increased by as much as an order of magnitude. This indicates that the energy dissipated in the column was small compared to the total electrical energy transferred to the gas.

(2) It has been observed that when the electric discharge in a cylinder strikes to the wall near the cathode and does not rotate, then the gas flowing through the cylinder and around the arc is not heated appreciably and the point of attachment at the anode burns out quite

rapidly.

(3) In the electrode configuration shown in Figure 29, the spacing between the cathode and anode is only about 1/8 inches. Other experimenters have found that with electrode spacings an order of magnitude greater, the potential drop across the arc was much the same as was measured in the experiments reported here, when the average gas enthalpy and pressure was in the same range.

If we admit the above hypothesis, then we must next inquire into the manner by which the applied magnetic field can influence the production rate of charged particles in the contracted regions of the discharge near the electrodes. Independent of the mechanism involved, the first requirement is that the electrons in these regions be either raised to a higher temperature or maintained at their original temperature over a longer portion of the arc channel by the action of the applied magnetic field. Evidence from experiments with the retrograde motion of the cathode spot indicate that the former is the more likely phenomenon. In these experiments, there is a strong indication that increasing the applied magnetic field eventually raises the electron temperature in the cathode spot to the point where the electrons are energetic enough to doubly ionize the gas atoms that are present in that region.

It must be conceded, at this point, that there is as yet insufficient evidence to allow any definite statement to be made concerning the reason for the increase in the arc potential due to the applied mangetic field. The discussion above, as to the possible mechanisms involved, must be considered as highly speculative and to some extent intuitive. Efforts to analyse the contracted electrode regions of the discharge

are still quite crude as no consistent technique of handling the temperature difference between the electrons and the heavy gas particles has yet been devised.

Before leaving this particular aspect of the arc discharge-gas flow interaction problem, it should be mentioned that in devising a mechanism to explain the higher charged particle production rate in the presence of a magnetic field, it is essential to simultaneously account for the mechanism by which the particles are removed from the contracted arc regions and injected into the gas flow at the higher rate.

XII. 2. 2. Efficiency

The efficiency with which the electric energy is transferred from the electric discharge to the gas was somewhere between .60 and .85 for all types of gases and over all enthalpy levels. Typical efficiencies for some experiments in argon and helium are plotted in Figure 34.

XII. 2. 3. Rotation Rate of Arc and Gas

No measurements were made of the anode spot rotation rate.

Static pressure measurements were made in the arc chamber. These are shown in Figure 41 for some runs. At the lower mass flow values, there is a fairly consistent tendency for the same measurement as in Section XII. 1. 3. to be higher when the magnetic field strength is higher. This indicates that there is probably a considerable amount of tangential velocity induced in the gas by the anode spot rotation.

XIII. HEAT TRANSFER MEASUREMENTS

XIII. 1. Heat Transfer to Nozzle

Following the development of the arc heater described above, it was decided to carry out some heat transfer measurements using the hot gas from the generator. A number of two-inch long copper cylindrical channels were constructed with bell-mouth inlets and mounted downstream of the arc, as shown in Figures 29 and 47. These nozzles were insulated both thermally and electrically from the rest of the equipment and were cooled by a water jacket. The power delivered to the cooling water was accurately determined by measuring the water flow rate and the rise in the temperature of the water with thermocouples. Most of the experiments were conducted using argon gas, but helium gas was used during some runs. Each run consisted of setting the electric power level and changing the gas mass flow rate over a wide range. For this reason the gas enthalpy changed by a factor of 8 to 9 in going from the highest mass flow rate to the lowest mass flow rate. Many independent runs were made to see if any influence of the gas enthalpy on Nusselt number could be detected, but the result was always negative over the region where the gas average equilibrium temperature was between 2500°K and 10,500°K. No attempt was made, therefore, to include the gas enthalpy as a parameter in the presentation of the results.

The nozzles were short enough so that at no time was there a fully developed velocity profile for Poiseuille pipe flow. The heat transfer rate could therefore be considered as that across a boundary layer.

For this reason the measured values of heat transfer rate are compared to those computed from formulae derived from heat transfer studies across a boundary layer on a flat plate.

All of the quantities which were measured are plotted as a function of the free stream Reynolds number, defined as follows:

$$Re = (\dot{m}d/A\mu_{F.S.})$$

$\dot{m}$ mass flow rate of the gas

d diameter of the nozzle

A cross-sectional area of the nozzle

$\mu_{F.S.}$ viscosity of the gas atoms computed at the average equilibrium temperature of the free stream.

Each set of measurements were carried out over a Reynolds number range of 100 - 10,000.

The heat transfer measurements are presented in two ways. First, the measured ratio of power absorbed by the nozzle to the power in the gas is plotted vs. the Reynolds number. Second, a Nusselt number is computed and plotted as a function of the Reynolds number. The Nusselt number is defined as follows:

$$Nu = St \cdot Re \cdot Pr$$

where

Re Reynolds number as previously defined

St $(d/4\ell)(P_N/P_G)$ = Stanton number

ℓ length of nozzle

P_N power absorbed by the cooling water of the nozzle

P_G power in the gas = $\dot{m}\,h$

Pr $C_p \mu/\kappa$ = Prandtl number = .662 for argon

C_p specific heat of the gas atoms in the free stream

κ thermal conductivity of the gas atoms in the free stream

The values of the transport coefficients used in reducing the data were those of the gas atoms only. This was done so that a common reference for comparison with other experiments could be used, since there is still little uniformity in the manner by which the coefficients are evaluated for a partially ionized gas. The values of the transport properties that were used were taken from Reference 22.

As is indicated in Figure 35, four series of experiments were made. Since some axial magnetic field was necessary to have the arc function properly the minimum magnetic field in the arc region during the experiments was 1100 gauss. However, in the first two series of experiments the copper nozzle was surrounded by an iron annulus which reduced the magnetic field in the nozzle to less than 50 gauss. During the first set of experiments the nozzle was shorted through an ammeter to the anode and the current measured. Comparing the results of series 1 and series 2 on Figure 35 it is seen that the heat transfer rate was consistently higher when the current is allowed to flow between the nozzle and the anode. The heat transfer equation (IV-11) indicates that this is to be expected, since the current carries with it the enthalpy of the electrons, which is delivered to the nozzle as the electrons enter the surface. In addition, the electrons entering the nozzle fall through a potential which is approximately equal to the work function of the metal $|e|\chi$ and each electron that enters the nozzle thus contributes this additional energy to the heat transfer. When the nozzle is

shorted to the anode, we should expect that, in addition to the power transferred from the gas to the nozzle due to frictional heat transfer, the power $(5/2\ kT/|e| + \chi)\ I$ should also be transferred to the nozzle. If we assume that there is no interaction between these two heat transfer mechanisms, it is possible to compute the value of $5/2\ kT/|e| + \chi$ by comparing the values of P_N obtained from the measurements of series I and series 2 and measuring the current I in the former. When this is done it is found that $5/2\ kT/|e| + \chi \approx 3.6$ volts and that by subtracting the power $3.6I$ from P_N of series 1, the resulting values P_N' are identical to those obtained in series 2 within experimental error. This is shown in Figure 36, where the corrected values of P_N' for series 1 were used to compute the Nusselt number that is plotted there. Since the work function of pure copper is 4.4 volts it is tentatively concluded that the copper surface of the nozzle was probably oxidized or otherwise modified so that the electrons fell through only 3.6 volts upon entering the surface rather than the 4.4 electron volt work function of pure copper. (The 5/2 kT is negligible compared to $|e|\chi$.)

The series of measurements 3 and 4 were made in an effort to see if the magnetic field had any detectable influence on the heat transfer rate. Although some spread in the experimental points occurred, there was no consistent trend in the data which was obtained from a fairly extensive group of experiments to indicate any reduction of heat transfer rate as the magnetic field was increased. Since the magnetic field strength can have quite a pronounced influence on the state of the gas as it enters the nozzle, due to the interaction of the

gas flow with the rotating anode spot, it is not possible to make any conclusive statements as to the effect of the magnetic field upon the heat transfer rate in these experiments. It is tentatively concluded, however, that the spread in the data on Figures 36 and 37 is mainly due to rotation or unevenness induced in the gas flow by the rotating discharge, the rotation rate of which changes with the magnetic field strength.

Dotted lines, representing laminar and turbulent heat transfer rates computed from formulae derived from experiments on flat plates, are plotted on Figures 36, 37, and 38. These lines are introduced only in order to give some reference level from which to compare the measured values and are not intended to indicate the true or expected heat transfer rate in the configuration studied. In particular, it is conventional to define the various gas properties such as density and viscosity in terms of the wall temperature in flat plate experiments, whereas in the nozzle experiments carried out and reported here the gas properties used in computing the Reynolds and Nusselt numbers were calculated on the basis of the free stream temperature. In obtaining the laminar heat transfer rate plot the following two equations were used:

$$q = \frac{.29}{(P_r)^{2/3}(Re)_d^{1/2}} \left(\frac{d}{x}\right)^{1/2} \rho u h$$

q local heat transfer rate

Pr Prandtl number as previously defined

$(Re)_d$ Reynolds number as previously defined

$\rho u h = P_G/A$ = power density of gas flow

x distance along the channel

This equation was integrated along the channel length to give the expression that has been plotted, e. g.,

$$Nu = 0.580\,(d/\ell)^{\frac{1}{2}}\,(Re)_d^{\frac{1}{2}}\,(Pr)^{1/3} \quad .$$

Similarily for the turbulent section of the heat transfer rate curve, the local and integrated heat transfer rate equation that were used are

$$q = \frac{.023}{Pr^{2/3}\,(Re)_d^{1/5}}\,(d/x)^{1/5}\,(P_G/A)$$

$$Nu = .0288\,(d/\ell)^{1/5}\,(Re)_d^{4/5}\,Pr^{1/3} \quad .$$

Figure 38 indicates that when the heat transfer results are plotted as the Nusselt number vs. the Reynolds number, measurements using argon and helium gas give results that are identical to within the experimental error.

The results presented in Figures 36, 37, and 38 can be correlated to within about $\pm$ 10 per cent by the following expression

$$Nu = .285\,\left\{(d/\ell)(Re)_d\right\}^{2/3}$$

The line represented by this equation is plotted on Figures 36, 37, and 38. This equation can be written alternatively as

$$P_N/P_G = (1.14/Pr)\left\{\frac{\ell}{d\,(Re)_d}\right\}^{1/3}$$

This relation indicates that over the region of (d/ℓ) tested during these experiments, the fraction of the power in the gas that is transferred to the nozzle does not depend upon the nozzle diameter but only upon its length for a fixed mass flow rate. Further experiments should

be carried out to determine if this relation is true over a much wider range of (d/ℓ) nozzles.

XIII. 2. Electrical Measurements Connected with the Nozzle

In the first series of experiments a current that flowed from the anode to the nozzle was measured. The values obtained from a number of runs is plotted in Figure 40. Over the Reynolds number range of 400 - 1500 this current was as much as 1/4 of the current in the arc. At some higher Reynolds number the anode to nozzle current dropped off to practically zero and in some cases rose rapidly again for higher Reynolds numbers. During these measurements, no changes could be detected in the characteristics of the arc heater, hence it is unlikely that the arc current transferred partially to the nozzle when the high anode to nozzle current was measured, although this is one possible explanation for the surprisingly high value of this current. When the nozzle was electrically insulated from the rest of the equipment, its potential relative to the anode was measured by using a Volt-ohmyst vacuum tube volt meter. The nozzle potential was always negative with respect to the anode but it appeared to vary in magnitude in a fairly random manner. However, when the potential between the nozzle and the anode V_N was divided by the arc potential drop V, the ratio was found to be quite constant at a value of about 0. 35. The results of measurements on series runs 2, 3, and 4 in argon gas are plotted in Figure 39. The nozzle can be considered as a probe and hence the potential that it develops can differ from the plasma potential by only a few volts. This indicates that in the arc configuration used in these studies, the anode potential drop was about 35 per cent of the total arc

potential drop and that the remaining 65 per cent of the potential drop occurred in the cathode region and the column, if one developed. In general, this statement can be rephrased to say that 35 per cent of the electric energy was transferred to the gas in the anode drop region and that the remaining 65 per cent of the electric energy was transferred to the gas in the cathode drop region.

XIV. CONCLUSIONS AND RECOMMENDATIONS

The analysis and experiments reported in this paper can only be considered as a preliminary survey of the very complicated field of energy transfer processes in partially ionized gases.

In the analysis, some departures from existing theoretical results of the conduction and diffusion processes in a plasma were obtained. These are listed below with a brief discussion of the possibility of checking the predictions experimentally.

(1) An electric current in the direction of (E x B) x B is predicted from the treatment of the general diffusion equations. Some difficulty is anticipated in devising an experiment to check this result, since as yet, even the Hall currents in a plasma have not been accurately measured.

(2) It is predicted that a magnetic field can influence the thermal conductivity of a plasma directly only through controlling (a) the ambipolar diffusion rate of the charged particles, and (b) the thermal diffusion of the charged particles.

There is good reason to hope that this result will be checked experimentally in the near future. Studies of the radial energy transfer out of arcs with and without magnetic fields along the discharge axis are presently under way in several laboratories. Provided that instabilities do not occur that may mask the results, clarification of the magnetic field influence on heat transfer rate should soon be available from the results of these experiments.

(3) When the plasma temperature and pressure is such that the

charged particle density is not too far from its equilibrium value, it has been found that the ambipolar diffusion of the charged particles makes a major contribution to the thermal conductivity of the plasma. This is equivalent to the manner in which the atom diffusion in a molecular gas influences the thermal conductivity of the mixture when the gas temperature is high enough to form an appreciable number of atoms.

The experiment discussed in (2) above can be modified slightly to check the above point. When the gas pressure is reduced enough an axial magnetic field should be able to inhibit the radial diffusion of the charged particles and hence the manner in which this diffusion affects the thermal conductivity can be determined.

The analysis carried out in this report is inadequate to fully describe all of the relevant processes occurring in electric discharges. The modifications and additions to the theory that should be made are outlined below:

(1) The effect of radiation upon the transport properties of the plasma must be included in the phenomenological equations. This can be accomplished in an elegant manner by considering the effects of radiation as due to the motion of photon particles. This assumption allows one to consider the plasma as a four particle system and thus fit all radiation effects logically into the phenomenological equations.

(2) The fact that the electron mass is much smaller than that of the atoms and ions means that the electrons are loosely coupled energetically to these heavier particles. This raises two basic problems:

(a) The velocity distribution of the electrons will not usually be Maxwellian in the presence of an electric field.

(b) The average energy, or temperature of the electrons will usually be higher than that of the ions and atoms when energy is being transferred from an applied electric field to the gas.

Many aspects of these problems have been studied extensively by groups working with glow discharges and to some extent those studying electrode effects in arcs. The latest and most comprehensive investigation along these lines appears to be that of Wu in Reference 14. Considerably more work must be done on this subject before these effects can be introduced into the general transport equations or phenomenological relations for a plasma. A concentrated effort should be placed upon investigations along these lines, as a general formulation of the subject would form the framework within which one could treat electrode and gaseous breakdown phenomena in a logical and consistent manner.

A complete similarity solution for a cylindrically symmetric electric discharge has been worked out. A number of parameters that appear in the analysis are listed below:

(1) The first parameter indicates that the amount of radial pressure that the discharge can produce due to the arc self magnetic field depends only upon the type of gas, the static pressure at the outer edge of the discharge and the temperature along the axis of the discharge.

(2) The second similarity parameter indicates that the power per unit length that the discharge can dissipate depends only upon the

type of gas and the temperature on the axis of the discharge.

(3) The third parameter indicates that for a given total current, the temperature on the axis of the discharge increases as the radius of the channel confining the discharge decreases.

Using the transport coefficients that have been computed in Appendix 1, the E - I characteristic for a confined arc in argon has been evaluated. The calculated curve is compared with an experimentally determined curve from Reference 30. The electric field in the experimental curve is roughly twice that computed from the theory, over most of the range of current. In general, this indicates that the electrical conductivity of the gas is actually somewhat lower, probably by about a factor of 2, than the computed value. More experimental evidence and analytical studies are required before this conclusion can be justified. Once the experimental results are considered to be completely reliable, then this experiment can be used to accurately measure the thermal and electrical conductivities of the plasma over a temperature range of $10,000^{\circ}K$ to about $100,000^{\circ}K$.

A study of the sheath structure that forms on walls that are in contact with hot plasmas is of importance from the standpoint of interpreting probe measurements and also in studying electrode behavior. The sheath that develops between a hot plasma and a cold wall when the gas is not too far from equilibrium has been analysed and found to have the following characteristics:

(1) A potential well develops between the gas and the wall when $(\frac{V_I}{2} - \chi) > 0$. The depth of the well is approximately $(\frac{V_I}{2} - \chi)$ volts and can effectively form an insulating layer between the wall and the

plasma.

(2) One side of the well extends out only a Debye distance from the wall. This part of the sheath can be influenced by space charge accumulation on the wall. The other side of the potential well extends into the plasma a distance that is controlled by the temperature gradient and hence by the configuration under study. This part of the potential well structure can only be controlled by changing the temperature gradients near the wall either by gasdynamic techniques or by changing the current density normal to the wall.

The experiments conducted with a concentric electrode arc heater in which the discharge was made to spin by an applied axial magnetic field indicated that this configuration embodies numerous serious defects, some of which are indicated below.

(1) The tangential gas flow which the rotating discharge sets up induces a secondary flow of hot gas along the electrode surfaces which results in serious energy losses and may burn out insulators between the electrodes.

(2) It is necessary to position the discharge axially by some mechanical technique, since it tends to blow out of the annulus. Experience has shown that at one atmosphere pressure or higher, it is not feasible to use an insulated ring as one electrode in order to axially position the discharge, since the hot gas very quickly burns up the insulation.

(3) High amplitude oscillations are encountered in the discharge potential and this, coupled with transient electrode phenomena, tend to make the arc behave in an erratic manner, that gives poor and uneven heating to the gas.

These defects occur in an annular configuration. When the electrode configuration was changed so that a point cathode aligned along the axis of the magnetic field was made to discharge to a ring anode on which the anode spot rotated rapidly due to the magnetic field, a marked improvement in the performance of this device as an arc heater occurred. Some of the characteristics of this configuration are summarized below.

(1) The potential drop across the arc depends only upon the average gas enthalpy for a given magnetic field strength.

(2) The arc voltage drop increases quadratically with the magnetic field strength for a given value of the average gas enthalpy.

(3) Over the range of pressure that the device was operated, no dependence of the potential drop on the pressure could be detected.

(4) The energy was transferred from the electric field to the gas with an efficiency of between 60 and 85 per cent.

A number of tentative conclusions can be drawn concerning the manner in which the energy is transferred to the gas from the discharge. These are based upon the results of the analysis, the experiments and some intuitive hypotheses.

(1) Arc columns in general can dissipate only a few kilowatts of power per centimeter of length when the temperature on the axis of the discharge is under $20,000^{\circ}K$.

(2) The production of charged particles in regions of the discharge where the electron temperature is considerably higher than the heavy gas particle temperature and their injection into the volume of the gas is a powerful means of transferring large quantities of energy

to the gas over very small areas and as such can account for most of the energy transfer from the discharge to the gas that occurs in many arc heater configurations.

(3) If it is desirable or necessary to use the arc column as the major heat source in the electric discharge, then the diameter of the column should be kept as small as possible. Rotating the column through the gas by using a transverse magnetic field is probably the best method of accomplishing this.

REFERENCES

1. Finkelnberg, W. and H. Maecker: Electric Arcs and Thermal Plasma. Handbuch der Physik, Vol. 22, pp. 254-494, Springer-Verlag, Germany, 1956.

2. Giannini, G. M.: The Plasma Jet. Scientific American, Vol. 196, pp. 80-84, 86, 88, (1957).

3. Browning, J. A.: Techniques for Producing Plasma Jets, "Dynamics of Conducting Gases". Northwestern University Press, Evanston, Illinois, 1960, pp. 126-138.

4. Vidya, Inc.: Arc Wind Tunnel Simulates Reentry. Aviation Week, Vol. 73, No. 13, p. 110, September 26, 1960.

5. John, R. R. and W. L. Bade: Recent Advances in Electric Arc Plasma Generation Technology. ARS Journal, Vol. 31, No. 1, pp. 4-17, January, 1961.

6. McGregor, W. K.: Performance of a D. C. Arc Excited Plasma Generator. USAF, AEDC TN 60-112, August, 1960.

7. Ducati, A. C. and G. L. Cann: Propulsion Properties of High Intensity Plasma Jets. AFOSR TN 57-748, February, 1958.

8. Cann, G. L. and A. C. Ducati: Energy Content and Ionization Level in an Argon Gas Jet Heated by a High Intensity Arc. Journal of Fluid Mechanics, Vol 4, pp. 529-537, (1958).

9. Brogan, T. R.: Preliminary Evaluation of Helium as an Electric Arc Heated Propellant. ARS Journal, Vol. 29, No. 9, pp. 662-663, September, 1959.

10. Clauser, F.: Plasma Dynamics. Chapter 5, Addison-Wesley Publishing Company, Inc., Reading, Massachusetts, 1960.

11. Chapman, D. S. and I. G. Cowling: The Mathematical Theory of Non-Uniform Gases. Cambridge University Press, 1953.

12. Spitzer, L., Jr.: Physics of Fully Ionized Gases. Interscience Publishers, New York, N. Y., 1956.

13. Pipkin, A. C.: The Electrical Conductivity of a Partially Ionized Gas. University of Maryland, TN BN-170, April, 1959.

14. Wu, Cheng-Sheng: The Effect of the Orientation of Electric and Magnetic Fields on the Electron Mean Energy and Drift Velocity in a Partially Ionized Gas. Proc. Royal Society, Series A, Vol. 259, pp. 518-530, December, 1960.

15. Hirschfelder, J. O.; C. F. Curtiss; R. B. Bird: The Molecular Theory of Gases and Liquids. John Wiley and Sons, New York, N. Y., 1954.

16. De Groot, S. R.: Thermodynamics of Irreversible Processes. Interscience Publishers, Inc., New York, N. Y., 1952.

17. Sommerfeld, A.: Thermodynamics and Statistical Mechanics. Academic Press, Inc., New York, N. Y., 1956.

18. Fowler, R.: Statistical Mechanics. 2nd ed., Cambridge University Press, 1955.

19. Von Engel, A.: Ionized Gases. Clarendon Press, Oxford, 1955.

20. Lehnert, B.: Diffusion Processes in the Positive Column in a Longitudinal Magnetic Field. Second United Nations International Conference on the Peaceful Uses of Atomic Energy. United Nations, Geneva, 1958.

21. Green, H. S.: Ionic Theory of Plasmas and Magnetohydrodynamics. Physics of Fluids, Vol. 2, No. 4, pp. 341-349, July-August, 1959.

22. Amdur, I. and E. A. Mason. Properties of Gases at Very High Temperatures. The Physics of Fluids, Vol. 1, No. 5, pp. 370-383, September-October, 1958.

23. Loeb, L. B.: Basic Processes of Gaseous Electronics. University of California Press, Berkeley, California, 1955.

24. Powers, W. E. and R. M. Patrick: Engineering Aspects of Magnetohydrodynamics. University of Pennsylvania, Philadelphia, Pennsylvania, March 9 and 10, 1961.

25. Early, H. C. and W. G. Dow: Preliminary Research on a Low Pressure Ionic Wind Tunnel. University of Michigan, Memorandum No. 41, 1949.

26. Sommerfeld, A.: Electrodynamics. Academic Press, Inc., New York, N. Y., 1952.

27. Sommerfeld, A.: Mechanics of Deformable Bodies. Academic Press, Inc., New York, N. Y., 1950.

28. Fowler, R. and E. A. Guggenheim: Statistical Thermodynamics. Cambridge University Press, 1956.

29. Maecker, H.: Uber die Charakteristiken zylindrischen Bögen. Zeitschrift für Physik, Vol. 157, pp. 1-29, 1959.

30. Maecker, H.: Messung und Auswertung von Bogenscharakteristiken (Ar, N_2). Zeitschrift für Physik, Vol. 158, pp. 392-404, 1960.

31. Spitzer, L., Jr. and R. Härm: Transport Phenomena in a Completely Ionized Gas. Physical Review, Vol. 89, No. 5, pp. 977-981, March, 1953.

32. Princeton Series, Vol. I: Editor: F. D. Rossini: Thermodynamics and Physics of Matter. Princeton, New Jersey, 1955.

33. Lin, S. C.; E. L. Resler; A. Kantrowitz: Electrical Conductivity of Highly Ionized Argon Produced by Shock Waves. Journal of Applied Physics, Vol. 26, No. 1, pp. 95-109, January, 1955.

34. Olsen, H. N.: Thermal and Electrical Properties of an Argon Plasma. The Physics of Fluids, Vol. 2, No. 6, pp. 614-623, November-December, 1959.

APPENDIX 1

TRANSPORT COEFFICIENTS OF A PARTIALLY IONIZED GAS

1.1. Calculation of the Transport Coefficients for a Partially Ionized Gas

The Chapman-Enskog treatment of the Boltzman equation has developed an expansion in Sonine polynomials that can be used to evaluate the transport coefficients of a gas mixture to any desired accuracy[2]. From this analysis, Hirschfelder, Curtiss, and Bird have derived a set of determinants that can be used to compute the first approximation to the coefficients. Correction terms for the calculation of some of the second approximations have also been worked out. When more than two components are present in the gas mixture the evaluation of the general expression for the transport coefficients becomes extremely tedious and in many cases is not feasible without undue expenditure of time and effort. A method of computing the viscosity and thermal conductivity coefficients approximately is obtained by expanding the respective determinants and keeping only the dominant term. This approach was suggested by an empirical equation for the viscosity of a multicomponent mixture derived by J. W. Buddenberg and C. R. Wilke and described in Reference 15, page 532. The multiple diffusion coefficients are computed exactly and then some approximations are made to simplify the expressions. Approximate expressions are computed for the thermal diffusion coefficients.

1.1.1. Interaction Cross-Sections and Transport Coefficient Parameters

In order to calculate the transport properties in a gas mixture, it is shown in Reference 15 page 524 that six interaction parameters for each type of collision must be computed. In the formulas that will be used later, these parameters are divided by the equivalent value for a binary collision involving rigid spherical particles. Numerous models, representing binary collisions between atoms-atoms, atoms-molecules, atoms-ions, etc., can be found in the literature. In particular, I. Amdur and E. A. Mason[22] have computed the transport coefficients for the noble gas atoms up to 15,000°K using data from molecular beam experiments to evaluate the constants of their collision models.

If it is assumed that the long range forces account for most of the collisions between ions and atoms then a simple theory of the interaction of the ions charge with the induced dipole of the colliding atom indicates that an inverse 5th power law holds for the collision and that the kinetic theory of "Maxwell molecules" adequately describes the relevant transport coefficients for ion-atom interactions. In this section the six parameters will be computed for particles with coulomb interaction only. When no other data is available it will be assumed that all other types of collisions can be adequately represented by the rigid spherical model interactions. These six interaction parameters make it possible to calculate the coefficients of viscosity, thermal conductivity and diffusion to a first approximation in a multiple component gas mixture. However, in order to obtain equal accuracy for

all three coefficients it is necessary to use the second approximation to the binary diffusion coefficients. As shown by Spitzer in Reference 31, when this is done the diffusion coefficient for the electrons in a completely ionized gas as computed by the Chapman-Enskog procedure agrees with that computed using the approach of Reference 31 to within a few per cent.

The Chapman-Enskog treatment of the Boltzmann equations gives the required relationship between the parameters of the binary collision and the transport coefficient parameters. The three necessary relations are

$$\chi(g,b) = \pi - 2b \int_{r_m}^{\infty} \frac{dr/r^2}{\left\{1 - b^2/r^2 - \frac{\phi(r)}{\frac{1}{2} m_{12} g^2}\right\}^{1/2}} \qquad \text{(A1-1)}$$

$$Q_{12}^{l}(g) = 2\pi \int_0^{\sigma_{12}} (1 - \cos^l \chi)\, b\, db \qquad \text{(A1-2)}$$

$$\Omega_{12}^{(l,s)}(T) = \left(\frac{kT}{2\pi m_{12}}\right)^{1/2} \int_0^{\infty} e^{-\eta} \eta^{s+1} Q_{12}^{l}(\eta) \frac{d\eta}{2} \qquad \text{(A1-3)}$$

The various symbols are defined as follows:

χ	angle of deflection of the particles upon collision
g	relative velocity of the two particles
b	distance of closest approach of the two particles
$\phi(r)$	potential energy of interaction of the two particles
m_{12}	reduced mass of the particles $= \dfrac{m_1 m_2}{m_1 + m_2}$
η	$\dfrac{\frac{1}{2} m_{12} g^2}{k T}$

Some differences in definition occur between Hirschfelder, Curtiss, and Bird and Chapman and Cowling. The definitions shown above are those adopted by the former. Since it is desirable to use the two references interchangeably, the following relationship occurs between the definitions occurring in both books:

$$Q_{12}^{(l)} = \frac{2\pi}{g}\,\phi_{12}^{(l)}$$

$$\Omega_{12}^{(l,s)}(T) = \Omega_{12}^{l}(s)$$

Since the term "cross-section" is used by many authors to mean any one of many different quantities that are used in this paper, a list of the most commonly used relations and their usual name is given below.

$$Q_{12}^{\circ}(g) = 2\pi \int_0^{\sigma_{12}} b\,db = \pi \sigma_{12}^{2}(g)$$

is the total collision cross-section for particles of relative velocity g.

$$Q_{12}^{'}(g) = 2\pi \int_0^{\sigma_{12}} (1-\cos\chi)\, b\,db$$

is the diffusion collision cross-section for particles of relative velocity g.

$$Q_{12}^{2}(g) = 2\pi \int_0^{\sigma_{12}} (1-\cos^2\chi)\, b\,db$$

is the momentum collision cross section for particles of relative velocity g. Since all of the above cross-sections are defined for a given relative particle velocity, they are not convenient to use when the particles have a Maxwell velocity distribution. For this reason a quantity is defined as the reference collision cross-section as follows:

$$g_{12}(T) = \frac{\Omega_{12}^{(1,1)}}{[\Omega_{12}^{(1,1)}]_{R.S}} \pi \sigma_{12}^2$$

1.1.1.1. Rigid Spherical Model

The generalized interaction cross-sections is defined as

$$[Q_{12}^{\ell}]_{R.S.} = \left[1 - \frac{1}{2}\frac{1+(-1)^{\ell}}{1+\ell}\right] \pi \sigma_{12}^2 \qquad \text{(A1-4)}$$

The subscript R. S. denotes the rigid spherical model. The interaction parameters are defined as follows:

$$[\Omega_{12}^{\ell,s}]_{R.S.} = \left(\frac{kT}{2\pi m_{12}}\right)^{1/2} \frac{(s+1)!}{2} [Q_{12}^{\ell}]_{R.S.} \qquad \text{(A1-5)}$$

These quantities are used to non-dimensionalize the values that occur for other collision models. The following notation is used:

$$Q_{12}^{\ell} / [Q_{12}^{\ell}]_{R.S.} = Q_{12}^{\ell *} \qquad \text{(A1-6)}$$

$$\Omega_{12}^{\ell,s} / [\Omega_{12}^{\ell,s}]_{R.S.} = \Omega_{12}^{\ell,s *} \qquad \text{(A1-7)}$$

$$\Omega_{12}^{(1,1)*} \pi \sigma_{12}^2 = g_{12} = \text{reference cross-section} \qquad \text{(A1-8)}$$

It will be necessary to evaluate these parameters for ℓ = 1, 2, and s = 1, 2, 3.

1.1.1.2. Coulomb Interactions

When the force between two particles is given by $F = \frac{e_1 e_2}{4\pi\varepsilon_0 r^2}$ the required cross-sections are given in Reference 11, page 178, by

$$Q_{12}^{(1)} = \frac{\pi}{2}\left(\frac{e_1 e_2}{4\pi\varepsilon_0 \frac{1}{2} m_{12} g^2}\right)^2 \ln\left(1 + 4 y_0'^2\right) \qquad \text{(A1-9)}$$

$$Q_{12}^{(2)} = \pi\left(\frac{e_1 e_2}{4\pi\varepsilon_0 \frac{1}{2} m_{12} g^2}\right)^2 \left\{\ln\left(1 + 4 y_0'^2\right) - \frac{4 y_0'^2}{1 + 4 y_0'^2}\right\} \qquad \text{(A1-10)}$$

In the above expressions the quantity y' is defined as follows:

$$y_0' = \frac{4\pi\varepsilon_0 kT}{e_1 e_2} d\eta = \frac{d\eta}{f_p} \qquad \text{(A1-11)}$$

$$f_p = \frac{e_1 e_2}{4\pi\varepsilon_0 kT} \qquad \text{(A1-12)}$$

Before the quantities $\Omega_{12}^{(l,s)}$ can be evaluated a number of assumptions must be made. The first is simple and causes no trouble:

$$4\, y_0'^2 >> 1 \quad .$$

For any reasonable assumption concerning d this relation is always true. The next problem is to determine the value of d. Most authors put d equal to the Debye shielding distance of the electrons. For the time being the value of d will be left arbitrary and given a dependence on the relative velocity of the colliding particles as follows:

$$d = b^{1+m}\left(\frac{\eta}{f_p}\right)^m \qquad \text{(A1-13)}$$

With these relations the logarithmic terms in the cross-sections reduces to the following expression:

$$\ln\left(1 + 4 y_0'^2\right) = \ln 4\left(\frac{b\eta}{f_p}\right)^{2(1+m)} \qquad \text{(A1-14)}$$

The cross-sections can now be simplified as follows:

$$Q_{12}^{1} = \pi f^2 \frac{(1+m)}{\eta^2} \ln\left(\frac{1}{2^{1+m}} \frac{b\eta}{f}\right) \tag{A1-15}$$

$$Q_{12}^{2} = 2\pi f^2 \frac{(1+m)}{\eta^2} \ln\left\{\left(\frac{4}{2.718}\right)^{\frac{1}{2(1+m)}} \frac{b\eta}{f}\right\} \tag{A1-16}$$

The interaction parameters are obtained from the integration of Eq. (A1-3) non-dimensionalized by Eq. (A1-5) as follows:

$$\Omega_{12}^{l,s} = \frac{\int_0^\infty e^{-\eta} \eta^{1+s} Q_{12}^{l}(\eta)\, d\eta}{(s+1)!\left[1 - \frac{1+(-1)^l}{2(1+l)}\right]\pi \sigma_{12}^2} \tag{A1-17}$$

Two types of integrals occur in Eq. (A1-17), the solutions of which are shown below:

$$\int_0^\infty e^{-\eta} \eta^k\, d\eta = k! \tag{A1-18a}$$

$$\int_0^\infty e^{-\eta} \eta^k \ln \eta\, d\eta = k\, g(k-1) + (k-1)! = g(k) \tag{A1-18b}$$

$g(0) = - C_\varepsilon = -.5772$

$g(1) = 1 - C_\varepsilon$ Euler's constant

$g(2) = 2(1 - C_\varepsilon) + 1$.

Using these relations and the $Q_{12}^{l}(\eta)$ of Eqs. (A1-15) and (A1-16) the following expressions are obtained for the interaction parameters.

$$\Omega_{12}^{1,1*}\pi\sigma_{12}^2 = \pi f^2 \frac{1+m}{2}\left\{\ln\left(2^{\frac{1}{1+m}}\frac{b}{f_0}\right) - c_\varepsilon\right\}$$

$$\Omega_{12}^{1,2*}\pi\sigma_{12}^2 = \pi f^2 \frac{1+m}{6}\left\{\ln\left(2^{\frac{1}{1+m}}\frac{b}{f_0}\right) + 1 - c_\varepsilon\right\}$$

$$\Omega_{12}^{1,3*}\pi\sigma_{12}^2 = \pi f^2 \frac{1+m}{24}\left\{2\ln\left(2^{\frac{1}{1+m}}\frac{b}{f_0}\right) + 3 - 2c_\varepsilon\right\} \qquad \text{(A1-19a)}$$

$$\Omega_{12}^{2,2*}\pi\sigma_{12}^2 = \pi f^2 \frac{1+m}{2}\left\{\ln\left[\left(\frac{4}{2.718}\right)^{\frac{1}{2(1+m)}}\frac{b}{f_0}\right] + 1 - c_\varepsilon\right\}.$$

The combinations of these parameters needed most are given below:

$$A_{12}^* = \frac{\Omega_{12}^{2,2*}}{\Omega_{12}^{1,1*}} = \frac{\ln\left[\left(\frac{4}{2.718}\right)^{\frac{1}{2(1+m)}}\frac{b}{f_0}\right] + 1 - c_\varepsilon}{\ln\left[2^{\frac{1}{1+m}}\frac{b}{f_0}\right] - c_\varepsilon}$$

$$B_{12}^* = \frac{5\Omega_{12}^{1,2*} - 4\Omega_{12}^{1,3*}}{\Omega_{12}^{1,1*}} = \frac{\ln\left[2^{\frac{1}{1+m}}\frac{b}{f_0}\right] + \frac{2}{3} - c_\varepsilon}{\ln\left[2^{\frac{1}{1+m}}\frac{b}{f_0}\right] - c_\varepsilon} \qquad \text{(A1-20)}$$

$$C_{12}^* = \frac{\Omega_{12}^{1,2*}}{\Omega_{12}^{1,1*}} = \frac{1}{3}\,\frac{\ln\left[2^{\frac{1}{1+m}}\frac{b}{f_0}\right] + 1 - c_\varepsilon}{\ln\left[2^{\frac{1}{1+m}}\frac{b}{f_0}\right] - c_\varepsilon}$$

1.1.1.3. Interactions for Ramsauer Effect Collisions

The electron-atom collisions in argon exhibit an anomalous behavior which can be explained by the phase changes in the quantum theory of collisions. The total collision cross-section and diffusion collision cross-section have been computed and measured over a wide energy range. In order to compute the interaction parameters for argon atom-electron collisions, the experimental curve for $Q_{e,a}'$ is fitted by the following function up to about 30 e. v.

$$Q'_{e,a} = \left\{ 4.83\, e^{-.82x} - 4.03 + 1.956\, x - .0489\, x^2 \right\} \times 10^{-20}\ m^2$$

$$x = (kT/.64\ e)\eta\ ;$$

$$Q^2_{e,a} = 1.034\ Q'_{e,a}$$

Although $Q'_{e,a}$ in the above function goes negative for $x > 40$, this does not affect the integrals up to temperature of 20,000°K. The expressions for the interaction parameters are shown below:

$$\Omega^{1,1*}_{e,a}\pi\sigma^2_{e,a} = q_{e,a} = \left\{ \frac{4.83}{(1+.82p_1)^3} - 4.03 + 5.868p_1 - .586p_1^2 \right\} \times 10^{-20}\ m^2$$

$$\Omega^{1,2*}_{e,a}\pi\sigma^2_{e,a} = \left\{ \frac{4.83}{(1+.82p_1)^4} - 4.03 + 7.824p_1 - .978p_1^2 \right\} \times 10^{-20}\ m^2$$

$$\Omega^{1,3*}_{e,a}\pi\sigma^2_{e,a} = \left\{ \frac{4.83}{(1+.82p_1)^5} - 4.03 + 9.78p_1 - 1.467p_1^2 \right\} \times 10^{-20}\ m^2 \qquad \text{(A1-19b)}$$

$$\Omega^{2,2*}_{e,a}\pi\sigma^2_{e,a} = 1.551 \left\{ \frac{4.83}{(1+.82p_1)^4} - 4.03 + 7.824p_1 - .978p_1^2 \right\} \times 10^{-20}\ m^2$$

$$p_1 = \frac{kT}{.64|e|}$$

Values of $q_{e,a}$, $A^*_{e,a}$, $B^*_{e,a}$, $C^*_{e,a}$, etc. are tabulated in Table 1.

1.1.1.4. Interactions for He-Atoms-Electron Collisions

Since no simple model can be found to represent the electron-helium atom interactions, they are treated in a manner similar to the argon atoms-electrons interactions. The diffusion cross-section curves from page 15 of Massey and Burhop is represented by the following equation:

$$Q'_{e,a} = \left\{ 5.0\, e^{-.035 p_2 \eta} + 1.20\, p_2 \eta\, e^{-.40 p_2 \eta} \right\} \times 10^{-20} \ m^2$$

$p_2 = (kT/|e|)$.

The momentum cross-section is postulated to follow the relation for particles interacting with an inverse 5th power law

$$Q^{(2)}_{e,a} = 1.034\, Q'_{e,a}$$

Using these cross-sections, the following interaction parameters are computed

$$\Omega^{1,1}_{e,a} \pi \sigma^2_{e,a} = g_{e,a} = \left\{ \frac{5.00}{(1+.035 p_2)^3} + \frac{3.60 p_2}{(1+.40 p_2)^4} \right\} \times 10^{-20} \ m^2$$

$$\Omega^{1,2}_{e,a} \pi \sigma^2_{e,a} = \left\{ \frac{5.00}{(1+.035 p_2)^4} + \frac{4.80 p_2}{(1+.40 p_2)^5} \right\} \times 10^{-20} \ m^2 \qquad \text{(A1-19c)}$$

$$\Omega^{1,3}_{e,a} \pi \sigma^2_{e,a} = \left\{ \frac{5.00}{(1+.035 p_2)^4} + \frac{6.00 p_2}{(1+.40 p_2)^6} \right\} \times 10^{-20} \ m^2$$

$$\Omega^{2,2}_{e,a} \pi \sigma^2_{e,a} = 1.551 \left\{ \frac{5.00}{(1+.035 p_2)^4} + \frac{4.80 p_2}{(1+.40 p_2)^5} \right\} \times 10^{-20} \ m^2$$

Values of $g_{e,a}$, $A^*_{e,a}$, $B^*_{e,a}$, $C^*_{e,a}$, etc. for the helium atom-electron interaction are tabulated in Table 2.

1.1.2. Transport Parameters

In calculating the transport coefficients in a gas mixture three generalized parameters are useful. The first is the second approximation to the binary diffusion coefficient and is defined below:

$$\mathcal{D}_{ij} = \frac{3}{16}\left(\frac{2\pi kT}{m_{ij}}\right)^{1/2} \frac{f_{ij}^{(2)}}{n\, q_{ij}} \qquad \text{(A1-21)}$$

The second parameter is the first approximation to the viscosity of a pure substance when i = j and is defined as follows:

$$\eta_{ij} = \frac{5}{32}\left(\frac{2\pi kT}{m_{ij}}\right)^{1/2} \frac{m_{ij}}{A_{ij}^{*}\, q_{ij}} \qquad \text{(A1-22)}$$

The third quantity is the first approximation to the thermal conductivity of a pure substance when i = j and is defined as follows:

$$[\kappa_{ij}]_{J=0} = \frac{75}{128}\left(\frac{2\pi kT}{m_{ij}}\right)^{1/2} \frac{k}{A_{ij}^{*}\, q_{ij}} \qquad \text{(A1-23)}$$

The quantity m_{ij} is the reduced mass defined by $m_{ij} = \dfrac{m_i\, m_j}{m_i + m_j}$.

The parameter q_{ij} is the reference collision cross-section for the interactions of particles of type i and type j. The term $f_{ij}^{(2)}$ is the correction term applied to the first approximation of the binary diffusion coefficient to obtain the second approximation.

1.1.3. Calculation of $f_{12}^{(2)}$

In order to calculate the second approximation to the binary diffusion coefficient it is necessary to evaluate the quantity defined below.

$$f_{12}^{(2)} = \frac{1}{1 - \Delta_{12}} \qquad \text{(A1-24)}$$

$$\Delta_{12} = \frac{(6\, C_{12}^{*} - 5)^2\, 2f}{60(X_\kappa + Y_\kappa)} \qquad \text{(A1-25)}$$

$$\mathcal{H} = \frac{1}{(n_1+n_2)^2}\left[\frac{n_1^2}{\mathcal{K}_{11}}\frac{m_1}{m_2} + \frac{2n_1n_2}{\mathcal{K}_{12}}\left\{1+\frac{15}{8A_{12}^*}\frac{(m_1-m_2)^2}{m_1m_2}\right\} + \frac{n_2^2}{\mathcal{K}_{22}}\frac{m_2}{m_1}\right]$$

$$X_\chi = \frac{1}{(n_1+n_2)^2}\left[\frac{n_1^2}{\mathcal{K}_{11}} + \frac{2n_1n_2}{\mathcal{K}_{12}} + \frac{n_2^2}{\mathcal{K}_{22}}\right] \qquad \text{(A1-26)}$$

$$Y_\chi = \frac{1}{(n_1+n_2)^2}\left[\frac{n_1^2}{\mathcal{K}_{11}}U^{(1)} + \frac{2n_1n_2}{\mathcal{K}_{12}}U^{(\gamma)} + \frac{n_2^2}{\mathcal{K}_{22}}U^{(2)}\right]$$

$$U^{(1)} = \frac{4}{15}A_{12}^* - \frac{1}{12}\left(\frac{12}{5}B_{12}^*+1\right)\frac{m_1}{m_2} + \frac{1}{2}\frac{(m_1-m_2)^2}{m_1m_2} \qquad \text{(A1-27)}$$

$$U^{(2)} = \frac{4}{15}A_{12}^* - \frac{1}{12}\left(\frac{12}{5}B_{12}^*+1\right)\frac{m_2}{m_1} + \frac{1}{2}\frac{(m_2-m_1)^2}{m_1m_2}$$

$$U^{(\gamma)} = \frac{4}{15}A_{12}^*\left\{\frac{(m_1+m_2)^2}{4m_1m_2}\frac{\mathcal{K}_{12}^2}{\mathcal{K}_{11}\mathcal{K}_{22}}\right\} - \frac{1}{12}\left(\frac{12}{5}B_{12}^*+1\right) - \frac{5}{32A_{12}^*}\left(\frac{12}{5}B_{12}^*-5\right)\frac{(m_1-m_2)^2}{m_1m_2}$$

This expression will be evaluated for the following collision models.

(1) Electron-ion -- coulomb interaction

(2) Electron-atom -- arbitrary interaction

(3) Ion-atom -- rigid spherical interaction.

1.1.3.1. Calculation of $f_{12}^{(2)}$ when the First Particle is an Electron

$$\mathcal{H} = \frac{1}{(n_1+n_2)^2\mathcal{K}_{12}m}\left[\frac{15}{4}\frac{n_1n_2}{A_{12}^*} + n_2^2\frac{\mathcal{K}_{12}}{\mathcal{K}_{22}}\right]. \qquad \text{(A1-28)}$$

$$U^{(1)} \approx \frac{1}{2m} \qquad \text{(A1-29)}$$

$$U^{(2)} \approx \frac{1}{2m}\left(\frac{5}{6} - \frac{2}{5}B_{12}^*\right) \qquad \text{(A1-30)}$$

$$U^{(Y)} = \frac{1}{2m}\left[\frac{2}{15}\frac{A_{12}^{*}\mathcal{K}_{12}^{2}}{\mathcal{K}_{11}\mathcal{K}_{22}} - \frac{5}{16A_{12}^{*}}\left(\frac{12}{5}B_{12}^{*}-5\right)\right] \tag{A1-31}$$

Investigating the order of magnitude of the various terms, one finds that $X_{\mathcal{K}} \approx m Y_{\mathcal{K}}$ hence $X_{\mathcal{K}}$ is neglected relative to $Y_{\mathcal{K}}$.

$$Y_{\mathcal{K}} = \frac{1}{2m(m_1+m_2)^2\mathcal{K}_{12}}\left[m_1^2\frac{\mathcal{K}_{12}}{\mathcal{K}_{11}} + m_2^2\left(\frac{5}{6}-\frac{2}{5}B_{12}^{*}\right)\frac{\mathcal{K}_{12}}{\mathcal{K}_{22}} + 2m_1m_2\left\{\frac{2}{15}\frac{A_{12}^{*}\mathcal{K}_{12}^{2}}{\mathcal{K}_{11}\mathcal{K}_{22}} - \frac{5}{16A_{12}^{*}}\left(\frac{12}{5}B_{12}^{*}-5\right)\right\}\right] \tag{A1-32}$$

Substituting these expressions into Eq. (A1-21), the following relation is obtained:

$$\frac{1}{\Delta_{12}} = \frac{30\left[m_1^2\frac{\mathcal{K}_{12}}{\mathcal{K}_{11}} + m_2^2\left(\frac{5}{6}-\frac{2}{5}B_{12}^{*}\right)\frac{\mathcal{K}_{12}}{\mathcal{K}_{22}}\right]}{(6C_{12}^{*}-5)^2\left(\frac{15}{4}\frac{m_1m_2}{A_{12}^{*}} + m_2^2\frac{\mathcal{K}_{12}}{\mathcal{K}_{22}}\right)} + \frac{60m_1m_2\left[\frac{2}{15}\frac{A_{12}^{*}\mathcal{K}_{12}^{2}}{\mathcal{K}_{11}\mathcal{K}_{22}} - \frac{5}{16A_{12}^{*}}\left(\frac{12}{5}B_{12}^{*}-5\right)\right]}{(6C_{12}^{*}-5)^2\left(\frac{15}{4}\frac{m_1m_2}{A_{12}^{*}} + m_2^2\frac{\mathcal{K}_{12}}{\mathcal{K}_{22}}\right)} \tag{A1-33}$$

Case I -- Electron-ion Interaction

$$A_{12}^{*} = A_{11}^{*} = A_{22}^{*}$$

$$B_{12}^{*} \approx 1 \quad ; \quad C_{12}^{*} \approx \frac{1}{3}$$

$$\frac{\mathcal{K}_{12}}{\mathcal{K}_{11}} = \frac{1}{\sqrt{2}}$$

$$\frac{\mathcal{K}_{12}}{\mathcal{K}_{22}} \approx \frac{1}{\sqrt{2m}} \tag{A1-34}$$

$$\Delta_{eI} = \frac{9\left(1 + \frac{15\sqrt{2}}{4}\frac{\sqrt{m}}{A_{eI}^*}\frac{n_e}{n_I}\right)}{13\left(1 + \frac{4\sqrt{2}}{13}A_{eI}^*\frac{n_e}{n_I} + \frac{30}{13}\sqrt{m}\left(\frac{n_e}{n_I}\right)^2 - \frac{3\sqrt{2m}}{4A_{eI}^*}\frac{n_e}{n_I}\right)} \qquad \text{(A1-35)}$$

Neglecting terms of order $m^{\frac{1}{2}}$ compared to 1,

$$\Delta_{eI} = \frac{9}{13 + 4\sqrt{2}\,A_{eI}^*\frac{n_e}{n_I}}$$

$$f_{eI}^{(2)} = \frac{\frac{13}{4} + \sqrt{2}\,A_{eI}^*\frac{n_e}{n_I}}{1 + \sqrt{2}\,A_{eI}^*\frac{n_e}{n_I}} \qquad \text{(A1-36)}$$

Case II -- Electron-atom Interaction

$$\frac{\chi_{12}}{\chi_{11}} = \frac{A_{ee}^* q_{ee} A_{ee}^*}{\sqrt{2}\,q_{ea} A_{ea}^*} \qquad \text{(A1-37)}$$

$$\frac{\chi_{12}}{\chi_{22}} = \frac{q_{aa} A_{aa}^*}{\sqrt{2m}\,q_{ea} A_{ea}^*}$$

$$f_{ea}^{(2)} = \frac{\frac{30\left(\frac{5}{6} - \frac{2}{5}B_{ea}^*\right)}{(6C_{ea}^* - 5)^2} + \frac{4\sqrt{2}\;A_{ee}^* q_{ee} n_e}{(6C_{ea}^* - 5)^2\;q_{ea} n_a}}{\frac{30\left(\frac{5}{6} - \frac{2}{5}B_{ea}^*\right)}{(6C_{ea}^* - 5)^2} - 1 + \frac{4\sqrt{2}\;A_{ee}^* q_{ee} n_e}{(6C_{ea}^* - 5)^2 q_{ea} n_a}} \qquad \text{(A1-38)}$$

This expression is evaluated for argon atom and helium atom collisions with electrons in Tables 1 and 2, respectively.

Case III

Calculation of $f_{12}^{(2)}$ for an ion-atom interaction when q_{12} is independent of the temperature. Since the correction term is negligible in this case, the details of the calculation will not be given. The final result can be expressed as follows:

$$f_{aI}^{(2)} = \frac{59 + 59\,\delta}{58 + 59\,\delta} \qquad \text{(A1-39)}$$

where δ is a parameter that varies from zero to infinity.

1.1.4. Evaluation of Diffusion Coefficients

The generalized diffusion coefficients in a 3-component gas have been worked out in Reference 32, page 797.

The L_{ij} of Eqs. (III-10) are given by the following expression

$$L_{ij} = \frac{n^2 w_i w_j m_i m_j}{\rho^2 p}\left(\sum_{k \neq i} w_k m_k^2 D_{ik} - \rho w_j D_{ij}\right) \qquad \text{(A1-40)}$$

where

$$D_{ij} = \mathcal{D}_{ij}\left[1 + \frac{w_\ell\left(\frac{m_\ell}{m_i}\mathcal{D}_{i\ell} - \mathcal{D}_{ij}\right)}{w_i \mathcal{D}_{j\ell} + w_j \mathcal{D}_{i\ell} + w_\ell \mathcal{D}_{ij}}\right] \qquad \text{(A1-41)}$$

The binary diffusion coefficients $\mathcal{D}_{ij}$ are given by Eq. (A1-17).

$$\mathcal{D}_{ij} = \mathcal{D}_{ji} = \frac{3}{16}\left(\frac{2\pi k T}{m_{ij}}\right)^{1/2} \frac{f_{ij}^{(2)}}{n q_{ij}}$$

In an ionized gas the components are labelled as follows:

1st component = electrons

2nd component = ions

3rd component = atoms

In evaluating expressions (A1-40), the following notations are used:

$$\epsilon = \frac{w_e}{w_I} \quad ; \quad a = \frac{w_a}{w_I}$$

$$b = \frac{q_{Ia}\, f_{eI}^{(2)}}{q_{eI}\, f_{Ia}^{(2)}} \quad ; \quad b_1 = \left(\frac{2m_e}{m_a}\right)^{1/2} \frac{q_{Ia}\, f_{eI}^{(2)}}{q_{eI}\, f_{Ia}^{(2)}}$$

$$c = \frac{q_{ea}\, f_{eI}^{(2)}}{q_{eI}\, f_{ea}^{(2)}} \quad ; \quad m = \frac{m_e}{m_a}$$

$$\eta = 1 + a\,c + \epsilon \frac{m\,c}{b_1} \approx 1 + a\,c$$

The coefficients can now be written as follows:

$$L_{11} = K \epsilon m \left\{ 1 + \frac{a}{c} - \frac{a(1-c)^2}{c\,\eta} \right\} \tag{A1-42}$$

$$L_{12} = -K \epsilon m \left\{ 1 - \frac{a(1-b_1)(1-c)}{b_1\,\eta} \right\} = L_{21} \tag{A1-43}$$

$$L_{13} = -K \epsilon m \frac{a}{c} \left\{ 1 + \frac{(1-c)(c-b_1)}{b_1\,\eta} \right\} = L_{31} \tag{A1-44}$$

$$L_{22} = K \left\{ \epsilon m + \frac{a}{b_1} - \frac{\epsilon m\, a\, c (1-b_1)^2}{b_1^2\,\eta} \right\} \tag{A1-45}$$

$$L_{23} = -K \frac{a}{b_1} \left\{ 1 - \frac{\epsilon m (1-b_1)(c-b_1)}{b_1 \eta} \right\} = L_{32} \qquad \text{(A1-46)}$$

$$L_{33} = K \frac{a}{b_1 c} \left\{ \epsilon m b_1 + c - \frac{\epsilon m (c-b_1)^2}{b_1 \eta} \right\} \qquad \text{(A1-47)}$$

where

$$K = \frac{3}{16} \frac{m_a^2 m f_{eI}^{(2)}}{g_{eI} k T (1+a+\epsilon m)^2} \left(\frac{2\pi k T}{m_{eI}} \right)^{1/2} \qquad \text{(A1-48)}$$

$$= \frac{m_e m_a}{|e|^2 (1+a)^2} \sigma_{sp}$$

neglecting the mass of the electrons compared to the atom and ion mass.

$$\sigma_{sp} = \frac{3}{16} \left(\frac{2\pi k T}{m_{eI}} \right)^{1/2} \frac{|e|^2 f_{eI}^{(2)}}{g_{eI} k T} \qquad \text{(A1-49)}$$

Due to the relations among the coefficients, only three need to be evaluated. Of the above set, L_{11}, L_{12}, and L_{22} are chosen. The dominant term of each of these expressions is now computed and shown below:

$$\frac{L_{11}|e|}{m_e^2 n_e} = \frac{\sigma_{sp}}{|e| n_I \eta} \left\{ 1 + \frac{a+c}{(1+a)^2 b} \left(\frac{m}{2} \right)^{1/2} \epsilon \right\} \qquad \text{(A1-50)}$$

$$\frac{L_{12}|e|}{m e m_a \nu_e} = \frac{\sigma_{sp}}{|e| \nu_I \eta} \frac{a+c}{(1+a)^2 b} \left(\frac{m}{2}\right)^{1/2} \frac{a - b(2m)^{1/2}}{a+c} \tag{A1-51}$$

$$\frac{L_{22}|e|}{m a^2 \nu_I} = \frac{\sigma_{sp}}{|e| \nu_I \eta} \frac{a+c}{(1+a)^2 b} \left(\frac{m}{2}\right)^{1/2} \eta \frac{a + b(2m)^{1/2} \epsilon m}{a+c} \tag{A1-52}$$

The following notation is now introduced:

$$\gamma = \frac{\sigma_{sp} \quad (a+c)}{|e| \nu_I \eta \quad (1+a)^2 b} \left(\frac{m}{2}\right)^{1/2} ; \quad \frac{a}{a+c} = \phi$$

$$\beta = \frac{(1+a)^2 b}{a+c} \left(\frac{2}{m}\right)^{1/2} ; \quad \beta_1 = ac ; \quad \delta = \frac{b(2m)^{1/2}}{a} \tag{A1-53}$$

With these definitions, the expression for L_{11}, L_{12}, and L_{22} reduce to the expressions given below:

$$\frac{L_{11}|e|}{m e^2 \nu_e} = \gamma(\beta + \epsilon) \tag{A1-54}$$

$$\frac{L_{12}|e|}{m e m_a \nu_e} = \gamma \phi (1 - \delta) \tag{A1-55}$$

$$\frac{L_{22}|e|}{m a^2 \nu_I} = \gamma \eta \phi (1 + \delta \epsilon m) \tag{A1-56}$$

When the limitation on the ratio of atom to ion density is imposed so that $\infty > a > 10^{-2}$, the above expressions can be simplified, since to within a few per cent $\phi = 1$ and $\delta = 0$. In this case the values are as follows:

$$\frac{L_{11}|e|}{n_e^2 n_e} = \gamma(\beta + \epsilon) \tag{A1-57}$$

$$\frac{L_{12}|e|}{n_e n_a n_e} = \gamma \tag{A1-58}$$

$$\frac{L_{22}|e|}{n_a^2 n_I} = \gamma\eta \tag{A1-59}$$

In discussing the heat flux equation, the expression $L_{21}\,L_{22} - L_{12}^2$ must be evaluated. This quantity is shown below:

$$L_{11}L_{22} - L_{12}^2 = n_e n_I m_e^2 m_a^2 \gamma^2 \{(\beta+\epsilon)\eta - \epsilon\} \tag{A1-60}$$

Other groups of these expressions will be frequently encountered in this report and are shown below in terms of the binary diffusion coefficients:

$$\gamma\eta = \frac{\alpha}{\beta} = \frac{|e|}{kT} \mathcal{D}_{Ia} \frac{n_a n}{(n_a + n_I)^2} \tag{A1-61}$$

$$\gamma\beta = \frac{\alpha}{\eta} = \frac{|e|}{kT} \mathcal{D}_{ea} \frac{n c}{n_I + n_a c} = \frac{\sigma_{sp}}{|e| n_I (1 + ac)} \tag{A1-62}$$

$$\alpha\gamma = \left(\frac{|e|}{kT}\right)^2 \mathcal{D}_{Ia}\,\mathcal{D}_{ea}\,\frac{n^2 n_a C}{(n_a + n_I)^2 (n_I + n_a C)} \qquad \text{(A1-63)}$$

1.1.5. Calculation of the Viscosity Coefficient

The general expressions for the viscosity coefficient in a component mixture is given by Reference 11, page 531, as follows:

$$[\eta]_i = \frac{\begin{vmatrix} H_{11} & H_{12} & \cdots & H_{1\nu} & n_1 \\ H_{12} & H_{22} & \cdots & H_{2\nu} & n_2 \\ \cdots & & & & \\ \cdots & & & & \\ H_{1\nu} & H_{2\nu} & \cdots & H_{\nu\nu} & n_\nu \\ n_1 & n_2 & \cdots & n_\nu & 0 \end{vmatrix}}{\begin{vmatrix} H_{11} & H_{12} & \cdots & H_{1\nu} \\ H_{12} & H_{22} & \cdots & H_{2\nu} \\ \cdots & & & \\ H_{1\nu} & H_{2\nu} & \cdots & H_{\nu\nu} \end{vmatrix}} \qquad \text{(A1-64)}$$

The components H_{ij} are given by the following expressions

$$H_{ii} = \frac{n_i^2}{\eta_{ii}} + \sum_{\substack{k=1 \\ k\neq i}}^{\nu} \frac{2 n_i n_k\, m_i m_k}{\eta_{ik}\,(m_i + m_k)^2}\left(\frac{5}{3 A_{ik}^*} + \frac{m_k}{m_i}\right)$$

$$H_{ij} = -\frac{2 n_i n_j\, m_i m_j}{\eta_{ij}\,(m_i + m_j)^2}\left(\frac{5}{3 A_{ij}^*} - 1\right) \qquad \text{(A1-65)}$$

The evaluation of these determinants requires a detailed knowledge of the collision parameters of the various particles. Since these are

hardly ever known with an accuracy that warrants the complete evaluation of expression (A1-64) some approximate method of determining $[\eta]_1$ is desirable. The off-diagonal terms H_{ij} can be made equal to zero by putting $A_{ij}^* = 5/3$. The equation for the viscosity now becomes

$$[\eta]_1 = \sum_i \frac{n_i^2}{H_{ii}} \qquad \text{(A1-66)}$$

This expression is relatively easy to evaluate and hence a modified form of it is used rather than Eq. (A1-64) for the calculation of the viscosity in which the A_{ij}^* appearing in H_{ii} are not put equal to 5/3, but to their appropriate values.

In order to obtain an estimate of the errors involved in making this approximation the general expression is evaluated for a two component system of atoms and ions and the answer compared to the value obtained from the approximate equation. The two results are found to be identical to within the order of $(m_e/m_a)^{\frac{1}{2}}$ compared to one; hence for the purposes of this report the approximation is satisfactory.

1.1.5.1. Computation of Viscosity for a Partially Ionized Gas

$$[\eta]_1 = \sum_i \frac{n_i^2}{H_{ii}}$$

$$\frac{\eta_{ii} H_{ii}}{n_i^2} = 1 + \sum_{\substack{k=1 \\ k \neq i}}^{3} 2 \frac{n_k \eta_{ii} m_i m_k}{n_i \eta_{ik} (m_i + m_k)^2} \left(\frac{5}{3 A_{ik}^*} + \frac{m_k}{m_i} \right)$$

Evaluate this expression first for the atoms:

$$\frac{\eta_{aa} H_{aa}}{w_a^2} = 1 + \frac{5/3 + A^*_{Ia}}{2a A^*_{aa}} \frac{q_{Ia}}{q_{aa}} + \frac{10}{3 A^*_{aa}} \left(\frac{m}{2}\right)^{1/2} \frac{\epsilon}{a} \frac{q_{ea}}{q_{aa}}$$

The equivalent expression for the ions becomes

$$\frac{\eta_{II} H_{II}}{w_I^2} = 1 + \frac{5/3 + A^*_{Ia}}{2 A^*_{II}} a \frac{q_{Ia}}{q_{II}} + \frac{10}{3 A^*_{II}} \left(\frac{m}{2}\right)^{1/2} \epsilon$$

Finally, evaluating it for the electrons, we obtain:

$$\frac{\eta_{ee} H_{ee}}{w_e^2} = 1 + \frac{\sqrt{2}\, A^*_{eI}}{\epsilon\, A^*_{ee}} + \frac{2a}{\epsilon} \frac{q_{ea}}{q_{ee}} \frac{A^*_{ea}}{A^*_{ee}}$$

Summing these together the value of $[\eta]_1$ is obtained, when $\epsilon \approx 1$.

$$[\eta]_1 = \frac{a\, \eta_{aa}}{a + \frac{5+3A^*_{Ia}}{6 A^*_{aa}} \frac{q_{Ia}}{q_{aa}}} + \frac{\eta_{II}}{1 + \frac{5+3A^*_{Ia}}{6 A^*_{II}} a \frac{q_{Ia}}{q_{II}}} + \frac{\eta_{ee}\, \epsilon}{\epsilon + \sqrt{2} + 2a \frac{q_{ea}}{q_{ee}} \frac{A^*_{ea}}{A^*_{ee}}} \qquad \text{(A1-67)}$$

As a check on the accuracy of the approximation, this expression is evaluated when $n_e = 0$ and compared with the value obtained from an accurate calculation of the viscosity for an atom-ion mixture. When all terms that are smaller than $(m_e/m_a)^{\frac{1}{2}}$ compared to one are neglected, then as $\epsilon \longrightarrow 0$, Eq. (A1-67) reduces to the following expression:

$$[\eta]_{Ia} = \eta_{aa} \frac{1 + a^2 + \frac{6 A^*_{II}}{5+3 A^*_{Ia}} \frac{q_{II}}{q_{Ia}} a}{\frac{A^*_{II}}{A^*_{aa}} \frac{q_{II}}{q_{aa}} + a^2 + \frac{6 A^*_{II}}{5+3 A^*_{Ia}} \frac{q_{II}}{q_{Ia}} a} \qquad \text{(A1-68)}$$

1.1.5.2. Viscosity of an Atom-Ion Gas Using the Exact Equation

Using the expression on page 530 of Reference 15, the viscosity for a binary mixture of atoms and ions is computed and the following result is obtained:

$$[\eta]_{Ia} = \eta_{aa} \frac{1 + a^2 + \frac{6 A^*_{II}}{5 + 3 A^*_{Ia}} \frac{g_{II}}{g_{Ia}} a}{\frac{A^*_{II}}{A^*_{aa}} \frac{g_{II}}{g_{aa}} + a^2 + \frac{6 A^*_{II}}{5 + 3 A^*_{Ia}} \frac{g_{II}}{g_{Ia}} a} \qquad \text{(A1-69)}$$

This expression is identical with Eq. (A1-68).

1.1.6. Calculation of the Thermal Conductivity

The thermal conductivity is treated in a manner similar to the viscosity. When all of the off diagonal terms are put equal to zero in the general expression for the thermal conductivity, (See, for example, Reference 15, page 537), the remaining expression is shown below:

$$[\mathcal{K}]_1 = \sum_i 4 \frac{w_i^2}{L_{ii}} \qquad \text{(A1-70)}$$

$$L_{ii} = \frac{4 w_i^2}{\mathcal{K}_{ii}} + \sum_{k \neq i} 2 w_i w_k \left\{ \frac{\frac{15}{2} m_i^2 + \frac{25}{4} m_k^2 - 3 m_k^2 B^*_{ik} + 4 m_i m_k A^*_{ik}}{(m_i + m_k)^2 A^*_{ik} \mathcal{K}_{ik}} \right\} \qquad \text{(A1-71)}$$

1.1.6.1. Computation of Thermal Conductivity for a Partially Ionized Monatomic Gas

The various values of $\mathcal{K}_{ij}$ are first normalized to $\mathcal{K}_{aa}$

$$\frac{K_{II}}{K_{aa}} = \frac{g_{aa} A^*_{aa}}{g_{II} A^*_{II}}$$

$$\frac{K_{Ia}}{K_{aa}} = \frac{g_{aa} A^*_{aa}}{g_{Ia} A^*_{aI}}$$

$$\frac{K_{ee}}{K_{aa}} = \frac{g_{aa} A^*_{aa}}{g_{ee} A^*_{ee}} \frac{1}{\sqrt{2m}}$$

$$\frac{K_{ea}}{K_{aa}} = \frac{g_{aa} A^*_{aa}}{g_{ea} A^*_{ea}} \frac{1}{\sqrt{2m}}$$

$$\frac{K_{Ie}}{K_{aa}} = \frac{g_{aa} A^*_{aa}}{g_{eI} A^*_{eI}} \frac{1}{\sqrt{2m}}$$

The element L_{aa} can now be evaluated

$$L_{aa} = \frac{4a^2}{K_{aa}} + \frac{a}{2} \frac{\left(\frac{55}{4} + 4A^*_{Ia} - 3B^*_{Ia}\right)}{A^*_{Ia} \frac{g_{aa} A^*_{aa}}{g_{Ia} A^*_{Ia}} K_{aa}} \qquad \text{(A1-72a)}$$

$$+ \frac{15a\epsilon}{A^*_{ea} \frac{g_{aa} A^*_{aa}}{g_{ea} A^*_{ea}} \frac{K_{aa}}{\sqrt{2m}}}$$

$$\approx \frac{4a}{K_{aa}} \left[a + \frac{59}{32} \frac{g_{Ia}}{g_{aa}}\right] \qquad \text{(A1-72b)}$$

To obtain this last approximate expression the values of A_{ij}^* and B_{ij}^* are put equal to 1, the values for rigid sphere interactions, and it is assumed that $\epsilon < 1/(2m)^{\frac{1}{2}}$.

The element L_{II} is evaluated next,

$$L_{II} = \frac{4}{K_{aa}} \frac{q_{II} A^*_{II}}{q_{aa} A^*_{aa}} + \frac{a}{2} \frac{\left(\frac{55}{4} + 4 A^*_{Ia} - 3 B^*_{Ia}\right)}{A^*_{Ia} \frac{q_{aa} A^*_{aa}}{q_{Ia} A^*_{Ia}} K_{aa}} + \frac{15 \epsilon}{\frac{q_{aa} A^*_{aa}}{q_{Ie}} \frac{K_{aa}}{\sqrt{2}m}} \qquad \text{(A1-73a)}$$

$$\approx \frac{4}{K_{aa}} \left[\frac{q_{II}}{q_{aa}} + \frac{59}{32} \frac{q_{Ia}}{q_{aa}} a \right] \qquad \text{(A1-73b)}$$

Similar approximations are made as in the evaluation of L_{aa}. The value obtained for L_{ee} is shown below.

$$L_{ee} = \frac{4\epsilon^2 \sqrt{m}}{K_{aa}} \frac{q_{ee} A^*_{ee}}{q_{aa} A^*_{aa}} + \frac{2\epsilon\left(\frac{25}{4} - 3 B^*_{eI}\right)}{\frac{q_{aa} A^*_{aa}}{q_{eI}} \frac{K_{aa}}{\sqrt{2}m}} + \frac{2a\epsilon\left(\frac{25}{4} - 3 B^*_{ea}\right)}{\frac{q_{aa} A^*_{aa}}{q_{ea}} \frac{K_{aa}}{\sqrt{2}m}} \qquad \text{(A1-74a)}$$

$$\approx \frac{4\epsilon}{K_{aa}} \frac{q_{ee}}{q_{aa}} \sqrt{m} \left\{ \epsilon + \frac{13\sqrt{2}}{8} + \frac{13\sqrt{2}}{8} \frac{q_{ea}}{q_{ec}} a \right\} \qquad \text{(A1-74b)}$$

The expression for the thermal conductivity now becomes

$$[K]_1 = K_{aa} \left\{ \frac{a}{a + \frac{59}{32} \frac{q_{Ia}}{q_{aa}}} + \frac{1}{\frac{q_{II}}{q_{aa}} + \frac{59}{32} \frac{q_{Ia}}{q_{aa}} a} + \frac{\epsilon \frac{q_{aa}}{q_{ee}} \frac{1}{\sqrt{m}}}{\epsilon + \frac{13\sqrt{2}}{8} + \frac{13\sqrt{2}}{8} \frac{q_{ea}}{q_{ee}} a} \right\} \qquad \text{(A1-75)}$$

Several aspects of this expression should be stressed as a general tendency exists to treat thermal conductivity of a plasma in a manner similar to electrical conductivity. An examination of the above equations indicates that the thermal conductivity of the plasma is very close to that of the atoms up to a quite high per cent ionization for some gases. This occurs because the coulomb cross-section, which accounts for the majority of the electron collisions is much greater than the atom-

atom or atom-ion cross-sections which counterbalances the effect of the low electrons mass. Even at 20 per cent ionization, the electrons contribute only a few per cent to the plasma thermal conductivity of helium.

A second point that should be stressed is that the method of calculating the transport coefficients by the Chapman-Enskog expansion does not include any dependence on the externally applied fields which can influence the charged particle motion. The transport coefficients depend only on the physical properties of the gas particles and their collision parameters. Any dependence of the thermal conductivity of a plasma on applied electric or magnetic fields must occur through the interactions of the various terms of the phenomenological equations, Eqs. (II-11) and (II-12). This important point will be discussed in detail in other sections of this paper.

The thermal conductivity for a pure plasma is obtained by putting a = 0 in Eqs. (A1-75).

$$[\mathcal{K}]_{eI} = \frac{\epsilon}{\epsilon A^*_{ee} + \frac{13}{4\sqrt{2}}} \frac{75}{128} \left(\frac{4\pi k T}{m_e}\right)^{1/2} \frac{k}{q_{ee}} \qquad \text{(A1-76)}$$

When this expression is compared to that obtained by Spitzer (Reference 12, page 89) the following relation holds

$$\frac{[\mathcal{K}]_{eI}}{\mathcal{K}_{sp}} = \frac{1.21\,\epsilon}{A^*_{ee}\,\epsilon + \frac{13}{4\sqrt{2}}} \qquad \text{(A1-77)}$$

When $\epsilon = 1$, the value of the thermal conductivity found in this report is about a factor of 3 lower than the value given by Spitzer.

1.1.7. Approximate Calculation of Thermal Diffusion Coefficients

Because of a general lack of information on collision parameters for electron-atom and ion-atom collisions, the assumption will be made that the only collisions that contribute to thermal diffusion are the electron-ion coulomb interactions. This approximation is good as long as the electron or ion interaction with the atom obeys an inverse 5th power law, which is used as a model for the interaction of a charged particle and an atom. This approximation is expected to be very poor when the Ramsauer effect occurs in the electron-atom collisions.

The definition for the thermal diffusion ratio, K_e and K_I in this paper is slightly different from the definition in References 11 and 15. The following equation shows the relation between the two for a two component gas mixture:

$$K_e = (n/n_e)\,(k_T)_e \qquad \text{(A1-78)}$$

Using the expression of Reference 15, page 541, to evaluate $(k_T)_e$ the following relation is obtained when terms of the order $m^{\frac{1}{2}}$ compared to 1 are neglected:

$$(k_T)_e = \frac{15}{13 + 4\sqrt{2}\, A^*_{eI} \frac{n_e}{n_I}} \quad \frac{n_e}{n_e + n_I} \qquad \text{(A1-79)}$$

When this expression is weighted for atom-electron collisions and substituted into Eq. (A1-78), the value for K_e shown below is obtained:

$$K_e = \frac{15}{(13 + 4\sqrt{2}\, A^*_{eI} \frac{n_e}{n_I})(1 + ac)} \qquad \text{(A1-80)}$$

To within an approximation similar to that used in obtaining Eq. (A1-80), the ion thermal diffusion ratio can be neglected.

$$K_I = 0 \qquad \text{(A1-81)}$$

1.2. Evaluation of the Transport Coefficients

There is at present a serious lack of data on the cross-sections for the interaction of ions with neutral atoms and molecules in the energy range of 1 electron volt. For this reason the data tabulated in this section can be only approximate. The various models chosen to represent the necessary interaction are discussed below.

1.2.1. Atom-Atom Collisions

Data for the transport properties of the noble gases from 1000 to 15000°K has been tabulated by Mason and Admur[22]. Where necessary, the data has been extrapolated to higher temperatures by fitting their data to a law of the form $q_{aa} = (q_{aa})_o (T/T_o)^n$. The only interaction parameters that had to be evaluated was A_{11}^* and B_{aa}^*. Using the table of values for A from Chapman and Cowling[11], page 172, the following values were chosen for argon and helium gas:

$$(A_{aa}^*)_A = 1.148; \quad (B_{aa}^*)_A = 1.0; \quad (q_{aa})_A = 14.80 \times 10^{-20} (T/10^4)^{.25} \text{ m}^2$$

$$(A_{aa}^*)_{He} = 1.195; \quad (B_{aa}^*)_{He} = 1.0; \quad (q_{aa})_{He} = 4.81 \times 10^{-20} (T/10^4)^{.33} \text{ m}^2$$

1.2.2. Electron-Electron Collisions

The cross-section for electron-electron, electron-ion, and ion-ion collisions was assumed to be identical and was evaluated using

Eq. (A1-15).* The necessary expressions are reproduced below for convenience:

$$q_{eI} = \pi \left(\frac{e_e e_I}{8\pi k T \varepsilon_0} \right)^2 \ln (\alpha_d)_{eI}$$

$$(\alpha_d)_{eI} = 1 + 4 \left(\frac{12\pi \varepsilon_0 k T}{e_e e_I} \right)^2 \left(\frac{\varepsilon_0 k T}{2|e|^2 n_e} \right) \qquad \text{(A1-82)}$$

1.2.3. Ion-Atom Collisions

The only information available on ion-atom interactions is from mobility studies. No information could be found covering the temperature range upward from 1,000°K. For this reason, some calculated values of Hornbeck and Varney were used. It was assumed that the temperature dependence was similar to the atom-atom interactions. The necessary data, taken from a table in Loeb[23] (page 71) is shown below:

$$\begin{aligned} (q_{Ia}/q_{aa})_A &= 3.20 \\ (A_{Ia}^*)_A &= 1.295 \\ (q_{Ia}/q_{aa})_{He} &= 3.60 \\ (A_{Ia}^*)_{He} &= 1.295 \end{aligned} \qquad \text{(A1-83)}$$

1.2.4. Electron-Atom Collisions

The interaction data for electron-atom collision has been computed from Eqs. (A1-19a and b), for both helium and argon. The only source of any appreciable error in the computations is in the specification of $Q_{ea}^{(2)}$. In general, it is felt that the cross-sections and parameters

---

* The term involving the logarithm of the relative velocity was averaged out of the integral.

can be accurate to $\pm$ 20 per cent.

The data is presented in Tables 1 and 2.

1.2.5. Evaluation of the Viscosity

The viscosity of argon and helium was computed over the temperature range where they are partially ionized. The final values are plotted in Figures 9 and 10, where they are compared to the values for the unionized gas. In general, the viscosity of a fully-ionized gas appears to be about a factor of 20 lower than when the gas is unionized.

1.2.6. Evaluation of the Thermal Conductivity

The various terms that contribute to the thermal conductivity of helium and argon while they are partially ionized is shown in Figures 11 and 12. The term arising from the ion and electron ambipolar diffusion gives by far the greatest contribution over most of the range of ionization, peaking at an ionization level of about 50 per cent. For convenience, the various terms contributing to the thermal conductivity are reproduced below.

$$\text{contribution from atoms} = \frac{K_{aa}}{1 + 1.465 \frac{g_{Ia}}{g_{aa} A^*_{aa}} \frac{\alpha}{1-\alpha}} \qquad \text{(A1-84)}$$

$$\text{contribution from electrons} = \frac{K_{aa} \epsilon \frac{g_{aa}}{g_{ee}} \frac{A^*_{aa}}{T_m}}{\epsilon A^*_{ee} + \frac{13}{4T^2} + \frac{1}{T^2}\left(\frac{25}{4} - 3B^*_{ea}\right)\frac{g_{ea}}{g_{ee}} \frac{1-\alpha}{\alpha}} \qquad \text{(A1-85)}$$

$$\text{contribution from ambipolar diffusion} = K_{aa} 2\alpha(1-\alpha) \frac{f^{(2)}_{Ia} g_{aa} A^*_{aa}}{g_{Ia}} \left(1 + \frac{|e| V_I}{\frac{5}{2} kT}\right)^2 \qquad \text{(A1-86)}$$

Since the thermal diffusion ratio K_e is small compared to $(|e|V_I)/(kT)$ it has been neglected in the above term.

When there is a considerable amount of energy in the electron excitation of the atoms and ions, the expression $\left(1+\frac{|e|V_I}{\frac{5}{2}kT}\right)^2$ should be replaced by

$$\left(\frac{\frac{5}{2}kT+h\nu_I+|e|V_I-h\nu_a}{\frac{5}{2}kT}\right)^2$$

When Finkelnburg[1] computed the thermal conductivity of argon, his analysis did not give him the term arising from the ion and electron ambipolar diffusion. The addition of this term is decisive in determining the operating characteristics of arcs, hence many of the models that are discussed in Reference 1 concerning arc column behavior must be critically reexamined and the conclusions that are drawn treated with reserve.

1.2.7. Evaluation of the Electrical Conductivity

The electrical conductivity is given by the following expression

$$\sigma = \frac{3}{16}\left(\frac{2\pi}{m_e kT}\right)^{1/2}\frac{|e|^2}{g_{eI}/f_{eI}^{(2)}+\frac{1-\alpha}{\alpha}g_{ea}/f_{ea}^{(2)}}$$

$$= \frac{33900\times10^{-18}}{g_{eI}/f_{eI}^{(2)}+\frac{1-\alpha}{\alpha}g_{ea}/f_{ea}^{(2)}}\left(\frac{10^4}{T}\right)^{1/2}\frac{mhos}{meter} \qquad \text{(A1-87)}$$

This expression is evaluated for argon and helium at a pressure of 1 atm. and over the temperature range of partial ionization. The results are plotted and shown in Figures 13 and 14.

APPENDIX 2

INSTRUMENTATION AND CALIBRATION OF EQUIPMENT

2.1. Motor Generator Set

A nominal 100 kw D. C. motor generator set was used to supply power to the arc and to the magnet. The set consisted of two units, each capable of delivering 50 kw over a wide voltage range. The unit used to supply power to the magnet had a reostat in the field circuit so that the output current could be controlled over a range of 20 - 350 amperes. The current and voltage delivered to the arc was controlled by the use of a series of ballast resistors.

The A. C. ripple voltage was checked and found to be less than 1 per cent under both open circuit and load conditions.

2.2. Magnet

A magnet that had been designed by Professor Anderson and used in cosmic ray studies was borrowed from the physics department. The magnet was powered from one side of the M. G. set and could be operated over a range of power from 0 to 50 kw.

The magnetic field strength was determined by using a flip-coil and measuring the induced charge on a ballistic galvanometer. The flip coils were calibrated on a standard magnet of 2250 gauss.

The magnetic field is plotted as a function of the current in the magnet in Figure 2-1.

2.3. Heater Flow System

Two separate water circuits were used for cooling the arc equipment. One flowed through a critical orifice and cooled the electrodes. The water flow rate was measured on a mercury manometer. Figure II-2 indicates the measured water flow rate as a function of the reading of the manometer. The second water circuit measured the power transferred from the hot gas to a cylinder downstream from the arc. The flow rate of this system was measured directly by determining the time to fill a 1 litre flask.

Tap water was used in all cooling circuits.

2.4. Gas Flow System

The gas was passed through a critical orifice meter before being fed into the arc. The orifice channel was immersed in the cold side of the water flow system so that by measuring the water temperature, the stagnation temperature of the gas would be known.

The pressure was measured on both sides of the critical orifice by pressure gauges.

2.5. Thermocouple System

The power in the cooling water was measured by using thermocouple banks. The cold junction was placed in the water flowing to the equipment and the hot junction in the heated water leaving the equipment, hence only the temperature increment given to the water was measured.

The thermocouples were calibrated by connecting the system to a dummy load where the water cooled a resistor through which a measured electrical power was dissipated.

The calibration curve of the thermocouples is shown in Figure II-3.

2.6. Spark Unit

The high voltage spark used to initiate the arc was obtained from a standard Schlieren spark source. The spark was delivered directly across the electrodes and was insulated from the M. G. set by a series of condensers and a coil in the high current arc circuit.

APPENDIX 3

ELECTROMAGNETIC PUMPING

The term "electromagnetic pumping", is applied to those processes in the arc where the self-magnetic field of the discharge interacts with some component of the discharge current in such a manner as to apply a force on the charged particles that tends to pump them out of the high current density region of the arc. In general, these forces occur in axisymmetric discharges when either the cross-sectional area of the discharge changes or when the column develops a curvature. In pinch discharges, the action of the above forces results in the development of the sausage and kink instabilities, respectively. When the discharge is surrounded by unionized gas it is possible for the column to deform in both of the above ways and still not become unstable. When this occurs, charged particles are pumped out of the regions of high current density and replaced by unionized gas. This gas is then ionized by electron bombardment and the discharge is thus maintained.

When a change in cross-sectional area of the conduction channel occurs a radial component of current develops. If the discharge current is along the positive z axis and the channel area increases, as z increases the charged particles are accelerated in the direction of increasing z. Conversely, if the discharge area decreases in the positive z direction then the charged particles are accelerated in the negative z direction. These considerations lead to the following general statement: When the cross-sectional area of a conducting

column of gas that is carrying an electric current changes, the charged particles in the column are accelerated in the direction of increasing area or decreasing current density.

Considerable experimental evidence is presented in Reference 1 to verify the above statement. Changes in cross-sectional area of the discharge at the points of attachment to the electrodes are discussed in sections XI and XII of this paper.

The forces that come into play when the column undergoes a change of curvature are best documented in the rail type of experiments or in the production of plasmoids. In both of these experiments the discharge path is turned through 180^{o} with a fairly small effective radius of curvature. The charged particles are accelerated in the direction of convex curvature.

TABLE 1

COLLISION CROSS-SECTIONS AND INTERACTION PARAMETERS

FOR COLLISIONS BETWEEN ARGON ATOMS AND ELECTRONS

Temperature ^{o}K $T/10^4$	Reference Cross-Section $q_{ea} \times 10^{20}$ m^2	Interaction Parameters			$30(\frac{5}{6} - \frac{2}{5} B_{ea}^*)$	$f_{ea}^{(2)}$	Electrical Conductivity mhos/meter
		A_{ea}^*	B_{ea}^*	C_{ea}^*	$(6 C_{ea}^* - 5)^2$		
.6	2.38	2.42	-.823	1.56	1.84	2.16	61.1
.7	3.05	2.34	-.548	1.51	1.91	1.93	463
.8	3.75	2.27	-.360	1.46	2.08	1.60	1080
.9	4.35	2.24	-.214	1.44	2.07	1.36	1850
1.0	4.98	2.21	-.082	1.42	2.10	1.20	2860
1.1	5.63	2.15	.032	1.39	2.20	1.11	3440
1.2	6.19	2.11	.139	1.36	2.33	--	4250
1.3	6.71	2.09	.240	1.35	2.30	--	5020
1.4	7.25	2.05	.337	1.32	2.45	--	5770
1.5	7.73	2.02	.432	1.30	2.53	--	6470
1.6	8.16	1.99	.533	1.28	--	--	7090
1.7	8.60	1.95	.622	1.25	--	--	7670
1.8	8.96	1.92	.721	1.24	--	--	8200
1.9	9.32	1.88	.818	1.21	--	--	8700

TABLE 2

COLLISION CROSS-SECTIONS AND INTERACTION PARAMETERS

FOR COLLISIONS BETWEEN HELIUM ATOMS AND ELECTRONS

Temperature ^{o}K $T/10^{4}$	Reference Cross-Section $q_{ea} \times 10^{20}$ m^2	Interaction Parameters A_{ea}^*	B_{ea}^*	C_{ea}^*	$\frac{30(\frac{5}{6} - \frac{2}{5} B_{ea}^*)}{(6 C_{ea}^* - 5)^2}$	$f_{ea}^{(2)}$	Electrical Conductivity mhos/meter
1.2	5.40	1.487	.907	.958	25.1	1.04	524
1.4	5.16	1.472	.959	.949	27.7	1.03	2,280
1.6	4.97	1.460	.985	.940	32.3	1.03	5,050
1.8	4.78	1.455	1.020	.938	32.7	1.02	8,020
2.0	4.63	1.440	1.052	.929	38.6	1.01	11,000
2.2	4.50	1.425	1.072	.919	47.0	1.00	14,000
2.4	4.37	1.420	1.097	.916	47.3	1.00	16,900
2.6	4.26	1.415	1.117	.913	51.3	1.00	19,400
2.8	4.16	1.410	1.135	.908	57.7	1.00	22,000
3.0	4.06	1.400	1.161	.902	67.0	1.00	23,800
3.2	3.98	1.393	1.175	.899	70.0	1.00	27,500
3.4	3.89	1.385	1.200	.893	84.2	1.00	30,500
3.6	3.81	1.378	1.207	.887	109.3	1.00	33,400

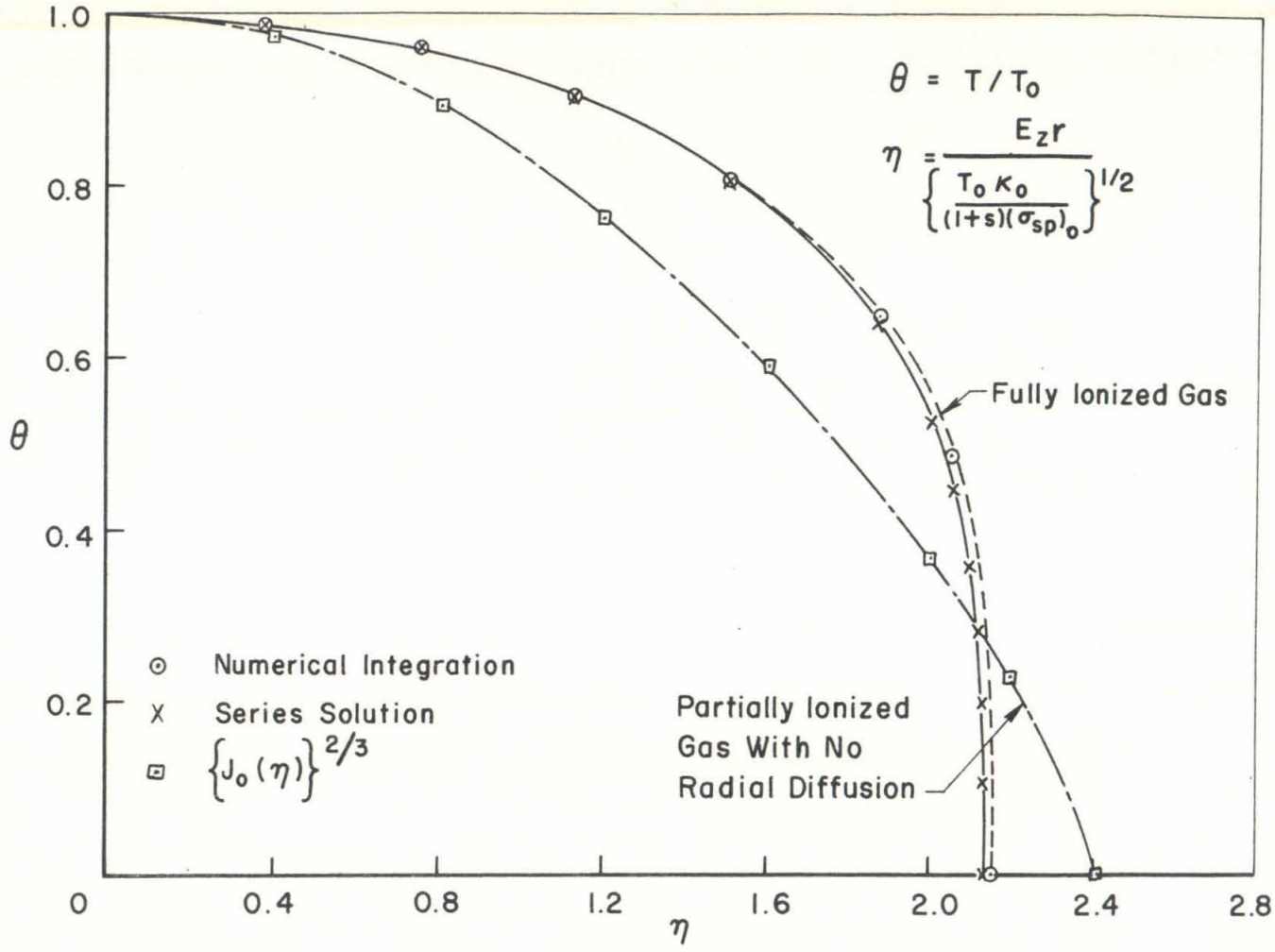

FIG. 1 TEMPERATURE PROFILES FOR IDEALIZED ARC COLUMNS

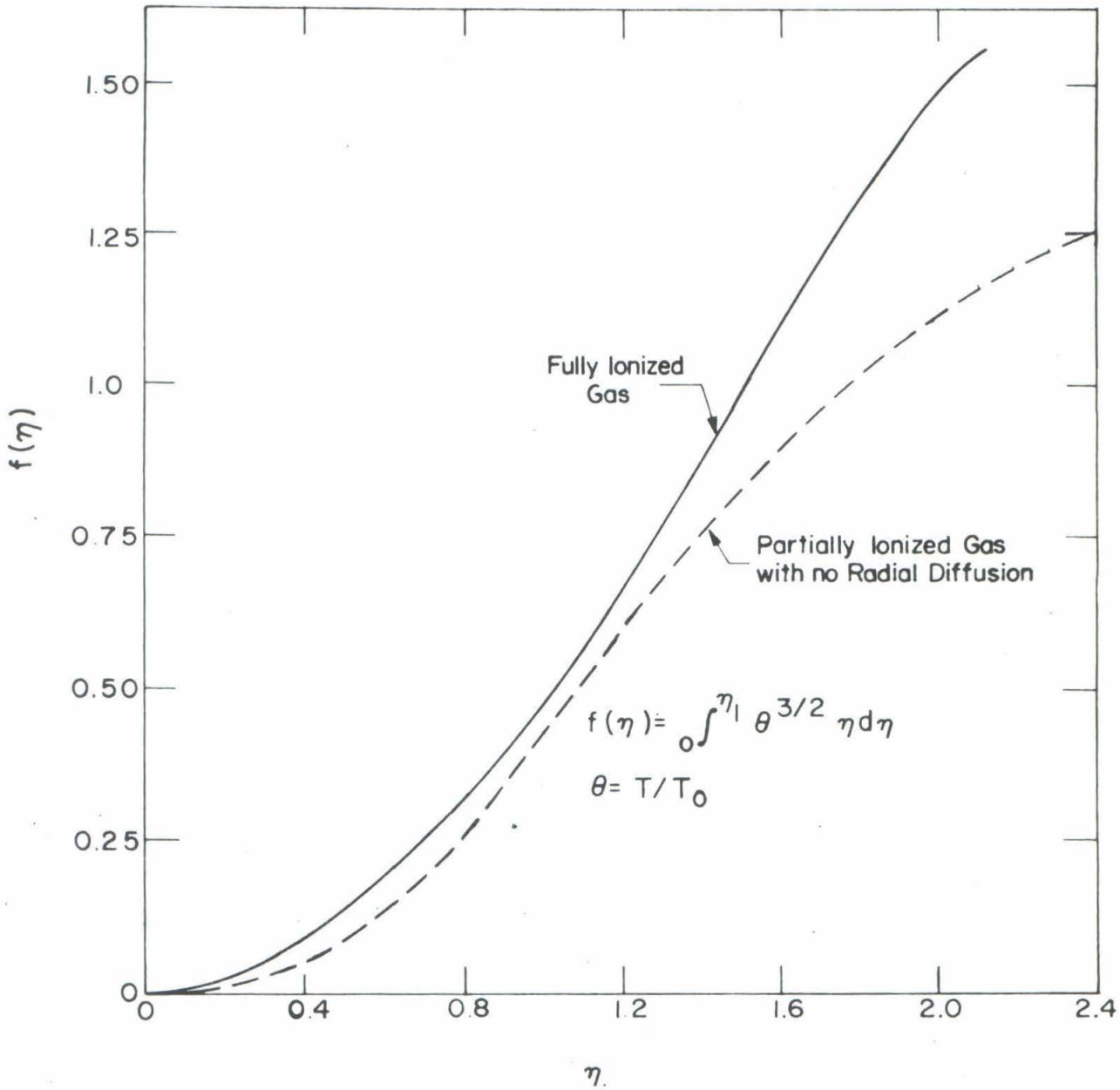

Fig. 2 CURRENT DENSITY INTEGRAL FOR IDEALIZED ARC COLUMNS

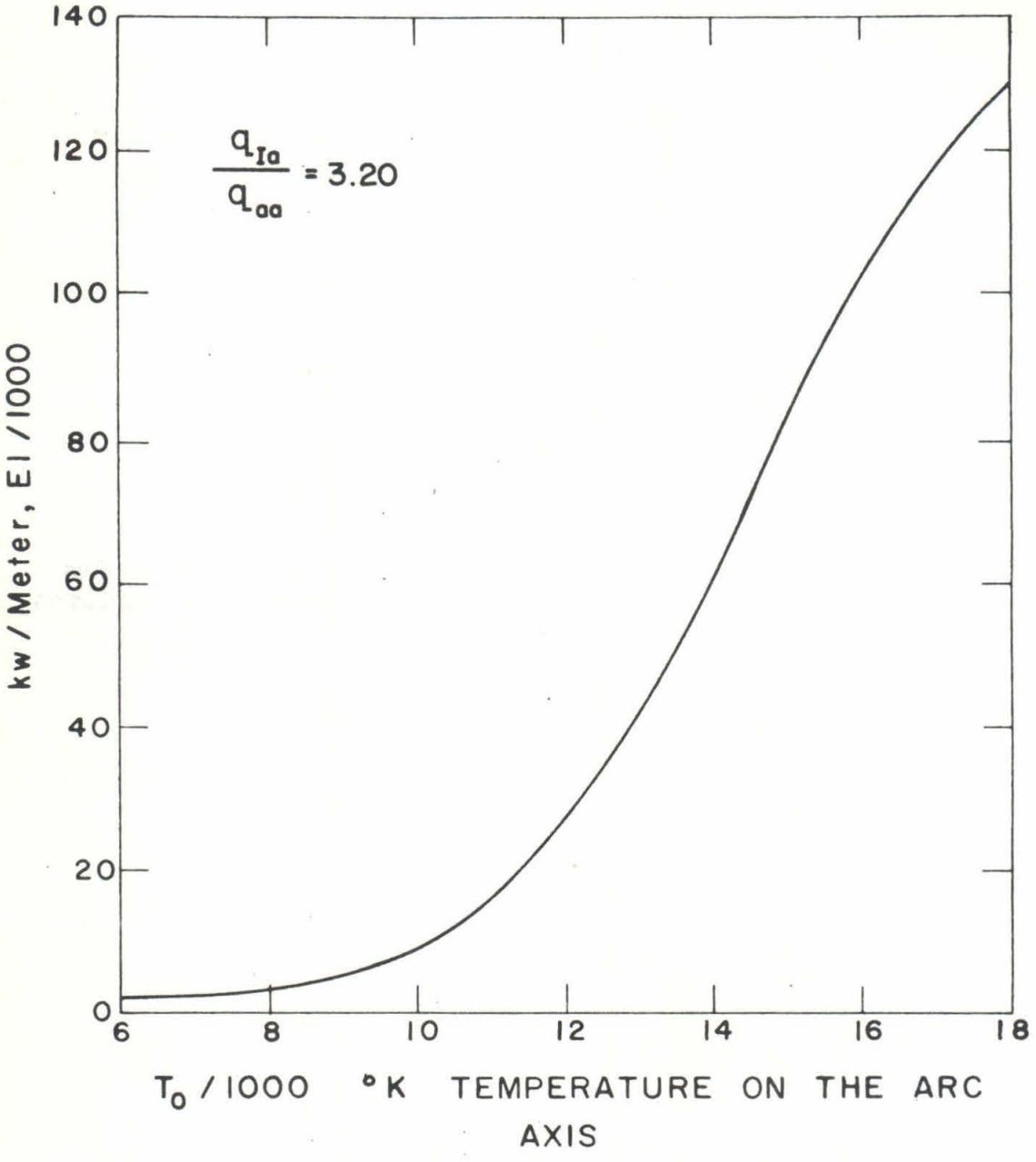

Fig. 3 POWER DISSIPATION PER UNIT LENGTH FOR AN ARC COLUMN IN ARGON AS A FUNCTION OF THE TEMPERATURE ON THE ARC AXIS.

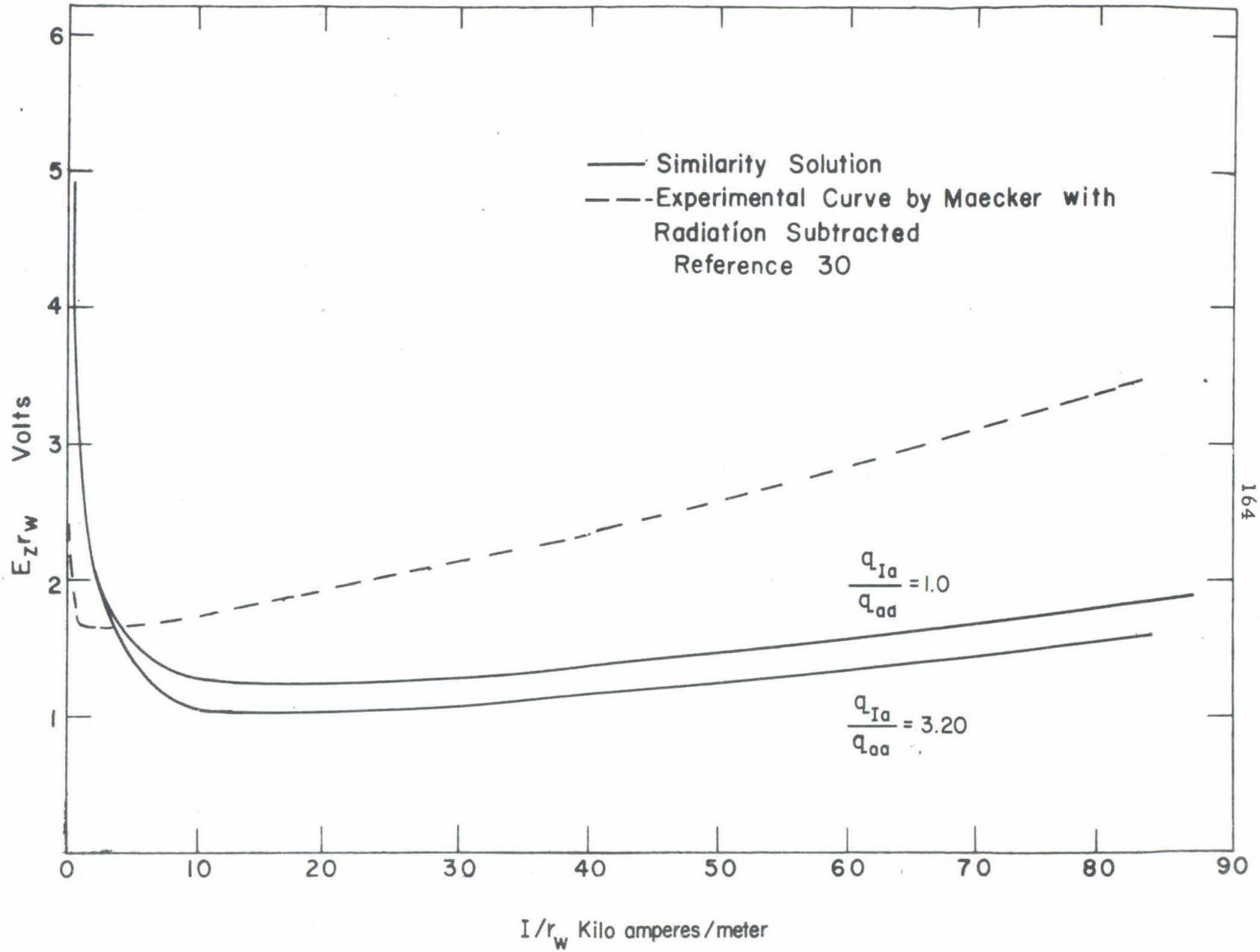

Fig. 4 CURRENT–VOLTAGE CHARACTERISTICS FOR AN ARC COLUMN IN ARGON CONFINED IN A CYLINDER OF RADIUS r_w, ONE ATMOSPHERE PRESSURE.

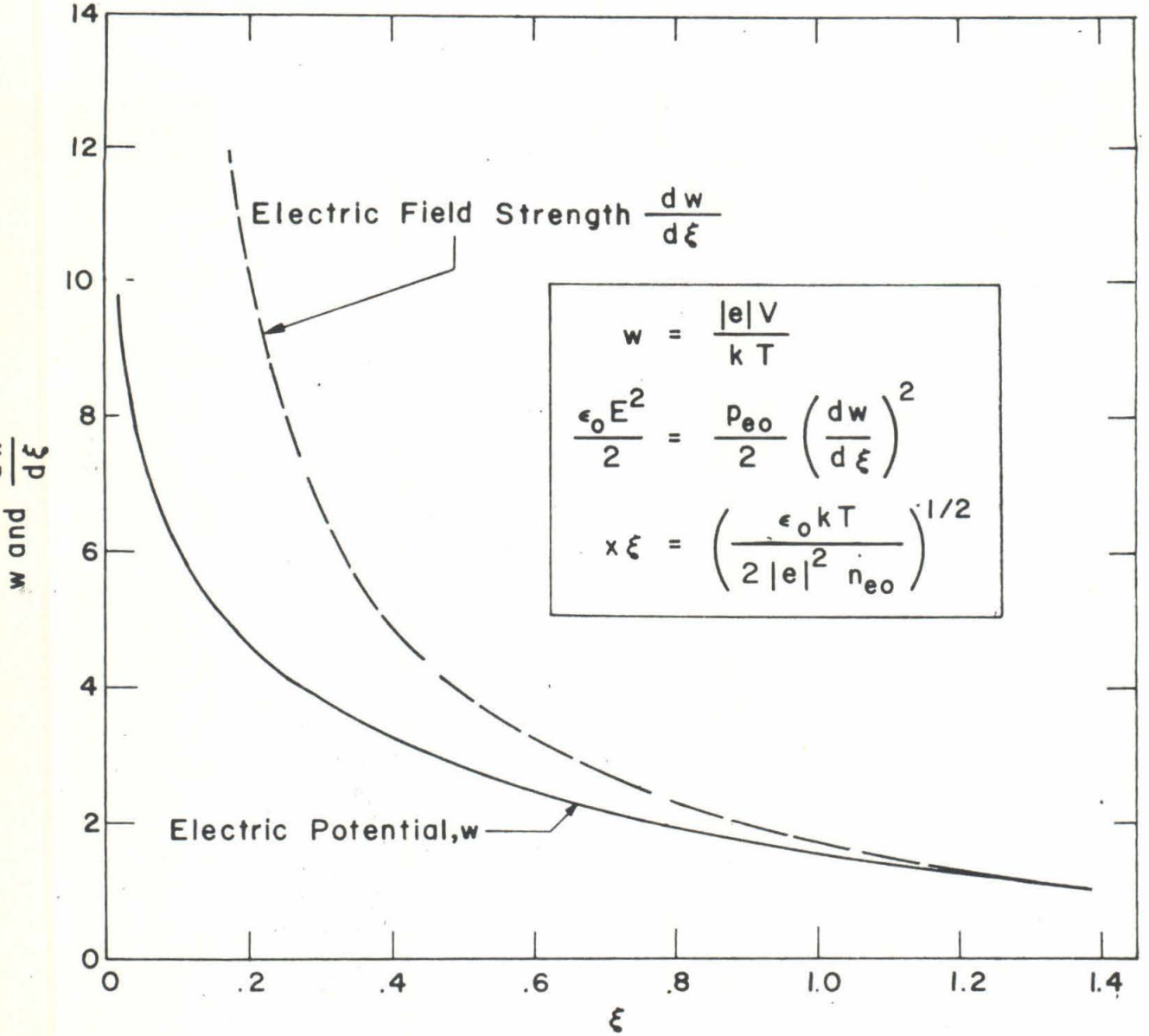

Fig. 5 POTENTIAL DISTRIBUTION AND ELECTRIC FIELD STRENGTH IN A SHEATH

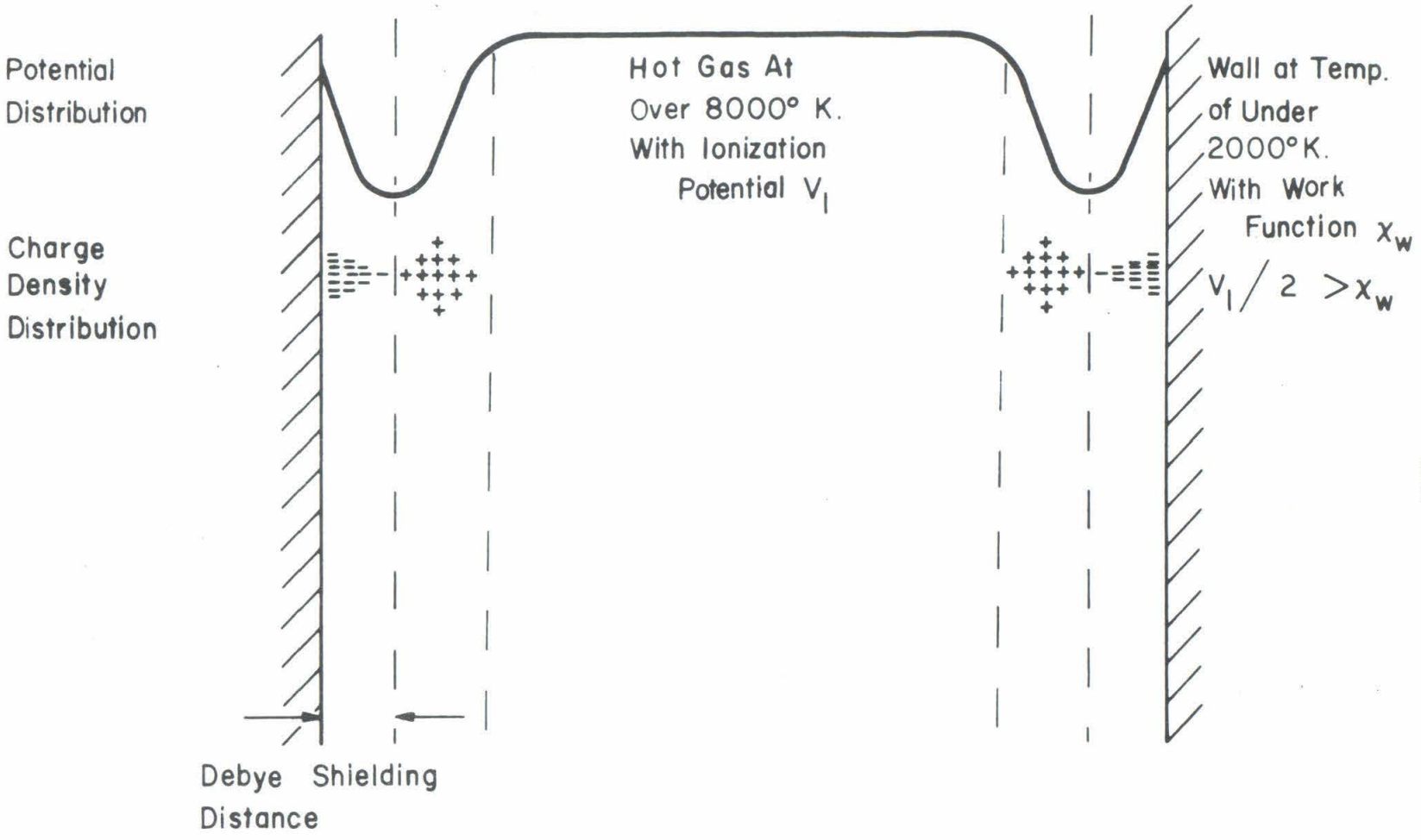

Fig 6 THE POTENTIAL DISTRIBUTION NEAR THE WALL IN A HOT PLASMA CONFINED IN A COLD CONTAINER

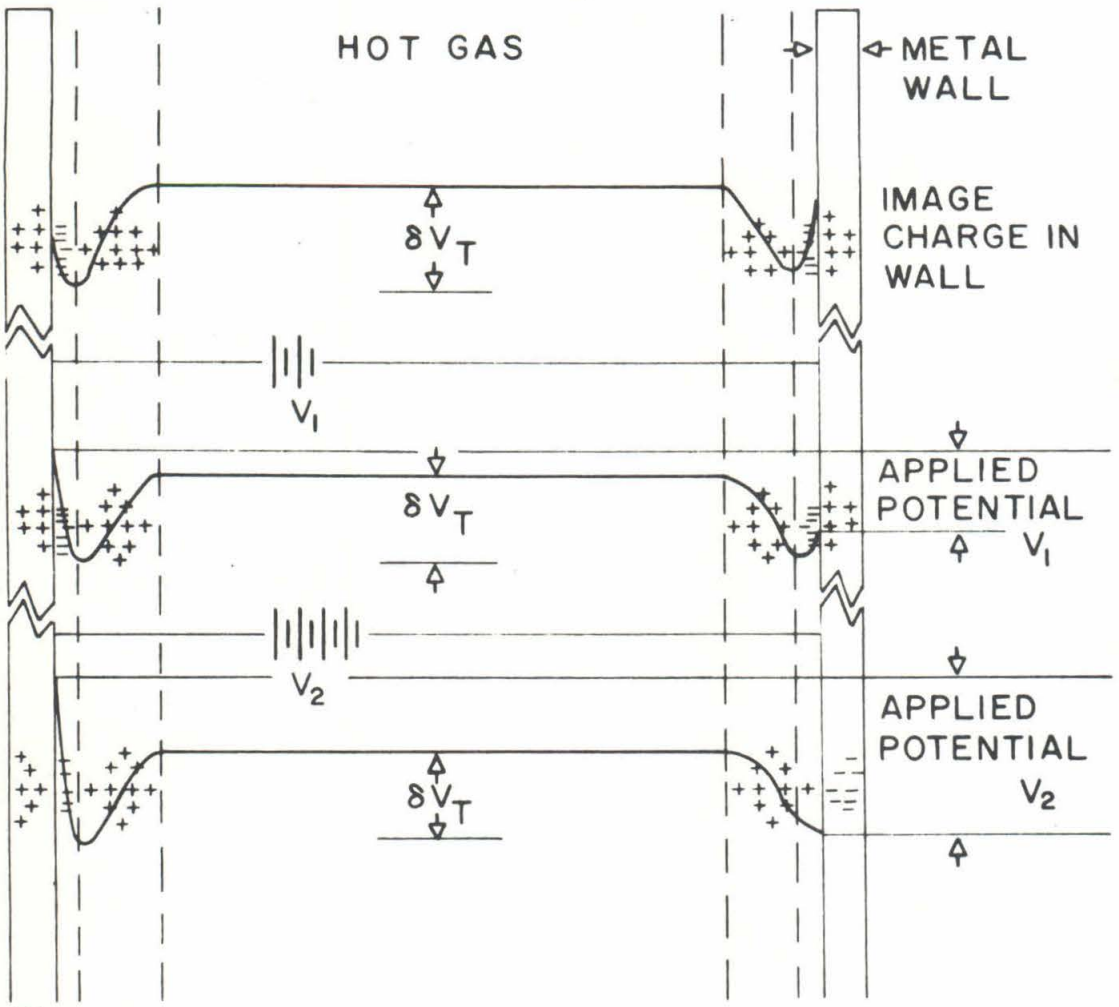

Fig.

Fig. 7 POTENTIAL DISTRIBUTION ACROSS EQUILIBRIUM SHEATHS WHEN NO CURRENT IS FLOWING BUT A POTENTIAL IS APPLIED BETWEEN THE TWO WALLS.

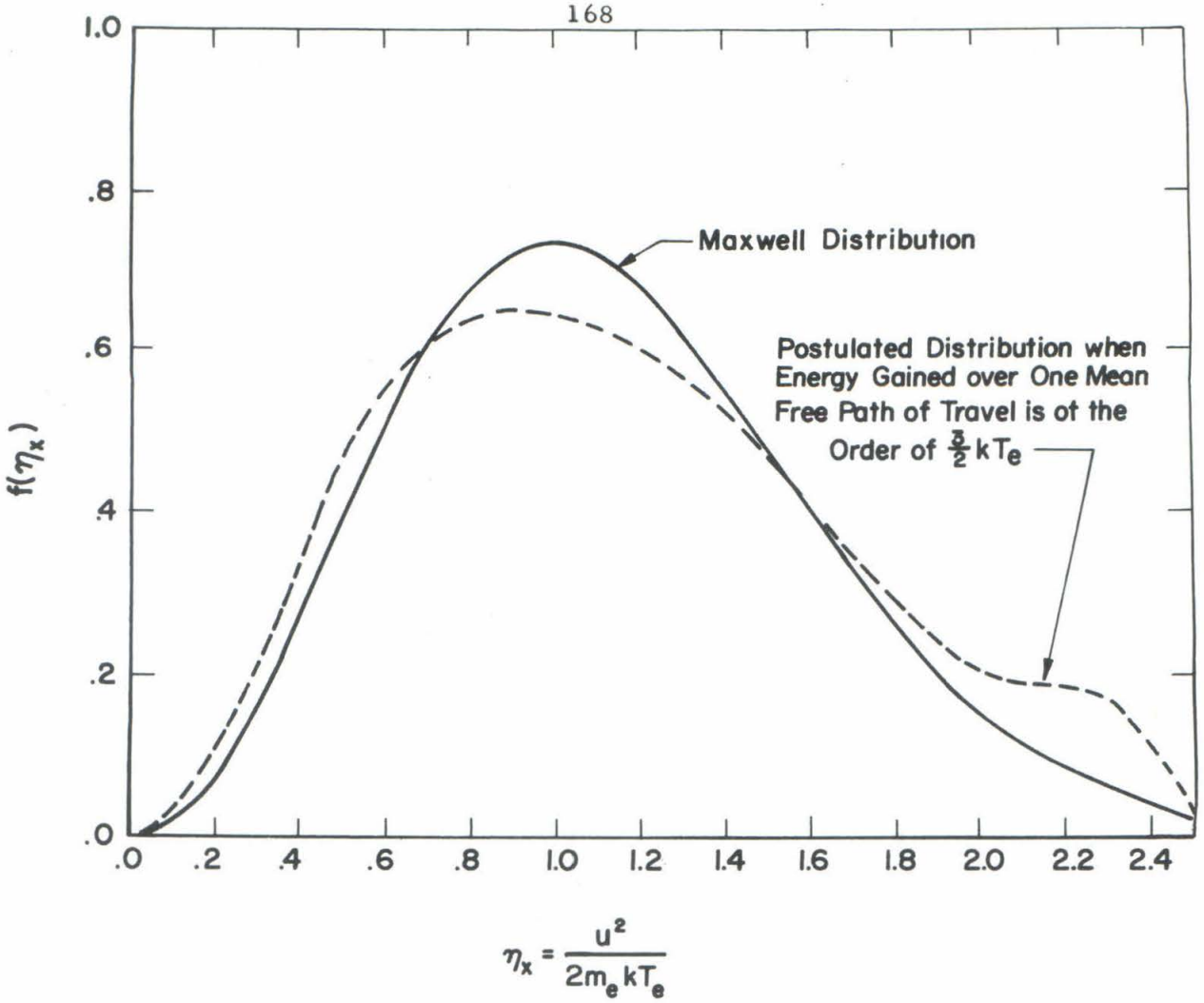

Fig. 8 POSTULATED ELECTRON ENERGY DISTRIBUTION IN A SHEATH WHEN NO CURRENT IS FLOWING

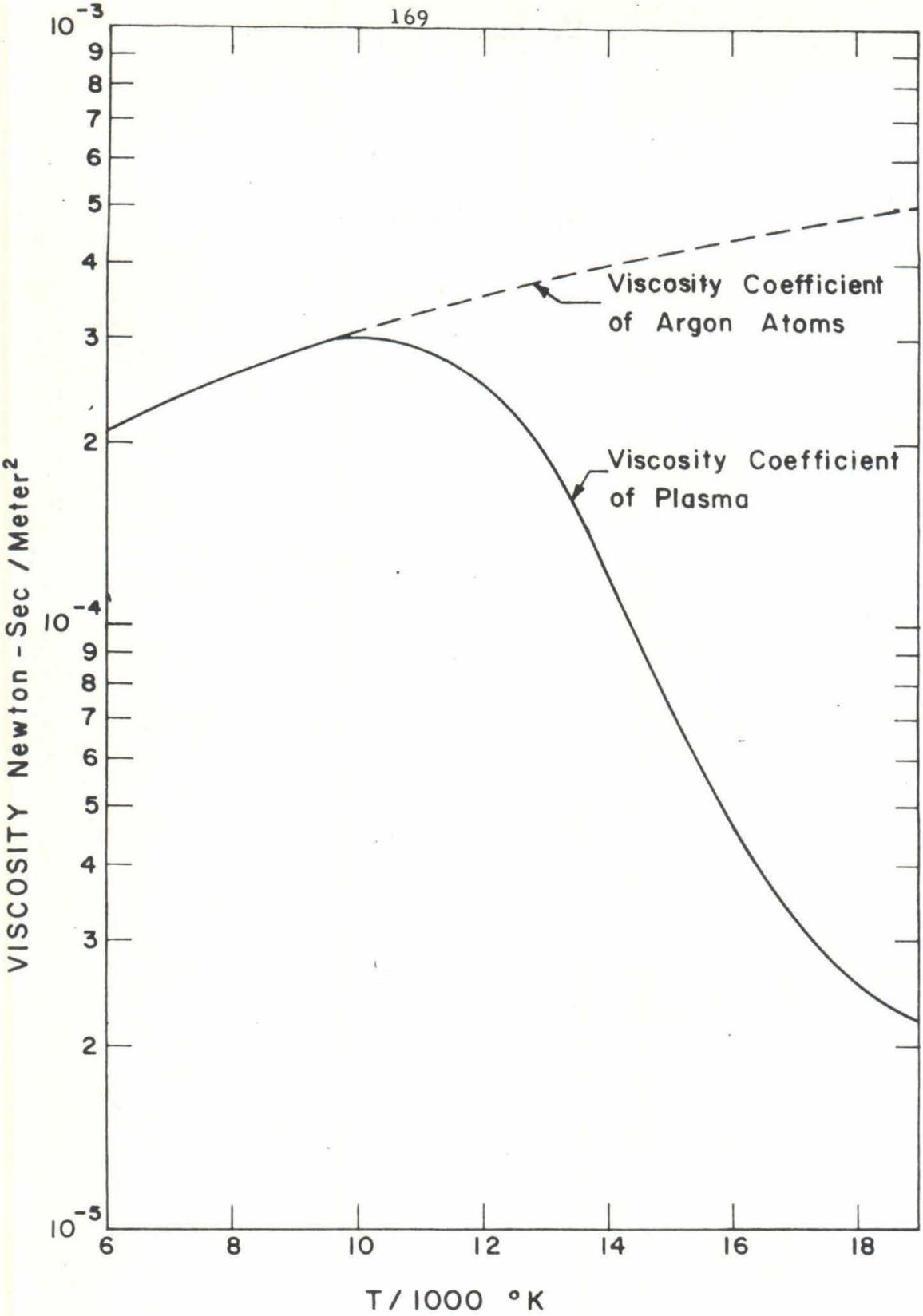

Fig. 9 VISCOSITY COEFFICIENT FOR ARGON PLASMA AT ONE ATMOSPHERE PRESSURE

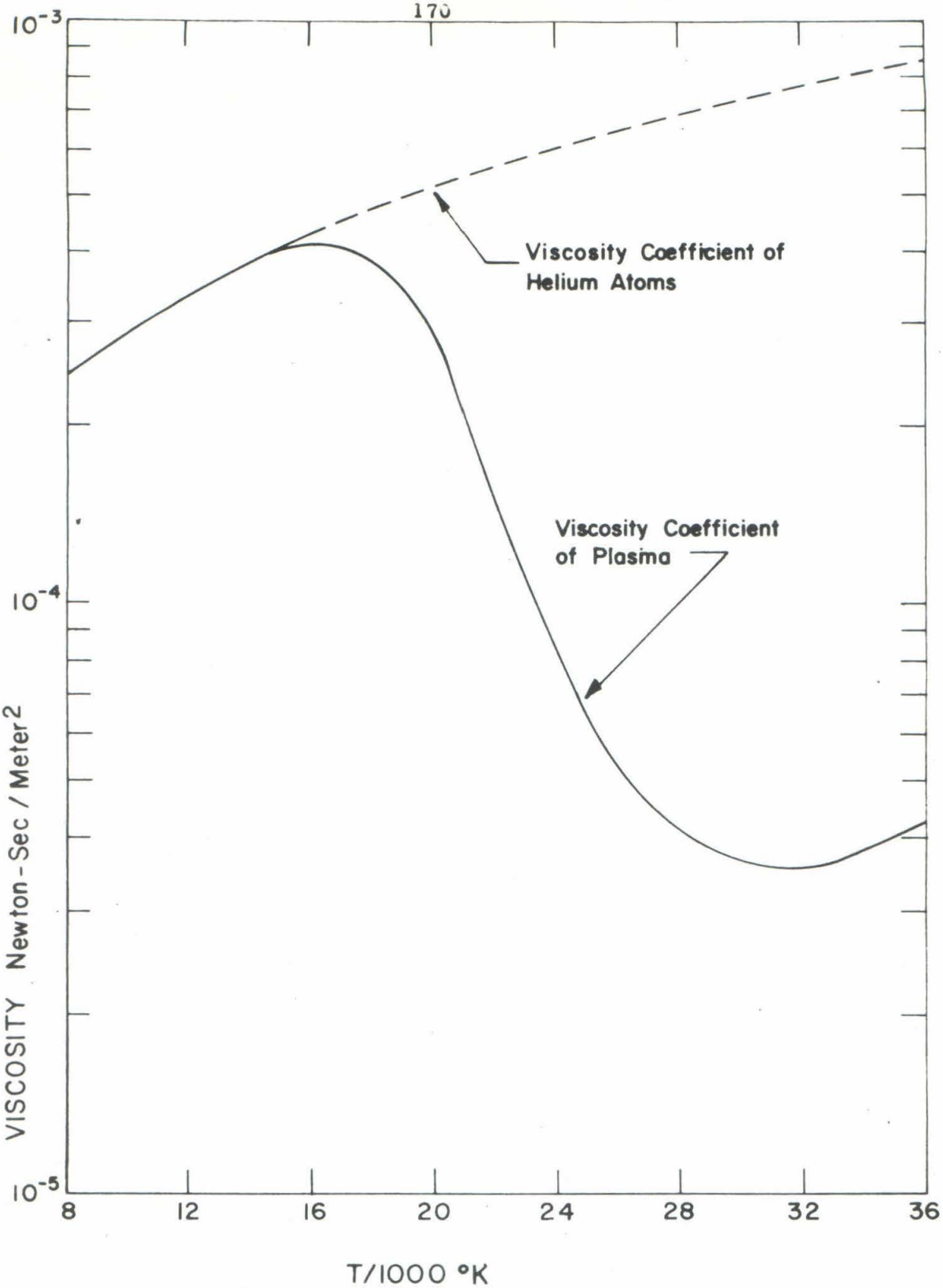

Fig 10 VISCOSITY COEFFICIENT FOR A HELIUM PLASMA AT ONE ATMOSPHERE PRESSURE

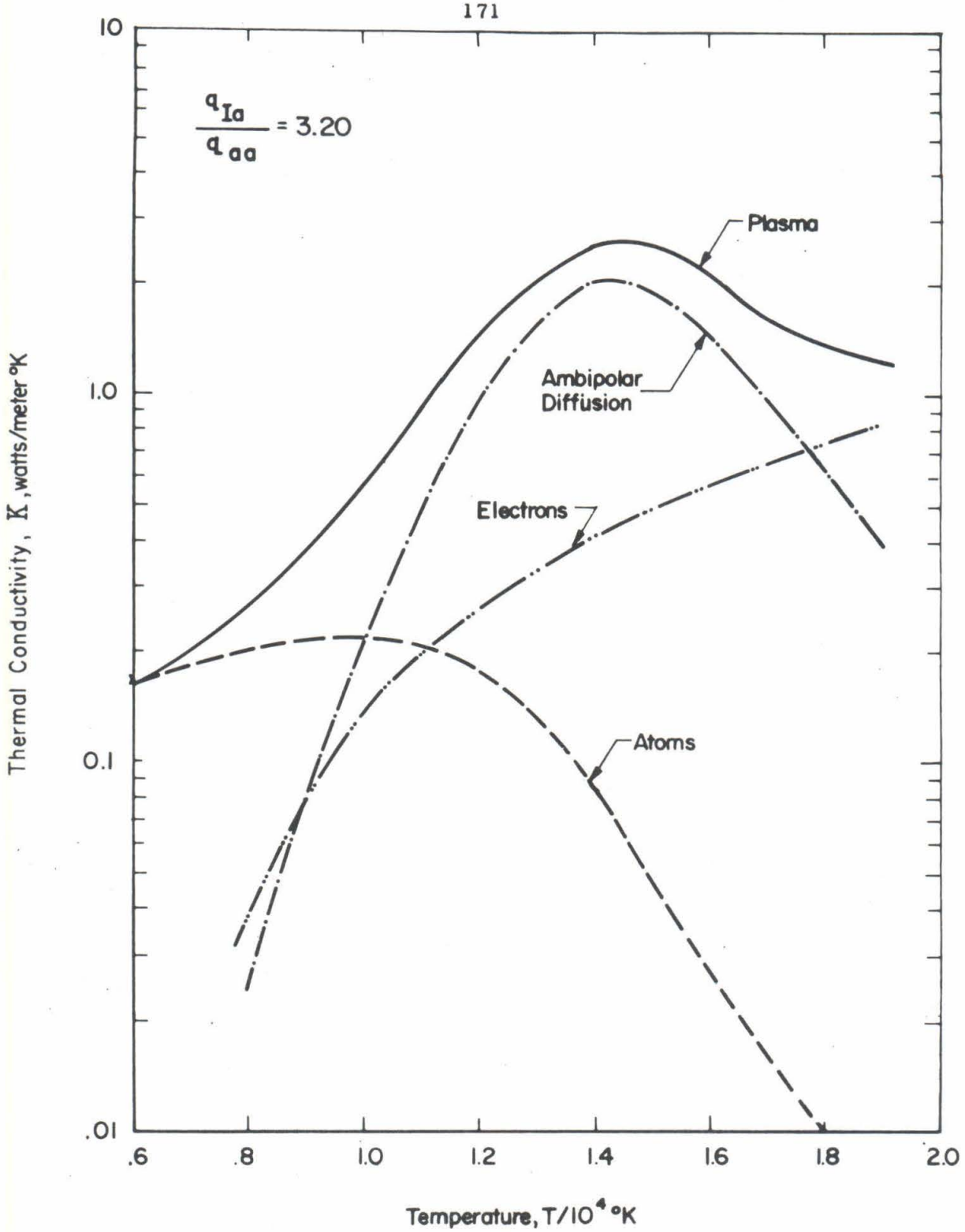

Fig. 11 THERMAL CONDUCTIVITY OF ARGON PLASMA AT ONE ATMOSPHERE PRESSURE

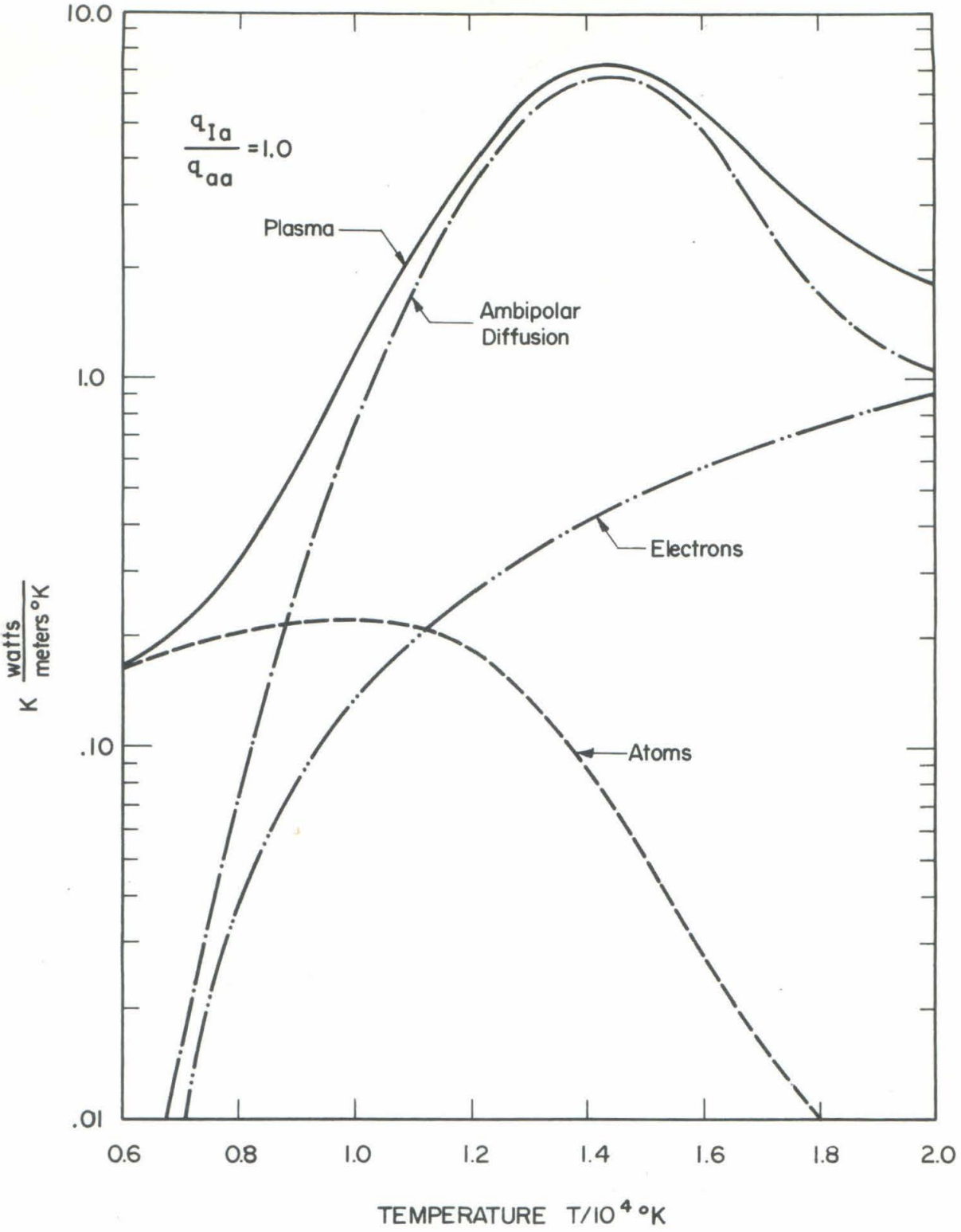

Fig. 11a THERMAL CONDUCTIVITY OF AN ARGON PLASMA AT ONE ATMOSPHERE PRESSURE

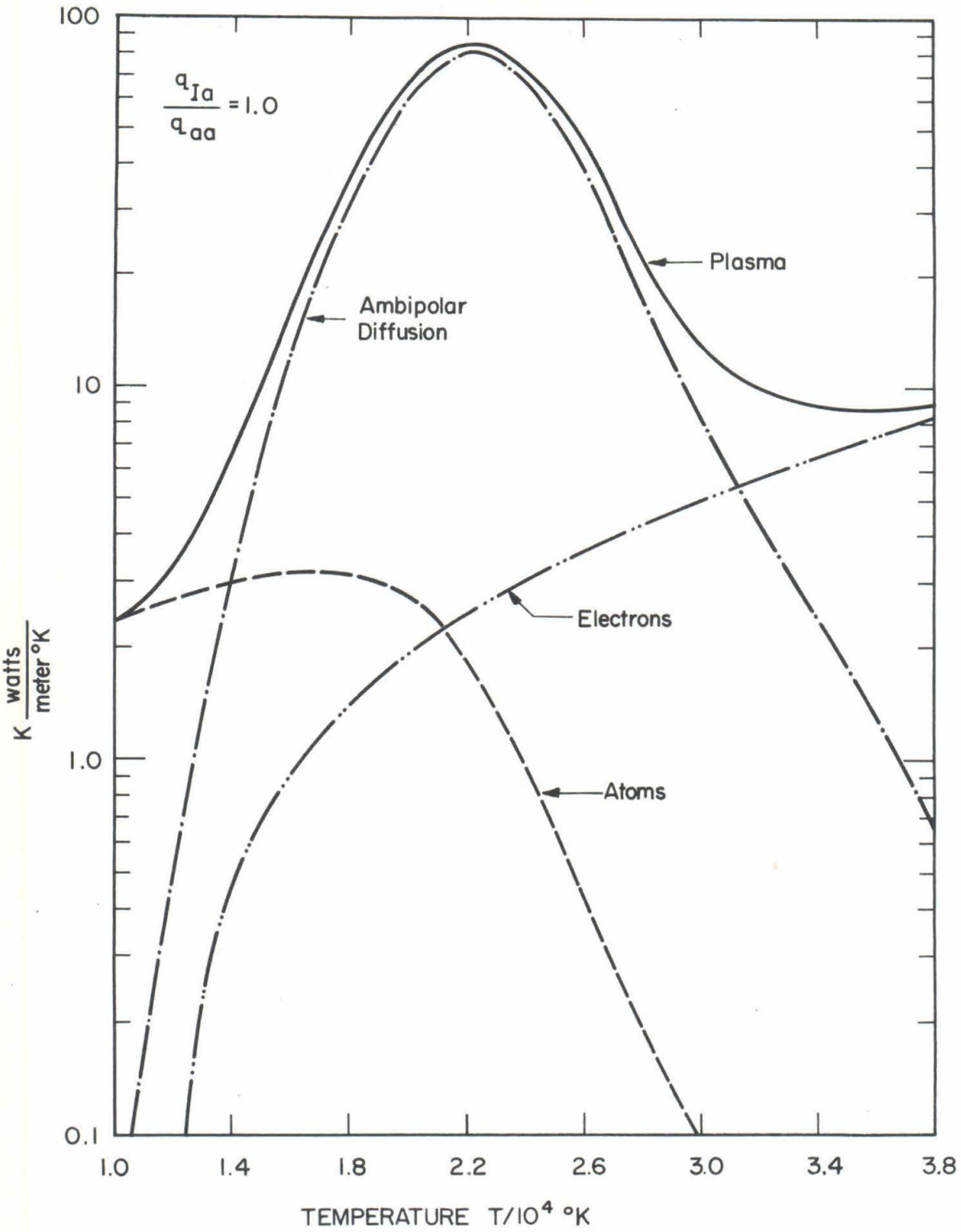

Fig. 12 THERMAL CONDUCTIVITY OF A HELIUM PLASMA AT ONE ATMOSPHERE PRESSURE

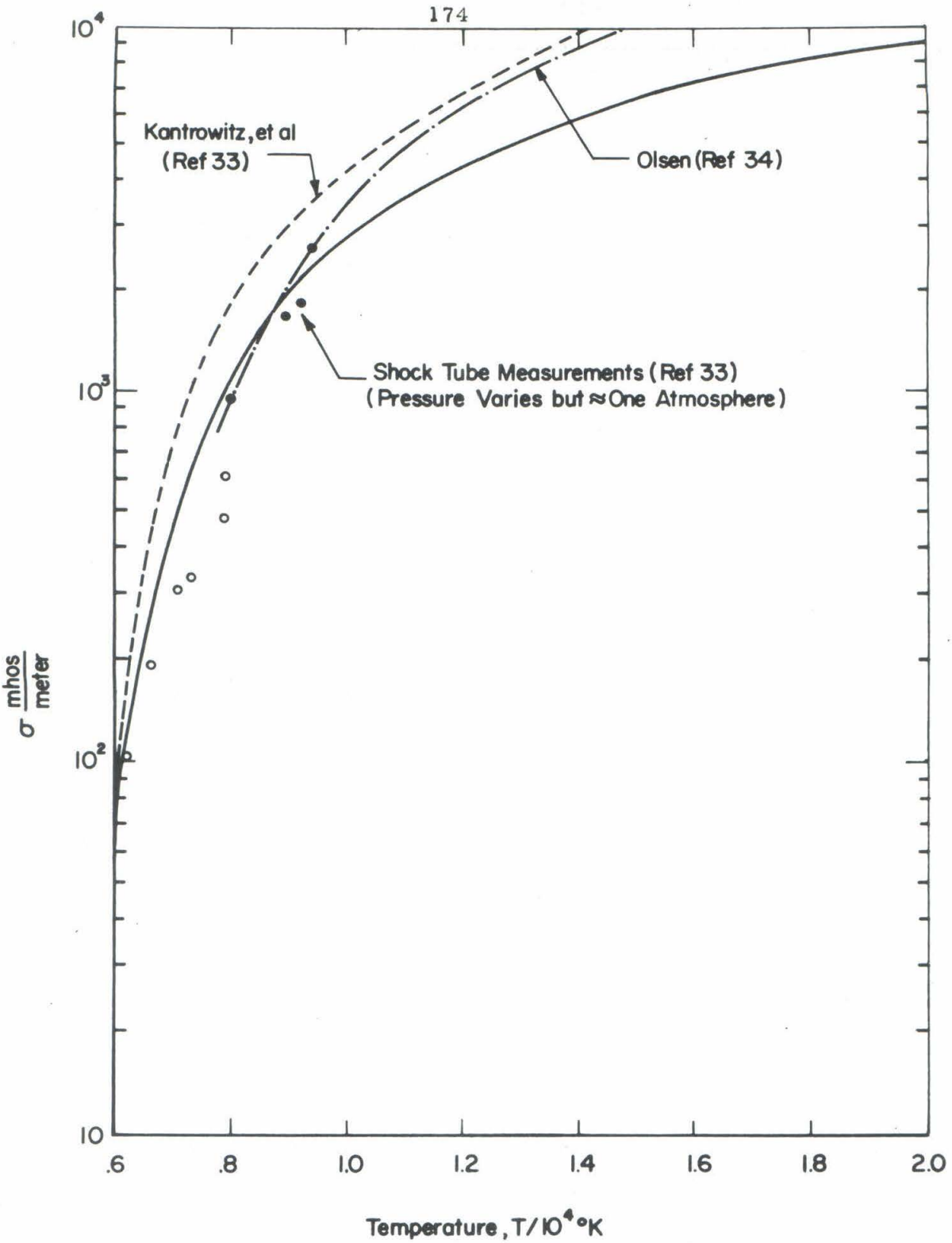

Fig.13 ELECTRICAL CONDUCTIVITY OF ARGON PLASMA AT ONE ATMOSPHERE PRESSURE

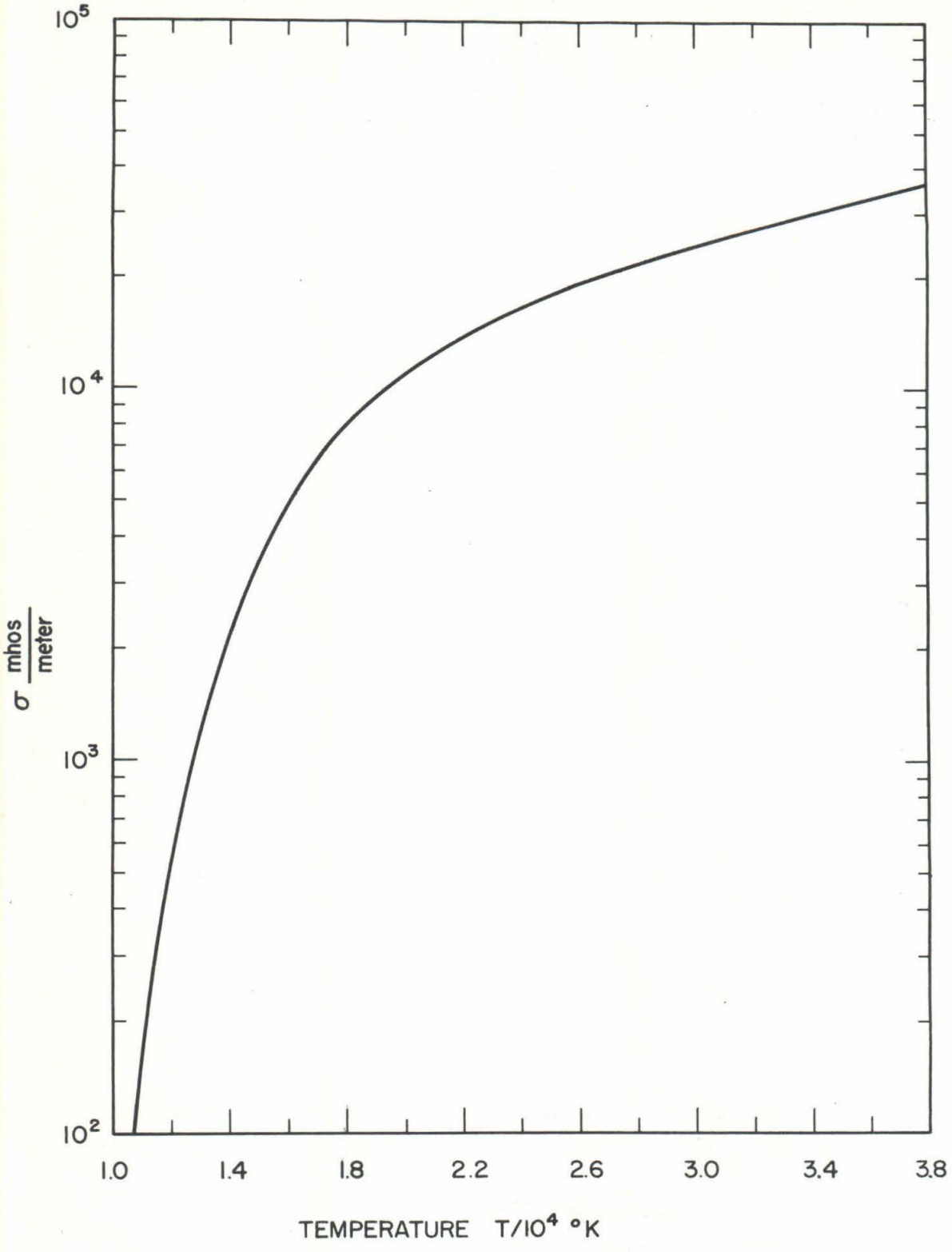

Fig. 14 ELECTRICAL CONDUCTIVITY OF HELIUM PLASMA AT ONE ATMOSPHERE PRESSURE

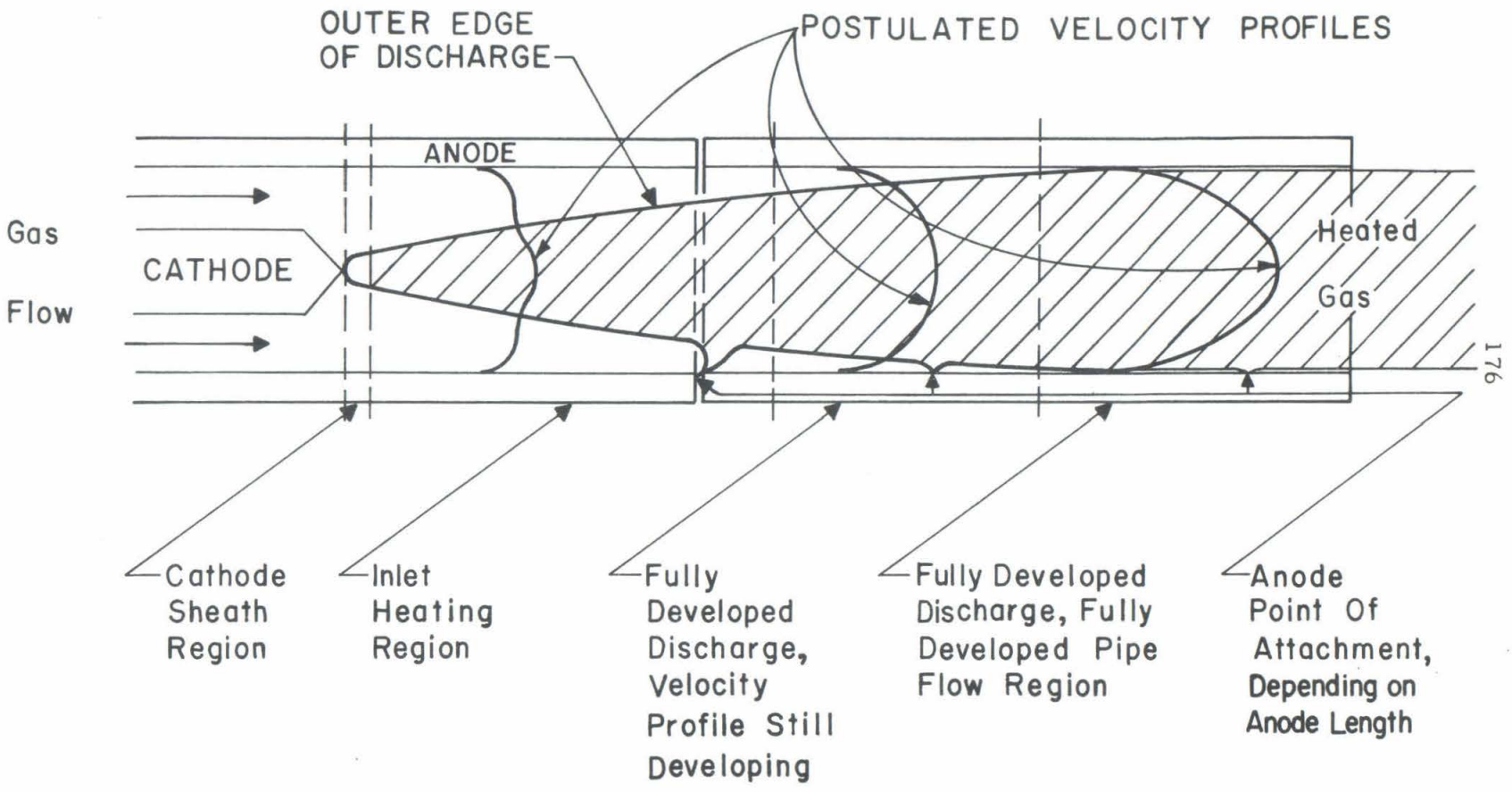

Fig. 15 WALL STABILIZED ARC

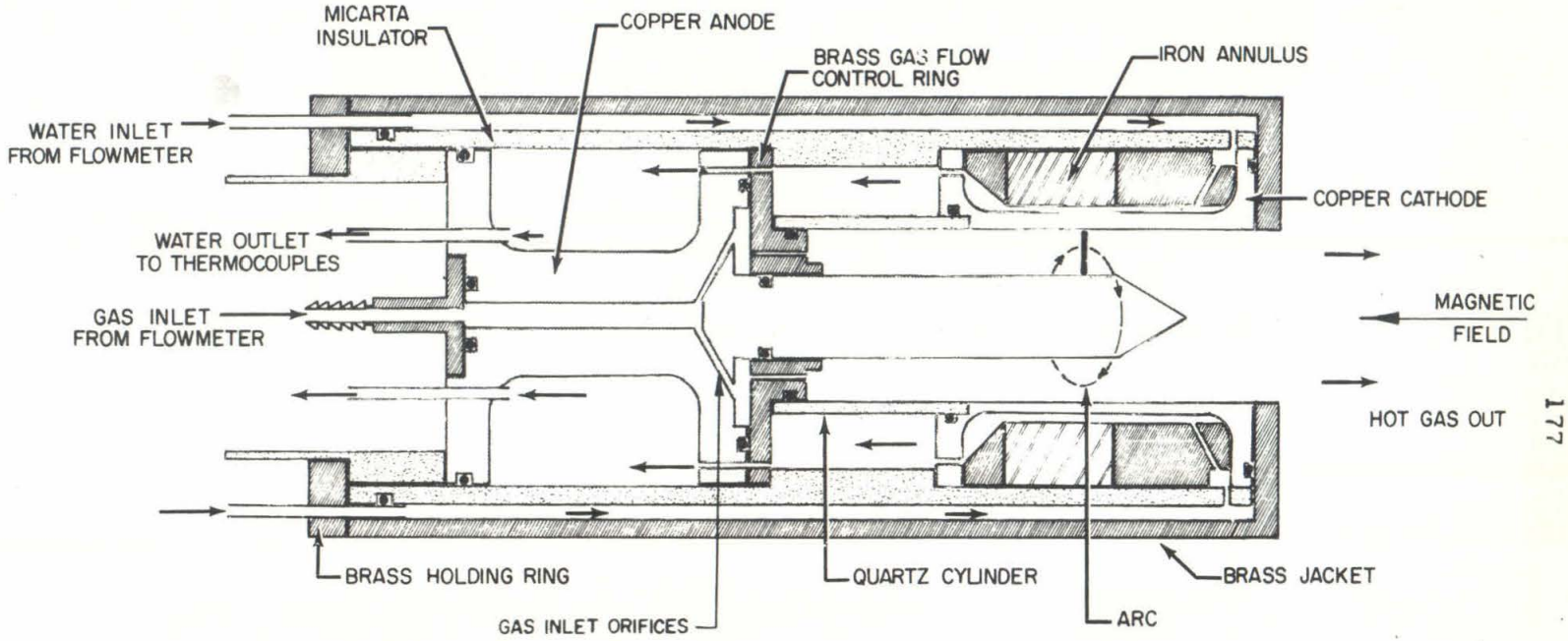

Fig. 16 ANNULAR ELECTRODE ARC HEATER

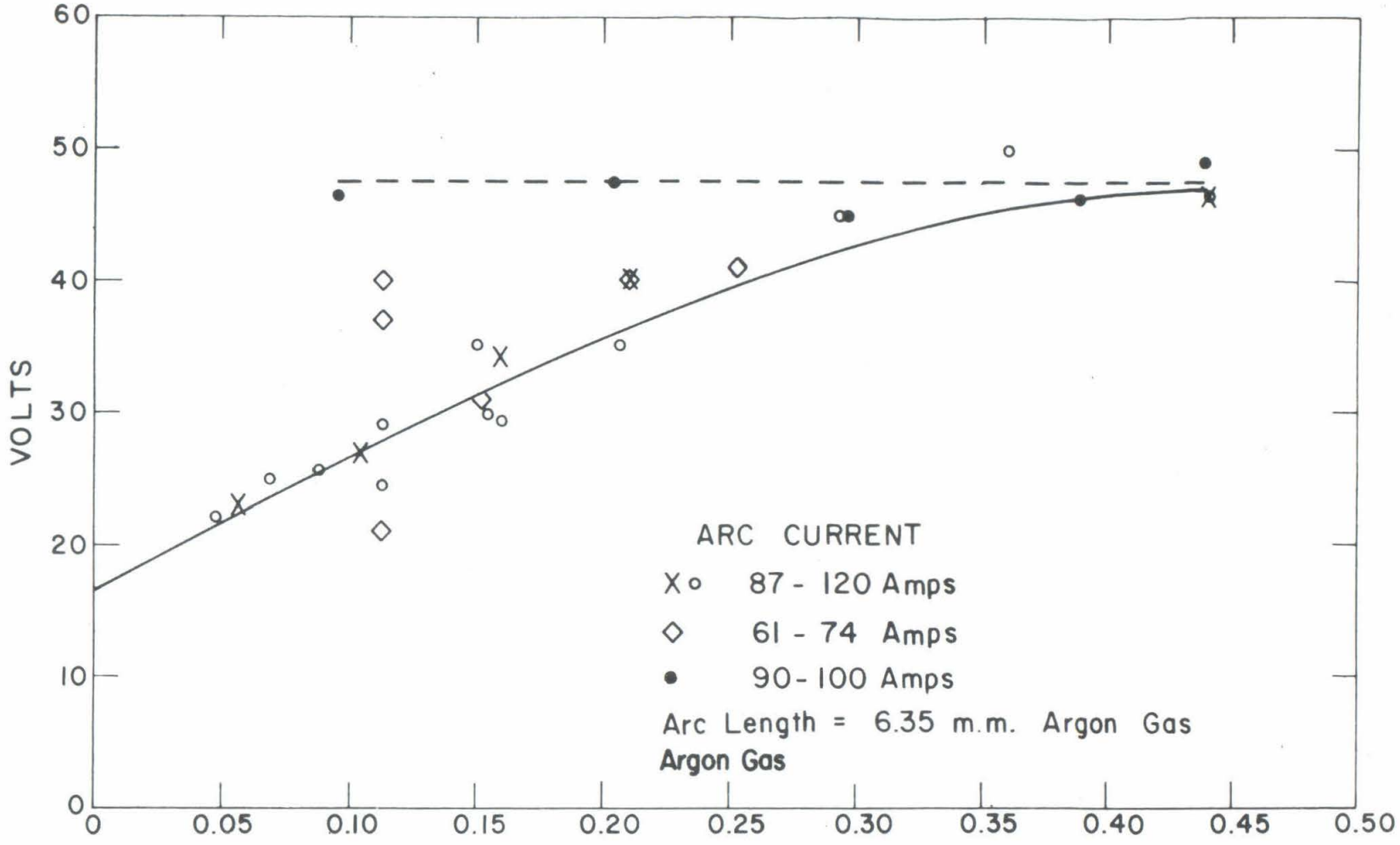

Fig.17 POTENTIAL DROP ACROSS THE ARC AS A FUNCTION OF THE MAGNETIC FIELD STRENGTH

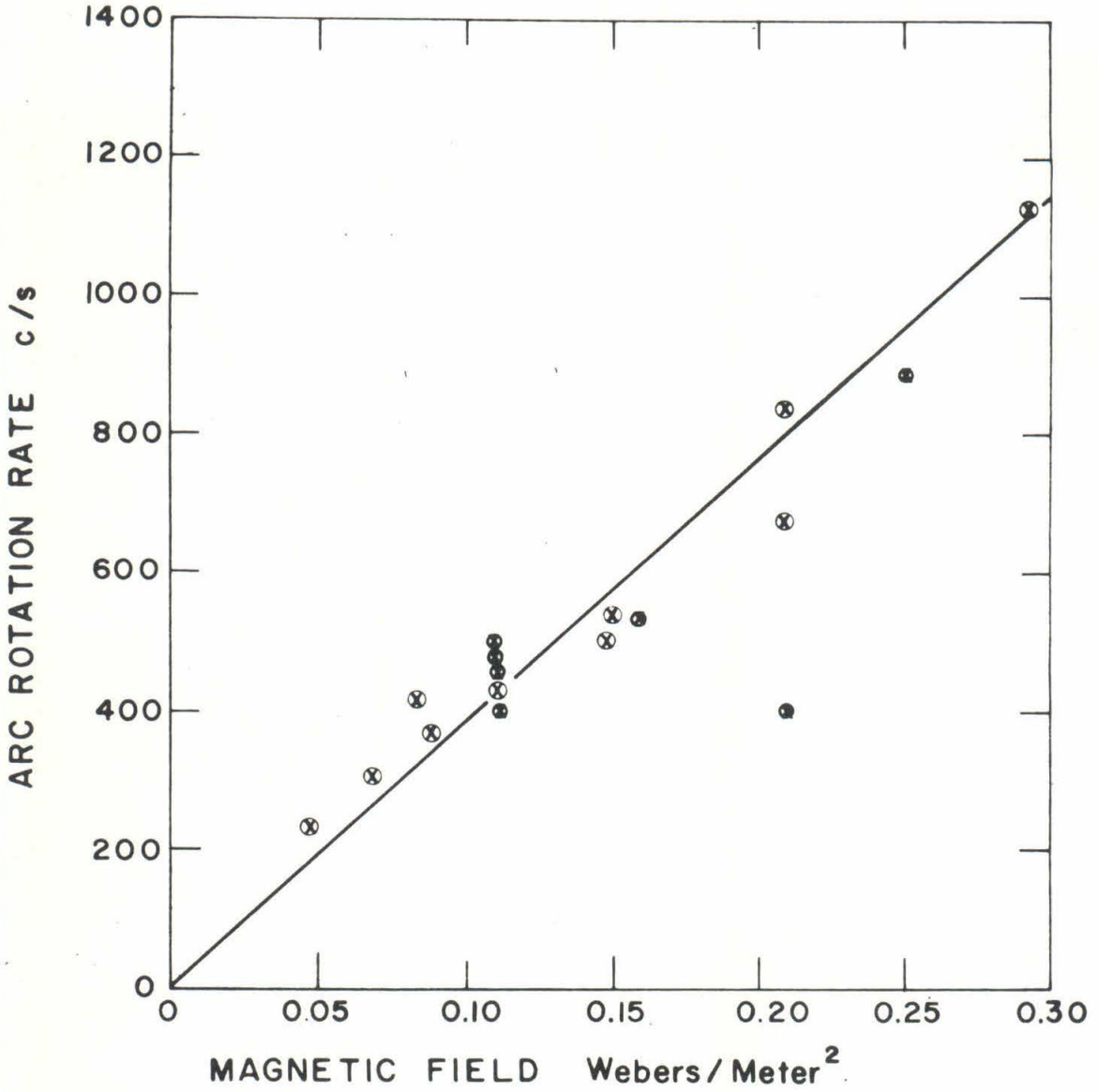

Fig. 18 ARC ROTATION RATE AS A FUNCTION OF THE MAGNETIC FIELD STRENGTH

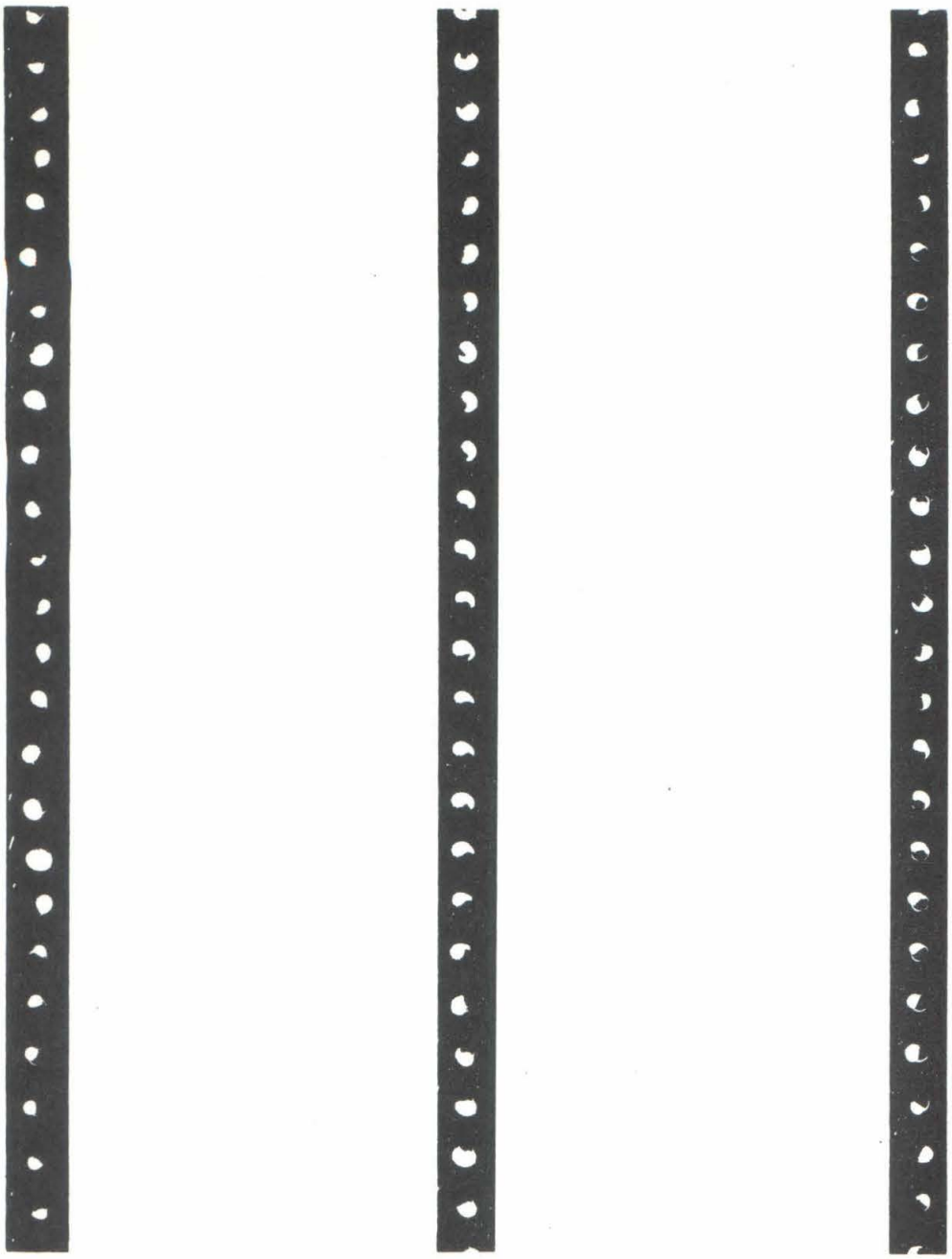

Fig. 19 FASTEX CAMERA PICTURES OF ROTATING ARC

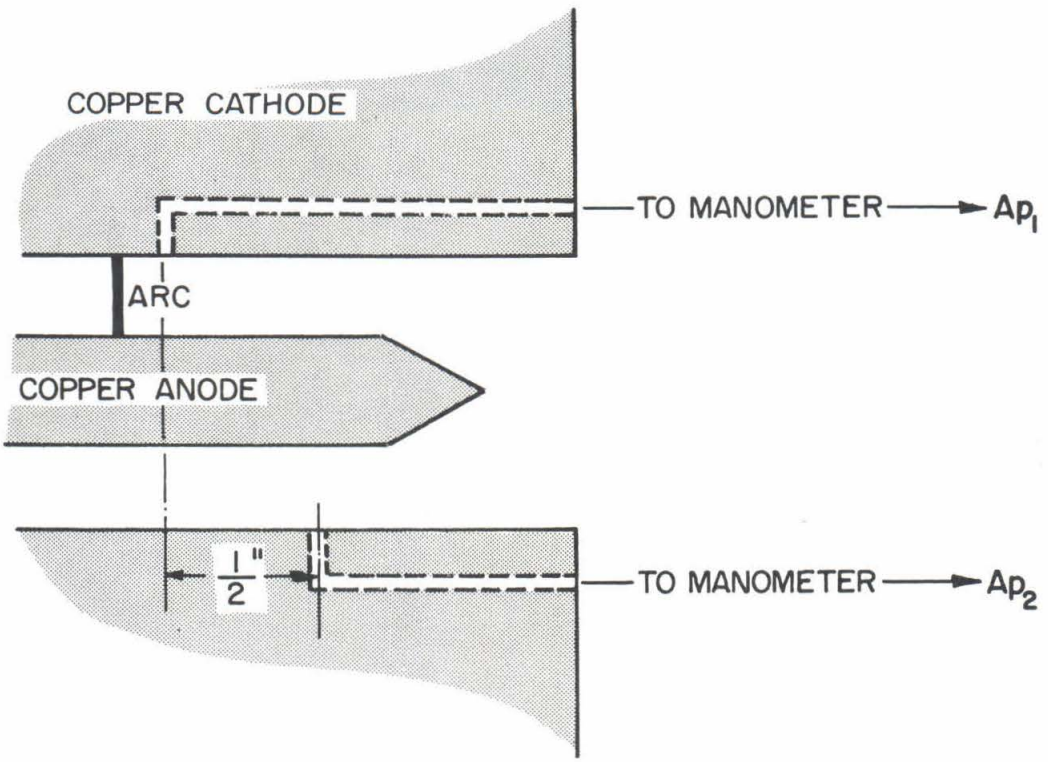

Fig. 20 STATIC PRESSURE ORIFICES

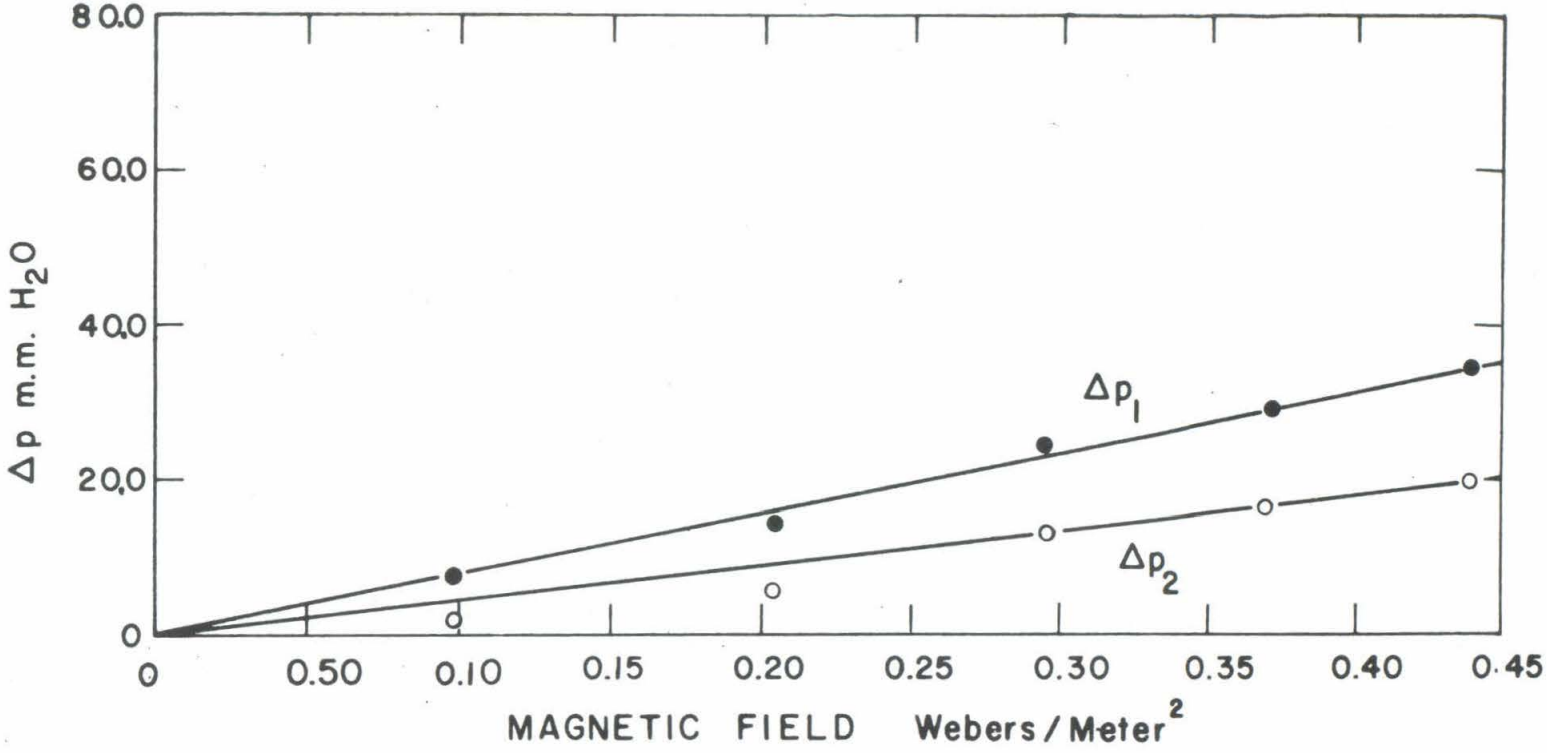

Fig. 21 RADIAL GAS PRESSURE DIFFERENTIAL AS A FUNCTION OF THE MAGNETIC FIELD STRENGTH

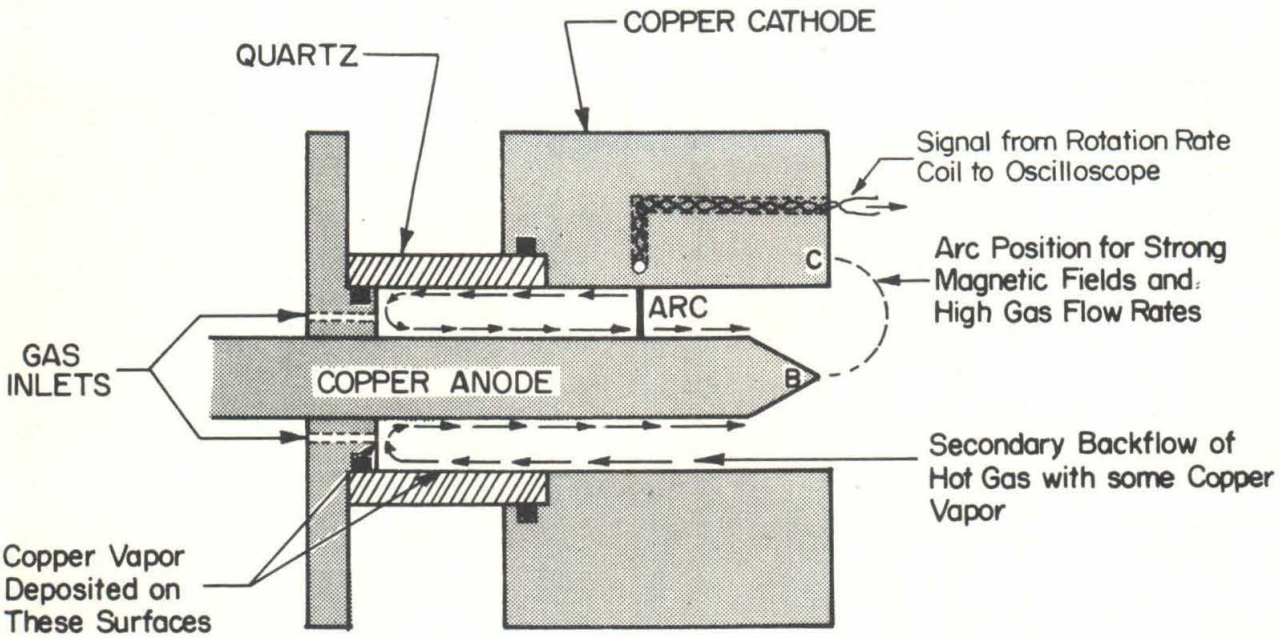

Fig.22 BACKFLOW OF HOT GAS INDUCED BY ARC ROTATION

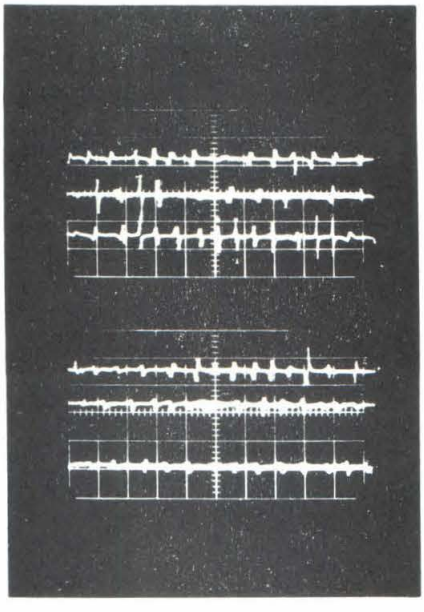

Fig. 23

SCALE: Vertical 2 m. volts/cm.
Horizontal 5 m. sec/cm.

Arc Current = 97 amperes

Magnetic Field = .0700 $\frac{\text{Webers}}{\text{Meter}^2}$

SIGNAL FROM ROTATION RATE MEASURING COILS MOUNTED IN THE ARC CATHODE.

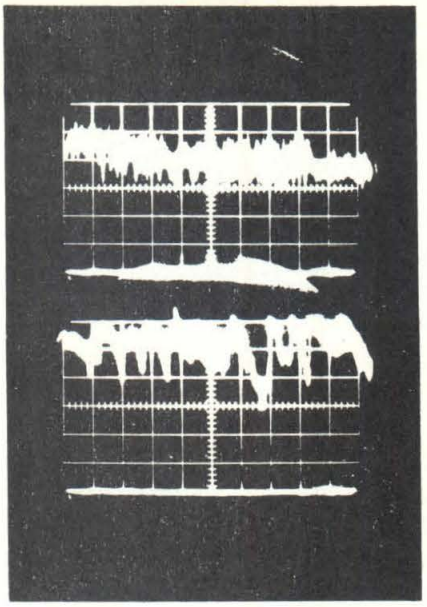

Fig. 24

SCALE: Vertical 10 volts/cm.
Horizontal 500 μ.sec/cm.

Arc Current = 55 amperes

Magnetic Field Strength = 0.44 $\frac{\text{Webers}}{\text{Meter}^2}$

ARC VOLTAGE OSCILLOGRAM SHOWING TWO MODES OF ARC OPERATION WITH AMPLITUDE AND FREQUENCY OF THE VOLTAGE FLUCTUATIONS.

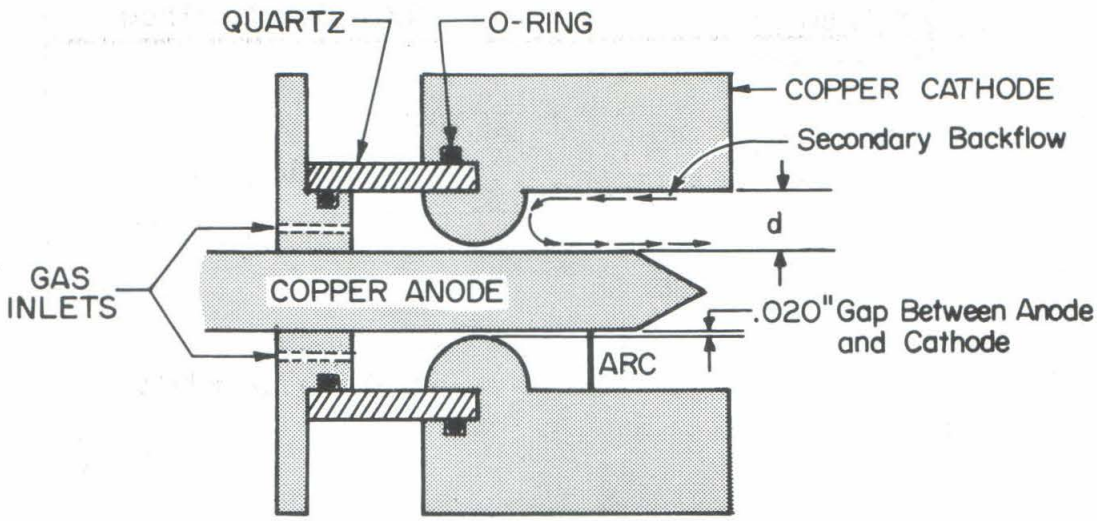

Fig.25 MODIFIED CATHODE TO REDUCE BACKFLOW ENERGY LOSSES and to PROTECT O-RING

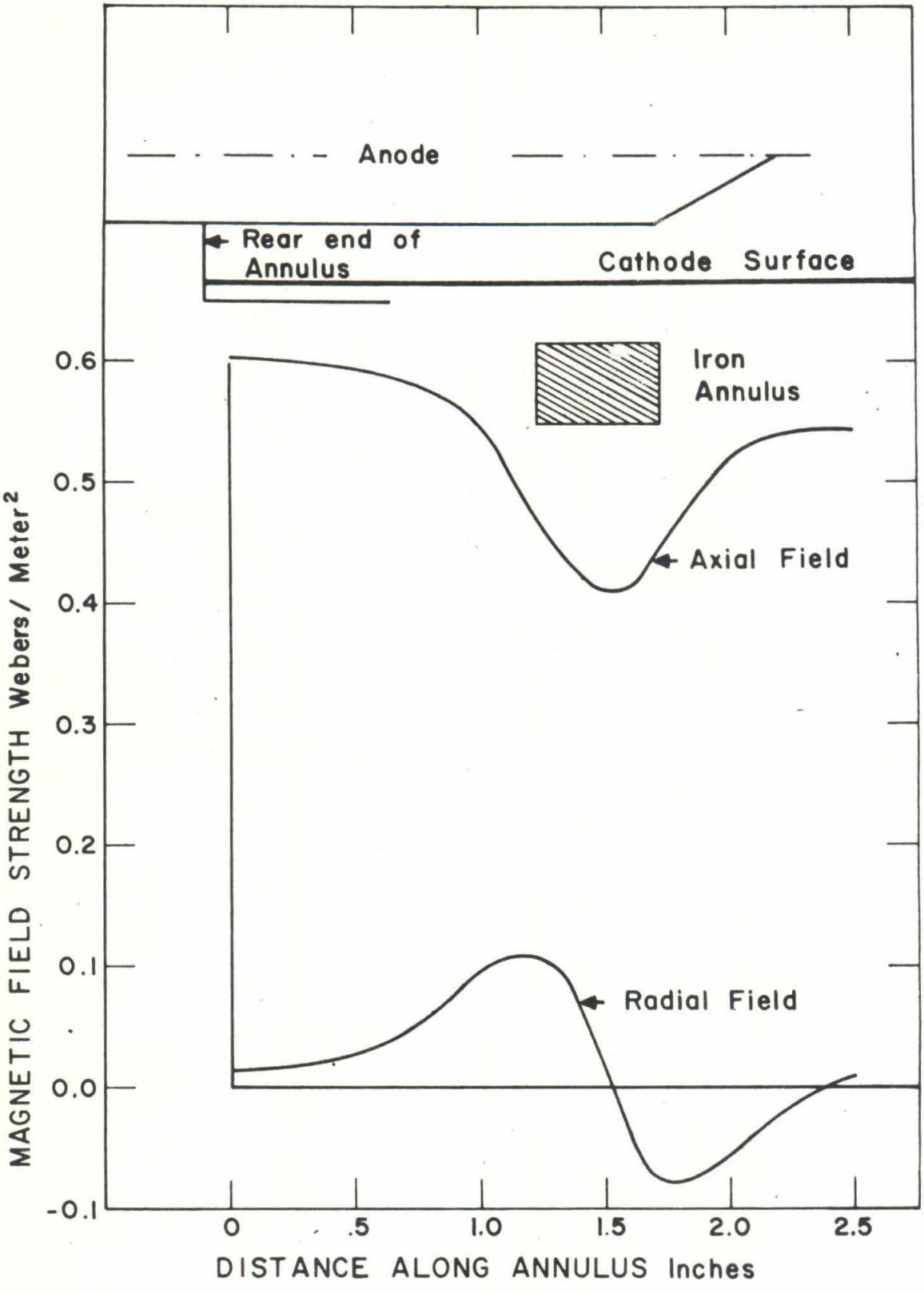

Fig. 26 AXIAL MAGNETIC FIELD PERTURBATION DUE TO IRON ANNULUS

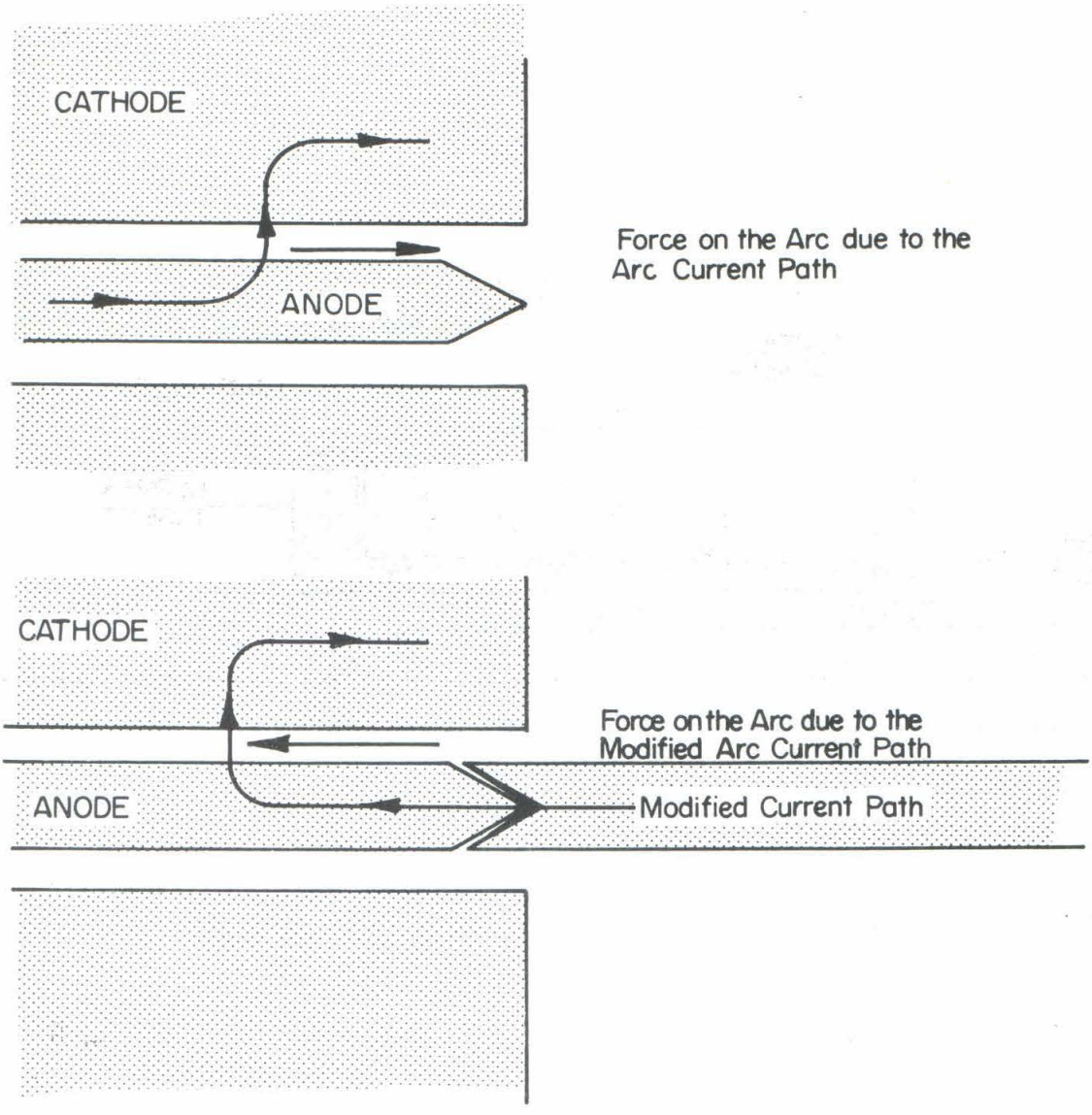

Fig. 27 AXIAL ELECTROMAGNETIC FORCE ON THE ARC DUE TO THE ARC CURRENT

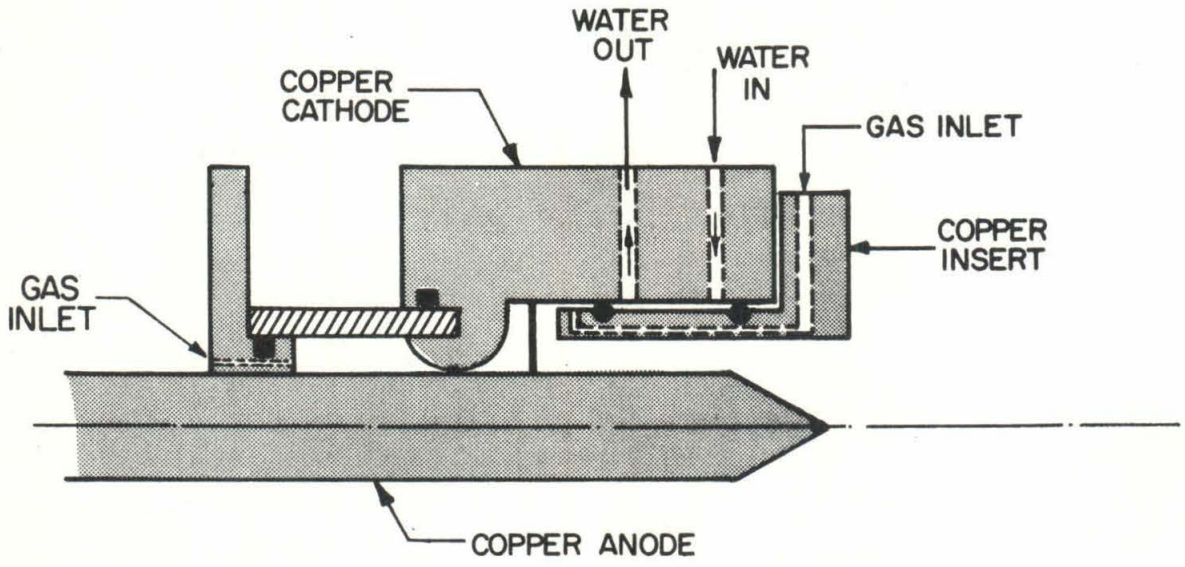

Fig. 28 COPPER INSERT USED TO POSITION THE ARC

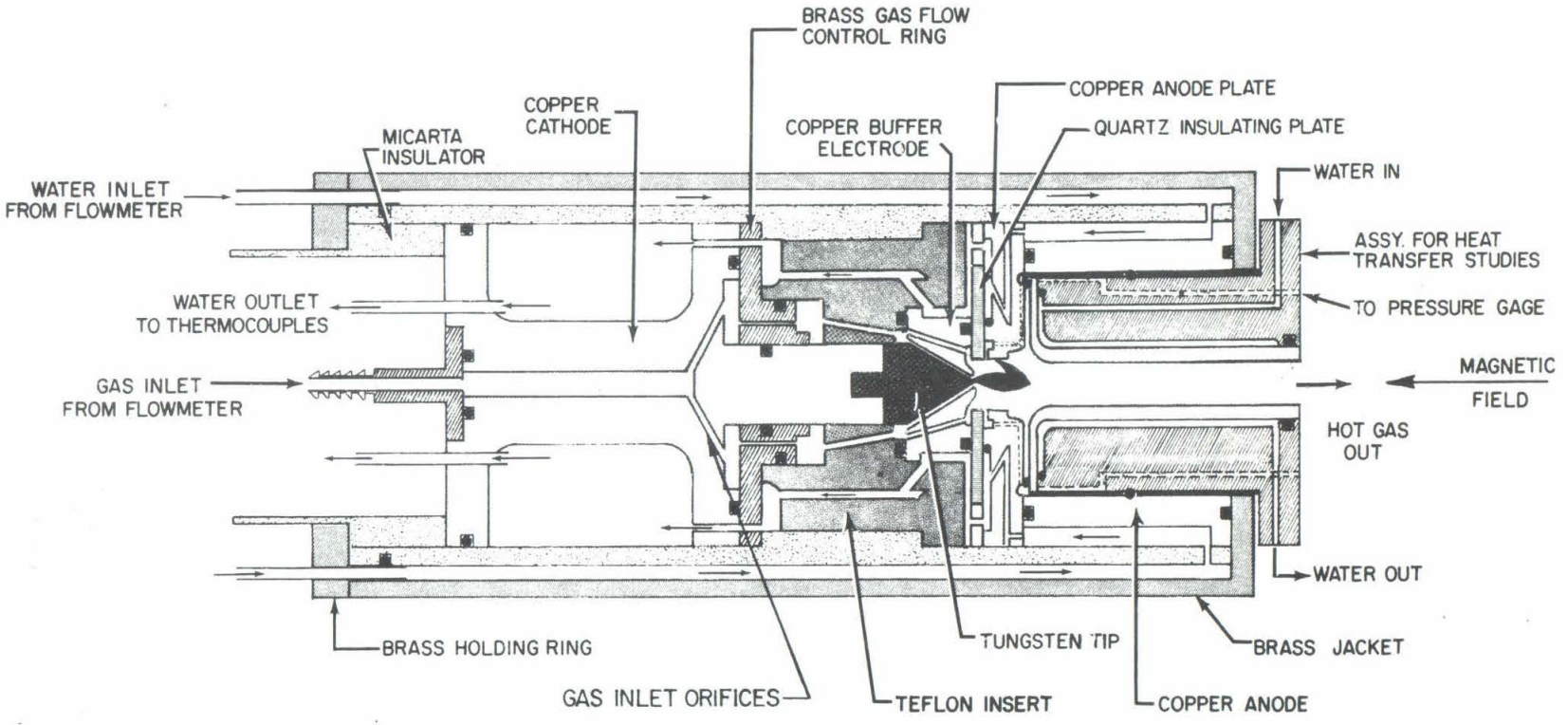

Fig. 29 POINT TO RING ELECTRODE ARC JET

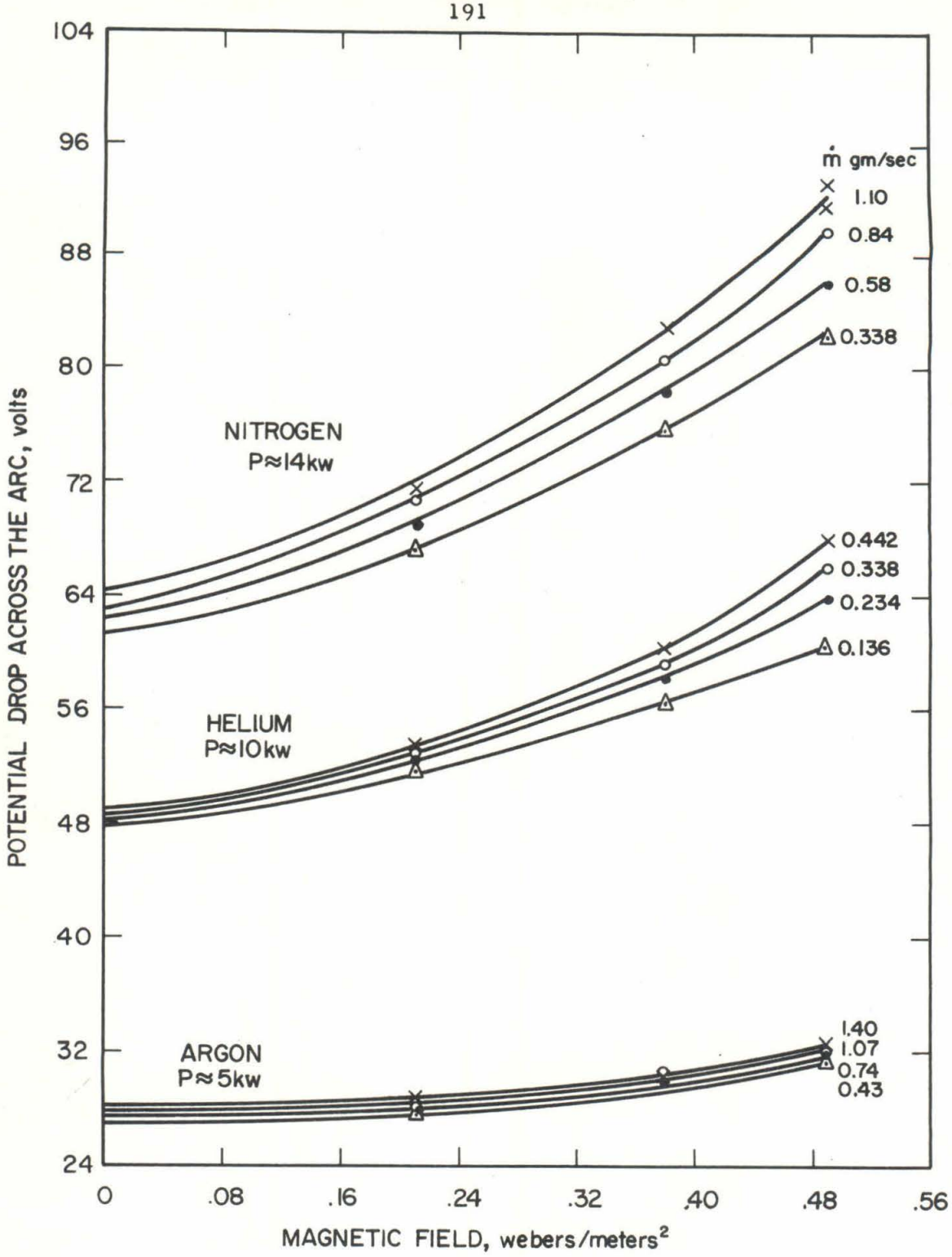

Fig. 30 ARC POTENTIAL DROP IN POINT TO RING ELECTRODE CONFIGURATION

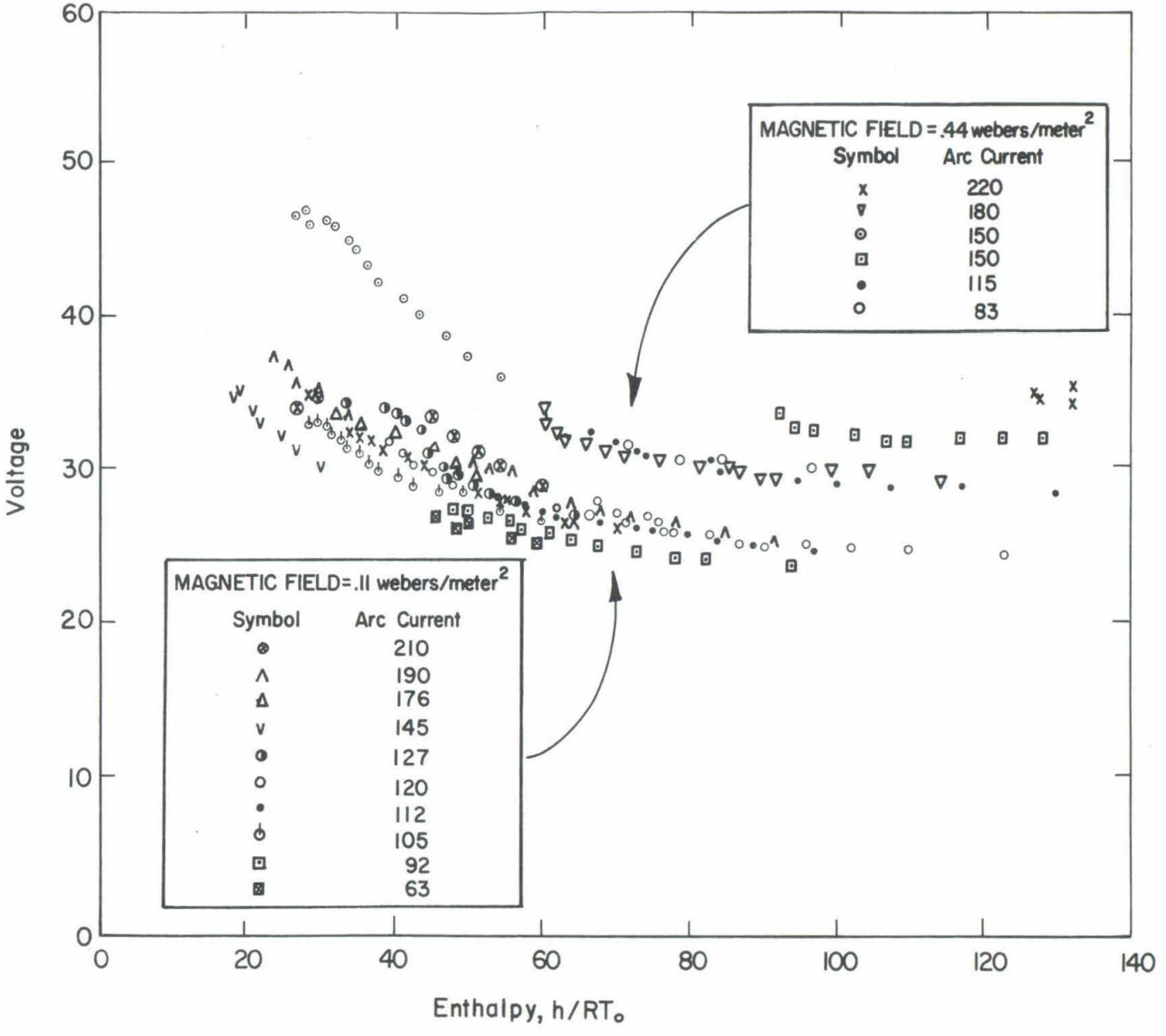

Fig. 31 ARC POTENTIAL DROP AS A FUNCTION OF THE AVERAGE ENTHALPY FOR ARGON

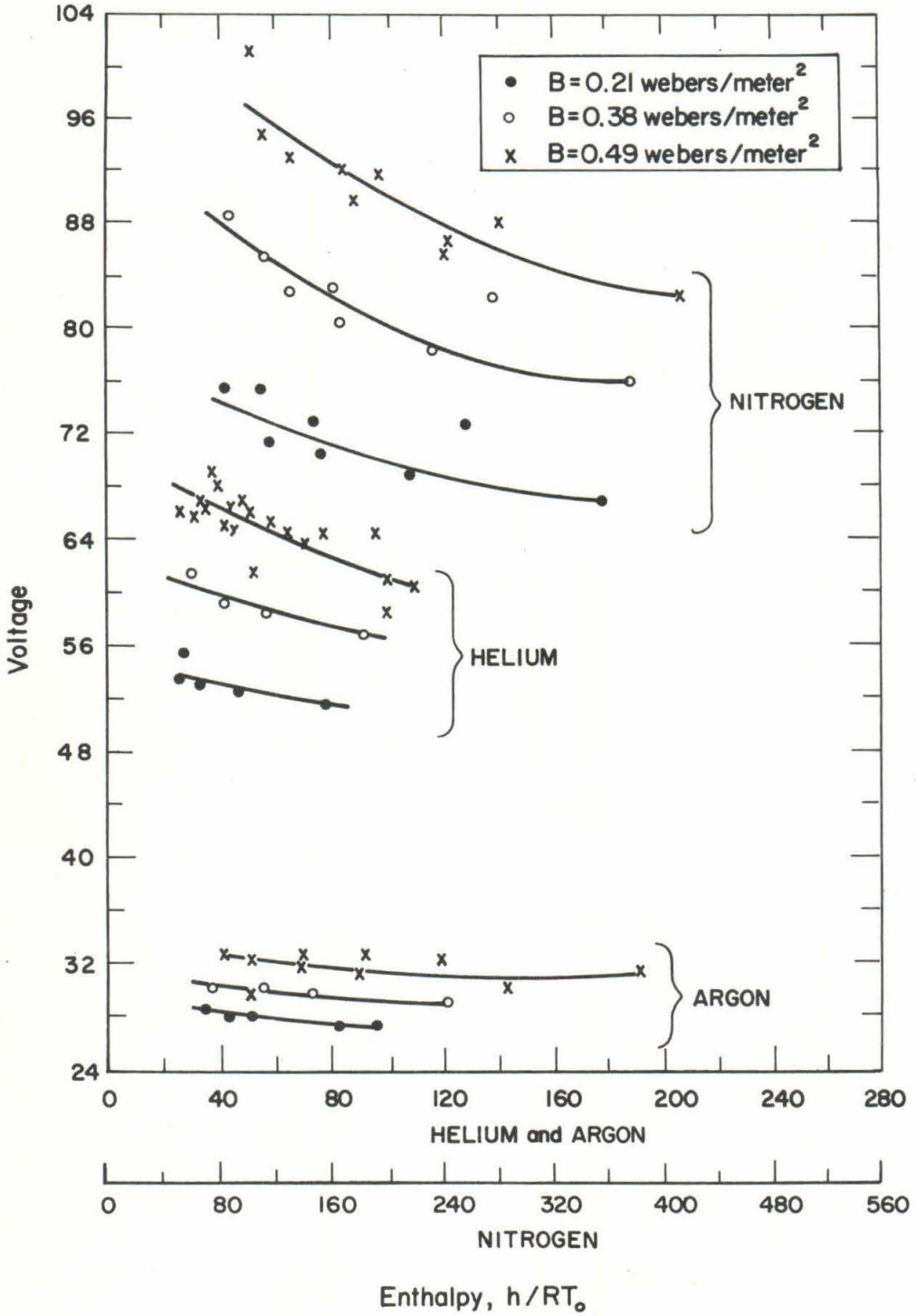

Fig. 32 POTENTIAL DROP ACROSS ARC FOR SOME REPRESENTATIVE GASES

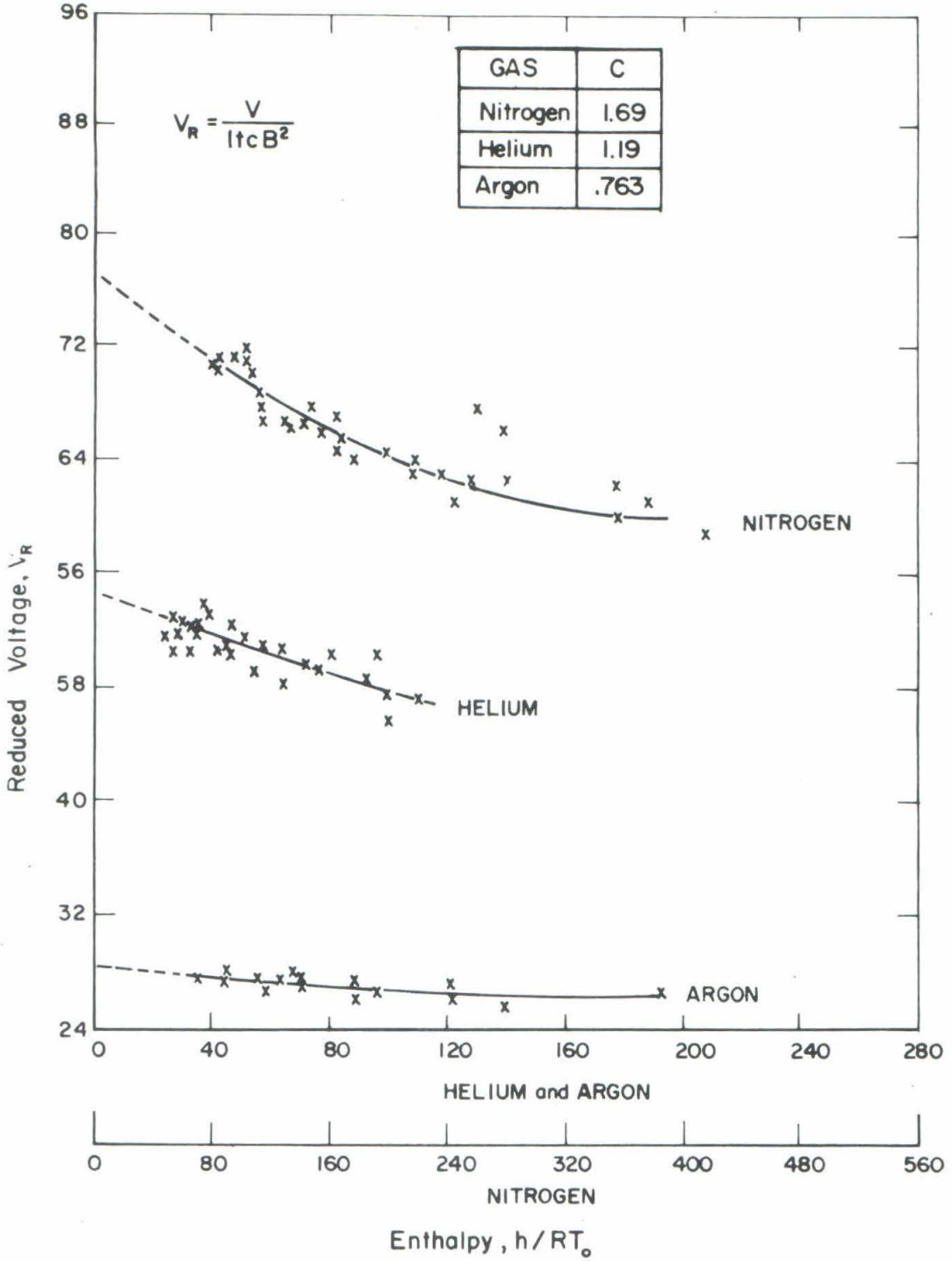

Fig. 33 REDUCED ARC POTENTIAL DROP

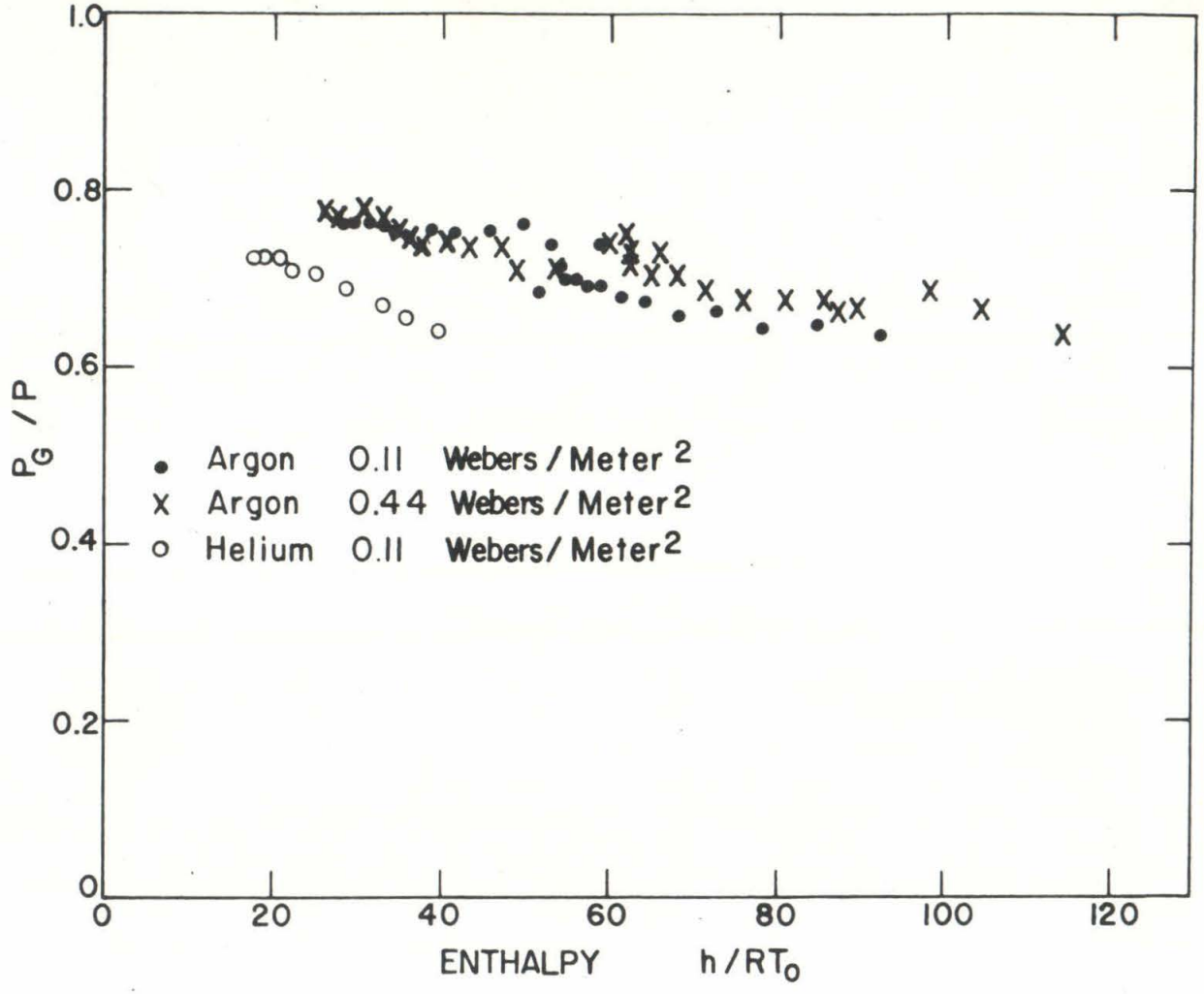

Fig. 34 EFFICIENCY OF ENERGY TRANSFER TO GAS

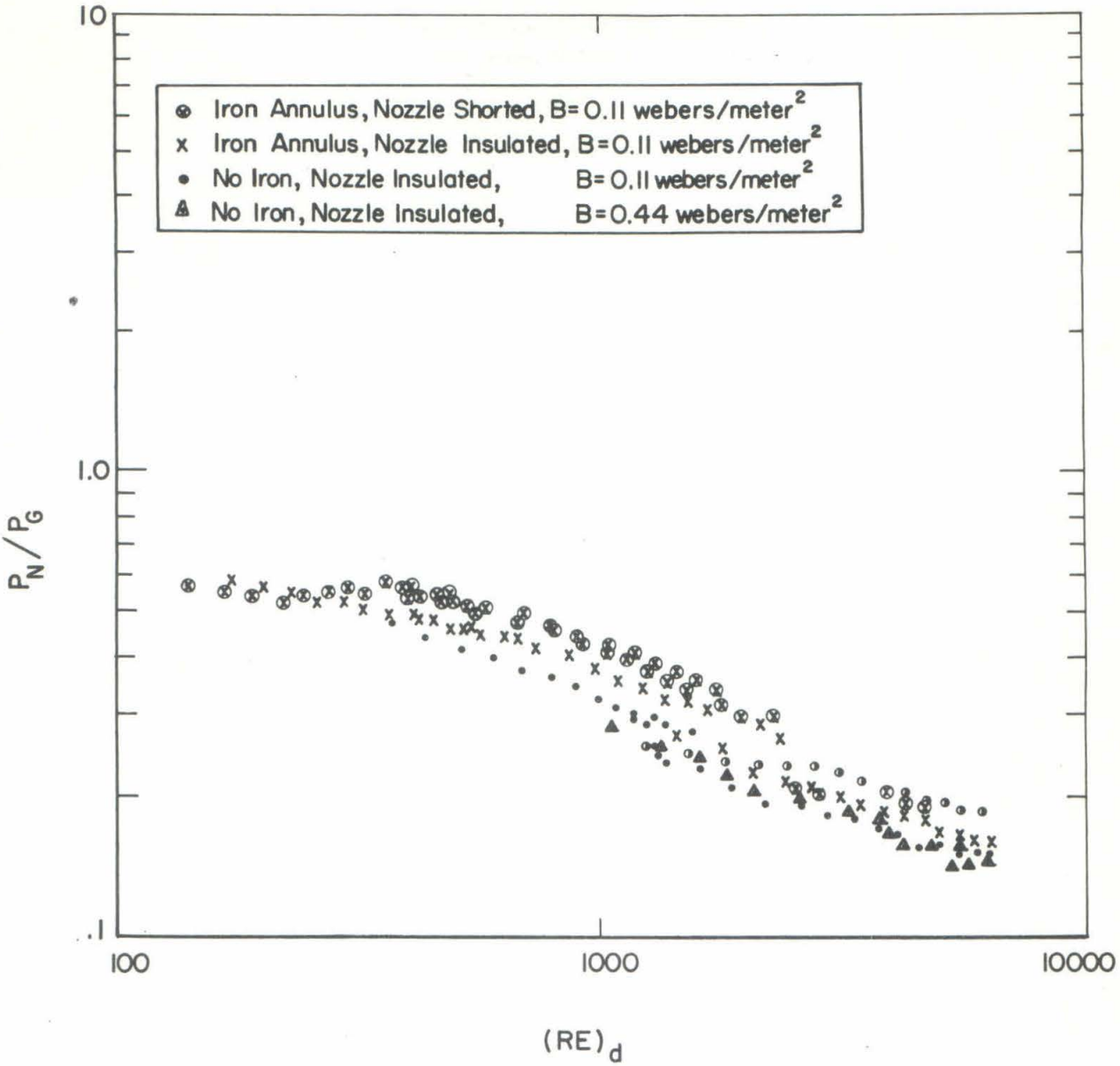

Fig 35 HEAT TRANSFER MEASUREMENTS TO CYLINDER I IN ARGON

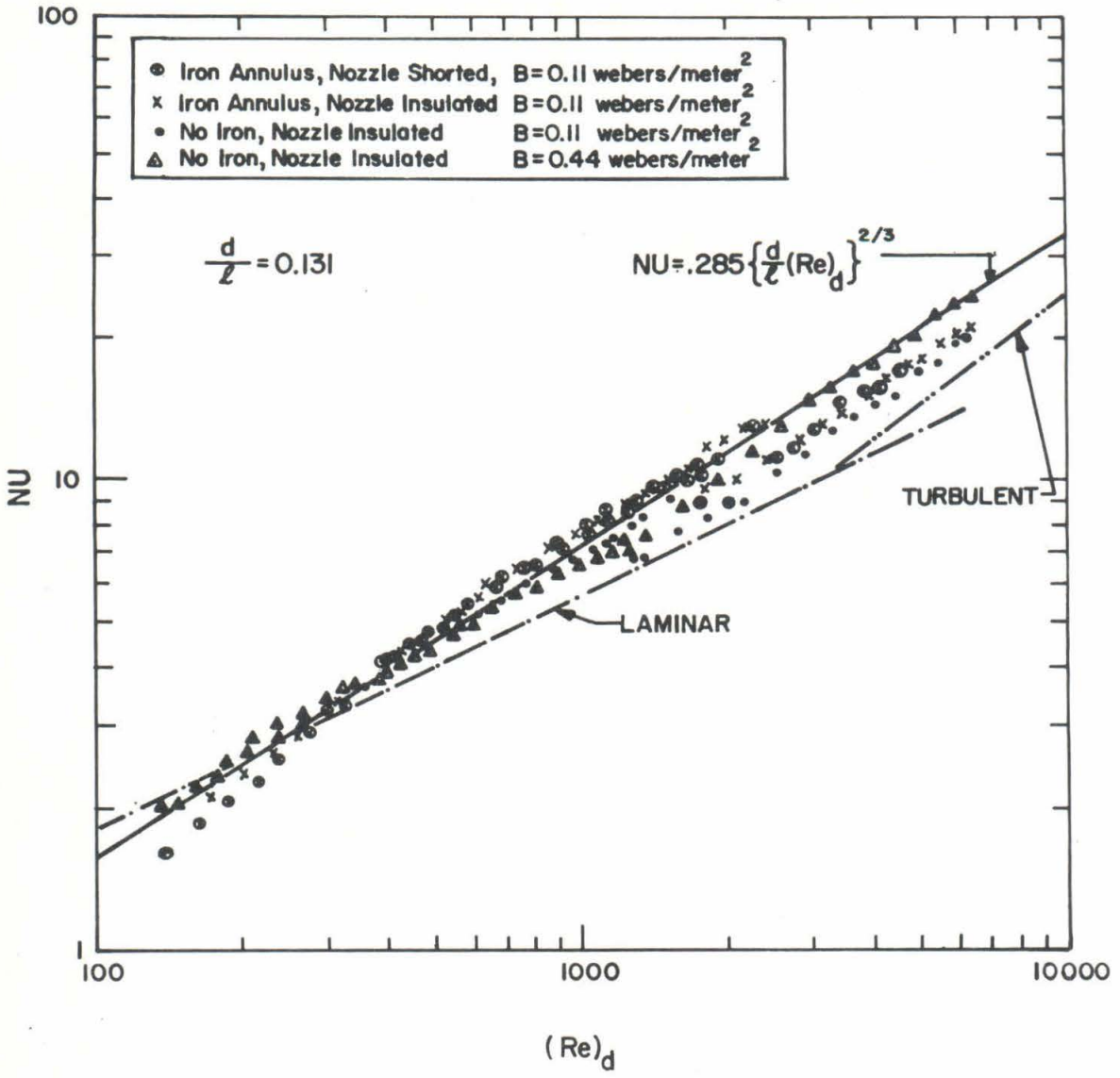

Fig 36 HEAT TRANSFER MEASUREMENTS TO CYLINDER I IN ARGON

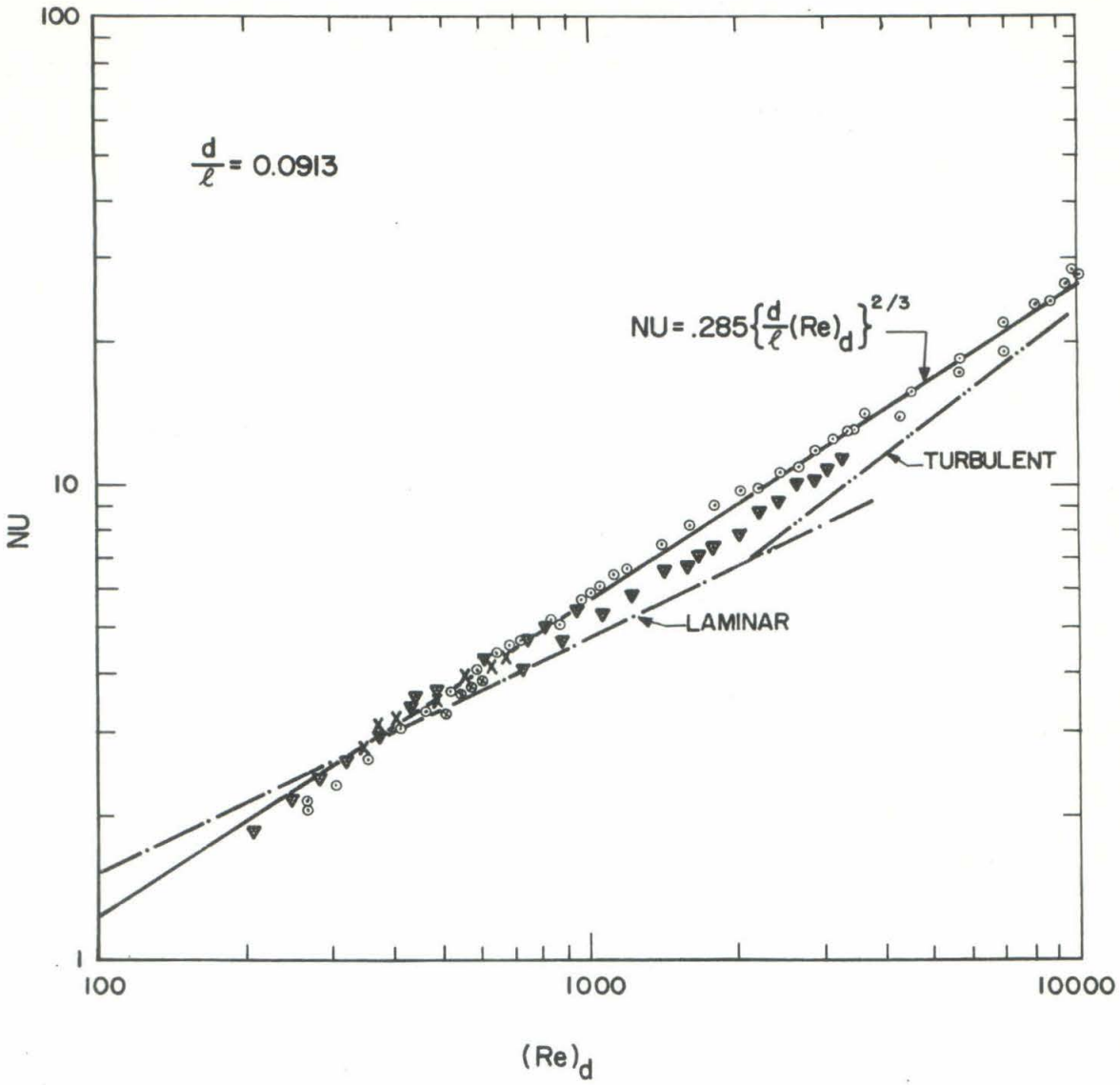

Fig. 37 HEAT TRANSFER MEASUREMENTS TO CYLINDER 2 IN ARGON

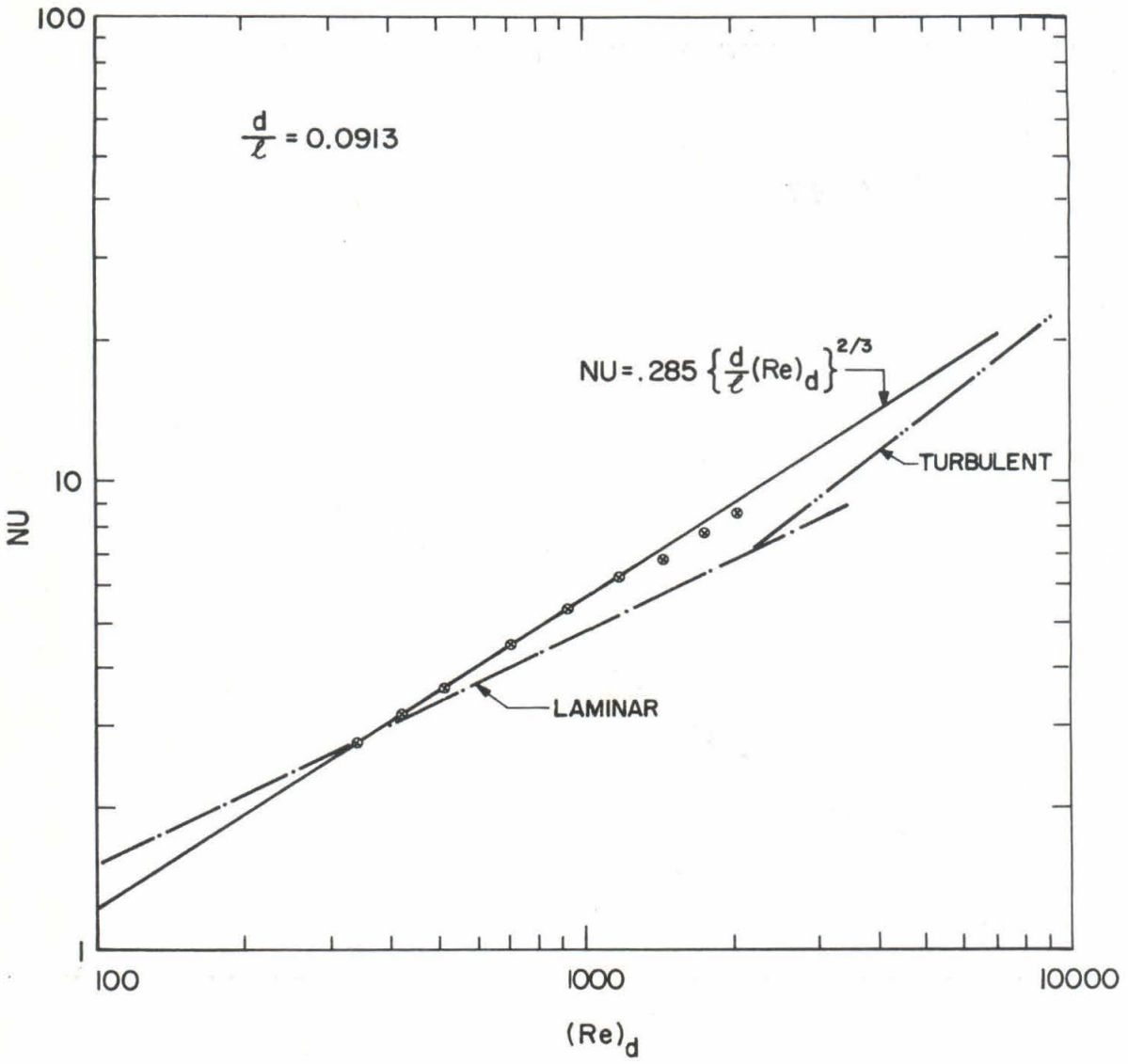

Fig. 38 HEAT TRANSFER MEASUREMENTS TO CLYINDER 2 IN HELIUM

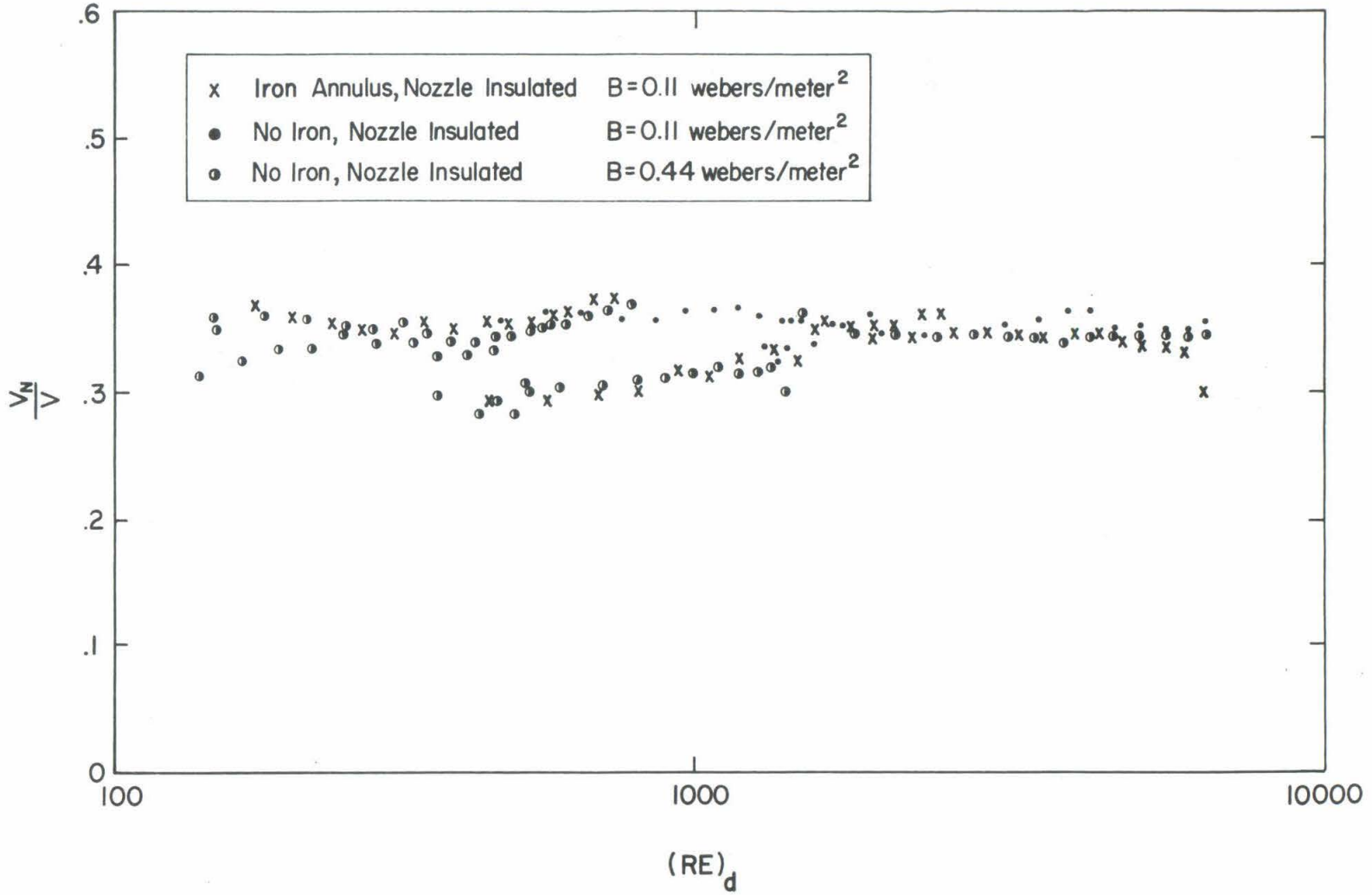

Fig. 39 OPEN CIRCUIT ANODE TO NOZZLE VOLTAGE DIVIDED BY ARC VOLTAGE, ARGON GAS

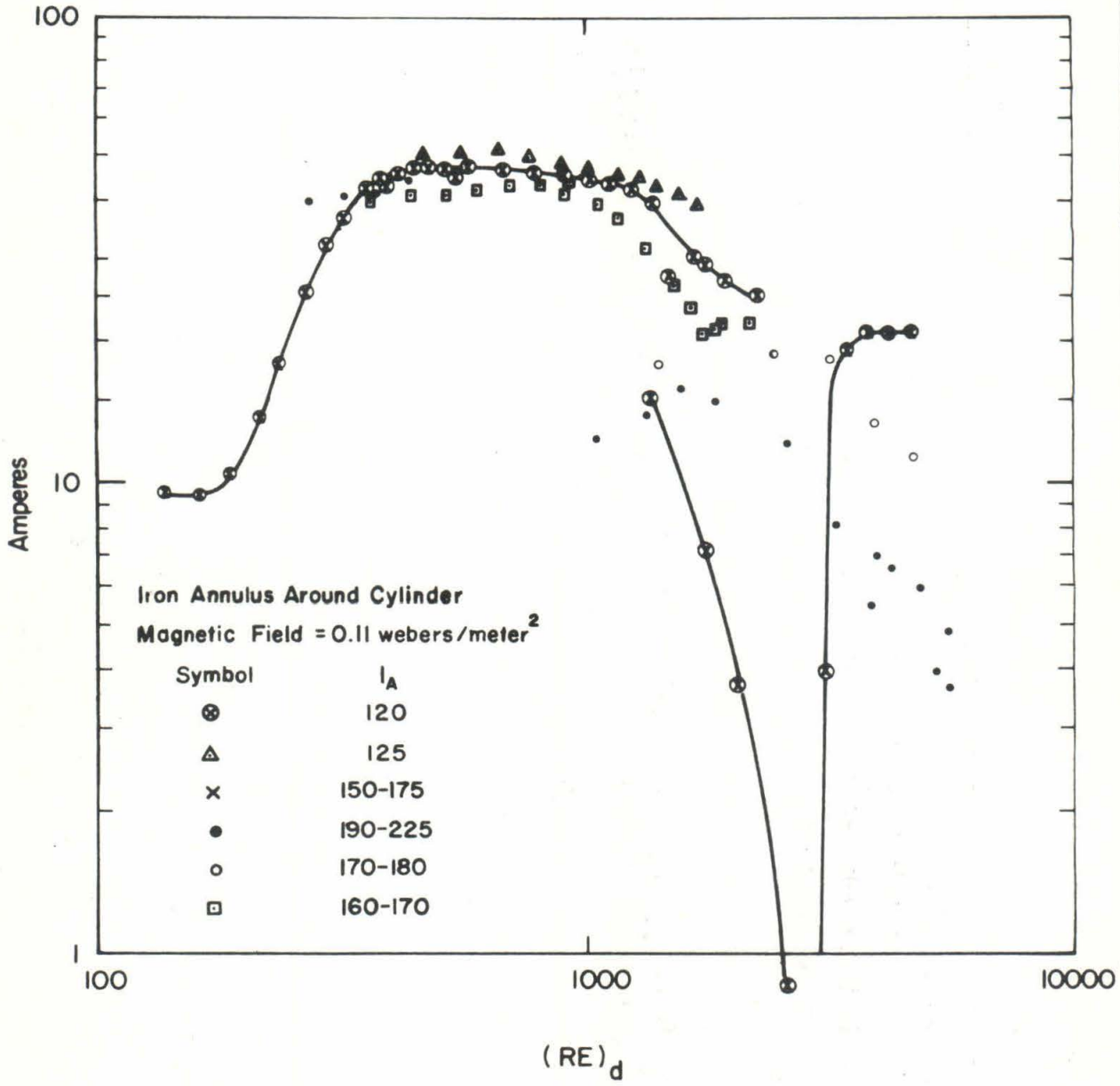

Fig. 40 ANODE TO NOZZLE CURRENT, ARGON GAS

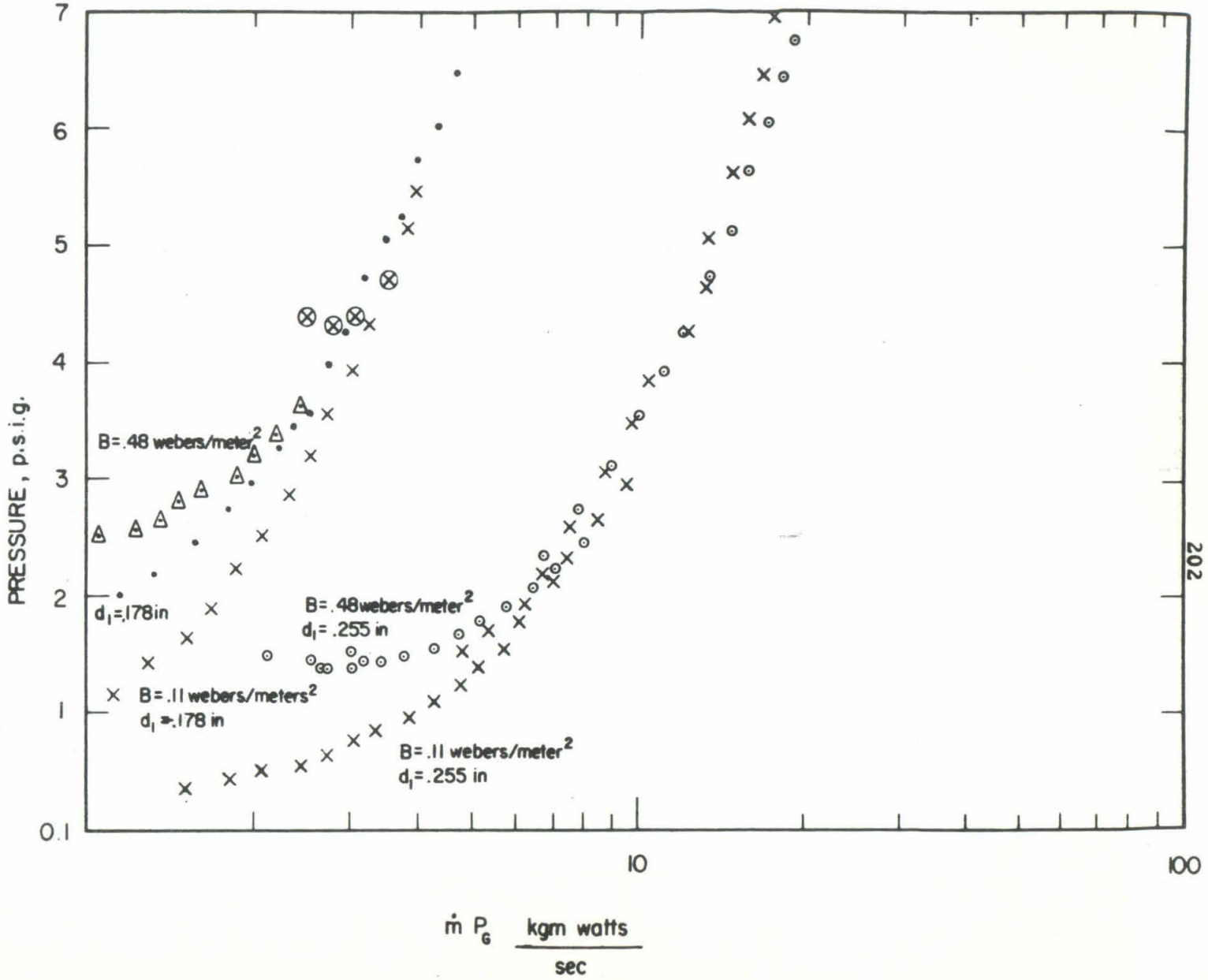

Fig. 41 STATIC PRESSURE IN THE ARC CHAMBER, ARGON GAS

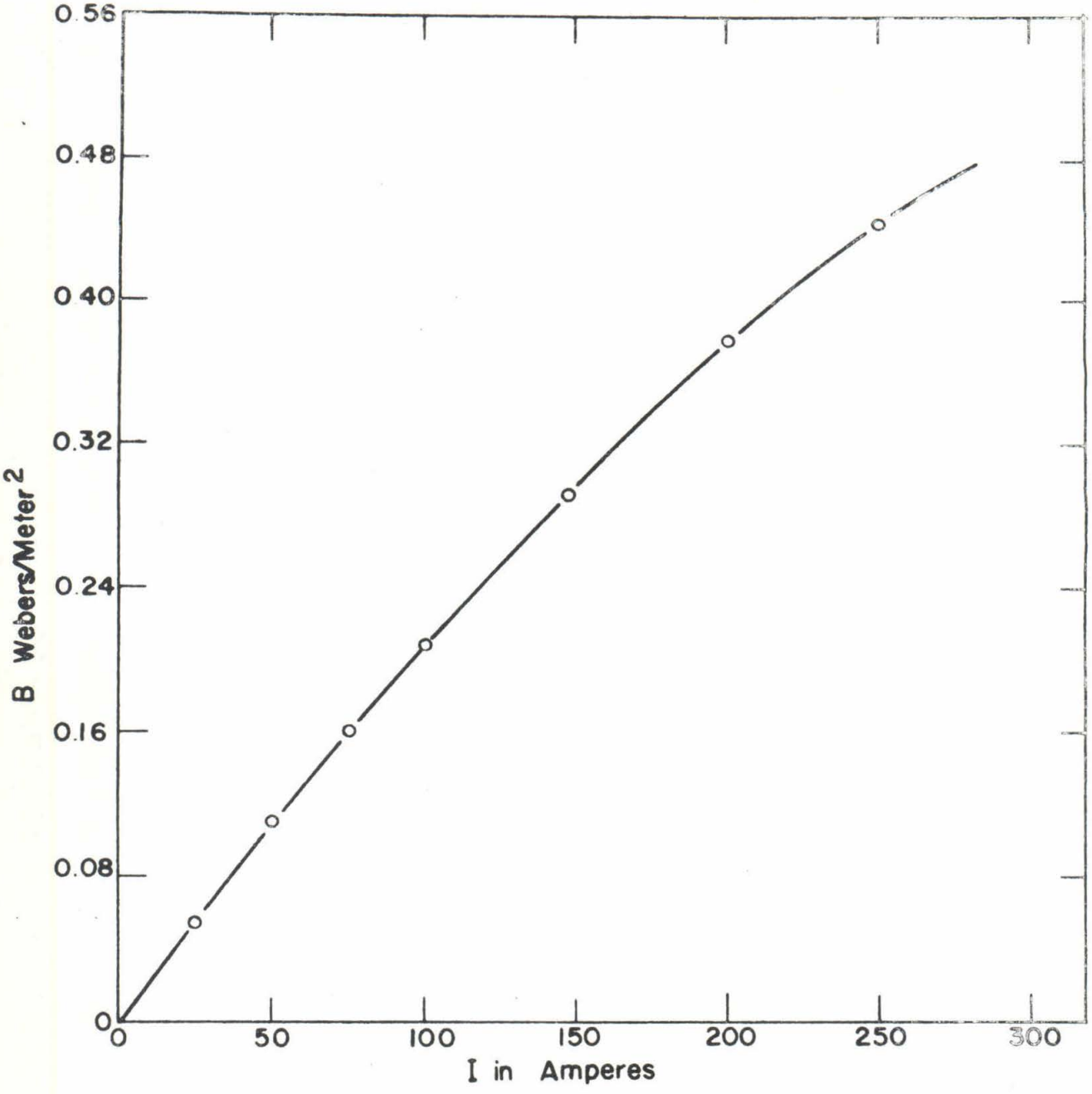

Fig. 2-1 MAGNET FIELD STRENGTH AS A FUNCTION OF THE MAGNET CURRENT.

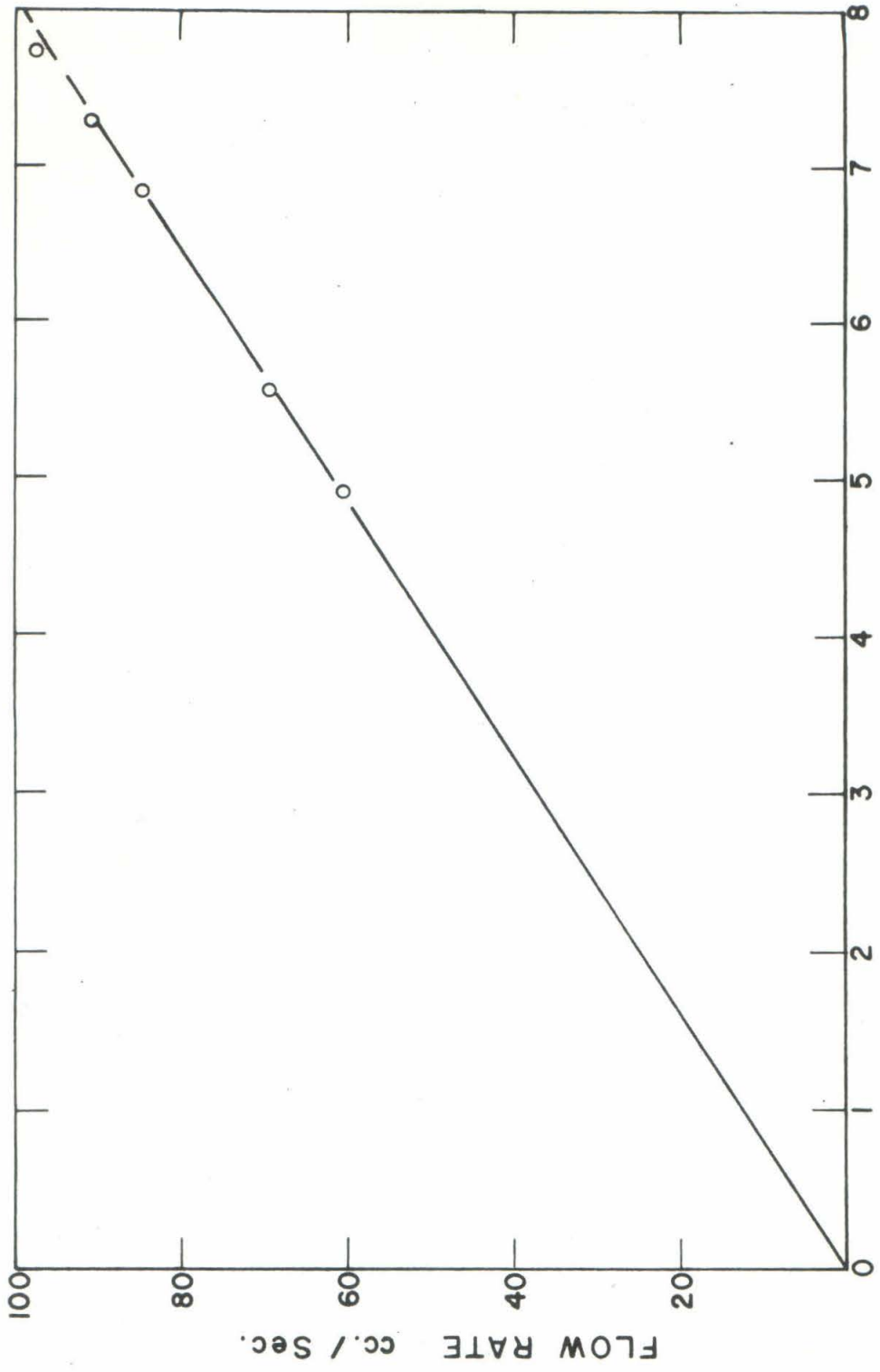

Fig. 2-2 CALIBRATION OF WATER FLOW METER

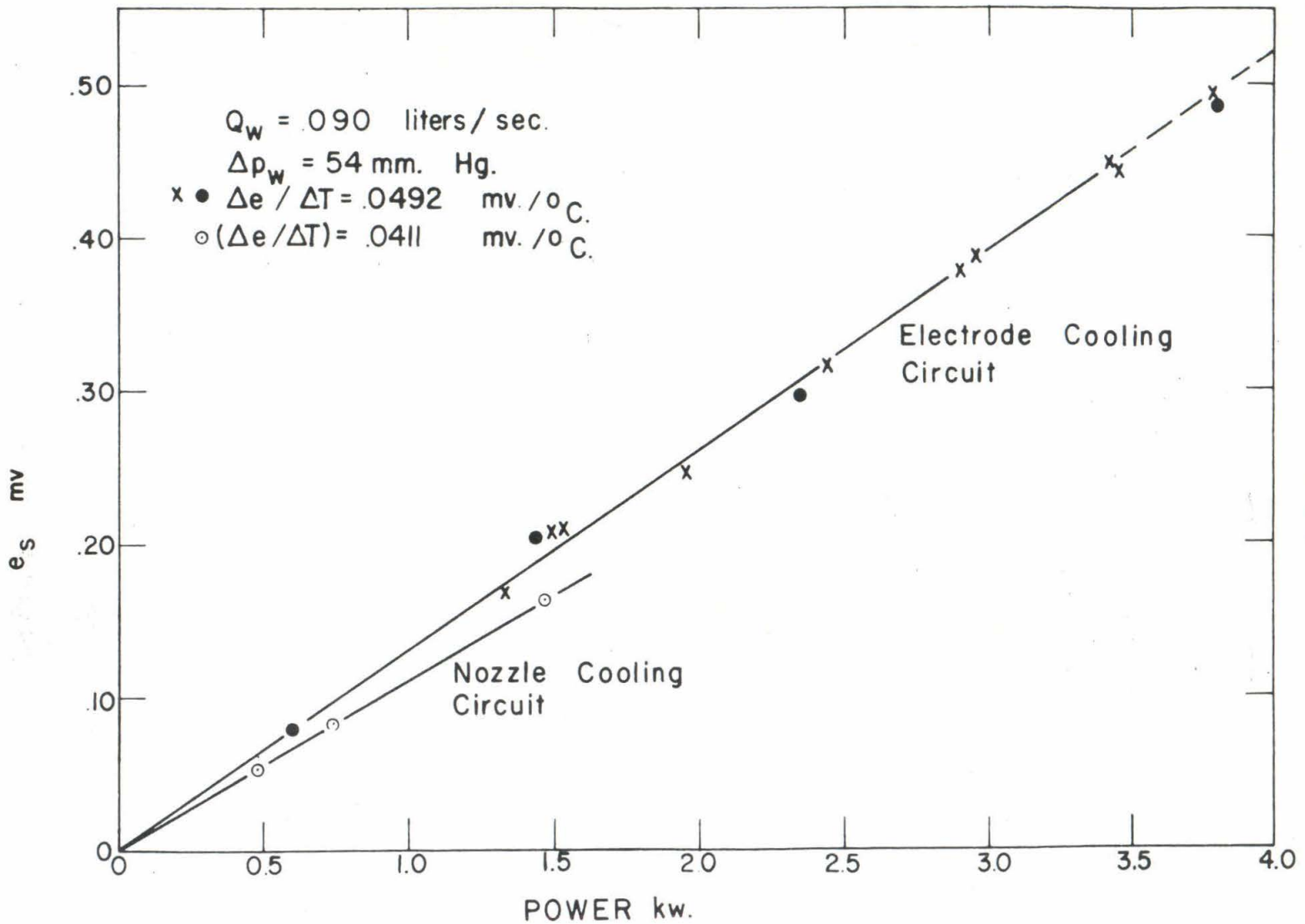

Fig. 2-3 CALIBRATION OF ELECTRODE WATER COOLING SYSTEM

DISTRIBUTION LIST

United States Army

U. S. Army Research Office (Durham)
Box CM, Duke Station
Druham, North Carolina
Attention: Information Processing Office
20 copies

Army Rocket and Guided Missile Agency
U. S. Army Ordnance Missile Command
Redstone Arsenal
Alabama
Attention: Technical Library
Attention: Mr. John Morrow
ORDXR-RMO

Commander
Army Ballistic Missile Agency
Redstone Arsenal
Alabama
Attention: ORDAB-IPL

Los Angeles Ordnance District
55 South Grand Avenue
Pasadena 2, California
Attention: Colonel P. H. Scordas
Attention: Mr. E. L. Stone
Attention: Mr. Typaldos, ORDEV-00

Chief of Ordnance
Department of the Army
ORDTB - Ballistic Section
The Pentagon
Washington 25, D. C.
Attention: Mr. George Stetson

Office of the Chief of Research and
Development
Department of the Army
Army Research Office
Washington 25, D. C.
Attention: Chief, Research Support Division

Commanding Officer
Diamond Ordnance Fuze Laboratories
Washington 25, D. C.
Attention: ORDTL 012

U. S. Army Ordnance
Ballistic Research Laboratories
Aberdeen Proving Ground
Maryland
Attention: Dr. Joseph Sternberg, Chief
Exterior Ballistics Laboratory
Attention: Dr. Raymond Sedney
Exterior Ballistics Laboratory

Commanding General
White Sands Missile Range
New Mexico
Attention: Technical Library

United States Navy

Director
U. S. Naval Research Laboratory
Washington 25, D. C.

U. S. Naval Ordnance Laboratory
White Oak
Silver Spring, Maryland
Attention: Dr. R. Kenneth Lobb
Aeroballistics Program Chief
Attention: Dr. A. E. Seigel
Chief, Ballistics Department
Attention: Dr. R. E. Wilson
Associate Technical Director
(Aeroballistics)

U. S. Naval Weapons Laboratory
Dahlgren, Virginia
Attention: Technical Library

U. S. Navy Department
David Taylor Model Basin
Applied Mathematics Laboratory
Washington 7, D. C.
Attention: Dr. F. N. Frenkiel

United States Air Force
Air Research and Development Command

Aeronautical Research Laboratories
Air Force Research Division
Air Research and Development Command
United States Air Force
Wright-Patterson Air Force Base
Ohio
Attention: Mr. Fred L. Daum, RRLD
Attention: Dr. Karl Gottfried Guderley, RRLM
Attention: Dr. Roscoe H. Mills, RRLD
Attention: RRLL

Wright Air Development Division
Air Research and Development Command
United States Air Force
Wright-Patterson Air Force Base
Ohio
Attention: WADD (WWAD - Library)
Attention: WADD (WWFEA - Reports Unit)
Attention: WWRMDF-2, Mr. Philip P. Antonatos
Attention: WWRMDF

Air Force Office of Scientific Research
Air Research and Development Command
United States Air Force
Washington 25, D. C.
Attention: Mechanics Division; Milton Rogers, Chief
Attention: SRGL (2 copies)

Directorate of Research Analysis
Air Force Office of Scientific Research
Air Research and Development Command
United States Air Force
Holloman Air Force Base
New Mexico
Attention: SRLS, Dr. Gerhard R. Eber

Air Force Ballistic Missile Division
Air Research and Development Command
United States Air Force
Air Force Unit Post Office
Los Angeles 45, California
Attention: Advanced Systems Division (WDTVV-3); Major E. W. Geniesse, Jr.
Attention: Penetration Division (WDTVV-4); 1/Lt. H. E. Hunter
Attention: AVCO Re-entry Vehicles Division (WDTVV-1); Capt. G. S. Lewis, Jr.

Air Research and Development Command
United States Air Force
Eglin Air Force Base
Florida
Attention: APGC (PGTRI, Technical Library)

Armed Services Technical Information Agency
Air Research and Development Command
United States Air Force
Arlington Hall Station
Arlington 12, Virginia
Attention: ASTIA (TIPCA)

National Aeronautics and Space Administration

NASA
Headquarters
1520 H Street, Northwest
Washington 25, D. C.
Attention: Dr. H. H. Kurzweg
Assistant Director of Research

NASA
George C. Marshall Space Flight Center
Huntsville, Alabama
Attention: Dr. Ernst D. Geissler, Director, Aeroballistics Division
Attention: M-AERO-A, Mr. Werner K. Dahm
Attention: Aeroballistics Division, M-AERO-E, Mr. T. G. Reed (3 copies)

NASA
Langley Research Center
Langley Field, Virginia
Attention: Librarian
Attention: Mr. Clinton E. Brown, Chief, Theoretical Mechanics Division, Bldg. 12
Attention: Dr. Adolf Busemann
Attention: Mr. Charles H. McLellan, 11-Inch Hypersonic Tunnel Section

NASA
Ames Research Center
Moffett Field, California
Attention: Library

NASA
Lewis Research Center
21000 Brookpark Road
Cleveland 35, Ohio
Attention: Library, Mr. George Mandel
2 copies

Miscellaneous Government Agencies

United States Atomic Energy Commission
P. O. Box 62
Oak Ridge, Tennessee
Attention: Library

U. S. Department of Commerce
National Bureau of Standards
Washington 25, D. C.
Attention: Dr. G. B. Schubauer
Chief, Fluid Mechanics Section

Universities and Non-Profit Organizations

Brown University
Division of Applied Mathematics
Providence 12, Rhode Island
Attention: Professor R. E. Meyer

Brown University
Division of Engineering
Providence 12, Rhode Island
Attention: Dr. Ronald F. Probstein

University of California at Berkeley
Aeronautical Sciences Department
Room 203, Mechanics Building
Berkeley 4, California
Attention: Professor S. A. Schaaf

University of California
Engineering and Mathematical
Sciences Library
Engineering II 8270
405 Hilgard Avenue
Los Angeles 24, California

University of California
Department of Engineering
Los Angeles 24, California
Attention: Professor A. F. Charwat
Attention: Professor John W. Miles

Case Institute of Technology
Department of Mechanical Engineering
University Circle
Cleveland 6, Ohio
Attention: Dr. G. Kuerti

Columbia University
Department of Mechanical Engineering
New York 27, N. Y.
Attention: Professor Robert A. Gross

Cornell University
Graduate School of Aeronautical Eng.
Ithaca, New York
Attention: Dr. William R. Sears
Attention: Library

University of Florida
Department of Aeronautical Eng.
Gainesville, Florida
Attention: Professor David T. Williams

Harvard University
Division of Eng. and App. Physics
Cambridge 38, Massachusetts
Attention: Dr. Howard W. Emmons

University of Illinois
Department of Aeronautical Engineering
Urbana, Illinois
Attention: Professor Harold O. Barthel
Attention: Dr. Allen I. Ormsbee

The Johns Hopkins University
Applied Physics Laboratory
8621 Georgia Avenue
Silver Spring, Maryland
Attention: Dr. L. L. Cronvich
Attention: Dr. F. K. Hill

The Johns Hopkins University
Department of Mechanics
Baltimore 18, Maryland
Attention: Dr. Francis H. Clauser
Attention: Dr. Stanley Corrsin
Attention: Professor L. S. G. Kovasznay

Lehigh University
Department of Physics
Bethlehem, Pennsylvania
Attention: Dr. Raymond J. Emrich

University of Maryland
Department of Aeronautical Engineering
College Park, Maryland
Attention: Professor S. F. Shen

University of Maryland
Institute for Fluid Dynamics and
Applied Mathematics
College Park, Maryland
Attention: Director
Attention: Professor J. M. Burgers
Attention: Professor Francis R. Hama
Attention: Professor S. I. Pai

Massachusetts Institute of Technology
Department of Aero and Astronautics
Aerophysics Laboratory
560 Memorial Drive
Cambridge 39, Massachusetts
Attention: Dr. Morton Finston

Massachusetts Institute of Technology
Department of Mathematics
Cambridge 39, Massachusetts
Attention: Professor C. C. Lin
Attention: Dr. George B. Whitham

Massachusetts Institute of Technology
Department of Mechanical Engineering
Cambridge 39, Massachusetts
Attention: Dr. A. H. Shapiro

Massachusetts Institute of Technology
Department of Aeronautical Engineering
Cambridge 39, Massachusetts
Attention: Professor E. Mollo-Christensen
Room 33-408
Attention: Dr. H. Guyford Stever

Massachusetts Institute of Technology
Department of Aeronautics and Astronautics
Cambridge 39, Massachusetts
Attention: Dr. Leon Trilling
Room 33-412

University of Michigan
Ann Arbor, Michigan
Attention: Engineering Library

University of Michigan
Willow Run Laboratories
P. O. Box 618
Ann Arbor, Michigan
Attention: BAMIRAC Library
Mr. Richard Jamron, Head
Information Handling Group

University of Michigan
Aeronautical Engineering Laboratories
North Campus
Ann Arbor, Michigan
Attention: Mr. James L. Amick

University of Michigan
Department of Aeronautical Engineering
Ann Arbor, Michigan
Attention: Dr. Arnold M. Kuethe

University of Michigan
Department of Aeronautical and
Astronautical Engineering
Ann Arbor, Michigan
Attention: Professor V. C. Liu
Attention: Professor William W. Willmarth

University of Michigan
Aeronautical and Astronautical
Engineering Laboratories
Aircraft Propulsion Laboratory
North Campus
Ann Arbor, Michigan
Attention: Professor J. A. Nicholls

University of Michigan
Department of Physics
Ann Arbor, Michigan
Attention: Dr. O. Laporte

University of Minnesota
Institute of Technology
Rosemount Aeronautical Laboratories
Rosemount, Minnesota
Attention: Mrs. Linda Caldon,
Librarian

New York University
Institute of Mathematics and Mechanics
53 Washington Square, South
New York 12, N. Y.
Attention: Library

North Carolina State College
Department of Mechanical Engineering
Raleigh, North Carolina
Attention: Professor R. M. Pinkerton

Northwestern University
The Technological Institute
Evanston, Illinois
Attention: Professor Ali Bulent Cambel

The Ohio State University
Department of Aeronautical and
Astronautical Engineering
2036 Neil Avenue
Columbus 10, Ohio
Attention: Professor John D. Lee
Attention: Professor Gavin L. VonEschen

Polytechnic Institute of Brooklyn
Aerodynamics Laboratory
527 Atlantic Avenue
Freeport, New York
Attention: Library
Attention: Professor Martin H. Bloom
Attention: Professor Antonio Ferri
Attention: Professor Paul A. Libby

Princeton University
School of Engineering
James Forrestal Research Center
Princeton, New Jersey
Attention: Library
Attention: Gas Dynamics Laboratory
Attention: Professor Sin-I Cheng
Attention: Dr. Luigi Crocco
Attention: Dr. Seymour Bogdonoff

Purdue University
School of Aeronautical and
Engineering Sciences
Wast Lafayette, Indiana
Attention: Aero. and Engineering
Sciences Library

Rensselaer Polytechnic Institute
Department of Aeronautical Engeering
Troy, New York
Attention: Library
Attention: Dr. Ting-Yi Li

University of Rochester
College of Engineering
Department of Mechanical Engineering
River Campus Station
Rochester 20, New York
Attention: Professor Martin Lessen

University of Southern California
Engineering Center
University Park
Los Angeles 7, California
Attention: Director
Attention: Dr. H. T. Yang

University of Southern California
Engineering Center
Aeronautical Laboratories Department
P. O. Box 1001
Oxnard, California
Attention: Mr. J. H. Carrington,
USCEC-ATL

Stanford University
Department of Aeronautical Engineering
Stanford, California
Attention: Professor Daniel Bershader
Attention: Dr. Milton Van Dyke

University of Texas
Defense Research Laboratory
P. O. Box 8029
Austin 12, Texas
Attention: Dr. M. J. Thompson

University of Virginia
Department of Physics
Charlottesville, Virginia
Attention: Dr. Jesse W. Beams

University of Washington
Department of Aeronautical Engineering
Seattle 5, Washington
Attention: Engineering Librarian
Attention: Professor R. E. Street

University of Wisconsin
Theoretical Chemistry Laboratory
P. O. Box 2127
Madison 5, Wisconsin
Attention: Dr. Joseph O. Hirschfelder

Yale University
Department of Mechanical Engineering
New Haven, Connecticut
Attention: Dr. Peter Wegener

Institute of the Aerospace Sciences
2 East 64th Street
New York 21, New York
Attention: Library

Industrial and Research Companies

Aeronautical Research Associates
of Princeton, Inc.
50 Washington Road
Princeton, New Jersey
Attention: Dr. Coleman duP. Donaldson

Aeronutronic
A Division of Ford Motor Company
Ford Road
P. O. Box 697
Newport Beach, California
Attention: Dr. L. L. Kavanau
Advanced Programs Staff

Aerospace Corporation, Inc.
Department of Theoretical Mechanics
Research Division
P. O. Box 95081
Los Angeles 45, California
Attention: Dr. Chieh-Chien Chang

Aerospace Corporation, Inc.
Aerodynamics and Propulsion Laboratory
P. O. Box 95085
Los Angeles 45, California
Attention: Dr. J. Logan, Director
2 copies

ARO, Inc.
Arnold Air Force Station
Tennessee
Attention: AEDC Library
Attention: Dr. B. H. Goethert
Director of Engineering
Attention: TS(T1)

ARO, Inc.
von Karman Gas Dynamics Facility
Arnold Air Force Station
Tennessee
Attention: Dr. J. Lukasiewicz, Chief
Attention: Mr. J. Leith Potter,
Manager, Research Branch

AVCO-Everett Research Laboratory
2385 Revere Beach Parkway
Everett 49, Massachusetts
Attention: Barbara A. Spence,
Technical Librarian

AVCO Research and Advanced
Development Division
201 Lowell Street
Wilmington, Massachusetts
Attention: Mr. A. Kahane
Assistant Technical Director
Attention: Dr. Frederick R. Riddell,
Tech. Ass't. to Pres. -S. Tec.

Boeing Airplane Company
Aero-Space Division
Seattle 24, Washington
Attention: Library 13-84

CONVAIR
A Division of General Dynamics Corp.
Astronautics Division
P. O. Box 1128
San Diego 12, California
Attention: Mr. K. J. Bossart, Tech. Dir.
Attention: Mr. W. B. Mitchell, 595-10

CONVAIR
A Division of General Dynamics Corp.
Scientific Research Laboratory
5001 Kearny Villa Road
San Diego 11, California
Attention: Mr. William H. Dorrance
Senior Staff Scientist
Mail Zone 1-162
Attention: Mr. Merwin Sibulkin
Staff Scientist

CONVAIR
A Division of General Dynamics Corp.
San Diego 12, California
Attention: Dr. H. Yoshihara
Chief of Fluid Dynamics Res.
Mail Zone 6-105

CONVAIR
A Division of General Dynamics Corp.
Aerospace Technology Section
P. O. Box 748
Fort Worth, Texas
Attention: Mr. R. C. Frost
Dept. 6-1
Mail Zone E63

CONVAIR
A Division of General Dynamics Corp.
Fort Worth, Texas
Attention: Mr. A. P. Madsen
Aerodynamics Group Eng.
Mail Zone E63
Attention: Mr. W. G. McMullen
Attention: Mr. Robert H. Widmer

CONVAIR
A Division of General Dynamics Corp.
Daingerfield, Texas
Attention: Mr. J. E. McMichael
Chief, Jet Engine Department

Cornell Aeronautical Laboratory, Inc.
P. O. Box 235
Buffalo 21, New York
Attention: Library
Attention: Dr. A. H. Flax
Attention: Mr. A. Hertzberg
Head, Aerodynamic Research

Douglas Aircraft Company, Inc.
Missiles and Space Systems
3000 Ocean Park Blvd.
Santa Monica, California
Attention: Library
Chief,
Aero/Astrodynamics Section
2 copies
Attention: Mr. R. J. Gunkel
Chief,
Aero/Astrodynamics Section

Douglas Aircraft Company, Inc.
827 Lapham Street
El Segundo, California
Attention: Dr. A. M. O. Smith

General Electric Company
Missile and Ordnance Systems Dept.
3198 Chestnut Street
Philadelphia 4, Pennsylvania
Attention: L. Chasen, Mgr. Libraries
Documents Library
Attention: Mr. P. J. Friel

General Electric Company
Space Sciences Laboratory
3750 D Street
Philadelphia, Pennsylvania
Attention: Mr. H. Lew

General Electric Company
Research Laboratory
P. O. Box 1088
Schenectady, New York
Attention: Dr. Henry T. Nagamatsu

Giannini Controls Corporation
1600 South Mountain Avenue
Duarte, California
Attention: Library

Grumman Aircraft Engineering Corp.
Bethpage, New York
Attention: Mr. Charles Tilgner, Jr.

Hughes Aircraft Company
Culver City, California
Attention: Mr. E. O. Marriott
Manager, Aerodynamics Dept.

Lockheed Aircraft Corporation
Missiles and Space Division
3251 Hanover Street
Palo Alto, California
Attention: Dr. W. A. Kozumplik
Head, Tech. Info. Center
Dept. 50-14, Bldg. 201

Lockheed Aircraft Corporation
Missiles and Space Division
Sunnyvale, California
Attention: Mr. R. N. Munson
Dept. 81-91

Lockheed Aircraft Corporation
Missiles and Space Division
P. O. Box 504
Sunnyvale, California
Attention: Mr. R. Smelt,
Chief Scientist

Lockheed Aircraft Corporation
Missile Systems Division
Sunnyvale, California
Attention: Mr. Maurice Tucker
Spacecraft and Missiles Research

Lockheed Aircraft Corporation
Missiles and Space Division
7701 Woodley Avenue
Van Nuys, California
Attention: Library

Lockheed Aircraft Corporation
Marietta, Georgia
Attention: Dr. W. F. Jacobs
Aerodynamics Dept. -72-07

Marquhardt Aircraft Company
P. O. Box 2013 - South Annex
Van Nuys, California
Attention: Technical Library

The Martin Company
Baltimore 3, Maryland
Attention: Mr. K. Jarmolow
Mail No. J-3033
Attention: Dr. Mark V. Morkovin
Mail No. J-3033

McDonnell Aircraft Corporation
Lambert-Saint Louis Municipal Airport
P. O. Box 516
St. Louis 66, Missouri
Attention: Mr. Kendall Perkins

The RAND Corporation
1700 Main Street
Santa Monica, California
Attention: Librarian
Attention: Dr. Carl Gazley, Jr.
Attention: Mr. E. P. Williams
Aero-Astronautics Dept.

Republic Aviation Corporation
Farmingdale, Long Island, New York
Attention: Engineering Library
Attention: Mr. R. W. Perry
Chief, Re-Entry Simulation Lab.
Applied Research and Dev.

Space Technology Laboratories, Inc.
P. O. Box 95001
Los Angeles 45, California
Attention: Technical Information Center
Document Procurement
Bldg. C, Room 2412
Attention: Dr. James E. Broadwell
Aerodynamics Research Section
Attention: Dr. C. B. Cohen
Attention: Dr. Luois G. Dunn, President
Attention: Dr. Andrew G. Hammitt, Head
Aerodynamics Research Section
Attention: Mr. Ernest I. Pritchard
Attention: Dr. George E. Solomon

Sperry Utah Engineering Laboratory
Division of Sperry Rand Corporation
322 North 21st Street West
Salt Lake City 16, Utah
Attention: Mr. Malcolm L. Matthews

Systems Corporation of America
1007 Broxton Avenue
Los Angeles 24, California
Attention: Dr. Paul D. Arthur

United Aircraft Corporation
Research Laboratories
East Hartford 8, Connecticut
Attention: Mr. John G. Lee

Internal

Mr. Paul E. Baloga
Dr. Julian D. Cole
Dr. Donald E. Coles
Dr. Anthony Demetriades
Dr. Toshi Kubota
Professor Lester Lees
Dr. H. W. Liepmann
Dr. Clark B. Millikan
Dr. Barry L. Reeves
Dr. Anatol Roshko

Dr. Frank Marble
Dr. S. S. Penner
Dr. W. D. Rannie
Dr. Edward Zukoski

Dr. Harry Ashkenas
Mr. George Goranson
Dr. James M. Kendall
Dr. John Laufer
Dr. Thomas Vrebalovich
Mr. Richard Wood

Aeronautics Library (2)
Hypersonic Files (3)
Hypersonic Staff and Research Workers (20)